

THE ROAD TO ENVIRONMENTAL CHEMISTRY IN REPUBLIC OF MOLDOVA PAVED BY THE ILLUSTRIOUS SCIENTIST AND RENOWNED ECOLOGIST VALERIU ROPOT

Tudor Lupascu^{a*} and Maria Sandu^b

^a*Institute of Chemistry, 3, Academiei str., Chisinau MD-2028, Republic of Moldova*

^b*Institute of Ecology and Geography, 1, Academiei str., Chisinau MD-2028, Republic of Moldova*

*e-mail: tudor.lupascu@ichem.md; lupascut@gmail.com

Abstract. In this paper, the main scientific and innovative results are presented, which were obtained by the talented chemist and renowned ecologist Valeriu Ropot throughout his scientific career. The results of scientific investigations are bestowed and analysed, focusing on the quality of the waters of the Dniester and the Prut Rivers, Dubasari reservoir on the Dniester River, as well as the main water bodies in the Republic of Moldova. Recommendations are also presented regarding the studies on the improvements of water purification technologies from the Dniester and Prut Rivers, including practical applications for the removal of fluoride, iron, ammonium, and sulphide ions from groundwater. Another aspect of the work is devoted to scientific studies related to the solving of problems concerning the treatment of wastewater from industrial enterprises in the agro-industrial complex and from economic units, and galvanic processes. The paper also presents some practical recommendations for reducing the negative impact on the environment, of the discharge of hundreds of thousands of tons of brine into the Dniester River as a result of the accident at the mineral fertilizer plant in the Stebnik town, Ukraine. Moreover, the paper brings into discussion the results of studies aimed at developing methods for determining organic and inorganic pollutants in natural waters.

Keywords: water, wastewater, chemical composition, treatment technology, pollutant.

Received: 26 October 2022

Introduction

In the beginning of the 70's (1972), the young doctor of chemistry Valeriu Ropot founded the Laboratory of Mineral Resources and Chemistry of Water within the Institute of Chemistry of the Academy of Sciences of Moldova. Later on, in 1992, at the initiative of the ecologist Valeriu Ropot the laboratory was re-profiled to the Laboratory of Ecological Chemistry due to the need to solve environmental problems that were escalating in the world, including in Bessarabia.

Environmental protection requires the implementation of a series of complex social, economic, scientific research and technical measures that will guarantee the preservation of the natural environment. These measures can have both a global character, impacting the vital interests of the entire population on earth, and a local character, by solving ecological problems.

Amongst the principal scientific objectives of the Laboratory of Ecological Chemistry within the Institute of Chemistry of the Academy of Sciences of Moldova, was the evaluation of natural minerals, research and establishment of

laws regarding the formation of the quality of surface and underground waters, as well as highlighting the processes and mechanisms of transformation of natural and anthropogenic pollutants in aquatic systems. Scientist Valeriu Ropot paid special attention to the development of high-performance technologies for making surface water potable, as well as those for treating wastewaters resulted from the activity of various economic units in the Republic of Moldova.

Under the leadership of Dr. Valeriu Ropot, a vast body of scientific research was carried out, concerning the mechanism of pollutant immobilization through mineral absorbents, and description of the role of active centres in the processes of pollutant migration and transformation in the aquatic environment were highlighted. Thus, the initial field of research was the evaluation of natural minerals (clays) used for the purification of winery wastewaters. The results of the study were appreciated with the Silver Medal at the Exhibition of Achievements of the National Economy of the USSR in 1975 - for implementing the technology at the Brandy Plant in Balti municipality, Republic of Moldova.

Table 1

Dynamics of the annual average values of the mineralization and the concentration of the main mineral components in the Dniester River water, Vadul lui Voda section, in the years 1961-1990 [1].

Years	Content, mg/L							
	K^+	Na^+	Ca^{2+}	Mg^{2+}	SO_4^{2-}	Cl^-	HCO_3^-	Dry residue
1961-1970	3-4	16-19	52-66	7-10	48-65	20-35	160-210	240-320
1971-1980	4-6	18-20	53-62	8-12	53-70	31-42	161-218	310-416
1981	5-6	19-24	56-63	10-13	67-84	41-52	160-270	318-338
1982	5-7	23-28	60-68	12-13	75-96	54-68	164-276	300-452
1983	9-70	22-230	59-90	14-84	87-280	65-502	185-330	316-1520
1984	16-21	68-75	86-92	24-40	128-160	115-145	214-290	497-670
1985	13-14	50-72	62-90	20-28	94-130	70-110	196-244	415-460
1986	12-13	36-58	62-69	16-18	92-102	62-72	164-300	410-488
1987	11-12	34-57	61-68	15-18	93-110	67-71	152-230	384-486
1988	9-11	33-58	54-70	12-17	76-108	50-68	168-220	338-490
1989	9-10	31-56	53-70	12-16	78-96	52-65	170-240	330-470
1990	5-6	20-25	52-68	10-12	72-84	35-52	160-210	320-406

Many scientific expeditions have been organized by the scientist Ropot Valeriu with the goal to study the quality of surface and underground waters, starting from the source and to the Black Sea, and respectively to the Danube along the Rivers of Dniester and Prut and many small rivers of the Republic of Moldova. The scientific research results obtained regarding the state of the surface and underground waters were reported in various scientific publications (1972-2002), presented at many national and international scientific conferences and used in the development of the National Strategic Action Program in the field of environmental protection, during the years 1995-2010-2020.

The scope of this paper is to put forward concisely the main achievements and contributions to the development of the field of environmental chemistry in the Republic of Moldova by the much-appreciated scientist and renowned ecologist Dr. Valeriu Ropot.

Background

Aspects regarding Dniester River water quality

A detailed study regarding the annual average values of the mineralization and concentration of the main mineral components in the Dniester River water, Vadul lui Voda section, was performed for the years 1961-1970, 1971-1980 and annually during 1981-1990 (Table 1) [1]. It was demonstrated that higher values of some indices (Na^+ , K^+ , SO_4^{2-} , Cl^- and mineralization) in the years 1983-1985 (Table 1) were the consequence of the serious accident at the mineral fertilizer complex in the Stebnic town (Ukraine) on 15 September 1983, when 1.35 million tons of salt (5 million m^3 of brine)

were discharged into the Dniester River. The brine reached the Novodnestrovsk reservoir and continued its course in the Dniester River on the Republic of Moldova territory.

Analysing the dynamics of the chemical indicators of water, until the year 1987, the scientist Ropot Valeriu found that in the water of the Dniester River, the mineralization and most of the mineral components were increasing.

Table 2

The maximum values (mg/L) of specific parameters in the water of Dniester River, Vadul lui Voda section (years 1987 and 1988).

Parameters	1987	1988	MAC*
Phenol	0.0008	0.0009	0.001
Anionic surfactants	0.26	0.27	0.5
Petroleum products	0.08	0.07	0.5
F^-	0.3	0.3	1.2
CN^-	-	-	0.05
AsO_2^-	traces	0.001	0.05
Se ($SeO_3^{2-}+SeO_4^{2-}$)	0.0001	0.0001	0.001
Mn^{2+}	0.003	0.002	0.1
Al^{3+}	0.12	0.11	0.5
Hg^{2+}	0.0006	0.0007	0.001
Cd^{2+}	0.0017	0.0015	0.001
Fe ($Fe^{3+}+Fe^{2+}$)	0.20	0.15	0.3
Cu^{2+}	0.12	0.12	1.0
Ni^{2+}	0.008	0.007	0.1
Cr^{3+}	0.003	0.003	0.01
Zn^{2+}	0.08	0.09	5.0
Ba^{2+}	0.016	0.018	0.1
Ag^+	0.0013	0.0014	0.05
Ti^{2+}	0.045	0.046	0.1
Co^{3+}	0.00016	0.00017	0.1
Sr^{2+}	1.08	1.08	7.0
Be^{2+}	0.00014	0.00014	0.0002
Mo^{3+}	0.0025	0.0026	0.5
Pb^{2+}	0.018	0.017	0.1

*MAC – maximum allowable concentration [2].

For example, the potassium content tripled (from 3-4 mg/L to 11-12 mg/L), sodium content doubled (from 16-19 mg/L to 34-57 mg/L), chlorides content increased from 20 mg/L to 50 mg/L and that of sulphates from 48 mg/L to 76 mg/L. The comparison of the average values of water mineralization also demonstrated a permanent increase from 240 mg/L to 488 mg/L, reaching an increase of 50% during the years 1961-1987.

The evaluation of the content of organic substances (phenol, anionic surfactants, petroleum products), fluorine, cyanide, arsenic, selenium and heavy metals in the Dniester River water (Vadul lui Voda section) was performed during the years 1987-1988, to ensure that the water can be used for drinking purposes (Table 2).

Based on the main *conclusions and recommendations* drawn from the study regarding the prevention of water pollution and removal of pollutants from the Dniester River, and also for other water basins [1], the ecologist Valeriu Ropot proposed a set of recommendations in the following directions:

1. *Legislation*: elaboration of legislative and normative acts for the protection and rational use of water resources;
2. *Organizational*: development of basins and territories schemes for complex use and water resources protection;
3. *Environmental monitoring*: organization of permanent monitoring of the state of natural resources on the Dniester River;
4. *Technological*: development of technological schemes of production at economic units that are friendlier to the environment, based on the production of a small volume of wastes, technologies with no waste and wastewater, implementation of wastewater recycling systems after treatment, *etc.*;

5. *Economic*: the development of criteria and methods for evaluating the damage caused by the pollution of water resources and the efficiency of the protection of water resources;
6. *Scientific*: carrying out complex scientific research combining theoretical and experimental methods in the field of environmental protection, rational use of water resources and implementation of the scientific results into practice;
7. *Social*: creating optimal conditions for human life, health and rest.

Scientist Ropot Valeriu mentioned that compliance with these recommendations would lead to the regulation of water consumption from the Dniester River basin and would increase the responsibility of consumers of water resources, improving the ecological condition of the hydrographic basin on the territory of the republic.

Optimization of the potabilization technology for water from the Dniester River [3,4]

With the purpose of evaluating the efficiency of the water treatment technology applied for Dniester River water with the goal to obtain potable water, the chemical composition of the water was studied after each treatment step. The analysis of the results presented in Table 3 highlights the fact that the chemical consumption of oxygen, determined by the CCO_{Cr} method was ≈ 4 times higher than that of CCO_{Mn} method and exceeded the maximum allowable concentration ($\text{CCO}_{\text{Cr}} = 3 \text{ mgO}_2/\text{L}$). The organic phosphorus and nitrogen detected in water imply the presence of organic micropollutants with complex structures, probably pesticides. Thus, it was concluded that the technology applied at the water treatment plant for Chisinau municipality did not allow obtaining qualitative drinking water.

Table 3

Chemical composition of the water from the Dniester River at different stages of treatment.

Parameters	Initial water	Water after the stage of coagulation and sedimentation	Water after the stage of filtration through sand filters	Drinking water
pH	7.97	7.67	7.67	7.8
CCO_{Cr} , mgO_2/L	18.96	13.8	11.4	9.8
Phenol total, mg/L	0.003	0.002	0.002	<0.001
Anionic surfactants, mg/L	0.54	0.04	0.026	0.024
NH_4^+ , mg/L	0.47	0.45	0.42	0.31
N-organic, mg/L	2.30	1.01	0.29	0.10
NO_3^- , mg/L	12.86	13.36	11.68	13.8
P-organic, mg/L	0.031	0.024	0.024	0.005
PO_4^{3-} , mg/L	0.26	0.12	0.10	0.10
Humic substances, mg/L	0.38	0.10	0.08	0.08

For the improvement of the water purification technology, the quality of water from Dniester River was assessed using 4 technological schemes presented in Table 4; their efficiency in water treatment from Dniester River is illustrated in Table 5. The analysis of the results (Table 5) allowed to conclude that Scheme 4 (D) was the most suitable for obtaining high-quality drinking water.

Table 4

Treatment schemes of Dniester River water.

No.	Process diagram	Continuity of processes
1	A	O(O ₃)→CF→D→FN→FCA
2	B	CF→D→O(O ₃)→FN→FCA
3	C	O(O ₃ /H ₂ O ₂)→CF→D→FN→FCA
4	D	PO(O ₃ /H ₂ O ₂)→CF→D→FN→IO→FCA

O- ozonation;

CF- coagulation-flocculation;

D-settlement; *FN*- sand filters;

FCA- filters with activated carbons;

PO- pre-ozonation;

IO- inter-ozonation.

Table 5

Efficiency of purification of water from the Dniester River by using different processes in treatment.

No.	Parameters	Water treatment efficiency (%) with the use of different options			
		A	B	C	D
1	CCO _{Cr}	66	19	77	94
2	N-organic	30	10	85	100
3	P-organic	70	20	89	96

Evaluation of the consequences of the accident at the mineral fertilizer plant in Stebnic town (Ukraine)

Unfortunately, on 15 September 1983, a serious accident occurred at the mineral fertilizer plant in Stebnic town (Ukraine). As a result of this accident, approximately 5 million m³ of concentrated wastewaters (brine) with a

concentration of 242.67 g/L were dumped into the Dniester River (on the Ukraine territory). The salty wastewaters contained fatty acids (0.01 g/L), potassium ions (20.06 g/L), sodium ions (36.19 g/L), magnesium ions (30.78 g/L), sulphates (60.58 g/L) and chlorides (97.09 g/L).

Brine, in the amount of about 1 million 350 thousand tons of salts, entered the reservoir of the Novodnestrovsk hydropower plant on the Dniester River. The height of the salt water layer was 10-12 m with a maximum salt concentration of 37 g/L. Although the salt content was decreasing during the water flow of the Dniester River, a high concentration still remained in the water, being dangerous for the river because it did not contain the oxygen necessary for the aquatic biota, and thus causing fish kills. The maximum concentration of chlorides and the mineralization value of the water of the Dniester River and the Novodnestrovsk reservoir after the discharge of wastewaters from the Stebnic plant are shown in Table 6 [5,6].

Resulting from the fact that the water from Lake Novodnestrovsk continues its course on the territory of the Republic of Moldova in the Dniester River, which is used to provide the population with drinking water, the Institute of Chemistry was actively involved in the scientific research of the composition of the water in the river. This theme was led by Dr. Valeriu Ropot, who contributed essentially to the evaluation of the composition of the water and the elaboration of special recommendations to solve the existing problem by using the Novodnestrovsk reservoir to avoid the disaster on the territory of the Republic of Moldova. The study demonstrated that the water in the reservoir needed to be discharged only from the surface and should not contain more than 2 g/L of salts (500-600 mg/L of chloride ions).

Table 6

Maximum concentration of chlorides and mineralization in Dniester River and Novodnestrovsk reservoir waters after the discharge of wastewaters from the Stebnic plant [5,6].

The supervision section	Date of water sample collection	Chloride concentration, g/L	Mineralization, g/L
Nikolaev town	16.09.1983	128.0	210.0
Galici town	18.09.1983	47.5	141.0
Zalescichi town	21.09.1983	36.0	114.0
Khotyn city	23.09.1983	34.0	105.0
Novodnestrovsk Lake	04.10.1983	12.0	37.0

The dynamics of ion content and water mineralization in Dniester River, Otaci city, upon entering the territory of the Republic of Moldova, demonstrates water pollution, especially with chlorine ions and total water mineralization (Table 7).

Dynamics of ion content and water mineralization in Dniester River, Vadul lui Voda town

As a result of the scientific research carried out and the recommendations given by the devoted scientist, Dr. Valeriu Ropot, the Dniester River water at Vadul lui Voda town (Chisinau Municipal Supply Station) contained from 40.3 to 500 mg/L of chlorides in October-December of 1983, with a maximum mineralization of 1383.1 mg/L on November 15, 1983 confirming the importance of the conducted scientific research that was continued in the years 1984-1985. Only in September 1984, the chloride content has decreased to 115 mg/L and the mineralization to 561.7 mg/L, and in August 1985 was attested a

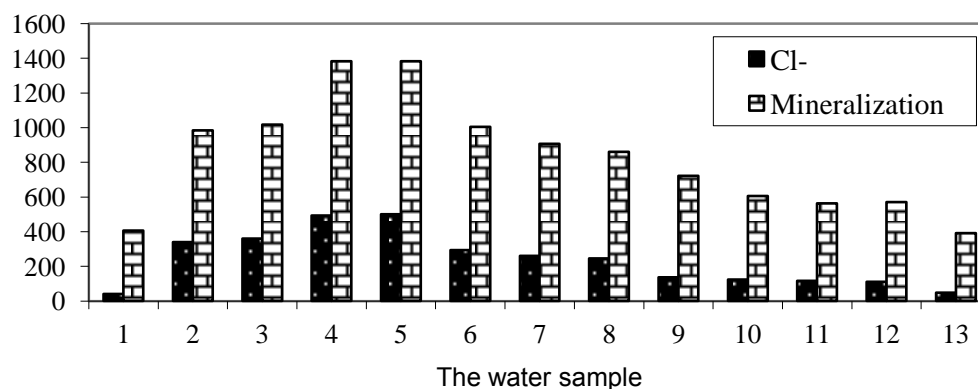
content of 47.8 mg/L of chloride ions and 391.3 mg/L mineralization (Figure 1) [5].

Moreover, the conducted research demonstrated a negative influence of the salts from the river water on the sludge (bottom sediment) from the Dubasari reservoir, which contained montmorillonite having sodium and potassium ions replaced by calcium ions. As a result, the dispersion and compaction of montmorillonite particles took place with the elimination of marsh gases. Dr. Valeriu Ropot studied the bottom sediment from Dniester River in sections at Camenca city, the Oxentia village and Dubasari lake, with its granulometric change and chemical composition being demonstrated (Table 8) [5]. To inform the scientific society, the results of the study and the special recommendations for solving the problem of the accident at the mineral fertilizer plant in Stebnic town (Ukraine) were presented at the international conference in Bucharest, Romania, in 2001 [7].

Table 7

Dynamics of ions content (mg/L) and water mineralization (mg/L) in Dniester River, Otaci city, the entrance on the Republic of Moldova territory [5,6].

Date of water sample collection	K^+	Na^+	Ca^{2+}	Mg^{2+}	Cl^-	SO_4^{2-}	NO_3^-	Mineralization
29.09.1983	9.0	34.0	61.4	16.8	60.0	70.0	6.7	367.9
01.10.1983	78.6	190.0	61.2	96.4	486.4	254.0	6.2	1273.9
04.10.1983	108.4	365.9	62.0	116.8	780.4	350.4	8.0	1876.9
09.10.1983	112.4	385.9	62.8	112.9	745.0	380.0	7.8	1904.3
12.10.1983	100.4	262.8	73.8	99.8	560.4	340.4	6.7	1561.4
10.11.1983	32.5	110.8	83.0	50.8	270.8	162.0	8.2	832.3
23.12.1983	27.2	100.0	95.0	45.8	225.0	158.4	8.6	780.0
02.02.1984	20.8	72.0	102.0	35.2	135.8	150.2	9.4	670.4
06.05.1984	14.8	49.2	88.8	28.8	120.6	125.8	6.8	556.8
23.09.1984	18.0	42.3	84.8	30.0	119.8	113.0	6.9	527.3
21.12.1984	13.8	40.0	72.8	29.8	95.0	86.5	9.5	457.4
05.04.1985	11.8	38.8	68.8	24.0	75.8	72.8	9.6	414.1
22.08.1985	11.2	36.0	66.0	18.0	65.0	68.0	7.4	377.0



1 – 19.10.1983
 2 – 25.10.1983
 3 – 30.10.1983
 4 – 09.11.1983
 5 – 15.11.1983
 6 – 30.11.1983
 7 – 01.12.1983
 8 – 10.12.1983
 9 – 02.02.1984
 10 – 24.07.1984
 11 – 24.09.1984
 12 – 05.04.1985
 13 – 22.08.1985

Figure 1. Dynamics of chloride (mg/mL) and mineralization in Dniester River water, Vadul lui Voda town (Water supply station of the Chisinau municipality), years 1983-1985 [5].

Following the consequences of the 1983 accident at the mineral fertilizer plant in the Stebnic town (Ukraine), the famous scientist Valeriu Ropot developed detailed studies and practical communications regarding the management of water resources in the conditions of a vulnerable environment [8].

Table 8

Content of mineral components in the bottom sediment from the Dubasari reservoir [5].

City and date of sample collection	$\text{CaSO}_4 \cdot 2\text{H}_2\text{O}$ % of the dry bottom sediment	CaCO_3	MgCO_3
Camenca town			
13.10.1983	0.57	8.24	0.004
Oxentia village			
13.10.1983	0.60	8.45	0.011
10.06.1986	0.025	5.71	0.038

Aspects regarding the water quality of Prut River

Considered a border river, almost along its entire length the Prut was not subjected to the scientific research necessary for water protection for a long time. As a result, it was found that there were a limited number of publications on the problems of the Prut River in the specialized literature. Starting with 1985, the researchers of the Institute of Chemistry of the Academy of Sciences of Moldova carried out systematic research on the evaluation of the water quality of

the Prut River and its tributaries. Since 1991, the research has been carried out jointly with collaborators of the Romanian Wastewater Treatment Research Institute, with joint publications [9,10].

The information presented in Table 9, regarding the content of heavy metals in the water and bottom sediments in the Prut River, Giurgiulesti village, proves that it was within the allowed limit for surface waters, being also accumulated in the silt of the river.

The average annual values of the water quality indicators of the Prut River on the Republic of Moldova territory in the years 1995 and 2000 are mentioned in Table 10 [11] and denote the increase in mineralization and the concentration of the main ions along the course of the river towards the Danube River.

Table 9

Content of heavy metals in water and bottom sediments in the Prut River, Giurgiulesti village.

Parameters	Water, mg/L	Bottom sediments, mg/kg
Iron ($\text{Fe}^{2+} + \text{Fe}^{3+}$)	0.3	900
Cooper (Cu^{2+})	0.005	40
Manganese (Mn^{2+})	0.004	500
Lead (Pb^{2+})	0.01	30
Zinc (Zn^{2+})	0.002	16
Cadmium (Cd^{2+})	traces	0.09

Table 10

Annual values of water quality indicators of the Prut River on the Republic of Moldova territory, 1995 and 2000 years [11].

Parameters	Sampling points									
	Lipcani		Costesti		Valea Mare		Cahul		Giurgiulesti	
	1995	2000	1995	2000	1995	2000	1995	2000	1995	2000
Suspensions, mg/L	45	42	22	20	104	87	83	70	82	56
Mineralization, mg/L	354	356	338	334	466	473	476	475	476	473
O ₂ dissolved, mg/L	9.8	10.3	11.2	11.2	6.3	7.2	9.3	9.5	7.8	8.1
Chloride, mg/L	42	45	34	35	41	41	35	32	34	32
Sulphates, mg/L	62	65	53	56	65	67	79	80	108	115
Hardness, mg eq./L	5.4	5.2	4.5	4.6	5.8	5.6	5.8	5.7	5.2	5.3
Fe _{total} , mg/L	0.2	0.2	0.2	0.2	0.3	0.3	0.4	0.4	0.4	0.4
Mn, mg/L	0.003	0.003	0.003	0.004	0.004	0.005	0.005	0.005	0.005	0.005
Zn, mg/L	0.0015	0.0015	0.002	0.002	0.009	0.009	0.008	0.008	0.006	0.006
Pb, mg/L	0.02	0.02	0.01	0.01	0.016	0.016	0.017	0.017	0.015	0.014
NH ₄ ⁺ , mg/L	0.054	0.062	0.03	0.031	0.38	0.40	0.022	0.023	0.012	0.010
Cu, mg/L	0.002	0.002	0.001	0.001	0.003	0.003	0.003	0.003	0.003	0.003
Cd, mg/L	traces	traces	traces	traces	0.0001	0.0001	0.0001	0.0001	traces	traces
NO ₂ ⁻ , mg/L	0.01	0.01	0.003	0.004	0.087	0.059	0.007	0.009	0.008	0.008
NO ₃ ⁻ , mg/L	4.94	1.73	4.02	2.25	6.45	1.97	6.85	3.92	6.72	3.74
P _{total} , mg/L	0.03	0.03	0.01	0.032	0.036	0.01	0.014	0.01	0.01	0.01
CBO ₅ , mgO ₂ /L	4.8	4.3	3.2	3.2	6.9	7.3	7.2	7.3	5.5	5.8
CCO _{Cr} , mgO ₂ /L	22.3	22.6	16.7	16.8	54.0	54.2	26.9	27.2	24.2	24.0
Volatile phenols, mg/L	0.002	0.002	0.001	0.001	0.007	0.008	0.005	0.005	0.003	0.003
Petroleum products, mg/L	0.04	0.04	0.04	0.03	0.1	0.2	0.12	0.2	0.04	0.03
Coli Index, mg/L	10 ⁵	10 ⁵	10 ⁴	10 ⁴	10 ⁶	10 ⁶	10 ⁶	10 ⁶	10 ⁵	10 ⁵

Petroleum products entered the river water, in a concentration of 0.04-0.2 mg/L. According to the study carried out at that time, the Prut River water corresponded to the quality class II-III (moderately polluted).

The concentration of mineral components in the aquatic basins and lakes waters in the republic

An important scientific study was also carried out regarding the water quality of the aquatic basins (AB) and lakes in the republic, resulting from the fact that the water was used for different purposes, especially irrigation and fish farming, and some were on the course of the rivers. The renowned scientist, Dr. Valeriu Ropot, evaluated the information on the characteristics (surface, depth, length, width, the volume of water, silty part, etc.) of the aquatic basins of rivers including: Novodnestrovsk, Dubasari (Dniester River), Ghidighici (Bac River), Comrat, Congaz and Taraclia (Ialpug River), Costesti-

Stanca (Prut River), Costesti-Ialoveni, Ulmu and Rezeni (Botna River), Ialoveni (Isnovat River) and Cuciurgan, Cahul, Ialpug and Cuhurlui lakes.

The chemical composition evaluation of the aquatic sources (Table 11) demonstrated high concentrations of Na^+ and SO_4^{2-} ions (AB Ghidighici, Bac River; AB Rezeni, Botna River; AB Comrat, Congaz, Taraclia, Ialpug River; Ialpug and Cuhurlui lakes), Cl^- (AB Comrat, Congaz, Taraclia, Ialpug River; Ialpug lake), dry residue and water hardness (AB Rezeni, Botna River; AB Comrat, Congaz, Taraclia, Ialpug River; Ialpug lake) [5]. The water from these aquatic basins and lakes according to the regulation regarding the environmental quality requirements for surface waters (Republic of Moldova) [12], was classified as polluted-very polluted (quality class IV-V). Moreover, it was determined that the chemical composition in the water basins and lakes water did not differ essentially from that of the rivers that feed them.

Table 11

The average values of the mineral components' concentrations (mg/L) in the Republic of Moldova aquatic basins and lakes, in the year 1987 [5].

<i>Aquatic basins (AB) and lakes</i>	K^+	Na^+	Ca^{2+}	Mg^{2+}	SO_4^{2-}	Cl^-	HCO_3^-	Fe_{total}	NO_3^-	PO_4^{3-}	M^*	H^{**}	pH
AB Novodnestrovsk, Dniester River	8.6	39.4	65.7	13.2	102.6	65.8	132	0.07	2.4	0.08	439	4.7	-
AB Dubasari, Dniester River	11.2	46.3	62.7	16.2	98.6	69.4	197	0.14	2.9	0.11	519	5.0	8.2
AB Costesti-Stanca, Prut River	7.2	37.6	71.2	21.8	118.7	72.0	220	0.12	2.4	0.09	454	5.4	7.8
AB Ghidighici, Bac River	15.0	95.0	57.0	63.0	266.0	85.0	410	0.11	4.5	0.08	764	6.7	8.6
AB Rezeni, Botna River	28.3	138.3	122.4	91.3	426.2	108.7	496	0.07	18.5	0.12	1165	13.7	8.4
AB Ulmu, Botna River	4.8	21.5	63.4	32.5	54.6	36.7	316	0.06	1.3	0.04	320	6.0	7.6
AB Costesti, Botna River	8.9	54.4	42.3	47.3	46.5	51.3	358	0.06	4.8	0.08	447	6.4	8.3
AB Ialoveni, Isnovat River	13.2	58.8	31.7	42.4	34.5	56.3	336	0.06	4.2	0.07	591	5.2	7.2
AB Cuciurgan, Cuciurgan River, alimentation from Turunciuc River	9.7	39.4	64.5	19.7	116.0	78.2	210	0.15	6.2	0.13	565	4.6	8.2
AB Comrat, Ialpug River	22.6	510	56.5	83.3	620.0	398.0	488	0.07	8.7	0.12	2183	9.6	8.6
AB Congaz, Ialpug River	28.4	560	58.4	94.5	580.0	412.0	473	0.08	9.4	0.12	2216	10.8	-
AB Taraclia, Ialpug River	15.3	520.5	64.2	89.8	750.0	463.0	390	0.08	7.5	0.10	2378	10.7	8.1
Lake Cahul	4.6	37.2	57.3	17.9	65.0	56.4	198	0.07	5.8	0.13	457	4.5	8.3
Lake Cuhurlui	7.2	98.7	59.4	31.7	262.0	69.4	210	0.08	6.4	0.16	740	5.7	8.4
Lake Ialpug	9.3	328.0	82.0	88.0	580.0	312.0	230	0.10	6.8	0.15	1650	11.5	8.3

*Mineralization

**Hardness, mg eq./L

Methods developed for water quality control

For the evaluation of the composition of natural and used waters under the leadership of the scientist Ropot Valeriu, a series of methods were developed for determining chemical substances in water: phenol [13], aromatic hydrocarbons [14], nitrates, nitrites, sulphates [15-20], cationic surfactants, *etc.* The nitrate determination method has been patented (USSR Patent, 12.01.1990, No. SU 1638619 [18]). The methods of analysis of the chemical parameters of water were published [19] to ensure chemistry teachers and pupils of higher classes were able carry out hydrochemical assessments.

The main argument for the contribution to the development of the National Strategic Action Program in the field of environmental protection, Chisinau, 1995

The practice accumulated in the field of water quality assessment and protection in the republic laid down the base of the essential contribution granted to the elaboration of the National Strategic Action Program in the field of environmental protection, years 1995-2010-2020, approved by the decree of the President of the Republic of Moldova Mircea Snegur, no. 321 on 6 October 1995. The quality requirements for water use in different fields were specified, including for drinking purposes, agriculture, and animal husbandry, and with specific technical-industrial properties proposed for industry, energy, transport and construction. The Program also mentioned the sources of pollution of natural waters and industrial sources of wastewaters existing in 1995 [21].

Proposals to be introduced in the National Strategic Action Program in the field of environmental protection:

Sources of water pollution

- 3.3.49. In the Republic of Moldova, as in other countries, the hydrographic network is a receiver for the discharge and use of water in different branches of the national economy. In the year 1994, approx. 350 mln m³ of wastewaters were released into the hydrographic network, including 182 mln m³ treated at the treatment stations according to normative documents existing at that time, 160 mln m³ insufficiently treated and 8 mln m³ without being subjected to any treatment, with increased content of pollutants.

- 3.3.54. A particular danger for the environment is presented by the sludge resulting from biological urban wastewaters treatment systems. In the year 1995, the sludge was placed

on special drying grounds. Thus, it is necessary to apply advanced methods - pressure filters, anaerobic fermentation with biogas production, *etc.*

Industrial wastewater sources

- 3.3.55. In the Republic of Moldova, industrial wastewaters, according to the chemical composition and degree of pollution, are very diverse. Waters with a predominant content of mineral salts of various metals, including heavy metals, come from the electronic and electro-technical industry, machines construction, equipment and materials production. The most dangerous for the environment are the waters used in the metal pickling and galvanizing processes; these contain heavy metals, have a strongly acidic or basic environment and cannot be discharged into sewage systems without being subjected to local purification. Non-ferrous metals can be recovered from these waters through various advanced methods, such as adsorption methods with ion exchangers, *etc.*

- 3.3.56. Wastewaters from the food industry, furniture, leather factories, textile industry, plastics' processing, *etc.*, contain many organic pollutants. Sometimes these contain substances that are quite toxic and "hard" biodegradable in the environment, such as polyphenols, organic acids, aldehydes, organic solvents, *etc.*, which need to be removed at local treatment installations, by oxidation, adsorption, *etc.* Only after this stage, wastewaters can be discharged into the sewage system and subsequently treated/cleaned along with household water in the urban biological purification systems.

- 3.3.57. In the future, it is indispensable to introduce efficient local wastewater treatment systems in the industry, which, combined with the municipal treatment systems, allow the use of dangerous substances and the reuse of water after treatment in closed circuits.

The contribution of the scientist Dr. Valeriu Ropot to the development of the National Strategic Program of Actions in the Field of Environmental Protection (1995) laid the base of the environmental policy in the stage of transition to the market economy, which was laid down in the Conception of the Environmental Policy of the Republic of Moldova, compartment "Protection and use of natural resources". The need and objectives of the Environmental Policy Concept of the Republic of Moldova was approved by Parliament Decision no. 605 on 02.11.2001 [22].

Table 12

Dynamic of chemical parameters and their concentration values in the Dniester River water (Republic of Moldova territory) [5].

Parameters	Sampling sections									
	Otaci		Vadul lui Voda		Bender		Slobozia		Olanesti	
	I	II	I	II	I	II	I	II	I	II
Mineralization, mg/L	540	480	650	500	730	530	760	560	820	600
Oxidability, mgO ₂ /L	30	12	40	13	45	14	54	16	60	18
pH, un.	8.0	7.6	8.1	7.7	8.2	7.8	8.3	7.8	8.4	7.9
Hardness, mg eq. /L	7.8	4.4	8.2	4.5	8.9	4.7	9.8	5.3	10.1	5.8
Ca ²⁺ , mg/L	80	66	86	68	92	74	97	78	100	82
Mg ²⁺ , mg/L	45	12	48	15	53	16	60	18	63	20
Na ⁺ , mg/L	70	46	78	50	84	55	86	60	88	64
K ⁺ , mg/L	20	12	22	14	23.5	16	24.5	20	26	22
SO ₄ ²⁻ , mg/L	130	75	136	80	141	84	157	90	164	94
Cl ⁻ , mg/L	160	36	165	45	170	48	183	52	190	58
P _{total} , mg/L	0.5	0.5	0.6	0.6	0.7	0.7	0.8	0.8	0.8	0.8
NO ₃ ⁻ , mg/L	10	10	12	12	15	15	18	18	20	20
Petroleum products, mg/L	0.04	0.04	0.05	0.03	0.05	0.04	0.05	0.05	0.06	0.06
Surfactants, mg/L	0.3	0.2	0.34	0.2	0.36	0.2	0.37	0.2	0.45	0.2

I – treatment of wastewaters and its discharge into natural aquifers;

II – implementation of efficient wastewaters treatment systems to ensure their reuse.

Evaluating the existing statistics regarding the hydrochemical and development information of the national economy, Dr. Ropot Valeriu conducted a study of the dynamics of chemical parameters in the Dniester River water on the Republic of Moldova territory in two versions:

I – treatment of wastewater and its discharge into natural aquifers;

II – implementation of efficient wastewater treatment systems to ensure their reuse.

As a result of the calculations, at the beginning of the 21st century, the composition of the water on different sections of the Dniester River has been predicted, the information is presented in Table 12 [5].

The concentration of biogenic elements (P_{total} and NO₃⁻) and petroleum products was expected to be approximately the same in both versions due to their presence in the rainwater entering in the rivers. It has been demonstrated that through the implementation of efficient wastewater treatment systems to ensure their reuse, the content value of most hydrochemical indices decreases, according to the proposal 3.3.57 from the National Strategic Action Program in the field of environmental protection, 1995 (in the future it is absolutely indispensable the introduction of effective local treatment systems for wastewaters of industrial sources, which along with the treatment systems, allow the use of dangerous substances and the reuse of treated water in closed circuits).

Biography of doctor of chemistry Valeriu Ropot

Valeriu Ropot was born on 7 November 1934 in Viisoara village, Hotin County, Romania. After graduating from the Faculty of Chemistry at the Moldova State University in 1957, he engaged in scientific research at the Institute of Chemistry of the Academy of Sciences of Moldova. Between 1960 and 1963, he completed his doctoral studies in the Laboratory of Analytical Chemistry, under the guidance of academician of Academy of Sciences of Moldova, Iurie Lealikov. He brilliantly defended his doctoral thesis in chemistry, titled “Variation of current intensity as a function of time in polarography and analytical applications” in 1968.



Doctor of chemistry Valeriu Ropot
(07.11.1934 - 05.03.2002)

Between 1964 and 1972 he worked as Scientific Secretary of the Institute of Chemistry of the Academy of Sciences of Moldova.

In 1972, doctor of chemistry Valeriu Ropot founded the Laboratory of Mineral Resources and Chemistry of Water within the Institute of Chemistry of the Academy of Sciences of Moldova. Later, in 1992, due to the need to solve environmental problems, which were intensifying in the world, including in Bessarabia, the laboratory was re-profiled as the Ecological Chemistry Laboratory. The main scientific objectives of the laboratory were aimed at researching and establishing the laws of formation of quality of surface and underground waters, highlighting the processes and mechanisms of transformation, immobilization of natural and anthropogenic pollutants in aquatic systems on carbonic and mineral adsorbents, the full utilization of secondary agricultural products to obtain new carbon catalysts and pharmaceutical products, *etc.* Dr. Valeriu Ropot paid special attention to the development of high-performance technologies for potabilization of surface and underground water, as well as technologies of treatment of wastewaters from various economic units in the Republic of Moldova.

Purification technologies of water from Dniester and Prut Rivers have been improved; many wastewater treatment processes from economic units of the agro-industrial complex, and units with galvanic processes, *etc.* have been implemented. The scientific research carried out by Dr. Valeriu Ropot allowed the application of methods to reduce the content of fluorine, iron, ammonium and sulphide ions in underground waters.

The scientific results are reflected in over 300 published works, including 3 monographs and 25 patents, *etc.* Under the leadership of Valeriu Ropot, a scientific school of hydrochemistry was formed in the Republic of Moldova, known far beyond its borders. He was an erudite supervisor for his disciples. In 1996, together with his 4 disciples, he was awarded the State Prize of the Republic of Moldova in the field of science, technology and production for a series of works in the field of natural water purification and wastewater purification technologies. For his outstanding scientific achievements, Dr. Valeriu Ropot was decorated with the "Civic Merit" medal and the "Glory of Work" Order; he was awarded the title "Emeritus Man and Emeritus Worker in the Protection of Nature".

Dr. Valeriu Ropot organized six expeditions to Dniester River from the source to the Black Sea, and to the Prut River starting from the Goverla Mountain to the Giurgiulesti commune. Moreover, he coordinated several international scientific events dedicated to water protection. The last international practical scientific seminar, held in the fall of 2001 with the title "Water resources management in the conditions of a vulnerable environment", which was organized by Dr. Valeriu Ropot with the financial support of the National Commission of the Republic of Moldova for UNESCO, is kept in our memory to date.

Conclusions

The results of the innovative, managerial and research activity of Valeriu Ropot, doctor of chemical sciences, talented chemist and renowned ecologist culminated into a great contribution to the environmental chemistry in Republic of Moldova and beyond its borders.

Under his guidance have been established the laws regarding the formation of surface and underground water quality, highlighting the processes and mechanisms of transformation, immobilization of natural and anthropogenic pollutants in aquatic systems on carbonic and mineral adsorbents.

The improvement of water purification technologies from the Dniester and Prut Rivers was achieved, as well as some practical recommendations were given regarding the removal of fluoride, iron, ammonium and sulphide ions from groundwaters.

Treatment procedures of wastewaters from economic units in the agro-industrial complex, units with galvanic processes, *etc.* were developed and implemented.

Argumentation of the practical recommendations helped to reduce the negative impact of the discharge of hundreds of thousands tons of brine into the Dniester River resulted from the accident at the mineral fertilizer plant in the city of Stebnik, Ukraine.

Methods for determining organic and inorganic pollutants in natural waters were developed.

Dr. Valeriu Ropot had essential contributions to the elaboration of the National Strategic Action Program in the field of environmental protection for the years 1995-2010-2020, approved by the decree of the President of Republic of Moldova Mircea Snegur no. 321 of October 6, 1995.

Acknowledgements

This work was prepared with the financial support of the national project "The reduction of the environmental and health impact of toxic chemicals through use of adsorbents and catalysts obtained from local raw material" DISTOX, No. 20.80009.7007.21.

References

1. Ropot, V.M. Problems of quality, use and protection of the Dniester River water resources. Chisinau, 1992, 49 p. (in Russian).
2. USSR State Standard, GOST 2874-82, Drinking Water. Moscow, 1984, 239 p. (in Russian). https://standartgost.ru/0/299-pitevaya_voda
3. Lupascu, T.; Sandu, M.; Nicolau, M.; Rusu, V.; Ropot, V.; Kerdivarenko, M. The current state of the Dniester River water quality and improvement of the technology of its purification for drinking needs. Collection of scientific articles "Water and health", Odessa, 2001, pp. 136-139. (in Russian).
4. Lupascu, T.; Ropot, V.; Nicolau, M.; Ballo, A.; Cosma, C. Studies of processes of the Dniester River water treatment for its utilization for drinking. The International Ecological Seminar Lviv – Vadul lui Voda "Tiras-96", 9-23 september, Chisinau, 1996, pp. 19-27. (in Romanian).
5. Ropot, V.; Stratulat, G.; Sandu, M.; Lupascu, T.; Rusu V.; Ciobanu M.; Dranca I.; Lozan, R.; Rusu, V. C.; Botan, V.; Shafranschii, V.; Vavelischii, M. Problems of quality, use and protection of water resources in the SSRM. Chisinau: Stiinta, 1991, 285 p. ISBN 5-376-01191-7. (in Russian).
6. Ropot, V. Dniester River pollution with toxically waste as a result of the accident at potassium fertilizers factory. The materials of the international ecological seminar "Tiras-96", Chisinau, 9-23 septembrie, 1996, pp. 3-12.
7. Ropot, V.; Sandu, M.; Lozan, R. The impact of Novodnestrivsc (Ukraine) hydro energetic complex concerning Dniester River water quality downstream the Republic of Moldova. 12-th Romanian International Conference on Chemistry and Chemical Engineering RICCE-12, Romania, Bucharest, September, 13-15, 2001, pp. 148-152.
8. Ropot, V.; Lozan, R.; Sandu, M.; Dumbraveanu, A. Studies and practical communications regarding the management of water resources under the conditions of a vulnerable environment. Chisinau, Universul, 2002, 205 p. (in Romanian).
9. Ropot, V.; Nicolau, M.; Curcaneanu, N.; Lozan, R.; Iliescu Ș.; Lupașcu, T.; Drancă, I.; Negru, M. Study on the Prut River water quality. *Bulletin of the Academy of Sciences of Moldova, Biological and Chemical Sciences*, 1994, 6, pp. 41-46. (in Romanian). <http://www.bsl.asm.md/archive>
10. Lupascu, T.; Sandu, M.; Rusu, V.; Ropot, V.; Revenco, M.; Kerdivarenko, M. The current state of water quality in the Prut River. Collection of scientific articles "Water and health", Odessa, 2001, pp. 132-136. (in Russian).
11. Ropot, V.; Sandu, M.; Revenco, M.; Mereanu, V.; Lupascu, T.; Rusu, V. Aspects regarding the current water quality of the Prut River. *Hydrotechnic Journal*, 2002, 47(2), pp. 34-38. (in Romanian). <https://rowater.ro/documente-de-interes-public/revista-hidrotehnica/>
12. Decision of Republic of Moldova Government no. 890 of 12.11.2013 for approving the Regulation regarding the environmental quality requirements for surface waters. Official Monitor no. 262-267 of 22.11.2013, art. no. 1006. (in Romanian). https://www.legis.md/cautare/getResults?doc_id=114535&lang=ro
13. Ropot, V.; Pinkas, M.; Lozan, R. Spectrophotometer determination of phenol in natural and wastewaters. The Republican Conference „Application of advanced methods and equipment for water treatment and drainless technology in the production of VPTIEMP”, Chisinau, 5-6 October, 1982, pp. 373. (in Russian).
14. Ropot, V.; Pinkas, M.; Lozan, R. Spectrophotometer determination of some aromatic hydrocarbons using DMAA. *Bulletin of the Academy of Sciences of Moldova, Biological and Chemical Sciences*, 1984, 6, pp. 74. (in Russian). <http://www.bsl.asm.md/archive?language=en-gb>
15. Lozan, R.; Ropot, V.; Sandu, M. Determination of nitrates and nitrites in natural waters. *Chemistry and water technology*, 1989, 11(2), pp. 120-122. (in Russian). <https://link.springer.com/journal/11962/volumes-and-issues>
16. Ropot, V.; Sandu, M.; Lozan, R. Determination of nitrate ions in natural waters. The XI National Conference of Analytical Chemistry, 24-25 September, 1992, Cluj-Napoca, pp. 78. (in Romanian).
17. Sandu, M.; Lozan, R.; Ropot, V. Determination of sulfates, nitrates and nitrites in galvanic wastewater. Republican Conference Waste-free technology, Chisinau, 1990, pp. 108-109. (in Russian).
18. Lozan, R.; Sandu, M.; Ropot, V. A method for determining nitrates. USSR Patent, 1990, No. SU 1638619 A1. (in Russian). <https://patents.su/3-1638619-sposob-opredeleniya-nitrat-ionov.html>
19. Sandu, M.; Lozan, R.; Ropot, V. Methods and instructions for water quality control. Chisinau, 1992, 160 p. ISBN 5-376-01636-1. (in Romanian).
20. Ropot, V.; Lozan, R.; Sandu, M. On the issue of the nitrates determining in natural waters. Materials of the XV Mendeleev Congress on General and Applied Chemistry, Minsk, 1993, pp. 156-157. (in Russian).
21. Ropot, V.; Sandu, M. Water quality. National Strategic Action Program in the field of environmental protection. Chisinau, 1995, pp. 18-24. (in Romanian).
22. Decision of the Parliament of the Republic of Moldova, no. 605 of 02.11.2001 regarding the approval of the Environmental Policy Concept of

the Republic of Moldova. Official Monitor no. 9-10 of 15.01.2002, art. 20. (in Romanian).
https://www.legis.md/cautare/getResults?doc_id=58192&lang=ro

Short biography of the authors



Maria Sandu, doctor of chemistry, is the associate researcher of the Laboratory of Natural and Anthropogenic Ecosystems of the Institute of Ecology and Geography, Republic of Moldova. She detains expertise in the fields of analytical chemistry, natural water quality and chemistry. Dr. Maria Sandu has a scientific activity of over 50 years, devoted to the assessment of the state of surface waters in the Republic of Moldova. She developed technologies for water purification and potabilization in Republic of Moldova, possessing invention patents and 465 scientific publications dedicated to natural water problems. In 2013 she was awarded the “Order of Work Glory” and in 2021 the “Order of the Republic” by the decree of the Republic of Moldova President.



Tudor Lupascu, academician, professor, doctor habilitate, head of the scientific Center of Ecological Chemistry and Environmental Protection, at the Institute of Chemistry (Republic of Moldova) is a remarkable personality and notorious scientist, and former director of the Institute of Chemistry (2001-2018), founder of the scientific school of chemistry of adsorbents. Acad. Tudor Lupascu is known to the scientific world due to complex scientific investigations, among which: synthesis of carbonaceous adsorbents with scheduled properties from local raw materials, useful for detoxification of the human body and protection of the environment; elaboration of biologically active substance Enoxil (from tannins) useful for medicine, veterinary and agriculture; new plastering materials for buildings surfaces from local raw materials. The prosperous scientific activity of academician Tudor Lupascu is eloquently described by the great number of scientific works that have exceeded 800. The scientific, innovational and managerial contribution of academician Tudor Lupascu was appreciated at home as well as abroad, being awarded many honorific titles, such as: Emeritus of the Republic of Moldova (2000); State Prize in Science and Technology (1996); Medals “Dimitrie Cantemir” (2010) and “Nicolae Testimitanu” (2010); Knight of the Orders “Labour Glory” (2010); “of the Republic” (2019); “Leonardo da Vinci” (2009); “Aurel Vlaicu” (2011) and “Pro Scientia et innovatio” with the rank of Officer (2019); Award of the Government of the Republic of Moldova “The most gifted inventor of the year” (2019); Gold Medal of OMPI (2009) and many, many others.

FROM (-)-SCLAREOL TO NORLABDANE HETEROCYCLIC HYBRID COMPOUNDS

Alexandru Ciocarlan 

Institute of Chemistry, 3 Academiei str., Chisinau MD 2028, Republic of Moldova
e-mail: algciocarlan@yahoo.com; alexandru.ciocarlan@ichem.md

Abstract. This review relates to the chemistry of the well-known biologically active natural labdane diterpenoid (-)-sclareol easily isolated from Clary sage (*Salvia sclarea* L.). This compound is used in industry, mainly for the synthesis of fragrances and natural analogues. The paper covers achievements reported in the respective publications from 2013 to 2021 on the synthesis, structure determination, and biological activity of molecular hybrid compounds bearing hydrazide and thiosemicarbazone fragments or diazine, 1,2,4-triazole, carbazole, 1,3-thiazole, 1,3,4-oxadiazole, and 1,3,4-thiadiazole units prepared basing on the studied compound.

Keywords: (-)-sclareol, norlabdane-heterocyclic compound, antimicrobial activity, biological activity.

Received: 24 April 2022/ Revised final: 28 September 2022/ Accepted: 04 October 2022

List of abbreviations and notations:

CDI	1,1'-Carbonyldiimidazole
CNBr	Cyanogen bromide
DCC	Dicyclocarbodiimide
DCM	Dichloromethane
DMAA	Dimethylacetamide
DMAP	4-Dimethylaminopyridine
DMF	<i>N,N</i> -Dimethylformamide
Et ₃ N	Triethylamine
EtOH	Ethanol
MCF-7	Breast cancer cells
MeOH	Methanol
MIC	Minimum inhibitory concentration
MW	Microwave irradiation
NMR	Nuclear magnetic resonance
r.t.	Room temperature
R-NCS	Substituted isothiocyanates
SAR	Structure-activity relationship
THF	Tetrahydrofuran
TMTD	Tetramethylthiuram disulfide
XRD	X-ray diffraction

Introduction

Due to its abundance in nature and significant practical importance, the chemistry of (-)-sclareol (**1**) has experienced an impressive development in recent years. The commercial labdane diterpenoid (-)-sclareol (**1**) isolated from Clary sage (*Salvia sclarea* L.) has many areas of industrial usage including food, pharmaceutical, tobacco industry, and perfumery. Based on this compound or some of its dinorlabdane **2-4** and

trinorlabdane **5-7** intermediates (Figure 1), as well as tetranorlabdane **8-10** and pentanorlabdane **11-13** (Figure 2), a great number of synthetic terpenic compounds or natural analogues were obtained. An example of this is the natural ambergris substituent Ambrox®, an important synthetic derivative of (-)-sclareol (**1**) with a pronounced ambergris-type odor. Some other biologically active drimanic sesquiterpenoids synthesized from diol **1** can be mentioned here, such as polygodial, warburganal, pereniporines A and B, and others.

Unlike other classes of compounds, such as alkaloids, terpenes that contain heteroatoms, especially nitrogen, are less numerous and less studied [1]. Urones, J. *et al.* performed one of the first syntheses of C₉ nitrogenated drimanes during the preparation of pereniporin A and 9-*epi*-warburganal [2]. Barrero, A.F. *et al.* reported some nitrogen-containing intermediates obtained during the synthesis of natural 9,11-drimen-8 α -ol from (-)-sclareol (**1**) [3]. A new 11-guanidinodrimene derivative of drimenol with an increased antifungal activity was reported by Zarraga, M. *et al.* [4]. Kuchkova, K.I. *et al.* accomplished the synthesis of 11-aminodrim-7-ene, a nitrogenated analogue of drimenol, from (-)-sclareol (**1**) *via* the corresponding oxime and nitrile [5]. The same authors communicated about a series of oximes, amides, 1,2,6- and 1,3,6-oxazines, *N*-oxide prepared from 11-dihomodriman-8 α -ol-12-one **5**

and 11-dihomodriman-8(9)-en-12-one **6**, two important derivatives of (-)-sclareol (**1**) [6,7]. Later, Kuchkova, K. *et al.* [8,9] described the synthesis of some di- and trinorlabdane isomeric amines *via* corresponding oximes, starting from dinorlabdane **2-4** and trinorlabdane **5-7** ketones, derived from (-)-sclareol (**1**).

In the desire to obtain γ -bicyclohomofarnesal (Ambral), which is the key intermediate in the synthesis of Ambrox® and others terpenes, de la Torre, M.C. *et al.* prepared some nitrogen containing intermediates like Weinreb amides and its unsaturated derivatives from (+)-sclareolide (**8**), one of the most important derivatives of (-)-sclareol (**1**) [10]. A bit later, Boukouvalas, J. *et al.* substantially improved de la Torres's method [10] and performed for the first time the synthesis of the antitumor diterpenoid (+)-zerumin B starting from the same (+)-sclareolide (**8**) [11]. Boukouvalas, J. and Wang, J.-X. reported the Weinreb amide together with an intermediate nitrile after the synthesis and structure revision of a novel labdane diterpenoid ottensinin based on (+)-sclareolide (**8**) [12]. Unlike previous transformations performed in the outside chain, Lungu, L. presented the synthesis of the cycle B C₇ functionalized tetra- and pentanorlabdane oximes and amines based on ketoester **10** and drimenone **12**, well known derivatives of (-)-sclareol (**1**) [13].

In the last decade, the (-)-sclareol (**1**) carbon skeleton has been intensively used for the synthesis of some natural N-containing labdane-type analogues [14]. The biologically active tetracyclic diterpenes 4-methyldecarboxyhaumanamide, 4-methyl decarboxyspongolactames A and C isolated from marine organisms and synthesized by Basabe, P. *et al.* from (-)-sclareol (**1**) belong to this series of nitrogenated spongianes [15].

Some of the authors mentioned above state that the presence of a heteroatom, such as nitrogen, often increases the biological activity of the compounds derived from (-)-sclareol (**1**) or (+)-sclareolide (**8**). An even greater increase can

be expected in the case of terpene compounds that contain heteroatomic fragments or different heterocyclic rings in their molecules. The publications on the synthesis, chemistry, and biological activity of non-terpeneic 1,2-diazines [16,17], 1,3-thiazole [18], 1,3,4-oxadiazole [19], 1,3,4-thiadiazole [19,20], 1,2,4-triazoles [19,21], and benzothiazole [22] are ascending nowadays.

It is well known that some ligands and their metal complexes bearing a thiosemicarbazone fragment show pronounced antibacterial, antifungal, antitumor, and antiviral activities [23,24]. Matesanz, A.I. *et al.* discussed a new family of Pt(II) and Pd(II) *bis*(thiosemicarbazone) compounds incorporating the 2,6-diacetylpyridine heterocyclic ring, which showed a high antiproliferative activity against cisplatin resistant A2780cisR cells and breast (MCF-7) cancer cells [25].

Starting from (-)- α -bisabolol, a series of thiosemicarbazones with high cytotoxicity and selectivity was prepared, and their structure-activity relationship was studied [26]. According to authors, some of thiosemicarbazones obtained from kaurenoic acid showed a significant antitrypanosomal activity [27]. A series of novel thiosemicarbazides, which exhibited considerable inhibitory effects on the growth of a wide range of cancer cell lines, was created by Vandresen, F. *et al.*, whose investigations were based on the natural monoterpene R-(+)-limonene [28].

The purpose of the present review is to discuss the current achievements in the field of the synthesis of hybrid norlabdane compounds containing heteroatomic fragments or heterocyclic rings, the chemistry of which is on the rise.

Background

Key norlabdane intermediates derived from (-)-sclareol

The (-)-sclareol (**1**) derivatives most frequently used for the synthesis of terpeno-heterocyclic hybrid compounds can be divided into several groups according to the number of atoms in their carbon skeletons (Figure 1).

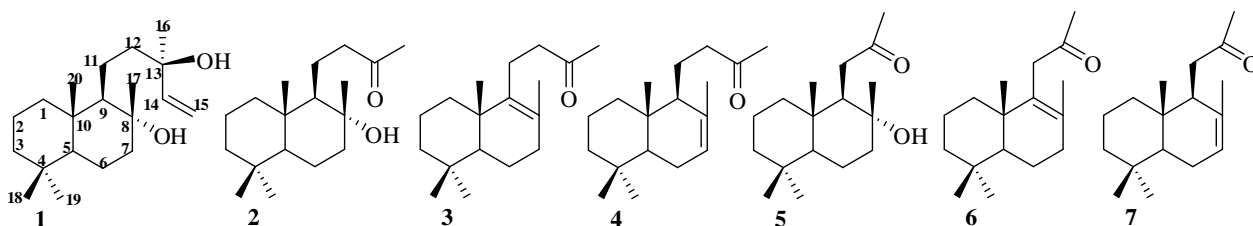


Figure 1. (-)-Sclareol (**1**) and its dinorlabdane **2-4** and trinorlabdane **5-7** derivatives [29,30].

One of the key dinorlabdane intermediate is methyl ketone **2** that can be easily prepared by the oxidative degradation of diol **1** according to [29]. Any further dehydration of compound **2** leads to isomeric ketones **3** and **4** [30] which are, as well, suitable starting materials for the synthesis of the target dinorlabdane heterocyclic hybrid compounds.

The methyl ketone **5** can be considered the head of the trinorlabdane compounds series, and it may be prepared from the commercial available (+)-sclareolide (**8**) according to the known procedure [31]. Its dehydration under the mentioned conditions [30] gives a mixture of chromatographically separable trinorlabdane ketones **6** and **7** in 4:1 ratio. The syntheses of molecular hybrids based on trinorlabdane compounds **5-7** are reported below. Both tetranorlabdane **9, 10** and pentanorlabdane **11-13** precursors depicted in Figure 2 were prepared by the known [32-34] and new [35,36] procedures and used further for the synthesis of the title compounds of these series.

Synthesis of norlabdane heterocyclic hybrid compounds

Among the first reported heterocyclic terpene compounds are those with diazine

units [37,38]. There, the authors used the $\Delta^{8,13}$ -bicyclohomofarnesenic acid **9**, a derivative of (-)-sclareol (**1**) as starting material and applied two synthetic pathways. The first method (method I) included a coupling reaction of chloroanhydride **14** obtained *in situ* from acid **9** with amines, such as 4-aminopyrimidine **15a**, 3-aminopyrazine **15b**, and 2-aminopyrimidine **15c**, under presented conditions (Scheme 1). As a result, amides **16a** and **16b** were obtained in 60% and 15% yields, respectively, and amide **16c** (16%) was isolated from the reaction mixture together with the major *bis*-acylamide **17** (54%).

Kuchkova *et al.* reported attempts to increase the reaction yields and selectivity and to prove that a *bis*-acylation reaction of 2-aminopyrimidine **15c** occurs under any condition [37,38]. The direct one-step acylations of aminodiazines **15a-c** with acid **9** in the presence of dicyclocarbodiimide (DCC) and 4-dimethylaminopyridine (DMAP) (Method II) were performed for that purpose (Scheme 1). As a result, amides **16a,b** were obtained in 53% and 52% yields, respectively, and in both cases, bicyclohomofarneseno-*N,N'*-dicyclohexylurea **19** was also formed (20% and 17%, respectively).

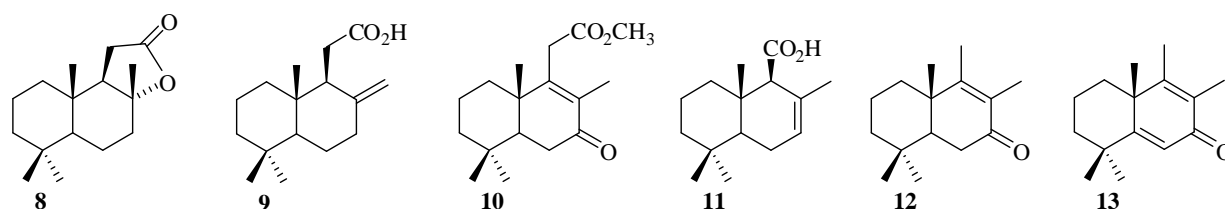
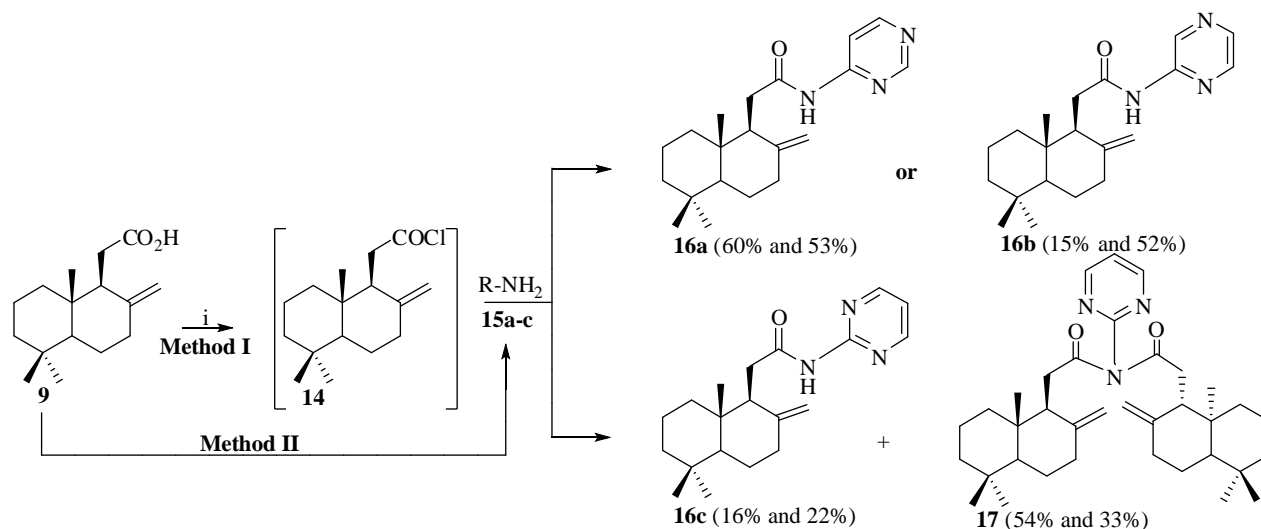


Figure 2. Tetranorlabdane **8-10** and pentanorlabdane **11-13** compounds [32-36].



Reagents and conditions: Method I: (i) $(\text{COCl})_2$, C_6H_6 , r.t. 1 h, Δ 1 h; (ii) R-NH_2 , DCM, Δ 2–15 h.

Method II: (i) R-NH_2 , DCC, DMAP, DCM, Δ , 5–28 h.

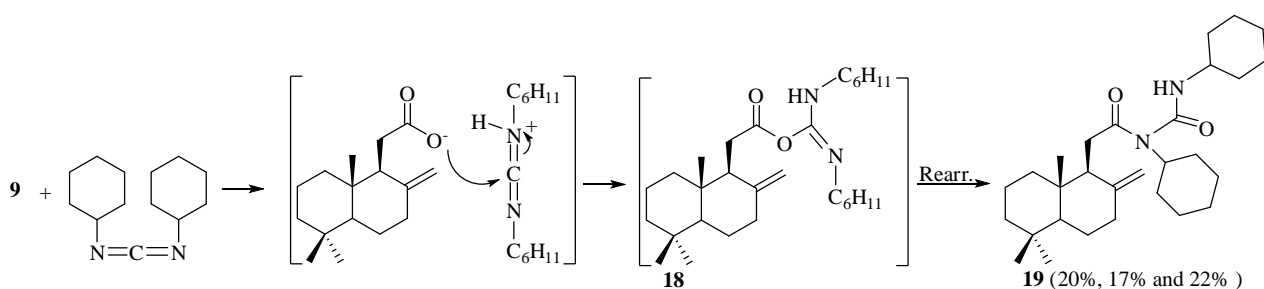
Scheme 1. Synthesis of diazines **16a-c** and **17** from $\Delta^{8,13}$ -bicyclohomofarnesenoic acid **9** [37,38].

From the reaction product of the interaction of acid **9** with 2-aminopyrimidine **15c**, together with amide **16c** (22%) and substituted urea **19** (22%), also *bis*-acylamide **17** was isolated in 33% yield. Based on the data obtained, those authors concluded that method I was more efficient in terms of yields and selectivity.

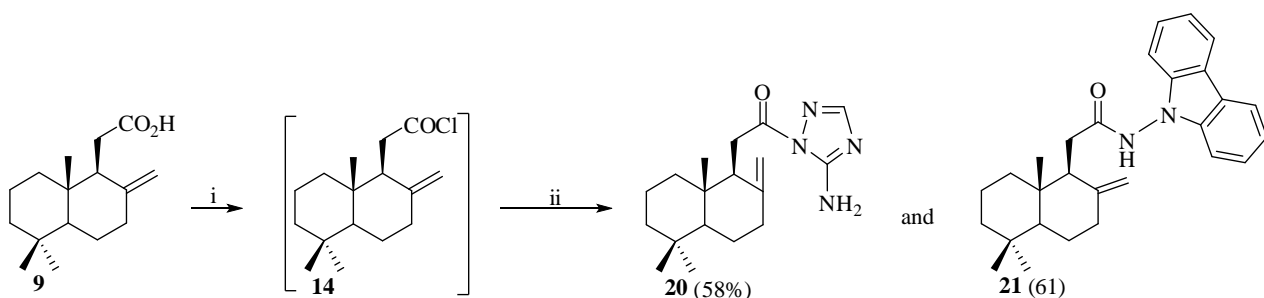
The proposed mechanism of compound **19** formation includes the protonation of a nitrogen atom from DCC, followed by a nucleophilic attack of a carboxyl ion, which leads to the intermediate **18** [38]. Its interaction with amines **15a-c** gives amides **16a-c** and *bis*-acylamide **17**, that fact being confirmed by the *N,N'*-dicyclohexylurea formation as by-product (Scheme 2). On the other hand, the rearrangement of intermediate **18** produces substituted urea **19**. The structures of the synthesized compounds were fully confirmed by the spectral methods and for *bis*-acylamide **17**, X-ray diffraction (XRD) was also performed.

In continuation, acid **9** was used for the synthesis of tetranorlabdane hybrids bearing 1,2,4-triazol and *N*-aminocarbazole units according to Scheme 3 and following the same method I applied in the synthesis of diazines [37,38]. As described above, acid **9** was converted into chloroanhydride **14** that interacted with 3-amino-1,2,4-triazole (amine 1) and *N*-aminocarbazole (amine 2) [39]. As a result of those transformations, hybrid compounds **20** and **21** containing substituted 1,2,4-triazole or *N*-aminocarbazole units, respectively, were obtained in 58% and 61% yields, and their structures were confirmed by both spectral methods and XRD.

Similar series of molecular hybrids containing diazine, 3-amino-1,2,4-triazole and *N*-aminocarbazole units were prepared by Aricu, A. *et al.* based on homodrimane acid **22** obtained earlier in five steps from (+)-sclareolide (**8**) [40] *via* its chloroanhydride **23** (Figure 3).



Scheme 2. Mechanism of formation of bicyclohomofarnezenoyl-*N,N'*-dicyclohexylurea **19** [37,38].



Reagents and conditions: (i) (COCl)₂, C₆H₆, r.t. 1 h, Δ 1 h; (ii) Amine I or II, DCM, r.t. 2 h and 10 h.

Scheme 3. Synthesis of tetranorlabdanes bearing 3-amino-1,2,4-triazole and *N*-aminocarbazole units [39].

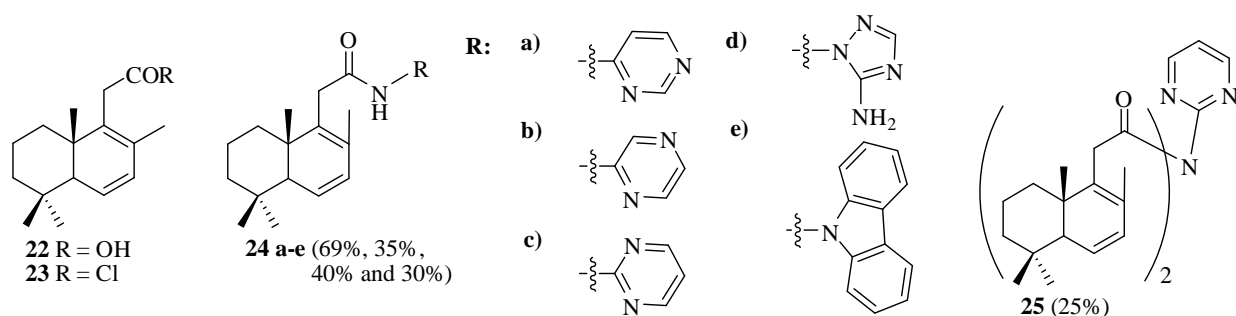


Figure 3. Hybrid homodrimane sesquiterpens **24a-e** and **25** derived from 11-homodrim-6,8-dien-12-oic acid **22** [40].

The same conditions as in Scheme 3 were applied in order to obtain, monoamides **24a-e** in 69%, 35%, 40%, 30%, and 40% yields, respectively. The *bis*-acylamide **25** was isolated from the reaction mixture in 25% yield together with diazine **24c**, thus confirming the hypothesis mentioned above.

Based on drimenic acid **11** and following the same chemical procedures, the syntheses of a series of pentanorlabdane heterocyclic compounds were described (Figure 4) [41]. The coupling reaction of chloroanhydride obtained *in situ* with 2-aminopyrimidine **15a**, 2-aminopyrazine **15b**, and 4-aminopyrimidine **15c** gave corresponding amides **26a-c** in 29%, 14%, and 11% yields, respectively, as well as amide **27c** (17%). Further interactions with *N*-aminocarbazol and 3-amino-1,2,4-triazole completed this series with amides **28e** and **29d**, obtained in 49% and 53% yields, respectively. Contrary to expectations, only the amides of the isodrimenic $\Delta^{8,9}$ **26a-c**, **28e**, and albicanic $\Delta^{8,12}$ **27c**, **29d** acids, as isomers of drimenic acid **11**, were obtained. This can be explained by the isomerization of the $C_{7,8}$ double bond in the tetrasubstituted and *exocyclic* ones upon interaction with oxalyl chloride. The structures of reported pentanorlabdane hybrid compounds containing diazine, 3-amino-1,2,4-triazole, and *N*-aminocarbazol units were fully

confirmed by the spectral data, and that of compound **28e** – by the crystallographic analysis.

Recently, a moderate number of publications devoted to the isolation or synthesis of tetranorlabdane compounds have appeared, and only in one of them, a tetranorlabdane pyridazinone hybrid **31** was reported [42]. The treatment of allyl bromide **30** derived from ketoester **10** with 6-(*p*-tolyl)-3(2*H*)-pyridazinone led to the desired hybrid compound **31** in 75% yield (Scheme 4). Contrary to that, the treatment of bromide **30** with 6-(*p*-tolyl)-4,5-dihydro-3(2*H*)-pyridazinone gave dimer **32** in 70% yield (Scheme 4), which can be explained by the different reactivity of (1,2)-diazines N-H bonds.

An attempt to substitute a bromine atom from a molecule of **30** by an acetoxy group gave the tetranorlabdane dimer **33** with an unprecedented carbon skeleton as the major product (86%) and acetate **36** (14%, route I) as the minor one. The mechanism of dimer **33** formation was also reported, where dimer **32** was described as an intermediate (Scheme 5). It involved the formation of some intermediates like carbocation **34** (route II), which, by a subsequent rearrangement of dienes and zwitterions **35a,b**, and **37**, and intermediate dimer **32**, gave dimer **33**. The structures of dimers **32** and **33** were proved by both spectroscopic and single-crystal XRD.

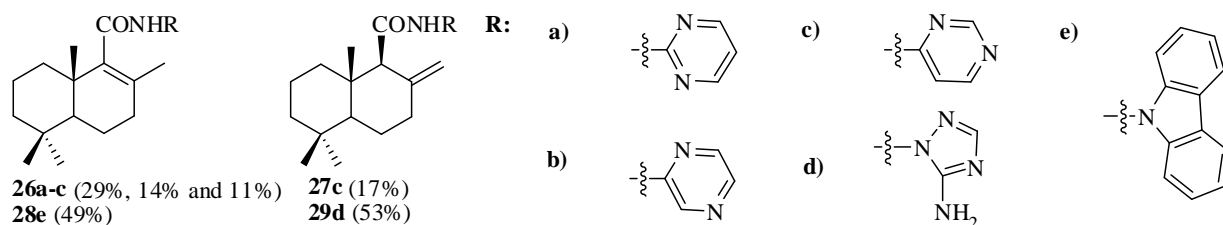
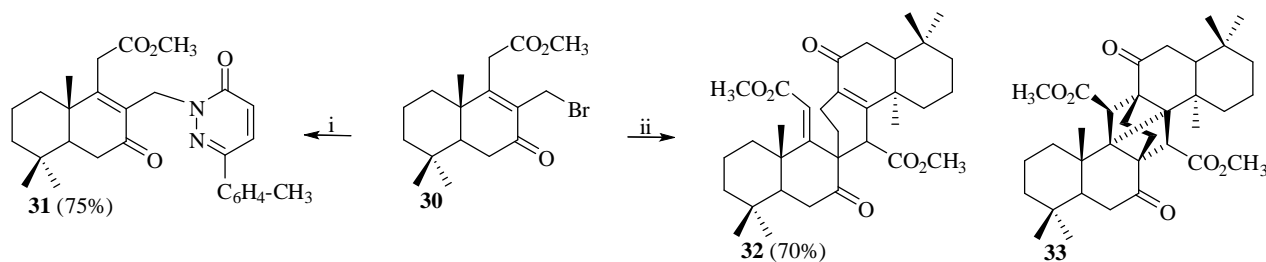


Figure 4. Syntheses of pentanorlabdane diazines **26a-c**, **27c**, carbazole **28e**, and 1,2,4-triazole **29d** [41].

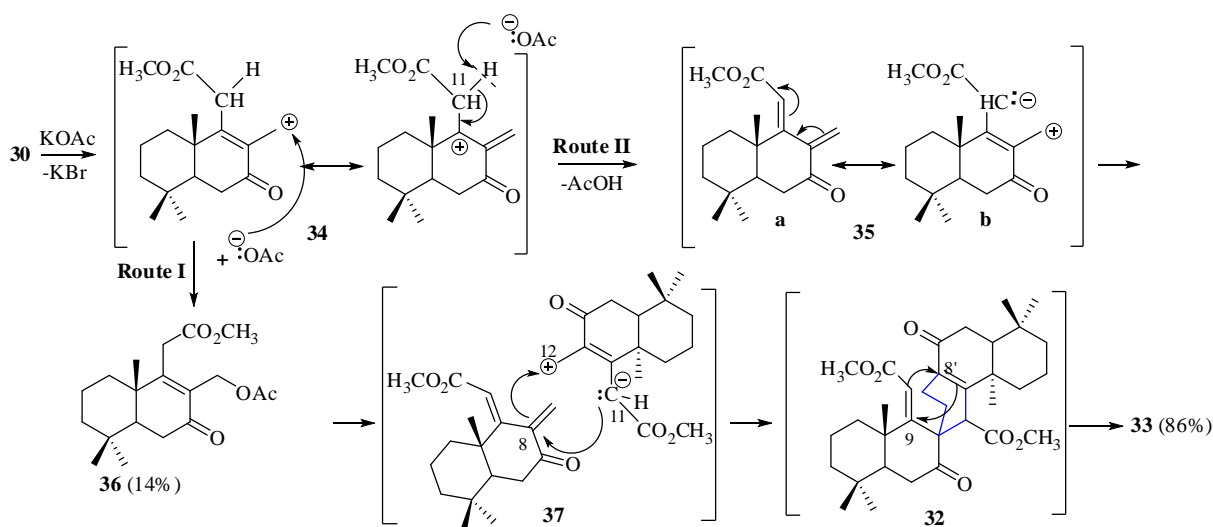


Reagents and conditions: (i) 6-(*p*-Tolyl)-3(2*H*)-pyridazinone, K_2CO_3 , DMAA, r.t., 48 h;
(ii) 6-(*p*-Tolyl)-4,5-dihydro-3(2*H*)-pyridazinone, K_2CO_3 , DMAA, r.t., 48 h.

Scheme 4. Synthesis of tetranorlabdane pyridazinone **31** and dimers **32**, **33** [42].

The monobrominated **38**, **39** and **41**, **42** and dibrominated derivatives **40** and **43** were prepared earlier from drimenone **12** and drimdienone **13** [34,43]. Those derivatives proved to be suitable intermediates for the synthesis of hybrid pentanorlabdane-pyridazinone compounds. By coupling the mentioned bromides with 6-(*p*-tolyl)-3(2*H*)-pyridazinone, Aricu, A. *et al.* [35] performed the synthesis of individual monosubstituted **44**, **45** and disubstituted **46**, **47** hybrid compounds by classical (3–24 h) and microwave assisted (20 min–1.5 h) methods in good and comparable yields (34–84%), as depicted in Figure 5. The structure of hybrid compound **47** was confirmed additionally by single-crystal XRD.

D'Ambrosio M. *et al.* continued the investigations in order to obtain new tetranorlabdane compounds bearing the hydrazinecarbothioamide fragment or the 1,2,3-triazole unit [44]. Unlike previous syntheses, commercially available (+)-sclareolide (**8**) was chosen as starting material, which was transformed into corresponding hydrazide **48** via the known procedure [45]. The latter, after treatment with substituted isothiocyanates at room temperature (4.5–5 h), generated corresponding hydrazinecarbothioamides **49a–d** (Scheme 6, method I). The same transformations were performed under MW-irradiation (5 min), resulting in higher yields (Scheme 6, method II).



Scheme 5. Mechanism of formation of tetranorlabdane dimer **33** [42].

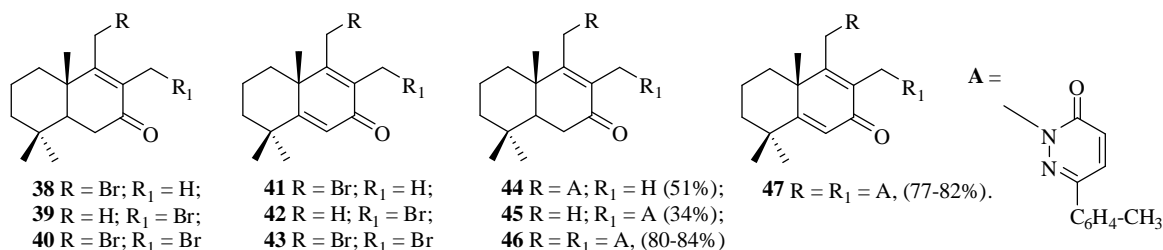
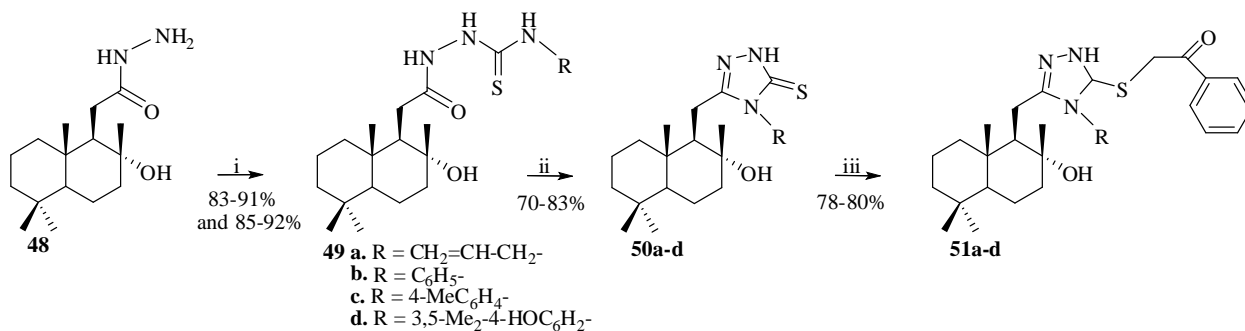


Figure 5. Synthesis of pentanorlabdane compounds with pyridazinone unit **44–47** [34,35,43].



Reagents and conditions: (i) Method I: RNCS, EtOH, r.t., 4.5–5 h; Method II: RNCS, EtOH, MW, 200 W, 5 min; (ii) NaOH, H₂O, 70°C, 2–3 h; (iii) Et₃N, Me₂CO, r.t., 2–3 h.

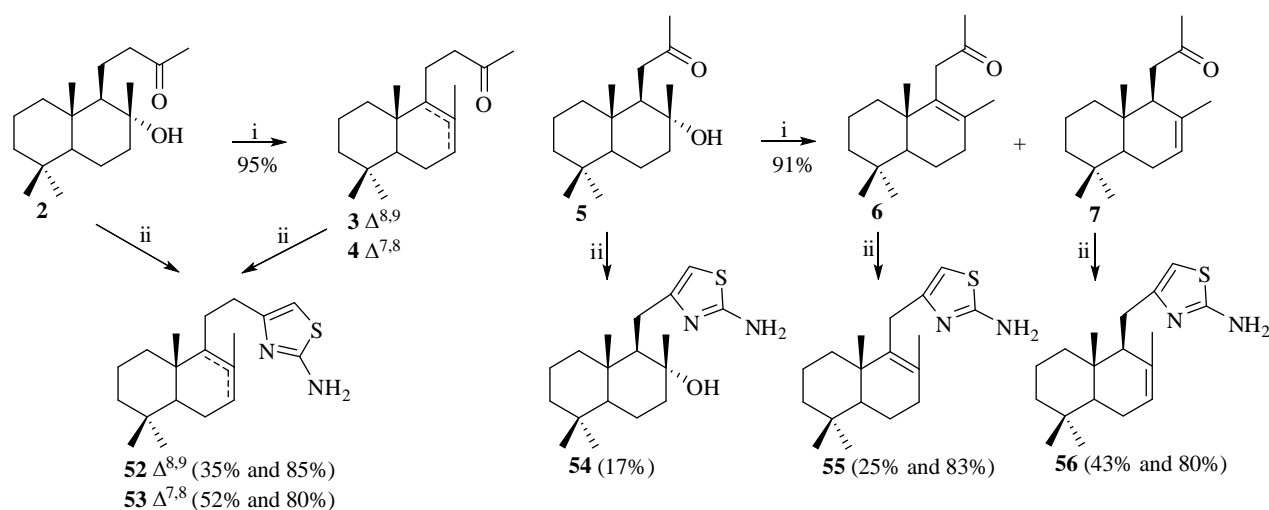
Scheme 6. Synthesis of tetranorlabdanes with hydrazinecarbothioamide fragment and substituted 1,2,4-triazole units [44].

The heterocyclization of compounds **49a-d** under alkaline aqueous solution conditions lead to *N*-substituted 1,2,4-triazoles **50a-d** which were easily alkylated with 2-bromoacetophenone giving *S*-substituted 1,2,4-triazoles **51a-d**. The structures of compounds **50c** and **51d** were confirmed by XRD.

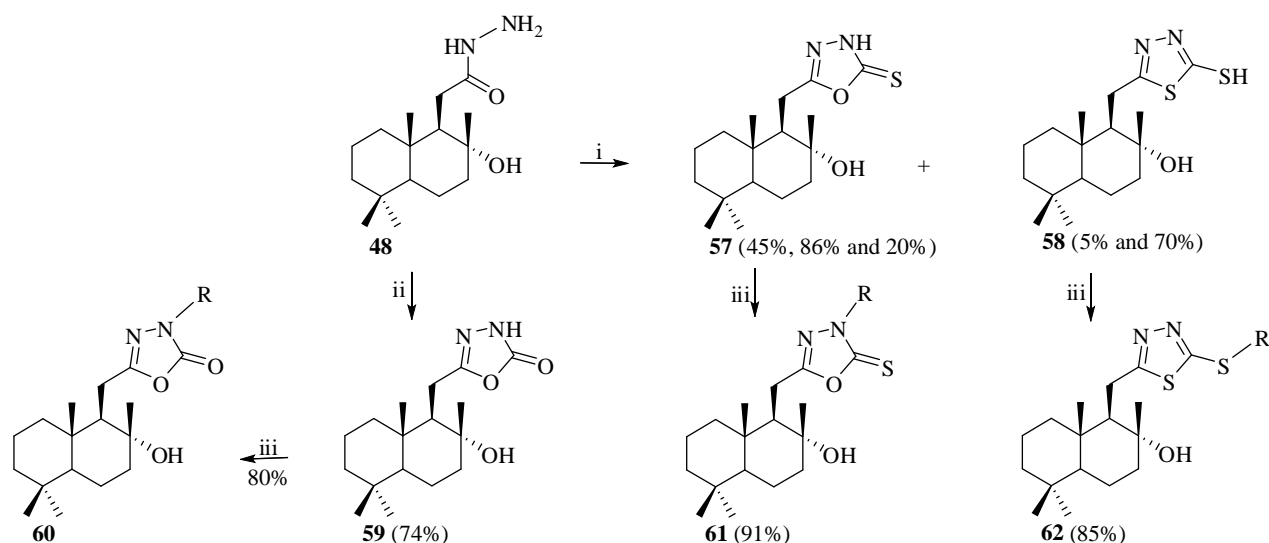
The synthesis of di- and trinorlabdane hybrids bearing a 2-amino-1,3-thiazole unit was reported by Blaja, S. [46]. The first series was obtained starting from hydroxyketone **2** which could be obtained directly by oxidation of (-)-sclareol (**1**) [29] and the second ketone **5** from (+)-sclareolide (**8**) [30]. The dehydration of ketones **2** and **5** after treatment with trimethylsilylmethanesulphonate led to chromatographically separable mixtures of ketones **3**, **4**, **6**, and **7** (Scheme 7). The standard conditions were used for individual

condensation-cyclization of ketones **3-7** [47] with thiourea and iodine in ethanol, thus giving dinorlabdane **52**, **53** and trinorlabdane **54-56** compounds bearing 2-amino-1,3-thiazoles units. Unfortunately, hydroxyketone **2**, under those conditions, suffered a dehydration favoured by iodine and formed only a mixture of compounds **3** and **4**.

Hydrazine **48** was used again for the synthesis of new tetranorlabdane compounds bearing 1,3,4-oxadiazole and 1,3,4-thiadiazole [48]. The reaction equilibrium of the compound **57** (45%→86%→20%) formation can be shifted to that of compound **58** (5%→70%) by the treatment of hydrazide **48** with an increasing amount of TMTD, 0.5→1.5 equivalents. The interaction of hydrazine **48** with CDI under the depicted condition (Scheme 8) [49] gave oxadiazole **59** in 74% yield.



Reagents and conditions: (i) $\text{MeSO}_3\text{SiMe}_3$, MeCN, r.t. 15 min; (ii) $\text{SC}(\text{NH}_2)_2$, I₂, EtOH, 12 h, Δ .
Scheme 7. Synthesis of di- and trinorlabdane compounds with 2-amino-1,3-thiazole unit [46].



Reagents and conditions: (i) TMTD, DMF, 90°C, 1.5 h; (ii) CDI, Et₃O, THF, 0°C, 3 h; (iii) RBr, Et₃N, Me₂CO, r.t., 3 h.
Scheme 8. Synthesis of tetranorlabdane 1,3,4-oxadiazole and 1,3,4-thiadiazole [48].

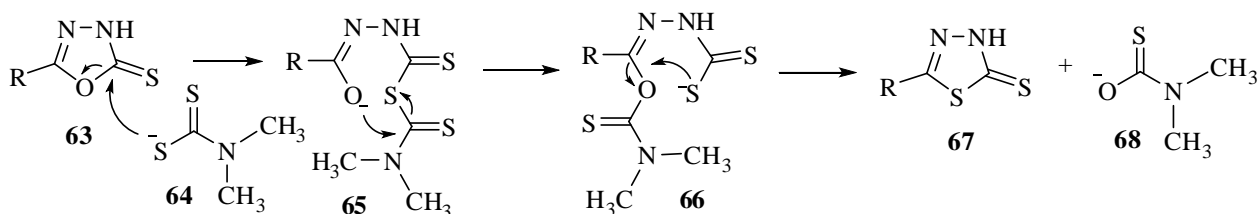
In continuation, hybrid compounds **57-59** were alkylated with bromoacetophenone ($R = -CH_2-C_6H_5$) under specified conditions yielding derivatives **60** (80%), **61** (91%), and **62** (85%). In addition to spectral data, the structures of oxadiazole **57** and thiadiazole **62** were confirmed by single-crystal XRD.

Boscheli, D.H. *et al.* mentioned that formation of thiadiazole **58** was surprising, still they presented the mechanism of oxadiazole cycle **63** conversion into thiadiazole cycle **67** (Scheme 9) [49]. As a result of acetohydrazide **48** interaction with TMTD, the *N,N*-dimethyldithiocarbamate ion **64** was formed. That ion attacks the oxadiazole cycle **63** causing its opening, and then two nucleophilic attacks follow in intermediates **65** and **66**, which leads to the formation of thiadiazole cycle **67** by elimination of the *N,N*-dimethylthiocarbamate ion **68**.

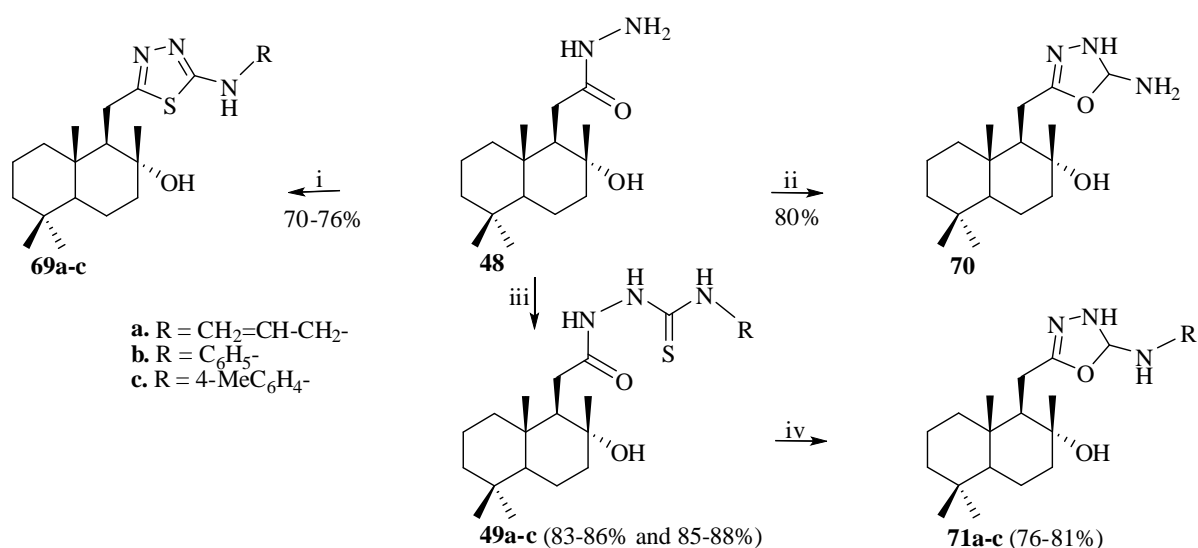
The syntheses of tetranorlabdane 2-aminosubstituted 1,3,4-thiadiazoles **69a-c** and 1,3,4-oxadiazoles **71a-c** were performed starting from hydrazine **48** [48]. Its interaction with CNBr in aqueous dioxane led to unsubstituted 2-amino-

1,3,4-oxadiazole **70** in 80% yield. The reaction of compound **48** with isothiocyanates in the presence of triethylamine (Et_3N) in water gave substituted 2-amino-1,3,4-thiadiazoles **69a-c** in 70–76% yields. The same transformation performed under slightly different conditions ($EtOH$, r.t. or MW) yielded intermediate hydrazinecarbothioamides **49a-c** (83-86% or 85-88%) which, after treatment with *N,N'*-dicyclohexylcarbodiimide, formed substituted 2-amino-1,3,4-oxadiazoles **71a-c** (Scheme 10).

Further, the synthesis of a series of new tetranorlabdane 2-functionalized 1,3,4-oxadiazoles **74-77** and 2-functionalized 1,3,4-thiadiazoles **78a,b** was performed based on the hydrazide of $\Delta^{8,9}$ -bicyclohomofarnesenic acid **72** (Scheme 11) [50]. The 2-amino substituted oxadiazoles **74a,b** were obtained from hydrazide **72** in two steps with 40-64% overall yields. One-step interactions of hydrazide **72** with CNBr led to 2-amino-1,3,4-oxadiazole **75** (91%), with CDI - to 2-keto-1,3,4-oxadiazole **76** (92%), with TMTD - to 2-thio-1,3,4-oxadiazole **77** (70%), and with RNCS - to 2-amino substituted thiadiazoles **78a,b** (75 and 72%).



Scheme 9. Mechanism of conversion of oxadiazole cycle **63** into thiadiazole **67** [48].

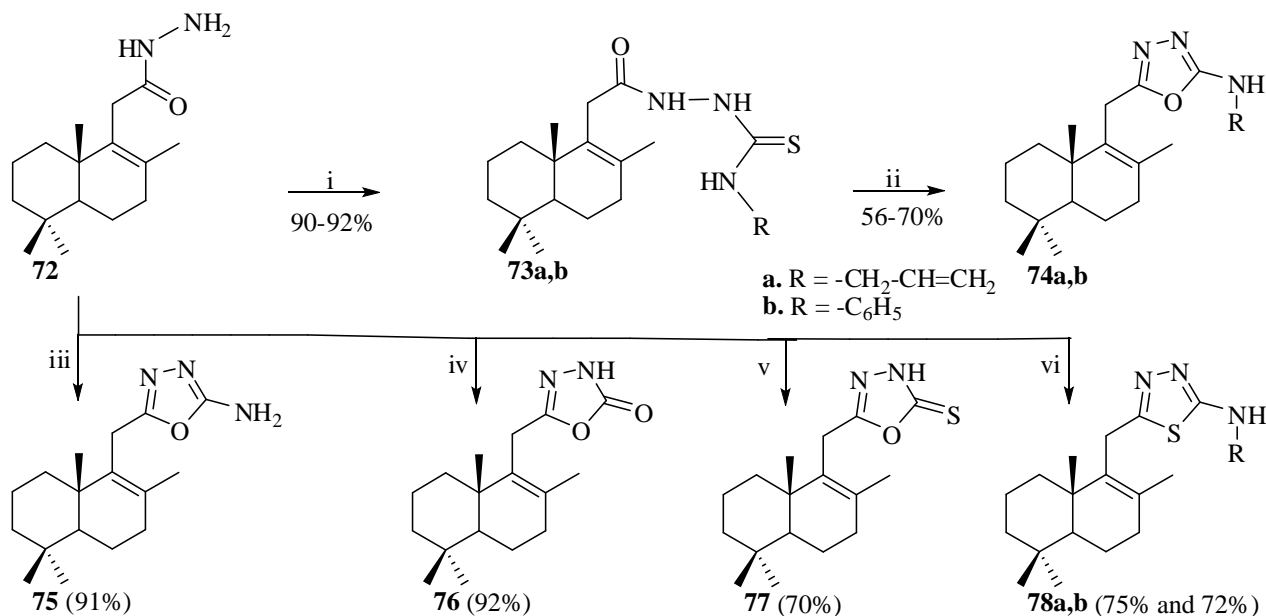


Reagents and conditions: (i) RNCS, Et_3N , Δ , 18 h; (ii) CNBr, $NaHCO_3$, dioxane (aq.), r.t., 1 h; (iii) RNCS, $EtOH$, r.t., 4-5 h or MW, 5 min; (iv) DCC, Me_2CO , $MeOH$, Δ , 5 h.

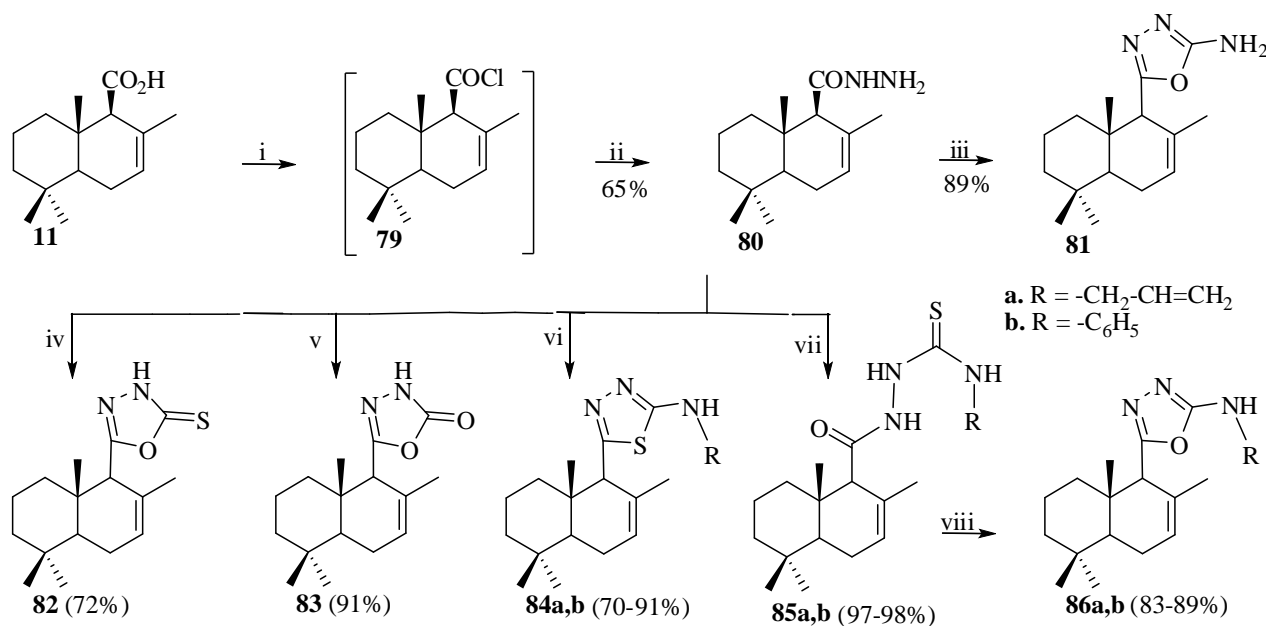
Scheme 10. Synthesis of tetranorlabdane compounds with unsubstituted and substituted 2-amino-1,3,4-oxadiazole and 2-amino-1,3,4-thiadiazole units [48].

Aricu, A. *et al.* applied the same strategy for the synthesis of new pentanorlabdane 2-functionalized 1,3,4-oxadiazoles **81-83**, **86a,b** and 1,3,4-thiadiazoles **84a,b** from

drimenic acid **11** via its chloranhydride **79** and hydrazide **80**, which led to the desired compounds in depicted yields (Scheme 12) [50].



Scheme 11. Synthesis of tetranorlabdane compounds with 2-functionalized 1,3,4-oxadiazole and 1,3,4-thiadiazole units [50].

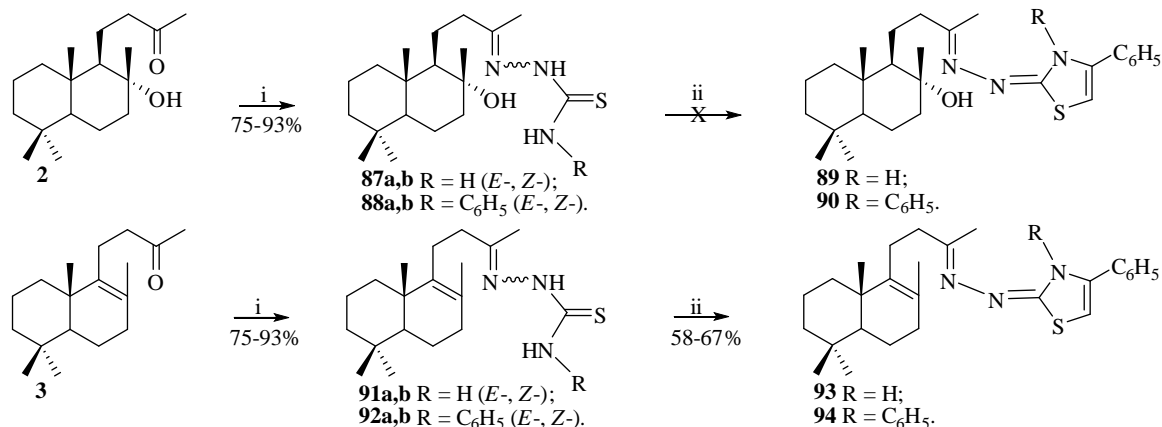


Scheme 12. Synthesis of pentanorlabdane compounds with 2-functionalized 1,3,4-oxadiazole and 1,3,4-thiadiazole units [50].

Aricu, A. *et al.* developed the synthesis of a large series of norlabdane compounds bearing thiosemicarbazone fragment or 1,3-thiazole cycle [51]. For this, a general procedure that included the interaction of ketones **2**, **3**, **5-7**, **10**, and **12** with thiosemicarbazide or 4-phenylthiosemicarbazide was used [52]. Under those conditions, ketones **2** and **3** gave dinorlabdane thiosemicarbazones **87a,b**, **88a,b** and **91a,b**, and **92a,b**, each as mixture of *E/Z* stereoisomers (Scheme 13). The following interaction of thiosemicarbazones **91a,b** and

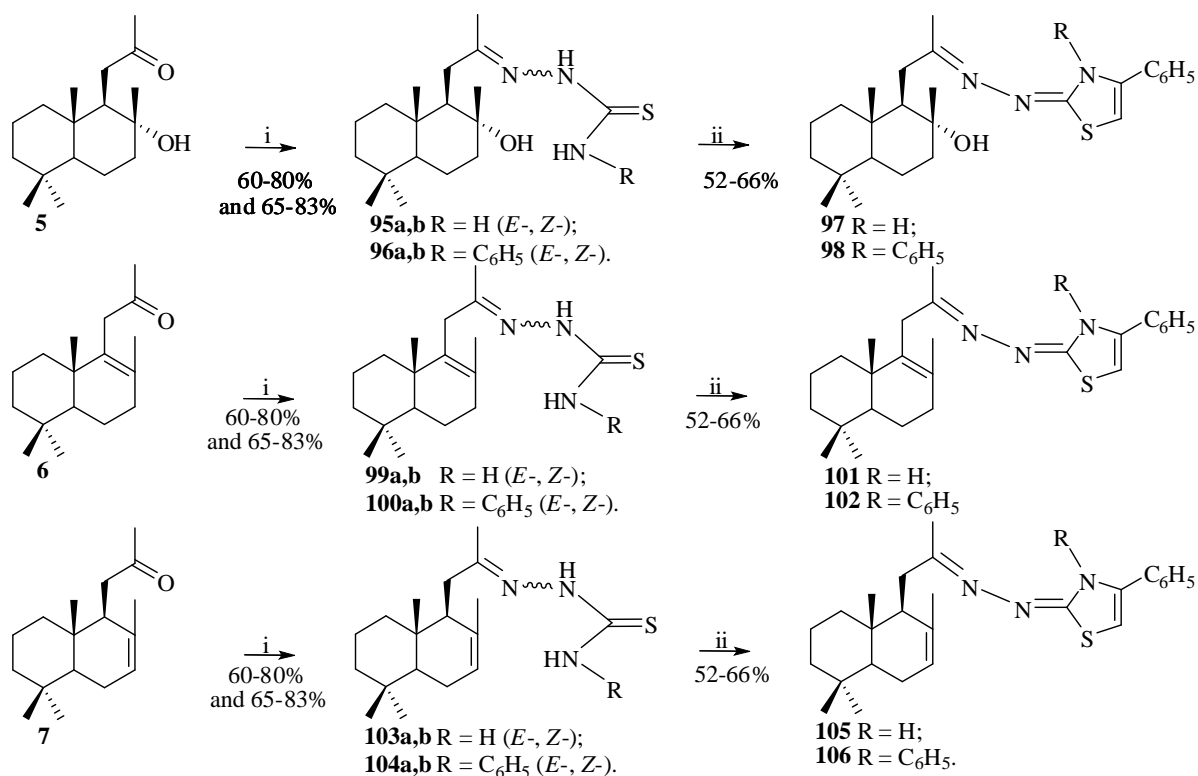
92a,b with 2-bromoacetophenone led to the target dinorlabdane compounds bearing 1,3-thiazole units **93** and **94** in 58-67% overall yields, but no reaction occurred in case of thiosemicarbazones **87a,b** and **88a,b**.

Using the same method, the mixtures of trinorlabdane (*E/Z*) thiosemicarbazones **95a,b-96a,b**, **99a,b-100a,b** and **103a,b-104a,b** were obtained from ketones **5-7** and converted without separation into desired trinorterpeno-1,3-thiazole hybrids **97**, **98**, **101**, **102**, **105**, and **106** in 31-55% overall yields (Scheme 14) [51].



Reagents and conditions: (i) NH₂NHCSNH₂ or NH₂NHCSNHC₆H₅, EtOH, 8-24 h, 60-80°C;
(ii) C₆H₅COCH₂Br, EtOH, 8-14 h, 20°C.

Scheme 13. Synthesis of dinorlabdane compounds containing thiosemicarbazone and 1,3-thiazole fragments [51].



Reagents and conditions: (i) NH₂NHCSNH₂ or NH₂NHCSNHC₆H₅, EtOH, 8-24 h, 60-80°C;
(ii) C₆H₅COCH₂Br, EtOH, 8-14 h, r.t.

Scheme 14. Synthesis of trinorlabdane compounds with thiosemicarbazone and 1,3-thiazole fragments [51].

Further, the known ketoester **10** and drimenone **12** [34] were used as starting materials for preparation of tetra- and pentanorlabdane thiosemicarbazones **107**, **108**, **111**, and **112** and corresponding 1,3-thiazoles **109**, **110**, **113**, and **114** (Scheme 15) by the method mentioned in [51]. In contrast to di- and trinorlabdane compounds presented in Schemes 13 and 14, the overall yields of the final tetra- and pentanorlabdane compounds were higher (57-74%).

Evaluation of antimicrobial activity of norlabdane heterocyclic hybrid compounds

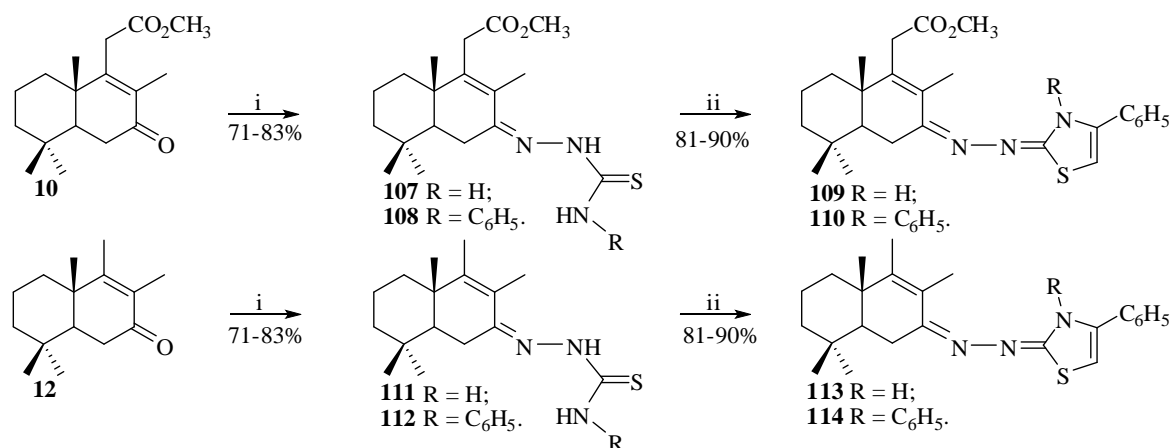
The majority of reported compounds were screened *in vitro* for their antimicrobial activity against pure cultures of fungi and bacteria.

Applying the agar diffusion assay [53] and using such reference drugs as Ampicillin, Chloramphenicol, and Nystatin, Mangalagiu, I.I. *et al.* evaluated the *in vitro* antibacterial and antifungal activity of the newly synthesized compounds (Scheme 1 and 2) against strains of gram-positive (*Staphylococcus aureus* ATCC 25923, *Sarcina lutea* ATCC 9341, *Bacillus cereus* ATCC 14579, *B. subtilis* ATCC), gram-negative (*Escherichia coli* ATCC 25922, *Pseudomonas aeruginosa* ATCC 27853) bacteria and three species of fungi (*Candida albicans* ATCC 10231, *C. glabrata* ATCC MYA 2950, *C. sake* ATCC) [38]. The most active of them proved to be the pyrimidine derivatives **16a,c**, both inhibiting the growth of five bacterial strains, except *P. aeruginosa*, with a 7-19 mm diameter of the inhibition zone. The pyrazine derivative **16b** showed an activity comparable to that of the no-diazine compound **19** against two strains of gram-positive bacteria (*S. aureus* and *B. cereus*), with an inhibition zone diameter of 10-19 mm,

and to *bis*-acylamide **17**, which inhibited only *S. aureus* species (10 mm). None of the mentioned compounds showed any antifungal activity. Kuchkova *et al.* also reported the structure-activity relationship (SAR) correlation concerning antimicrobial activity of the synthesized compounds [38].

Contrary to expectations, the tetranorlabdane pyridazinone hybrid compound **31**, in contrast to bromide **30** (MIC= 2.0 and 2.5 µg/mL) and dimer **32** (MIC= 3.5 and 4.0 µg/mL) (Scheme 4), did not show any antimicrobial activity against any of the tested species of fungi (*Aspergillus niger*, *Penicillium frequentans*, *Alternaria alternata*) or against both gram-negative (*Pseudomonas aeruginosa*) and gram-positive (*Bacillus polymyxa*) bacteria strains [42].

Some of the pentanorlandane pyridazinone hybrids described by Aricu, A. *et al.* showed good antimicrobial activity against five fungi species (*Aspergillus flavus*, *Fusarium solani*, *Penicillium chrysogenum*, *P. frequentans*, and *Alternaria alternata*) and against both gram-positive (*Bacillus polymyxa*) and gram-negative (*Pseudomonas aeruginosa*) bacteria [35]. The *in vitro* antimicrobial assessments performed according to procedures previously described [54,55] revealed good antifungal activity of monosubstituted hybrid **45** at MIC= $15 \cdot 10^{-1}$ µg/mL and high antifungal and antibacterial activities of disubstituted hybrid **47** at MIC= $5 \cdot 10^{-3}$ and $3.2 \cdot 10^{-2}$ µg/mL, respectively, compared to the reference compounds Caspofungin and Kanamycin (Figure 6). The antifungal and antibacterial activities of the disubstituted pentanorlabdane pyridazinone hybrid compound **47** [35] have been patented [56].



Reagents and conditions: (i) $\text{NH}_2\text{NHCSNH}_2$ or $\text{NH}_2\text{NHCSNHC}_6\text{H}_5$, EtOH, 8-24 h;
(ii) $\text{C}_6\text{H}_5\text{COCH}_2\text{Br}$, EtOH, 4-6 h, r.t.

Scheme 15. Synthesis of tetra- and pentanorlabdane compounds with thiosemicarbazone and 1,3-thiazole fragments [51].

Both tetranorlabdane hydrazine carbothioamide **49c** and *N*-substituted 1,2,4-triazole **50d** also manifested a comparatively high antimicrobial activity on the same microbe species (Scheme 5) as reported by D'Ambrosio, M. *et al.* [44]. Both compounds showed promising nonselective antifungal (MIC= 0.125 and $9.4 \cdot 10^{-2}$ µg/mL, respectively) and antibacterial (MIC= $6.4 \cdot 10^{-2}$ and $4.7 \cdot 10^{-2}$ µg/mL, respectively) activities, which are much higher than that of the reference compounds Caspofung and Kanamycin.

Compounds **49c** and **50d** were tested also for cytotoxicity on human ovarian carcinoma cells A2780 and A2780cis, as well as on noncancerous human embryonic kidney cells HEK293, and they showed the activity at IC₅₀ (9-11 mM, 14-15 mM and 18-17 mM, respectively). Those values are much smaller compared to those of Cisplatin (IC₅₀= 0.6, 11.0 and 4.3 mM).

The tetranorlabdane 1,3,4-oxadiazoles and 1,3,4-thiadiazoles (Schemes 7 and 9) reported by Aricu, A. *et al.* [48] were tested against fungal species *Aspergillus niger*, *Fusarium solani*, *Penicillium crysogenum*, *P. frequentans*, and *Alternaria alternata* and bacteria strains *Pseudomonas aeruginosa* and *Bacillus polymyxa*. Compounds **58** (Scheme 7) and **69a** (Scheme 9) showed high antifungal activity at MIC= $3.2 \cdot 10^{-2}$ and 0.25 µg/mL, respectively, and antibacterial activity at MIC= $9.4 \cdot 10^{-2}$ and 0.5 µg/mL, respectively. The activity of the reported compounds is much higher than that of the used standards Caspofungin and Kanamycin. The intellectual property rights on high antifungal and antibacterial activities of the tetranorlabdane 1,3,4-thiadiazole **58** were confirmed by the respective patent [57]. The same authors [50] reported some additional results of the biological activity assessment on the mentioned above microbial species of tetra- and pentanorlabdane oxadiazoles and thiadiazoles presented in Schemes 10 and 11. According to them, tetranorlabdane oxadiazole **76** possess higher antifungal and antibacterial activities (MIC= 0.125 and 2.5 µg/mL) than the standards, and pentanorlabdane hydrazinecarbothioamide showed moderate activities at MIC= 2.0 and 48 µg/mL.

In another paper, Aricu, A. *et al.* [51] reported the results of the biological investigation of the series of di-, tri-, tetra- and pentanorlabdane thiosemicarbazones and 1,3-thiazoles presented in Schemes 12-14. Compounds **88a,b** and **95a,b** were tested against the same species as mentioned in [48,50] and showed both antifungal or

antibacterial activities, a bit higher than those of the standards at MIC= 0.25 and 0.19 µg/mL, and MIC= 4.0 and 3.0 µg/mL, respectively. The series of the patented bioactive norlabdane heterocyclic compounds can be completed by trinorlabdane thiosemicarbazones **95a,b** [51] drawn on Scheme 11, which have shown a promising antifungal activity. These mixtures of isomers were claimed as antifungal agents in [60].

As a result of the microbiological evaluation, it was established that substituted 1,2,4-triazole **20** and *N*-aminocarbazole **21** hybrids depicted in Scheme 3 possess obvious growth stimulating properties [39]. Both compounds were used as components of nutrient media for the cultivation of *Nostoc linckia* cyanobacterium. Those compounds substantially increase the antioxidant activity of the cyanobacterium biomass under the specified conditions, at the following concentrations for **20** (0.062–0.064 g/L) and **21** (0.060–0.062 g/L), respectively [58,59]. The antimicrobial assessments of the reported norlabdane heterocyclic hybrids frequently proved their antifungal and antibacterial activities. Those data were reported elsewhere and also claimed by the author and colleagues. All those mentioned compounds are of a real interest for medicine and agriculture as antifungal and antibacterial agents.

Conclusions

The available scientific data on a new direction of research in the chemistry of labdane diol (-)-sclareol, namely, the synthesis of norlabdane heterocyclic hybrids and some of its intermediates, published from 2013 to the present time, are reviewed.

The analysed publications pointed out a new class of biocompatible and biologically active terpeno-heterocyclic hybrids and led to the synthesis of numerous series of norlabdane compounds with hydrazide or thiosemicarbazonic moieties and diazine, triazole, carbazolic, thiazole, oxadiazole or thiadiazole heterocyclic structural units.

Many of the mentioned compounds showed excellent *in vitro* antimicrobial activity on several species of fungi and two bacterial strains, and two of them – a moderate cytotoxic activity. It should be noted here that the preparation methods and the properties of biologically active hybrids have been patented.

Based on the above, it can be concluded that (-)-sclareol and the heterocyclic hybrid compounds derived from it are a promising object of research.

Funding

This work is part of the project PLANTERAS 20.80009.8007.03 “New substances with preventive and therapeutic potential based on natural compounds of plant origin and modern methods of organic synthesis” within the State Program (2020-2023) financed by the National Agency for Research and Development of the Republic of Moldova.

References

1. Aricu, A. Synthesis of nitrogen-containing compounds from higher terpenoids. *Chemistry Journal of Moldova*, 2011, 6(1), pp. 10–28. DOI: [https://dx.doi.org/10.19261/cjm.2011.06\(1\).15](https://dx.doi.org/10.19261/cjm.2011.06(1).15)
2. Urones, J.G.; Diez, D.; Gomez, P.M.; Marcos, I.S.; Basabe, P.; Moro, R.F. Drimane homochiral semisynthesis: pereniporin A, 9-*epi*-warburganal and C-9 nitrogenated drimanes. *Natural Product Letters*, 1998, 11(2), pp. 145–152. DOI: <https://doi.org/10.1080/10575639808041211>
3. Barrero, A.F.; Alvarez-Manzaneda, E.J.; Chahboun, R.; Diaz, C.G. New routes toward drimanes and *nor*-drimanes from (-)-sclareol. *Synlett*, 2000, 2000(11), pp. 1561–1564. DOI: <https://doi.org/10.1055/s-2000-7924>
4. Zarraga, M.; Zarraga, A.M.; Rodrigues, B.; Perez, C.; Paz, C.; Paz, P.; Sanhueza, C. Synthesis of a new nitrogenated drimane derivative with antifungal activity. *Tetrahedron Letters*, 2008, 49(32), pp. 4775–4776. DOI: <https://doi.org/10.1016/j.tetlet.2008.05.092>
5. Kuchkova, K.I.; Arycu, A.N.; Vlad, P.F. Synthesis of 11-aminodrim-7-ene from drimenol. *Chemistry of Natural Compounds*, 2009, 45(3), pp. 367–370. DOI: <https://doi.org/10.1007/s10600-009-9341-y>
6. Kuchkova, K.I.; Arycu, A.N.; Vlad, P.F.; Deleanu, K.; Nikolescu, A. Synthesis of *N*-containing drimane sesquiterpenoids from 11-dihomodriman-8 α -ol-12-one. *Chemistry of Natural Compounds*, 2010, 46(4), pp. 539–544. DOI: <https://doi.org/10.1007/s10600-010-9671-9>
7. Kuchkova, K.I.; Arycu, A.N.; Barba, A.N.; Vlad, P.F.; Lipkovskii, Ya.; Simonov, Yu.A.; Kravtsov, V.Kh. Synthesis of nitrogen-containing drimane sesquiterpenoids from 11-dihomodriman-8(9)-en-12-one. *Chemistry of Natural Compounds*, 2011, 47(2), pp. 223–228. DOI: <https://doi.org/10.1007/s10600-011-9888-2>
8. Kuchkova, K.I.; Aricu, A.N.; Barba, A.N.; Secara, E.S.; Vlad, P.F.; Ungur, N.D. Synthesis of 12-amino-11-dihomodrimane sesquiterpenoids from norambreinolide. *Chemistry of Natural Compounds*, 2014, 50(3), pp. 458–461. DOI: <https://doi.org/10.1007/s10600-014-0986-9>
9. Kuchkova, K.I.; Arycu, A.N.; Secara, E.S.; Barba, A.N.; Dragalin, I.P.; Vlad, P.F.; Ungur, N.D. Synthesis of 13-amino-14,15-dinorlabd-8(9)-ene from sclareol. *Russian Chemical Bulletin*, 2014, 63(9), pp. 2074–2076. DOI: <https://doi.org/10.1007/s11172-014-0703-7>
10. De la Torre, M.C.; Garcia, I.; Sierra, M.A. Straightforward synthesis of the strong ambergris odorant γ -bicyclohomofarnesal and its *endo*-isomer from *R*-(+)-sclareolide. *Tetrahedron Letters*, 2002, 43(36), pp. 6351–6353. DOI: [https://doi.org/10.1016/S0040-4039\(02\)01392-8](https://doi.org/10.1016/S0040-4039(02)01392-8)
11. Boukouvalas, J.; Wang, J.-X.; Marion, O.; Nzdi, B. Synthesis and stereochemistry of the antitumor diterpenoid (+)-zerumin B. *The Journal of Organic Chemistry*, 2006, 71(17), pp. 6670–6673. DOI: <https://doi.org/10.1021/jo0610154>
12. Boukouvalas, J.; Wang, J.-X. Structure revision and synthesis of a novel labdane diterpenoid from *Zingiber ottensii*. *Organic Letters*, 2008, 10(16), pp. 3397–3399. DOI: <https://doi.org/10.1021/ol8011919>
13. Lungu, L. Synthesis of new nitrogen-containing drimane and homodrimane sesquiterpenoids from sclareolide. *Chemistry Journal of Moldova*, 2015, 10(2), pp. 58–61. DOI: [https://dx.doi.org/10.19261/cjm.2015.10\(2\).07](https://dx.doi.org/10.19261/cjm.2015.10(2).07)
14. Frija, L.M.T.; Frade, R.F.M.; Afonso, C.A.M. Isolation, chemical, and biotransformation routes of labdane-type diterpenes. *Chemical Reviews*, 2011, 111(8), pp. 4418–4452. DOI: <https://doi.org/10.1021/cr100258k>
15. Basabe, P.; Blanco, A.; Boderio, O.; Martin, M.; Marcos, I.S.; Diez, D.; Mollinedo, F.; Urones, J.G. Expedient synthesis of nitrogenated spongianes: 4-methyldecarboxyspongolactams. *Tetrahedron*, 2010, 66(13), pp. 2422–2426. DOI: <https://doi.org/10.1016/j.tet.2010.01.091>
16. Butnariu, R.M.; Mangalagiu, I.I. New pyridazine derivatives: synthesis, chemistry and biological activity. *Bioorganic & Medicinal Chemistry*, 2009, 17(7), pp. 2823–2829. DOI: <https://doi.org/10.1016/j.bmc.2009.02.028>
17. Mangalagiu, I.I. Recent achievements in the chemistry of 1,2-diazines. *Current Organic Chemistry*, 2011, 15(5), pp. 730–752. DOI: <https://doi.org/10.2174/138527211794519050>
18. Dondoni, A.; Marra, A. Thiazole-mediated synthetic methodology. *Chemical reviews*, 2004, 104(5), pp. 2557–2600. DOI: <https://doi.org/10.1021/cr020079l>
19. Othman, A.A.; Kihel, M.; Amara, S. 1,3,4-Oxadiazole, 1,3,4-thiadiazole and 1,2,4-triazole derivatives as potential antibacterial agents. *Arabian Journal of Chemistry*, 2019, 12(7), pp. 1660–1675. DOI: <https://doi.org/10.1016/j.arabjc.2014.09.003>
20. Hu, Y.; Li, C.-Y.; Wang, X.-M.; Yang, Y.-H.; Zhu, H.-L. 1,3,4-Thiadiazole: synthesis, reactions, and applications in medicinal, agricultural, and materials chemistry. *Chemical Reviews*, 2014, 114(10), pp. 5572–5610. DOI: <https://doi.org/10.1021/cr400131u>
21. Neuhaus, W.C.; Moura-Letts, G. Alumina-promoted synthesis of *N*-aryl-1,2,4-triazoles from substituted hydrazines and imides. *Tetrahedron Letters*, 2016, 57(45), pp. 4974–4977.

- DOI: <https://doi.org/10.1016/j.tetlet.2016.09.086>
22. Gao, X.; Liu, J.; Zuo, X.; Feng, X.; Gao, Y. Recent advances in synthesis of benzothiazole compounds related to green chemistry. *Molecules*, 2020, 25(7), pp. 1675–1690.
DOI: <https://doi.org/10.3390/molecules25071675>
 23. Rajasekaran, A.; Murugesan, S. Synthesis and antimicrobial evaluation of thiosemicarbazones (I). *ChemInform*, 2003, 34(7), pp. 544–545.
DOI: <https://doi.org/10.1002/chin.200307105>
 24. Beraldo, H.; Gambinob, D. The wide pharmacological versatility of semicarbazones, thiosemicarbazones and their metal complexes. *Mini-Reviews in Medicinal Chemistry*, 2004, 4(1), pp. 31–39.
DOI: <https://doi.org/10.2174/1389557043487484>
 25. Matesanz, A.I.; Leita, I.; Souza, P. Palladium(II) and platinum(II) *bis*(thiosemicarbazone) complexes of the 2,6-diacetylpyridine series with high cytotoxic activity in cisplatin resistant A2780cisR tumor cells and reduced toxicity. *Journal of Inorganic Biochemistry*, 2013, 125, pp. 26–31.
DOI: <https://doi.org/10.1016/j.jinorgbio.2013.04.005>
 26. Da Silva, A.P.; Martini, M.V.; de Oliveira, C.M.A.; Cunha, S.; de Carvalho, J.E.; Ruiz, A.L.T.G.; da Silva, C.C. Antitumor activity of (-)- α -bisabolol-based thiosemicarbazones against human tumor cell lines. *European Journal of Medicinal Chemistry*, 2010, 45(7), pp. 2987–2993.
DOI: <https://doi.org/10.1016/j.ejmech.2010.03.026>
 27. Haraguchi, S.K.; Silva, A.A.; Vidotti, G.J.; Dos Santos, P.V.; Garcia, F.P.; Pedrosa, R.B.; Nakamura, C.V.; de Oliveria, C.M.A.; da Silva, C.C. Antitrypanosomal activity of novel benzaldehyde-thiosemicarbazone derivatives from kaurenoic acid. *Molecules*, 2011, 16(2), pp. 1166–1180.
DOI: <https://doi.org/10.3390/molecules16021166>
 28. Vandresen, F.; Falziroli, H.; Almeida Batista, S.A.; da Silva-Giardin, A.P.B.; de Oliveira, D.N.; Catharino, R.R.; Ruiz, A.L.T.G.; de Carvalho, J.E.; Foglio, M.A.; da Silva, C.C. Novel *R*-(+)-limonene-based thiosemicarbazones and their antitumor activity against human tumor cell lines. *European Journal of Medicinal Chemistry*, 2014, 79, pp. 110–116.
DOI: <https://doi.org/10.1016/j.ejmech.2014.03.086>
 29. Hua, S.-K.; Wang, J.; Chen, X.-B.; Xu, Z.-Y.; Zeng, B.-B. Scalable synthesis of methyl *ent*-isocopalate and its derivatives. *Tetrahedron*, 2011, 67(6), pp. 1142–1144.
DOI: <https://doi.org/10.1016/j.tet.2010.12.008>
 30. Cucicova, C.; Aricu, A.; Secara, E.; Vlad, P.; Ungur, N. Process for producing 14,15-bisnorlabdane-8(9)-en-13-one. *MD Patent* 2013, No. 4248.
 31. Kuchkova, K.I.; Chiumakov, Yu.M.; Simonov, Yu.A.; Bocelli, G.; Panasenkov, A.A.; Vlad, P.F. A short efficient synthesis of 11-monoacetate of drimane-8 α -11-diol from norambreinoloide. *Synthesis*, 1997, 1997(9), pp. 1045–1048.
DOI: <https://doi.org/10.1055/s-1997-1302>
 32. Stoll, M.; Hinder, M. Odor and composition XI. Study of transesterification-dehydration of lactone of 1,1,6,10-tetramethyl-6-hydroxy-decalyl-5-acetic acid. *Helvetica Chimica Acta*, 1954, 37(6), pp. 1859–1866. (in French).
DOI: <https://doi.org/10.1002/hlca.19540370632>
 33. Vlad, P.F.; Vorob'eva, E.A. Synthesis of drim-8-en-7-one. *Chemistry of Natural Compounds*, 1983, 19(2), pp. 139–141.
DOI: <https://doi.org/10.1007/BF00580546>
 34. Koltsova, M.N.; Mironov, G.N.; Malinovskii, S.T.; Vlad, P.F. Synthesis of drim-8(9)-en-7-one, drima-5,8(9)-dien-7-one, and their 11,12-dibromo derivatives from norambreinoloide. *Russian Chemical Bulletin*, 1996, 45(1), pp. 208–214.
DOI: <https://doi.org/10.1007/BF01433763>
 35. Aricu, A.; Ciocarlan, A.; Lungu, L.; Barba, A.; Shova, S.; Zbancioc, Gh.; Mangalagiu, I.I.; D'Ambrosio, M.; Vornicu, N. Synthesis, antibacterial and antifungal activities of new drimane sesquiterpenoids with azaheterocyclic units. *Medicinal Chemistry Research*, 2016, 25(10), pp. 2316–2323.
DOI: <https://doi.org/10.1007/s00044-016-1665-0>
 36. Ciocarlan, A.; Lungu, L.; Blaja, S.; Dragalin, I.; Aricu, A. The use of some non-conventional methods in chemistry of bicyclohomofarnesenic methyl esters. *Chemistry Journal of Moldova*, 2020, 15(2), pp. 69–77.
DOI: <https://dx.doi.org/10.19261/cjm.2020.791>
 37. Kuchkova, K.; Aricu, A.; Barba, A.; Vlad, P.; Shova, S.; Secara, E.; Ungur, N.; Zbancioc, Gh.; Mangalagiu, I.I. An efficient and straightforward method to new organic compounds: homodrimane sesquiterpenoids with diazine units. *Synlett*, 2013, 24(6), pp. 697–700.
DOI: <https://doi.org/10.1055/s-0032-1318253>
 38. Kuchkova, K.; Aricu, A.; Secara, E.; Barba, A.; Vlad, P.; Ungur, N.; Tuchilus, C.; Shova, S.; Zbancioc, Gh.; Mangalagiu, I.I. Design, synthesis, and antimicrobial activity of some novel homodrimane sesquiterpenoids with diazine skeleton. *Medicinal Chemistry Research*, 2014, 23(3), pp. 1559–1568.
DOI: <https://doi.org/10.1007/s00044-013-0720-3>
 39. Kuchkova, K.I.; Arycu, A.N.; Sekara, E.S.; Barba, A.N.; Vlad, P.F.; Makaev, F.Z.; Mel'nik, E.; Kravtsov, V.Kh. Synthesis and structure of homodrimane sesquiterpenoids containing 1,2,4-triazole and carbazole rings. *Chemistry of Natural Compounds*, 2015, 51(14), pp. 684–688.
DOI: <https://doi.org/10.1007/s10600-015-1384-7>
 40. Duca, Gh.; Aricu, A.; Lungu, L.; Tenu, N.; Ciocarlan, A.; Gutu, Y.; Dragalin, I.; Barba, A. Synthesis of new homodrimane sesquiterpenoids containing diazine, 1,2,4-triazole and carbazole rings. *Chemistry Journal of Moldova*, 2018, 13(1), pp. 69–73.
DOI: <https://dx.doi.org/10.19261/cjm.2017.458>

41. Aricu, A.N.; Kuchkova, K.I.; Secara, E.S.; Barba, A.N.; Dragalin, I.P.; Ungur, N.D.; Mel'nik, E.; Kravtsov, V.Kh. Synthesis and structure of drimane sesquiterpenoids containing pyrimidine, pyrazine, 1,2,4-triazole, and carbazole rings. *Chemistry of Natural Compounds*, 2018, 54(3), pp. 455–460.
DOI: <https://doi.org/10.1007/s10600-018-2378-z>
42. Ciocarlan, A.; Aricu, A.; Lungu, L.; Edu, C.; Barba, A.; Shova, S.; Mangalagiu, I.I.; D'Ambrosio, M.; Nicolescu, A.; Deleanu, C.; Vornicu, N. Synthesis of novel tetranorlabdane derivatives with unprecedented carbon skeleton. *Synlett*, 2017, 28(05), pp. 565–571.
DOI: <https://doi.org/10.1055/s-0036-1588651>
43. Ciocarlan, A.; Edu, C.; Biriiac, A.; Lungu, L.; Aricu, A.; D'Ambrosio, M.; Shova, S.; Nicolescu, A.; Deleanu, C.; Vornicu, N. Synthesis of polyfunctional drimanes from drim-7,9(11)-diene and drim-8-en-7-one. *Synthetic Communications*, 2013, 43(22), p. 3020–3033.
DOI: <https://doi.org/10.1080/00397911.2012.762105>
44. Lungu, L.; Ciocarlan, A.; Barba, A.; Shova, S.; Pogrebnoi, S.; Mangalagiu, I.; Moldoveanu, C.; Vornicu, N.; D'Ambrosio, M.; Babak, M.V.; Arion, V.B.; Aricu, A. Synthesis and evaluation of biological activity of homodrimane sesquiterpenoids bearing hydrazinecarbothioamide or 1,2,4-triazole unit. *Chemistry of Heterocyclic Compounds*, 2019, 55(8), pp. 716–724.
DOI: <https://doi.org/10.1007/s10593-019-02526-1>
45. Styngach, E.P.; Malinovskii, S.T.; Bets, L.P.; Vlad, L.A.; Gdanets, M.; Makaev, F.Z. Crystal and molecular structure of (1*S*,2*S*,4*aS*,8*aS*)-*N*-(*N*-allyldiaminomethanethione)-1-(2-hydroxy-2,5,5,8a-tetramethyldecahydro-naphthalenyl) acetamide. *Journal of Structural Chemistry*, 2005, 46(4), pp. 765–769.
DOI: <https://doi.org/10.1007/s10947-006-0199-6>
46. Blaja, S. Synthesis of new di- and trinorlabdane compounds with 2-amino-1,3-thiazole units. *Chemistry Journal of Moldova*, 2019, 14(2), pp. 72–78.
DOI: <https://dx.doi.org/10.19261/cjm.2019.609>
47. Tsai, C.-Y.; Kapoor, M.; Huang, Y.-P.; Lin, H.-H.; Liang, Y.-C.; Lin, Y.-L.; Huang, S.-C.; Liao, W.-N.; Chen, J.-K.; Huang, J.-S.; Hsu, M.-H. Synthesis and evaluation of aminothiazole-paeonol derivatives as potential anticancer agents. *Molecules*, 2016, 21(2), pp. 145–153.
DOI: <https://doi.org/10.3390/molecules21020145>
48. Lungu, L.; Ciocarlan, A.; Smigon, C.; Ozer, I.; Shova, S.; Gutu, I.; Vornicu, N.; Mangalagiu, I.; D'Ambrosio, M.; Aricu, A. Synthesis and evaluation of biological activity of homodrimane sesquiterpenoids bearing 1,3,4-oxadiazole or 1,3,4-thiadiazole units. *Chemistry of Heterocyclic Compounds*, 2020, 56(5), pp. 578–585.
DOI: <https://doi.org/10.1007/s10593-020-02703-7>
49. Boschelli, D.H.; Connor, D.T.; Bornemeir, D.A.; Dyer, R.D.; Kennedy, J.A.; Kuipers, P.J.; Okonkwo, G.C.; Schrier, D.J.; Wright, C.D. 1,3,4-Oxadiazole, 1,3,4-thiadiazole, and 1,2,4-triazole analogs of the fenamates: *in vitro* inhibition of cyclooxygenase and 5-lipoxygenase activities. *Journal of Medicinal Chemistry*, 1993, 36(13), pp. 1802–1810.
DOI: <https://doi.org/10.1021/jm00065a002>
50. Aricu, A.N.; Kuchkova, K.I.; Secara-Cushnir, E.S.; Barba, A.N.; Ungur, N.D.; Vornicu, N. Synthesis and antimicrobial activity of new drimane and homodrimane sesquiterpenoids with oxadiazole and thiadiazole fragments. *Chemistry of Natural Compounds*, 2020, 56(4), pp. 656–662.
DOI: <https://doi.org/10.1007/s10600-020-03115-x>
51. Blaja, S.P.; Lungu, L.V.; Kuchkova, K.I.; Ciocarlan, A.G.; Barba, A.N.; Vornicu, N.; Aricu, A.N. Norlabdane compounds containing thiosemicarbazone or 1,3-thiazole fragments: synthesis and antimicrobial activity. *Chemistry of Natural Compounds*, 2021, 57(1), pp. 101–110.
DOI: <https://doi.org/10.1007/s10600-021-03292-3>
52. Mohareb, R.M.; Wardakhan, W.W.; Elmegeed, G.A.; Ashour, R.M.S. Heterocyclizations of pregnenolone: Novel synthesis of thiosemicarbazone, thiophene, thiazole, thieno[2,3-*b*]pyridine derivatives and their cytotoxicity evaluations. *Steroids*, 2012, 77(14), pp. 1560–1569.
DOI: <https://doi.org/10.1016/j.steroids.2012.09.004>
53. Reeves, D.S.; Phillips, I.; Williams, J.D.; Wise, R. Disc methods of sensitivity testing and other semiquantitative methods. *Laboratory methods in antimicrobial chemotherapy. Part I.* Churchill Livingstone: Edinburgh, 1978, pp. 8–23.
54. Usta, A.; Yaşar, A.; Yılmaz, N.; Güleç, C.; Yaylı, N.; Karaoğlu, Ş.A.; Yaylı, N. Synthesis, configuration, and antimicrobial properties of novel substituted and cyclized 2',3"-thiazachalcones. *Helvetica Chimica Acta*, 2007, 90(8), pp. 1482–1490.
DOI: <https://doi.org/10.1002/hlca.200790154>
55. National Committee for Clinical Laboratory Standards (NCCLS) Antimicrobial Susceptibility Standards (ATS) for M7 (CMI) and M100. 2003
56. Aricu, A.; Mangalagiu, I.; Ciocarlan, A.; Lungu, L.; Zbancioc, Gh.; Vornicu, N. 11,12-*Bis-p*-tolyl-piridazonyl-drim-5(6),8(9)-diene-7-one exhibiting antifungal and antibacterial properties. MD Patent No.4370B1, 2015.
57. Aricu, A.; Lungu, L.; Ciocarlan, A.; Vornicu, N. (1*R*,2*R*,8*aS*)-1-((5-Mercapto-1,3,4-thiadiazol-2-yl) methyl)-2,5,5,8a-tetramethyldecahydro naphthalen-2-ol compound with antifungal and antibacterial properties. MD Patent No. 4580C1, 2019.
58. Cucicova, C.; Rudic, V.; Aricu, A.; Cepoi, L.; Rudi, L.; Secara, E.; Valuta, A.; Barba, A.; Miscu, V.; Vlad, P.; Chiriac, T. *N*-($\Delta^{8,13}$ -Bicyclohomofarnesenoylamino)carbazole

- compound and process for cultivation of *Nostoc linckia* cyanobacterium with its use. MD Patent No. 4326, 2013.
59. Cucicova, C.; Rudic, V.; Aricu, A.; Cepoi, L.; Rudi, L.; Secara, E.; Valuta, A.; Barba, A.; Miscu, V.; Vlad, P.; Chiriac, T. *N*-($\Delta^{8,13}$ -Bicyclohomofarnesenoyl)-3-amino-1,2,4-triazole compound and process for cultivation of *Nostoc linckia* cyanobacterium with its use. MD Patent No. 4327, 2013.
 60. Aricu, A.; Ciocarlan, A.; Lungu, L.; Blaja, S.; Vornicu, N. (*Z/E*)-2-(1-((1*R*,2*R*,8*aS*)-2-hydroxy-2,5,5,8*a*-tetramethyldecahydronaphtalen-1-yl)propan-2-iliden)hydrazincarbothioamide for use as antifungal agent. MD Patent No. 4769.

NEW ASPECTS FOR THE ESTIMATION OF THE STATE OF THE NATURAL WATER

Viacheslav Shvydkiy^{a*}, Sergey Dolgov^b, Alexander Dubovik^{a,c},
Mikhail Kozlov^a, Alisa Povkh^a, Lyudmila Shishkina^a, Gheorghe Duca^d

^aEmanuel Institute of Biochemical Physics, Russian Academy of Sciences, 4, Kosygin str., Moscow 119334, Russia

^bInstitute of Geography, Russian Academy of Sciences, 29, p.4, Staromonetny lane, Moscow 119017, Russia

^cA.N.Nesmeyanov Institute of Organoelement Compounds, Russian Academy of Sciences,
28, Vavilov str., Moscow 119991, Russia

^dInstitute of Chemistry, 3, Academiei str., Chisinau MD-2028, Republic of Moldova

*e-mail: slavuta58@gmail.com; phone: (+749)59 397 493; fax: (+749)91 374 101

Abstract. The hydrochemical composition and physicochemical properties of natural water samples from various sources in the Voronezh and Moscow regions have been studied. The highest mineralization of water was found in the snow collected near the highway, and the highest content of N-containing compounds in the water of the Usman River in the Voronezh reserve. Two model systems are proposed for assessing the state of the aquatic environment UV spectroscopy with spectrum decomposition by the Gauss method and spontaneous aggregation of lecithin in a polar medium. The presence of various organic, N- and P-containing compounds, even at low concentrations, leads to significant changes in the lecithin ability to form nanosized aggregates and change their electrophoretic properties. Based on the performed investigation, it was determined that the size of lecithin aggregates decreases, and the value of their zeta potential increases with an increase in the content of hydrophobic compounds in natural water.

Keywords: lecithin, hydrochemical index, water quality, UV-Vis spectroscopy, Gauss method.

Received: 01 June 2022/ Revised final: 07 September 2022/ Accepted: 12 September 2022

Introduction

The natural aquatic medium is a complex multicomponent system determined by the chemical composition of the boundary phases [1]. The pronounced self-organizing ability of water due to the hydrogen bonds formation has led to the expansion of studies on the liquid water structure. To the beginning of the 21st century many experimental data were obtained proving both the influence of low doses of inorganic salts and aminoacids on the nanostructured state of water, and peculiarities in the action of the biologically active substances and the low intensity physical factors on systems of varying complexity [2,3]. Also, ultra-low concentrations of the biologically active substances in systems are enough to be interrelated with a change of the physicochemical properties of water [4-6]. The formation of the supramolecular complexes with the linear sizes of 1-100 µm is also revealed in the water prepared from melted snow [7].

The normal functioning of the complex system is associated with oxidative processes, which play an important role not only in evaluating water quality, but also in metabolism

regulation of the biological objects of varying complexity [8,9]. Hydrogen peroxide present in the natural aquatic medium is one of the necessary participants to support the balance of its redox reactions [1,8,10] and an initiator of the lipid peroxidation (LP) in the biological system [9]. Upon entry into the body, all biologically active substances take part in the regulation of oxidative processes in tissues and significantly affect the structural state of biological membranes [11] at doses close enough to the background [3,11,12]. Similarity, the LP processes in the membrane, cellular and organ levels [13] whose stationary is supposed by the physicochemical regulatory system allows to propose new aspects to evaluate the effect of aquatic medium of components on the state of the LP processes in biological objects.

The aim of this work was to study the physicochemical properties of natural water samples from different sources, and to evaluate their influence on the biological membranes using the ability of the natural phospholipids (some of the biologically active substances components of membranes) to form nanosized particles in the polar medium.

Experimental

Materials

Chemically pure salts of ammonium chloride, sodium nitrite, potassium nitrate, potassium dihydrogen phosphate pre-dried for 2 hours at 105°C were used as standards for the determination of biogenic elements. Reagents used for spectrophotometric measurements (Griess reagent, Nessler reagent, Nitrover 5 nitrate reagent (HACH Company), ammonium molybdate, ascorbic acid) were of “chemically pure” and “pure for analysis” grades.

Sampling points description

The samples were collected from the natural water from Usman (Voronezh nature reserve) and Don (Voronezh region), Dubna and Sestra rivers (near settlement Ustie-Strelka, Moscow region). Samples of snow from the ice of the Usman river, in the pine forest and the grove of leafy trees, the water from the well (Voronezh nature reserve) and snow near the motor road in Rylysk city were also analysed. All samples were collected between March 10 and 21, 2021. The geographic location of samples in Voronezh and Moscow regions are presented in Table 1.

Determination of the hydrochemical indices

Water samples were filtered prior to analysis through a “blue ribbon” paper with pores of 3-5 µm. The quantitative content of the NH_4^+ , NO_2^- , NO_3^- and $(\text{PO}_4)^{3-}$ ions and the mineralization index were determined by photometric methods according to the method described elsewhere [14,15].

Isolation of lipids and analysis of their phospholipid composition

A 10% solution of the soy bean lecithin (BIOLEK, Ukraine) was used as analogue of the natural phospholipids. The fractional composition of its phospholipids was determined by thin layer chromatography according to the

standard procedure [16]. Glass plates 90×120 mm, type G silica gel (Sigma, USA) and the solvent mixture of chloroform:methanol:glacial acetic acid:distilled water as a mobile phase in a volume ratio of 12.5:7.5:2:1 were used. Five chromatographic lines were analysed according to procedure described elsewhere [16]. Methodological details on analysis of the fractional phospholipid composition was reported previously [17].

UV-Vis spectroscopy

The UV-Vis spectroscopy measurements of solutions of lecithin in distilled and natural water were carried out in 10 mm quartz cuvettes using a Shimadzu UV-1700 PharmaSpec (Japan) spectrophotometer. The obtained UV spectra were mathematically processed by the Gauss method using the Excel solver, by minimizing the sum of the squares of the difference between the experimental and calculated spectra under the following conditions: coincidence of the contour of the original spectrum with the calculated one after approximation at the level of 1×10^{-3} - 1×10^{-4} .

Determination of the particle size and ζ -potential by dynamic light scattering method

The aggregation of lecithin in aquatic medium was studied by dynamic light scattering measurements using a Malvern Zetasizer Nano-ZS analyzer (Malvern Instruments Ltd., UK) equipped with a He – Ne laser (4 mW and wavelength 633 nm) and automated program for data processing. The solution was put into an optic cell (10×10 mm). The measurements were carried out at 25°C and a 173° fixed scattering angle. The data were processed with Zetasizer Software 6.20. The particle size was presented as the hydrodynamic diameter d . The ζ -potential measurements of the lecithin nanoparticles in aquatic medium were also performed using dynamic light scattering.

Table 1

The geographic location of samples in Voronezh and Moscow regions.

Sampling point no.	Sampling location	Date of sampling	Coordinates	
			Latitude, N	Longitude, E
1	Usman river, Voronezh nature reserve	10.03.21	51.87924	39.65948
2	Snow from ice, Usman river, Voronezh nature reserve	10.03.21	51.87924	39.65948
3	Snow in the grove of leafy trees, Voronezh nature reserve	10.03.21	51.87924	39.65948
4	Snow in the pine forest, Voronezh nature reserve	10.03.21	51.88088	39.65217
5	Snow near the bridge over the river Seim on the Rylysk - Lgov motor road	13.03.21	51.94973	36.30433
6	Don river near the Novozhivotinnoe village	11.03.21	51.88958	39.16353
7	Usman river, near Orlovo village	14.03.21	51.76638	39.60188
8	Usman river, near Usman workers' settlement	14.03.21	52.01232	39.72948
9	Well in floodplain of the Usman river, 70 m from the coastline	14.03.21	52.01232	39.72948
10	Dubna river, near settlement Ustie-Strelka	21.03.21	56.71014	37.22877
11	Sestra river, near settlement Ustie-Strelka	21.03.21	56.71324	37.22524

It is defined as the electrostatic potential at the slipping (shear) plane outside a charged particle moving in an electric field, where the viscous forces and the electrostatic forces are balancing each other [18]. The velocity of a particle in an electric field is commonly referred to as its electrophoretic mobility, which can be used to obtain the zeta potential of the particle by application of the Henry equation (Eq.(1)).

$$U_E = 2\varepsilon \zeta f(ka) / 3\eta \quad (1)$$

where, ζ - zeta potential;

U_E - electrophoretic mobility;

ε - dielectric constant;

η – viscosity, $f(ka)$ - Henry's function.

Electrophoretic determinations of zeta potential are most commonly made in aqueous media and moderate electrolyte concentration, $f(ka)$ in this case is 1.5, and is referred to as the Smoluchowski approximation. Therefore, the calculation of zeta potential from mobility is straightforward for systems that fit the Smoluchowski model, *i.e.* particles larger than about 0.2 μm dispersed in electrolytes containing more than 10^{-3} M salt.

Smoluchowski's equation was used to calculate the value of the ζ -potential [19] from the electrophoretic mobility. In all experiments the lecithin concentration was 30 $\mu\text{g/mL}$ (4.3×10^{-5} mol/L). Measurements were proceeded during 2 – 2.5 hours after preparation of solutions to reach the dynamic balance. The measurement of each sample was repeated for at least five times.

Statistical procedure

The data were processed with a standard statistic method using MS Excel product, and by KINS program [20]. The significance of differences was evaluated using the *t*-Student's distribution. The experimental data are presented in the form of the average arithmetic means with their mean square errors ($M \pm m$).

Results and discussion

In March 2021, expedition surveys of water bodies in the Voronezh and Moscow regions were carried out. For research, samples were collected of both water and snow in adjacent areas with different vegetation cover. Data regarding the concentrations of the different ions and pH of samples from Voronezh region are presented in Table 2.

Table 2

Hydrochemical indices of studied samples from Voronezh region.

Point no.	Point of sampling	pH	Mineralization, mg/L	$[N-NH_4^+]$, mg/L	$[N-NO_2^-]$, mg/L	$[N-NO_3^-]$, mg/L	$[P-PO_4^{3-}]$, mg/L
1	Usman river, Voronezh nature reserve	8.22	389	3.92 ± 0.55	0.84 ± 0.21	0.70 ± 0.20	0.47 ± 0.17
2	Snow from ice, Usman river - Voronezh nature reserve	6.85	29.4	2.18 ± 0.31	0.017 ± 0.008	6.0 ± 1.7	0.466 ± 0.004
3	Snow in the grove of leafy trees, Voronezh nature reserve	6.38	15.0	1.24 ± 0.17	0.001 ± 0.0	0.094 ± 0.026	0.001 ± 0.0
4	Snow in the pine forest, Voronezh nature reserve	6.36	10.1	1.00 ± 0.14	0.0	0.040 ± 0.011	0.0
5	Snow near the bridge over the river Seim on the Rylysk - Lgov motor road	6.86	4670	3.03 ± 0.42	0.051 ± 0.026	0.0	0.064 ± 0.029
6	Don river near the Novozhivotinnoe village	8.10	227	0.459 ± 0.064	0.011 ± 0.005	0.51 ± 0.14	0.057 ± 0.034
7	Usman river, Orlovo village	8.14	341	2.97 ± 0.42	0.019 ± 0.009	0.42 ± 0.12	0.37 ± 0.17
8	Usman river, Usman workers settlement	8.56	349	3.43 ± 0.48	0.22 ± 0.08	0.69 ± 0.19	0.99 ± 0.36
9	Well in floodplain of the Usman river, 70 m from the coastline	8.71	343	0.81 ± 0.11	0.014 ± 0.007	0.040 ± 0.011	0.066 ± 0.030

As may be observed from the data, there are substantial differences between values of these indices depending on the location of sampling. Thus, snow is characterized by pH values which are close to neutral, while all natural water samples had alkaline pH. Besides, both the level of mineralization and concentration of all studied ions had the lowest values in samples of snow from the pine forest and the grove of leafy tress, and the highest ones were identified in the snow collected near the motor road. The lowest values for both pH and concentrations of NH_4^+ , NO_2^- , NO_3^- and $(\text{PO}_4)^{3-}$ ions were determined in the sample of the Don water, and the well water had the lowest value of nitrate ions.

It was shown on model systems previously that aquatic medium components have an impact on the changes of the state of the oxidative processes in the medium, as well as in the biological objects present in that medium [12,21]. To evaluate these changes, two model systems were used: UV-Vis spectroscopy with the mathematical analysis spectra by the Gauss method and the spontaneous aggregation of lecithin in distilled water and in the presence of investigated samples of the aquatic medium.

The analysis of UV-spectra revealed that samples of natural water from different sources can be divided in three groups: *group 1*: water from Dubna and Sestra rivers, Moscow region, and Don river, Voronezh region; *group 2*: water from the snow samples (with ice of Usman river, in the pine forest and in the grove of leafy tress, Voronezh nature reserve; snow near the motor road, Voronezh region), *group 3*: water of Usman river (points 1, 7, 8 and 9 (Table 1).

UV-spectra of the natural water samples of group 1 have only two absorption bands, one of which is presented in all three samples at $\lambda = 208\text{--}210\text{ nm}$. It is suggested that absorption

bands are typical for the carbonyl and *N*-containing organic compounds and phenols in water. The second absorption band is situated at $\lambda = 227.2, 238.6$ and 245.0 nm for water from the Dubna, Sestra and Don rivers, correspondingly. Presumably, this band is due to the presence of organic acids, compounds with conjugated double bonds and compounds with carbonyl groups, respectively. As an example, UV-spectrum of the Don water is presented in Figure 1.

As follows from the UV-spectra of the group 2 samples, the content of chemical substances is according to the sampling location. In particular, the snow in the pine forest with the lowest values of all hydrochemical indices (Table 1) has only three absorption bands ($\lambda = 236.4\text{ nm}, 254.0\text{ nm}$ and 291.9 nm) with a low absorbance ($A < 0.020$). This suggests the presence of organic substances with conjugated double bonds and carbonyl groups. Although snow in the grove of leafy trees has four absorption bands ($\lambda = 197.6\text{ nm}, 218.3\text{ nm}, 241.3\text{ nm}$ and 260.7 nm), their absorbance is low. Thus, the most intense band ($\lambda = 197.6\text{ nm}$) has $A = 0.0535$. In the snow samples from the ice of the Usman river and near the motor road, there are also four absorption bands in the UV-spectra. The most intense absorption band has the maximum λ in the region $195\text{--}197\text{ nm}$ due to the presence of the hydrophobic compounds such as esters and compounds with unconjugated double bonds. However, organic acids and compounds with carbonyl groups were also identified in these samples, and polycyclic compounds - in the snow sample collected near the motor road (Figure 2). It was expected that the sample of snow near the motor road would have the highest values of both the hydrochemical indices (Table 2) and intensity of the absorption band in UV-spectra.

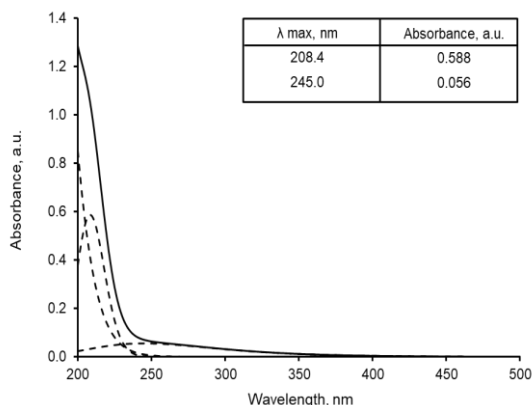


Figure 1. UV-spectrum of water from the Don river and its Gaussian.

(here and further: solid curve is initial and calculate spectra, dotted lines are its Gaussian)

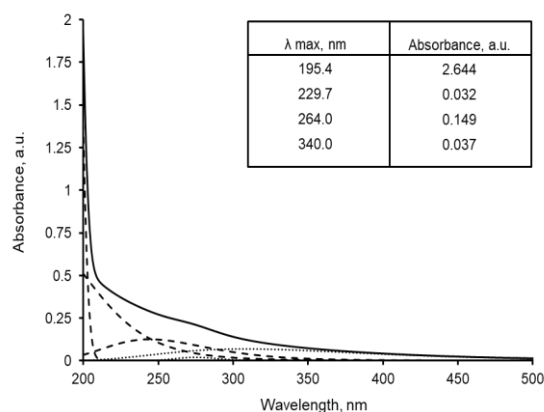


Figure 2. UV-spectrum of snow from the motor road and its Gaussian.

The number of the absorption bands and their intensity in the UV-Vis spectra of group 3 water samples are due to an inhabitation of people near the sampling location. Thus, two absorption bands are found only in the water from the Usman river (point 8, Table 1) characterized by a high content of hydrophobic compounds ($\lambda = 201.2$ nm, $A = 2.203$) and the presence of compounds with a conjugated double bonds ($\lambda = 230.2$ nm, $A = 0.370$). In the sample of the well water were identified organic acids and *N*- and *P*-containing compounds ($\lambda = 221.3$ nm, $A = 0.135$; $\lambda = 254.7$ nm; $A = 0.1345$; $\lambda = 332.3$ nm, $A = 0.018$) which were detected in accordance with a high content of NH_4^+ , NO_2^- and NO_3^- ions (Table 2). Samples of the Usman river water from Voronezh natural reserve (point no. 1) and near Orlovo village (point no. 7) contain a large number of hydrophobic compounds and other substances (as an example, the UV-Vis spectrum of sample no. 7 is presented in Figure 3).

The above presented analysis of the literature data allows us to conclude that the substantial changes in the chemical composition of the aquatic medium should affect the structural state and physicochemical properties of membranes of the biological objects. Indeed, the determination of the hydrodynamic diameters of the nanosized particles from lecithin and their ζ -potential in the presence of the natural aquatic samples supports this conclusion.

It is well-known that lecithin is a mixture of natural lipids and the proportion of phospholipids (PL) in its total lipid composition is at least 50%. Among PL, phosphatidylcholine is the main fraction. Earlier it was shown that the aqueous solution of lecithin is the adequate model system

of the evaluation both presence of toxicants in the water medium and their influence on biological objects [12,21]. It should be noted that samples of the natural objects of different batches differ in terms of the quantitative ratio of PL fractions and share of PL in the total lipid composition [17]. The PL composition of the lecithin batch used is shown in Table 3. The share of PL of the lecithin batch used in the total lipid composition was $65.5 \pm 5.0\%$ ($n = 8$).

The substantial differences in values of the hydrochemical indices and chemical composition of studied samples of the natural water cause changes in the ability of lecithin to aggregate (Figure 4). As seen, the main traction of lecithin ($87.0 \pm 0.85\%$) consists of particles with an average size of 995 ± 115 nm, whereas $13.0 \pm 0.5\%$ belong to nanosized particles with 109 ± 12 nm in *d*. In the presence of the Don and Usman rivers water samples (points no 1 and 6, Table 1) the lecithin aggregates consist of practically one fraction, 1.2–1.3 times smaller in size.

Table 3

The fractional composition of phospholipids in the used lecithin.

<i>Fraction of phospholipids</i>	<i>Share of fraction (%P)</i>
Lysoforms of phospholipids	3.03 ± 0.26
Sphingolipids	3.47 ± 0.42
Phosphatidylcholine	84.1 ± 1.4
Phosphatidylinositol+	2.67 ± 0.32
phosphatidylserine	
Phosphatidylethanolamine	1.89 ± 0.38
Cardiolipin	3.19 ± 0.45
Phosphatidic acid	1.64 ± 0.54

Number of chromatographic lines $n = 5$.

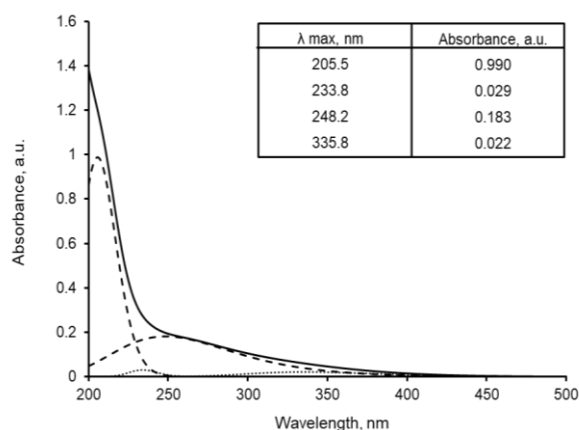


Figure 3. UV-spectrum of water from the Usman river near Orlovo village. (here and further: solid curve is initial and calculate spectra, dotted lines are its Gaussian)

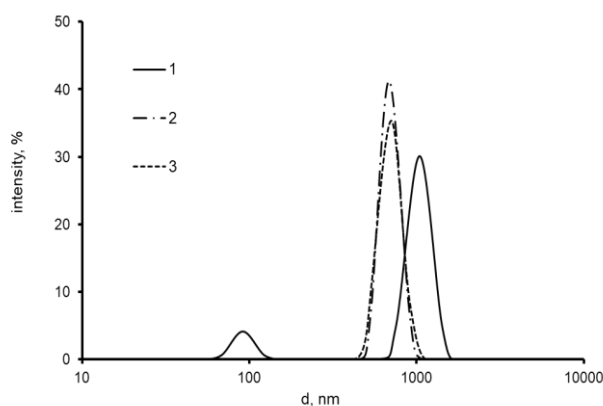


Figure 4. Size distribution (*d*) by intensity curves of lecithin aggregates in distilled water (1) and in the presence of the natural water from Don (2) and Usman (3) rivers (Voronezh nature reserve).

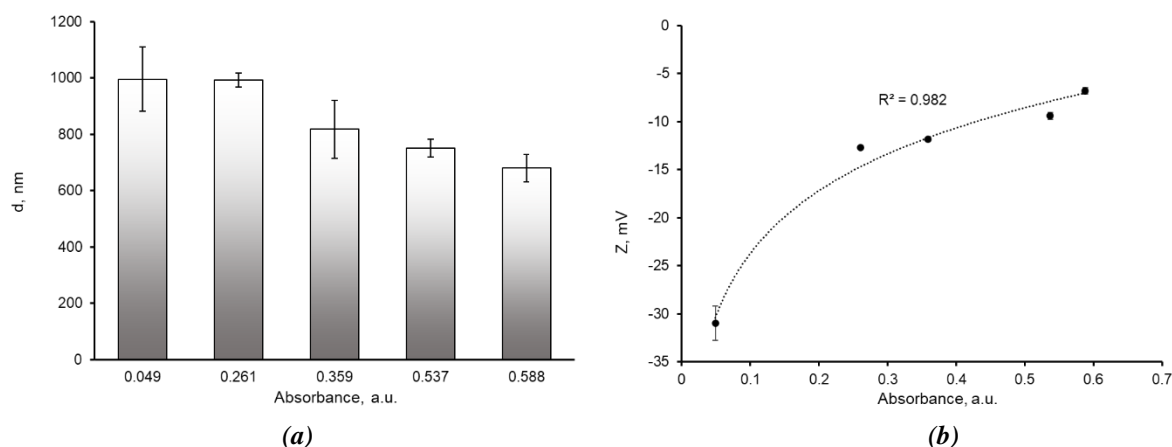


Figure 5. Size (d) particles of lecithin in the distilled water and in the presence of the natural water (a) and ζ -potential of the lecithin aggregates in the presence of the natural water (b) from Dubna (point no 10), Sestra (point no 11), Don (point no 6) and Usman (point no 1) rivers vs the contain of the hydrophobic compounds in the medium.

Table 4
Values of ζ -potential of the lecithin aggregates in the presence of natural water samples.

Samples	ζ -potential, mV
Dubna (point no 10)	-11.83 ± 0.05
Sestra (point no 11)	-12.72 ± 0.07
Usman (point no 1)	-9.41 ± 0.36
Usman (point no 7)	-12.97 ± 0.17
Usman (point no 8)	-14.7 ± 0.22
Usman (point no 9)	-7.98 ± 0.28
Don (point no 6)	-6.78 ± 0.33
Snow (point no 4)	-25.5 ± 0.66

Besides, in samples from the natural water from Dubna, Sestra, Don and Usman (points no. 1, 6, 10 and 11 rivers, an increase of the size of hydrodynamic diameters (d) is attended by the reduction in content of the hydrophobic compounds (Figure 5(a)). However, the most substantial influence of the presence of different additives in the natural water are revealed for magnitudes of ζ -potential of the lecithin aggregates (Table 4). In distilled water, the ζ -potential value is -31.0 ± 1.8 mV ($n=8$).

Noteworthy, the decrease in the negative value of the ζ -potential of the lecithin nanosized particles in the presence of the studied water samples is accompanied by an increase of the hydrophobic compounds in the natural aquatic medium in accordance with the parabolic function (Figure 5(b)).

Conclusions

From the obtained hydrochemical and spectrophotometric data, three groups of water bodies can be distinguished, the properties of

which are probably associated with different watersheds and ecological conditions. In particular, the snow near the road, compared to the snow in the background areas, is subject to significant pollution with the content of predominantly reduced forms of biogenic elements (3.03 mg $\text{N-NH}_4^+/\text{L}$, 0.051 mg $\text{N-NO}_2^-/\text{L}$) and high mineralization (4670 mg/L).

The presented two model systems (mathematical analysis of the UV spectra of natural water using the Gauss method and spontaneous aggregation of lecithin in distilled water and in the studied samples of natural water) showed that the presence of various organic, N - and P -containing compounds, even at low concentrations, leads to significant changes in the ability of lecithin to form nanosized aggregates in an aqueous medium (a decrease in size by 1.2–1.3 times, with an increase in the content of hydrophobic compounds in natural water), as well as to change the electrophoretic mobility of biological membranes in biological objects. A significant increase in the ζ -potential was noted in all samples of natural waters. The greatest increase in the ζ -potential, in particular, is shown in a sample of the natural water of the Don River, up to -6.88 mV compared to distilled water (control) -31.0 mV. This indicates the possible influence of the composition of natural water on the functioning of biomembranes in the cells of living organisms. The structure of biomembranes and their functions are closely interrelated, and this plays an important role in the normal functioning of biological objects. This effect still needs to be studied in detail.

Acknowledgments

The study was performed under Government contract 44.4 (state registration no. 0084-2019-0014) at the Emanuel Institute of Biochemical Physics of the Russian Academy of Sciences.

The author Gh.D. is grateful to the Moldovan State Program (2020-2023) project no. 20.80009.5007.27 "Physico-chemical mechanisms of redox processes with electron transfer involved in vital, technological and environmental systems".

References

1. Gurikov, Yu.V.; Bondarenko, N.F. Natural water as an oxidizing system. *Russian Journal of Physical Chemistry A*, 2001, 75(7), pp. 1103–1106. (in Russian).
2. Lo, Sh.; Li, V. Nanostructures in a very dilution water solutions. *Russian Chemical Journal*, 1999, 43(5), pp. 40–48. (in Russian).
DOI: <http://www.chem.msu.ru/rus/jvho/1999-5/40.pdf>
3. Burlakova, E.B. Peculiarities in the action of the biologically active substances at the ultra-low doses and the physical factors of the low intensity. *Russian Chemical Journal*, 1999, 43(5), pp. 3–11. (in Russian).
DOI: <http://www.chem.msu.ru/rus/jvho/1999-5/3.pdf>
4. Zhernovkov, V.E.; Roshchina, I.A.; Zubareva, G.M.; Shmatov, G.P.; Lokshin, B.V.; Palmina, N.P. The study of thyrotropin-releasing hormone effect in a wide concentration range on the aquifer system by IR-spectroscopy method. *Water*, 2010, 2, pp. 58–68.
DOI: <https://doi.org/10.14294/WATER.2010.4>
5. Belov, V.V.; Belyaeva, I.A.; Shmatov, G.P.; Zubareva, G.M.; Palmina, N.P. IR spectroscopy of thin water layers and the mechanism of action α -tocopherol in ultra low concentrations. *Doklady Physical Chemistry*, 2011, 439(1), pp. 123–126.
DOI: <https://doi.org/10.1134/S0012501611070013>
6. Kononov, A.I.; Maltseva, E.L.; Ryzhkina, I.S.; Murtazina, L.I.; Kiseleva, Yu.V.; Kasparov, V.V.; Palmina, N.P. Formation of nanoassociates is a factor determining physicochemical and biological properties of highly diluted aqueous solutions. *Doklady Physical Chemistry*, 2014, 456(2), pp. 86–89.
DOI: <https://doi.org/10.1134/S0012501614060050>
7. Smirnov, A.N.; Savin, A.V.; Sigov, A.S. Structural transformation in liquid water. *Biophysics*, 2020, 65(2), pp. 354–357.
DOI: <https://doi.org/10.1134/S0006350920020232>
8. Shvydkii, V.O.; Shtamm, E.V.; Skurlatov, Yu.I.; Vichutinskaya, E.V.; Zaitseva, N.I.; Semenyak, L.V. Intoxication of the natural aqueous medium resulting from disbalance of redox and free-radical intrabasin processes. *Russian Journal of Physical Chemistry B*, 2017, 11(4), pp. 643–651.
DOI: <https://doi.org/10.1134/S1990793117040248>
9. Vigo-Pelfrey, C. *Membrane Lipid Oxidation*. vol. III. Boston: CRC Press, 1991, 300 p.
10. Shtamm, E.V.; Pural, A.P.; Skurlatov, Yu.I. The role of hydrogen peroxide in natural aquatic media. *Russian Chemical Reviews*, 1991, 60(11), pp. 1228–1248. (in Russian). DOI: <https://doi.org/10.1070/RC1991v060n11ABEH001141>
11. Burlakova, E.B.; Varfolomeev, S.D. Eds. *Bioantioxidants: yesterday, today and tomorrow. Chemical and biological kinetics: New horizons*. Vol. 2: Biological Kinetics. CRC Press: London, 2005, pp. 1–33.
DOI: <https://doi.org/10.1201/b12196>
12. Shishkina, L.N.; Kozlov, M.V.; Povkh, A.Yu.; Shvydkiy, V.O. Role of the lipid peroxidation in the assessment of the consequences of exposure to chemical toxicants on bio-objects. *Russian Journal of Physical Chemistry B*, 2021, 15(5), pp. 861–867.
DOI: <https://doi.org/10.1134/S1990793121050080>
13. Orlicki, R.; Cienciala, C.; Krylova, L.P.; Pielichowski, J.; Zaikov, G.E. Eds. *Functioning similarity of the physicochemical regulatory system of the lipid peroxidation on membrane and organ levels. Pharmaceutical and Medical Biotechnology. New Perspectives*. Nova Science Publishers: New York, 2013, pp. 151–157.
<https://novapublishers.com/shop/pharmaceutical-and-medical-biotechnology-new-perspectives/>
14. GOST 33045-2014. *Water. Methods for determination of nitrogen-containing matters*. Interstate Council for Standardization, Metrology and Certification, Moscow, 2014. (in Russian).
<https://files.stroyinf.ru/Data2/1/4293766/4293766954.pdf>
15. GOST 18309-2014. *Water. Methods for determination of phosphorus-containing substances*. Interstate Council for Standardization, Metrology and Certification, Moscow, 2019. (in Russian).
<https://files.stroyinf.ru/Data/584/58485.pdf>
16. Findlay, J.B.C.; Evans, W.H. Eds. *Biological Membranes: A Practical Approach*. Mir: Moscow, 1990, 424 p. (in Russian).
17. Marakulina, K.M.; Kramor, R.V.; Lukanina, Yu.K.; Plashchina, I.G.; Polyakov, A.V.; Fedorova, I.V.; Chukicheva, I.Yu.; Kutchin, A.V.; Shishkina, L.N. Effect of the nature of phospholipids on the degree of their interaction with isobornylphenol antioxidants. *Russian Journal of Physical Chemistry A*, 2016, 90(2), pp. 286–292.
DOI: <https://doi.org/10.1134/S0036024416020187>
18. Jain, K.; Mehndzhiyski, A.Y.; Zozoulenko, I.; Wagberg, L. PEDOT:PSS nano-particles in aqueous media: A comparative experimental and molecular dynamics study of particle size, morphology and z-potential. *Journal of Colloid and Interface Science*, 2021, 584, pp. 57–66.
DOI: <https://doi.org/10.1016/j.jcis.2020.09.070>

19. Hunter, R.J. Zeta Potential in Colloid Science: Principles and Applications. Academic Press: London, 1988, 398 p.
<https://www.elsevier.com/books/zeta-potential-in-colloid-science/hunter/978-0-12-361961-7>
20. Brin, E.F.; Travin, S.O. Modeling the mechanisms of chemical reactions. Chemical Physics, 1991, 10(6), pp. 830–837. (in Russian).
21. Shishkina, L.N.; Kozlov, M.V.; Mazaletskaya, L.I.; Povkh, A.Yu.; Shvydkiy, V.O.; Sheludchemko, N.I. Regulatory system of lipid peroxidation as a basis for ecological testing. Russian Journal of Physical Chemistry B, 2020, 14(3), pp. 498–503.
DOI: <https://doi.org/10.1134/S1990793120030240>

PREPARATION OF COMPOSITE BASED ON CAFFEIC ACID AND FUMED SILICA AND EVALUATION OF ITS ANTIOXIDANT AND ANTIMICROBIAL PROPERTIES

Oksana Stavinskaya^{a*}, Iryna Laguta^a, Pavlo Kuzema^a, Iryna Skorochod^b,
Alla Roy^b, Ivan Kurdish^b

^a*Chuiko Institute of Surface Chemistry of National Academy of Sciences of Ukraine,
17, General Naumov str., Kyiv 03164, Ukraine*

^b*D.K. Zabolotny Institute of Microbiology and Virology of National Academy of Sciences of Ukraine,
154, Zabolotny str., Kyiv 03143, Ukraine
e-mail: okstavinskaya@yahoo.com

Abstract. The aim of this work was the preparation of a composite comprising caffeic acid (CA) and fumed silica (A300), and comparison of antioxidant and antimicrobial properties of CA in solution and in composite. The CA+A300 composite with CA content of about 25 mg/g was obtained using the sorptive modification of silica with CA solution under fluidized bed conditions. Antioxidant properties of the CA solution and the CA+A300 composite were studied using DPPH[•] and Folin-Ciocalteu assays, in addition OH[•] and NO[•] scavenging activity and antimicrobial properties against *Staphylococcus aureus* 209 strain were estimated. The results have shown that CA is very effective in the reaction with DPPH[•] radicals and that the inclusion of CA in the composite results in the slowing down of this reaction. The CA solution and the CA+A300 composite had a similar activity as NO[•] radicals' scavengers and as antimicrobial agents, whereas the CA solution was more effective in inhibition of OH[•] radicals. It has been assumed that the difference in activity between the CA+A300 composite and the CA solution may be due to the gradual release of CA from the composite into reaction mixtures and by the increase in this release as CA is consumed in the reactions.

Keywords: caffeic acid, fumed silica, composite, antioxidant, radical scavenger, antimicrobial activity.

Received: 20 June 2022/ Revised final: 05 August 2022/ Accepted: 10 August 2022

Introduction

Fumed silica is a biocompatible and bioactive powder used as an auxiliary ingredient for preparation of the medicines and dietary supplements. While silica itself can adsorb a large number of various toxic molecules, acting as a detoxifying or wound healing agent [1], its function in the formulations may be to improve the stability of the active components against oxidation, to reduce the drugs hygroscopicity, to introduce hydrophobic compounds into aqueous solutions or hydrophilic compounds into lipophilic media, etc. [2-4].

The most common ways to prepare bioactive composites based on silica and bioactive compounds are the following: 1) co-milling the silica powder together with active ingredients, 2) chemical immobilization of the active molecules involving silica silanol groups, 3) adsorption/deposition of bioactive compounds on silica surface from the solutions [5-8]. In contrast to the previously described case of

adsorption/deposition from excess solutions [6,9,10], adsorption/deposition under fluidized bed conditions was shown to preserve the high dispersion of silica nanoparticles, thus allowing silica to further act as an adsorbent and a detoxifying agent [9]. The technique also allows depositing of a high amount of active substances on silica surface, which is not restricted by the value of their equilibrium adsorption.

One of the main reasons for the inclusion of bioactive compounds, in particular antioxidants, in the composites is to provide their gradual release into solution or reaction medium. This slows the consumption of the compounds and ensures their prolonged action. For the case of silica-based composite, the rate of the active substances release apparently depends on the interaction of these substances with silica surface. Unfortunately, the most common antioxidants such as ascorbic acid, caffeic acid (CA), most polyphenols have a low affinity to silica, with free energies of adsorption being usually less than

20-40 kJ/mol [11], so one can expect that such substances will be readily released from the composite into appropriate solution or reaction medium.

The aim of the work was to prepare the composite comprising the antioxidant CA and fumed silica *via* the adsorption/deposition under fluidized bed conditions, and to compare the antioxidant and antimicrobial properties of CA in solution and in composite. The paper also includes the results on the release of CA from the composite into aqueous and ethanol solutions/mixtures. The results of the study will be useful for the preparation of silica-based formulations that possess both the biological activity of adsorbed molecules and the adsorption properties of silica powder.

Experimental

Materials

The following reagents and solvents were used in this study: caffeic acid, 2,2-diphenyl-1-picrylhydrazyl radical (DPPH[•]), Folin-Ciocalteu reagent, Greiss reagent, sodium nitroprusside, ferrous sulphate, brilliant green, ethanol (96%), phosphate buffered saline, hydrogen peroxide (all from Merck, Germany). Fumed silica (A-300, 99.7% purity) was obtained from State Enterprise “Kalush Test Experimental Plant of the Institute of Surface Chemistry of NAS of Ukraine” (Kalush, Ukraine).

Methods and instruments

Composite preparation was done as follows: 10 g of the silica powder was placed in the reaction vessel equipped with a stirrer and then 5 mL of the 270 mM CA solution in 96% ethanol were gradually dropped to the vessel under permanent intensive stirring; then the mixture was stirred for one more hour to provide good distribution of CA over the silica surface. The obtained powder was heated for 5 hours under reduced pressure at 40°C to remove the solvent. The calculated content of CA in the resulted composite was 24.4 mg per 1 g of silica or ~2.4 wt. %.

Thermogravimetric and differential thermogravimetric analysis (TG-DTG) was performed using a Q-1500D Derivatograph (MOM, Hungary) in air with the heating rate of 10°/min within the 20–800°C range.

DPPH[•] radical scavenging evaluation of CA solutions and CA+A300 composite was performed by using 2,2-diphenyl-1-picrylhydrazyl (DPPH[•]) radical scavenging method as described by Brand-Williams W. *et al.* [12]. Briefly, 1 mL

of CA solutions of various concentrations was poured into glasses and 2 mL of 70% ethanol and 2 mL of 0.15 mM DPPH[•] solution were consecutively added. A quantity of 7.5 mg of composite was weighted into glass, and 60 mL of 70% ethanol and 40 mL of 0.15 mM DPPH[•] solution were added. The solution/suspension was shaken at 25°C for 5÷120 min; then, in the case of the composite, the supernatant was separated from the solid phase. The change in concentration of stable radicals in the mixtures during the reaction was determined from the change in absorption at the maximum of 520 nm for tested solutions as compared to absorption value for blank solution. The blank solution was prepared by mixing 3 mL of 70% ethanol with 2 mL of 0.15 mM DPPH[•] solution. The stoichiometry of the reaction of CA with DPPH[•] radicals was investigated as follows. The course of the reaction at different [CA]/[DPPH[•]] molar ratios was studied and the ([CA]/[DPPH[•]])₅₀ ratio corresponding to the inhibition of 50% of the original amount of DPPH[•] was found. The doubled value of ([CA]/[DPPH[•]])₅₀ gives the theoretical effective concentration of the antioxidant required to reduce 100% of the radicals, and the value inverse to this concentration determines the stoichiometry of the reaction [12].

Folin-Ciocalteu assay on CA solutions and the CA+A300 composite was done according to a previously described method [13]. Briefly, to measure the total phenolic content for CA solutions of various concentrations, 45 mL of distilled water, 5 mL of Folin-Ciocalteu reagent, 20 mL of 20% sodium carbonate solution and 25 mL of water were consecutively added to 5 mL of tested solution. The solution was stirred for various time periods, the absorbance at 750 nm (*D*₇₅₀) was measured and the dependence of *D*₇₅₀ value on CA concentration was determined. In the case of CA+A300 composite, 7.5 mg of the composite was placed into glasses, followed by addition of 50 mL of distilled water, 5 mL of Folin-Ciocalteu reagent, 20 mL of 20% sodium carbonate solution and 25 mL of water.

NO[•] and OH[•] radicals scavenging assays for CA solution and the CA+A300 composite were performed by Griess-Ilosvay reaction and Fenton reaction, respectively [14,15]. To carry out the tests, a CA solution of about 4.5 mM/L and a suspension of composite in distilled water with the composite content of 0.035 g per 1 mL were used. The antioxidant quantities in solution and in suspension were equal.

The antimicrobial activity of CA solution and CA+A300 composite was studied using the

“wells” method. A volume of 0.1 mL of a 24-hour suspension of *Staphylococcus aureus* 209 strain was applied on the surface of the agar medium [16]. “Wells” with a diameter of 8 mm were made with a sterile drill, into which 0.015 μL of a CA solution (with concentration of about 4.5 mM/L) or a CA+A300 composite suspension (with the composite content of 0.035 g per 1 mL) was added. The cups were placed in a thermostat at 28°C for 48÷72 hours. The diameter of the zone of bacterial growth inhibition under the action of the solution/suspension was determined.

The release of the CA from the composite into solutions/reaction mixtures was studied under constant solution volume conditions. Fixed volumes (100 mL) of water or 70% ethanol solution were added to 7.5 mg of the composite; the glasses with the suspensions were placed into a shaking water bath (Jeio Tech BS-11, UK) and shaken at 25°C for 1÷120 min. The concentration of CA in the solutions after various time intervals was evaluated from the changes in absorbance of the solution at a wavelength of 312-315 nm. The degree of the antioxidant release was determined as the percentage of CA released regarding to its total amount in the composite.

The CA release under given conditions, when the antioxidant reacts with dissolved substances, was examined according to the procedure described above, with the Folin-Ciocalteu assay or DPPH test reaction mixtures being used instead of pure water or 70% ethanol solution, respectively. The amount of CA transferred from the composite into water-based and ethanol-based reaction mixtures during Folin-Ciocalteu and DPPH tests was estimated using the calibration data obtained during the assays performed for CA solutions of various concentrations (0.01÷0.10 mM).

The UV-Vis spectra of solutions and reaction mixtures were recorded using a Lambda 35 spectrophotometer (Perkin Elmer, USA) at 25°C in the wavelength range of 200–800 nm.

Results and discussion

In order to confirm that after sorptive modification of silica A300 with CA and subsequent solvent removal the modifying agent remains in the composite, TG-DTG studies have been carried out. TG-DTG data on the weight loss of the bulk CA, original silica, and CA+A300 composite upon the temperature increase is given in Figure 1.

For the bulk CA sample, above 99% of the weight loss occurs within the temperature interval

of 150–600°C (Table 1) as a result of the thermal decomposition and thermal-oxidative degradation processes. For the A300 sample, about three quarters of its total weight loss is in the region of 20–150°C and is mainly due to removal of physically adsorbed water; the further weight loss of ~1% in the temperature range of 150–600°C may be related to removal of strongly bound water or water formed as a result of silanol groups dehydroxylation. As to the CA+A300 composite, the weight loss in the region of 20–150°C is about 1% higher than in the case of A300, suggesting that ~1 wt.% of ethanol still remains in the composite after its drying.

Table 1

Parameters derived from TG-DTG studies.			
Sample	Weight loss, %		Total weight loss, %
	20-150, °C	150-600, °C	
A300	2.7	1.0	3.8
CA	0.2	99.3	100.0
CA+A300	3.6	3.6	7.2

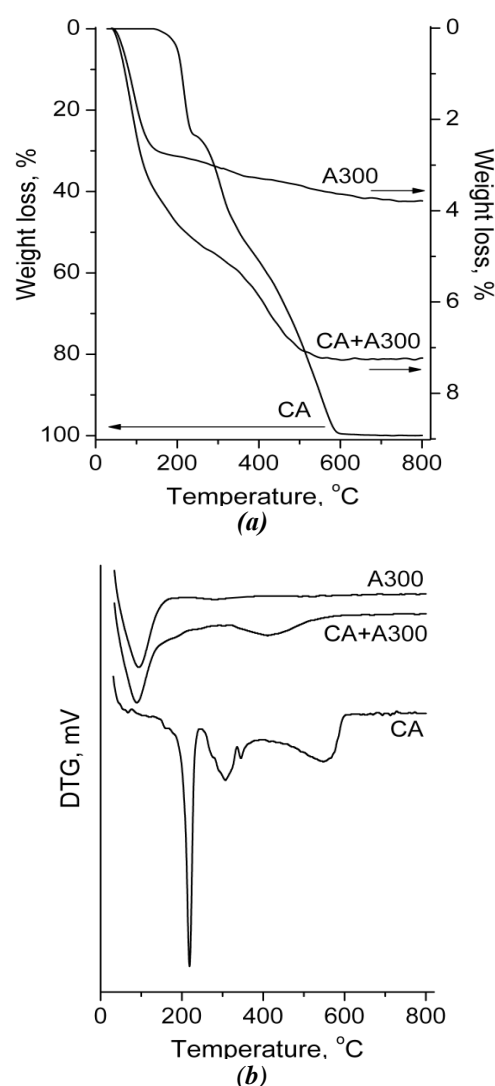


Figure 1. TG (a) and DTG (b) curves for A300, CA, and CA+A300 composite.

In the temperature range of 150–600°C, corresponding to the CA degradation, the weight loss for the composite is by 2.6% higher than in the case of the A300 sample. This value is close to the calculated CA content in the composite (~2.4%, see the Experimental part), with additional 0.2% being attributed to the further loss of the solvent and/or the products of its interaction with silica surface (thermal decomposition of ethoxysilyl groups). Thus, the TGA data confirms that the quantity of CA in the composite is about 25 mg/g.

The data on the inhibition of DPPH[•] radicals by the CA solutions of various concentrations is given in Figure 2, and the data that allow determining the stoichiometry of this reaction is presented in Figure 3 indicating that $([CA]/[DPPH^{\bullet}])_{50}$ value, corresponding to the inhibition of 50% of the original amount of DPPH[•] radicals, is about 0.11. Thus, the doubled $([CA]/[DPPH^{\bullet}])_{50}$ value is ~0.22, and the value reciprocal to 0.22 (~4.5) gives the stoichiometry of the reaction. This result is in agreement with

literature data, indicating that each molecule of CA can reduce in average 4.5 molecules of DPPH[•] [12].

The data on the inhibition of DPPH[•] radicals by the CA+A300 composite is given in Figure 4; for comparison, curve 2 also shows the inhibition of DPPH[•] radicals by the CA solution with the equivalent amount of antioxidant. In the case of the composite, scavenging of the radicals during the first hour of the reaction occurs much more slowly than in the case of the CA solution. This appears to be caused by gradual desorption of CA from silica surface. The final percentage of radicals inhibited by the composite and by the solution during two hours is ~57% and ~65%, respectively; thus, one can conclude that, during 2 hours, the main portion of antioxidant was released from the composite into solution and participated in the reaction.

Figure 5 presents similar data on the interaction of CA, both individual and included in the composite, with the Folin-Ciocalteu reagent in aqueous medium.

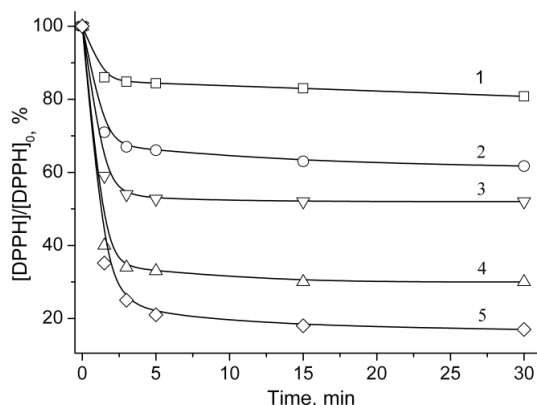


Figure 2. Inhibition of DPPH[•] radicals in the reaction with CA solutions at a molar $[CA]/[DPPH^{\bullet}]$ ratio of 0.05; 0.075; 0.10; 0.15; 0.30 (curves 1-5, respectively).

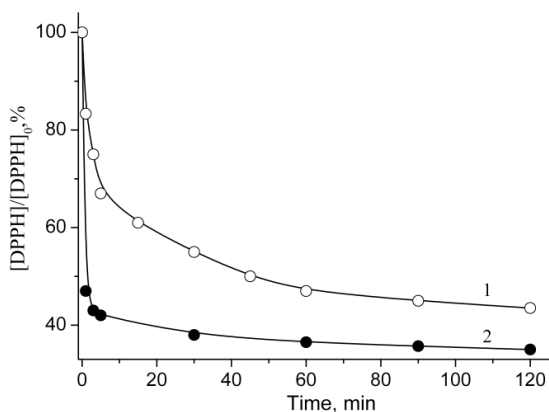


Figure 4. Inhibition of DPPH[•] radicals in the reaction with the CA+A300 composite (curve 1) and with an equivalent quantity of individual CA (curve 2).

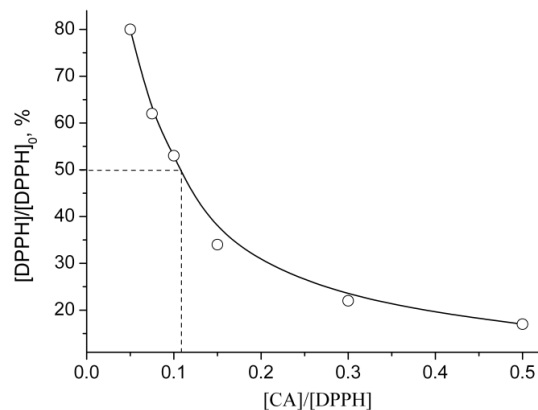


Figure 3. Percentage of residual DPPH[•] radicals in the reaction mixture versus the $[CA]/[DPPH^{\bullet}]$ molar ratio.

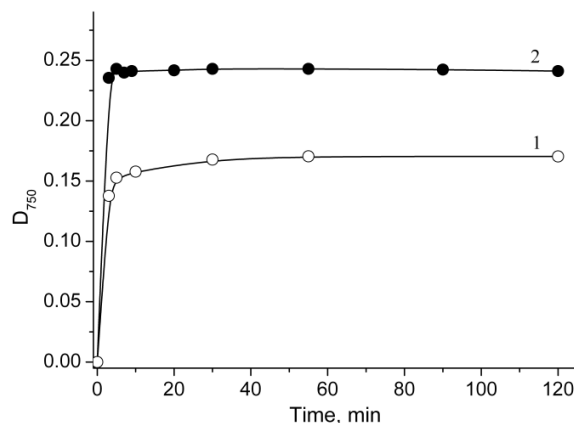


Figure 5. Change in D_{750} value during Folin-Ciocalteu test for the CA+A300 composite (curve 1) and for an equivalent quantity of individual CA (curve 2).

The data also shows that individual CA interacts with the reagent rapidly, with the changes in absorbance values at 750 nm during 2–120 min of the reaction being within 1÷2% of its average value. For the CA+A300 composite, during the same time interval an increase in D_{750} values by about 20% is observed, although only ~70% of the total quantity of antioxidant available in the composite appears to interact with the Folin-Ciocalteu reagent.

Figures 6 and 7 present the data on the release of CA into pure solvents and into the reaction mixtures containing DPPH[•] radicals or Folin-Ciocalteu reagent. Curves 1 in the Figures 6 and 7 illustrate the release of CA from the composite into 70% ethanol and into pure water, respectively, with the composite-to-volume ratio being the same as in the DPPH[•] and Folin-Ciocalteu tests. The data show quick, within 10–30 min, equilibration of CA concentration in the solutions, while the percentage of CA released into water and ethanol being about 55 and 60%, respectively.

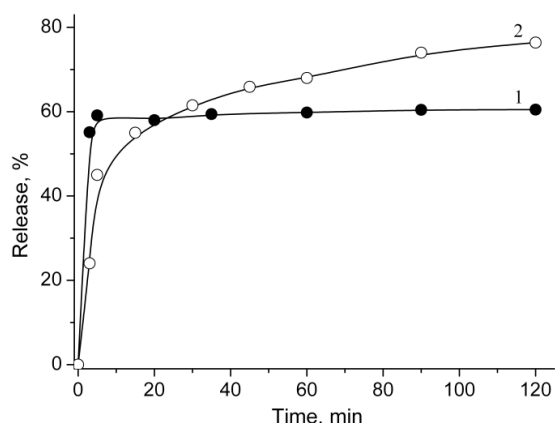


Figure 6. Percentage of CA released from the composite into 70 % ethanol (curve 1) and into the reaction mixture of the DPPH[•] test (curve 2).

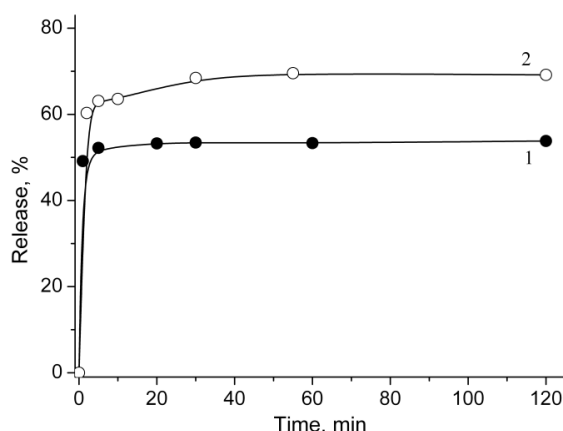


Figure 7. Percentage of CA released from the composite into pure water (curve 1) and into the reaction mixture of the Folin-Ciocalteu test (curve 2).

The release of only about a half of the total amount of CA is not the expected result. For example, in the case of a composite comprising A300 silica and another antioxidant - ascorbic acid - that is also weakly bound to silica, the release of ~90% of this antioxidant into aqueous media during 30 min was observed [4]. The lower release of CA into both solvents may be caused by the lower affinity of the CA for the solvents and its higher affinity for silica surface [11,17-19]. Thus, according to [4,11,17], the free energy of adsorption on silica surface for CA and ascorbic acid is about -40 and -30 kJ/mol, respectively, while the solubility of these antioxidants in water (ethanol) is ~1 (15) g/L for CA and 330 (27) g/L for ascorbic acid [18-20].

Curve 2 in Figure 6 gives the calculated values on the CA release into reaction mixture during the DPPH[•] test. (This data were derived from the data on the inhibition of DPPH[•] radicals by the CA+A300 composite, curve 1 in Figure 4, taking into account the stoichiometry of the reaction and the data on the CA content in the composite.) As one can see from Figure 6, the percentage of CA released from the composite into the mixture gradually increases during the entire time of observation and after 2 h reaches a value approximately 25% higher than the amount of CA released into 70% ethanol. The similar increase in the CA release was observed for water-based solutions, when the reaction mixture of Folin-Ciocalteu assay was used instead of pure water (Figure 7, curve 2). (This data, were derived from Figure 5, curve 1 data, using the preliminary found dependence of the D_{750} value on the concentration of CA in Folin-Ciocalteu reaction mixture.) Thus, for the case of reaction mixtures, the data obtained shows a prolongation of CA desorption and a noticeable increase in the overall amount of CA released. It can be assumed that the consumption of CA molecules in the reactions with DPPH[•] radicals or with Folin-Ciocalteu reagent leads to a decrease in CA concentration in the mixtures and, therefore, to the release of additional amount of antioxidant from the composite.

The CA solution and the CA+A300 composite were also tested in the reactions with NO[•] and OH[•] radicals and as antimicrobial agents against *Staphylococcus aureus* 209 bacterial strain. The results (Table 2) show that the CA solution and the CA+A300 composite suspension have a similar activity as NO[•] radicals scavengers and as antimicrobial agents; on the other hand, the CA solution was more effective in inhibition of OH[•] radicals.

Table 2

Antiradical and antimicrobial activity of CA solution and CA+A300 composite.

Sample	OH [•] radical scavenging activity, %	NO [•] radical scavenging activity, %	Diameter of the zone of bacterial growth inhibition, mm
A300	-	-	-
CA solution	9.8	33.8	12÷14
CA+A300 composite	0.1	34.6	12÷14

These results agree with the above data on the CA release from the composite into solutions/reaction mixtures. Indeed, in the case of very reactive OH[•] radicals, the rate of CA release is not sufficient to scavenge OH[•] radicals. In the case of the antimicrobial test or in the reaction with NO[•] radicals, the tests duration is long enough (several days and 2.5 hours, respectively) for the main part of CA to be released into the reaction medium (Table 2).

Conclusions

The CA+A300 composite comprising CA and fumed silica A300 was obtained using the sorptive modification of silica with CA solution under fluidized bed conditions; antioxidant and antimicrobial properties of the CA solution and the CA+A300 composite were compared.

The results have shown that CA itself and the CA+A300 composite are effective antioxidants and antimicrobial agents. Under chosen experimental conditions, the CA+A300 composite and the equivalent amount of individual CA possessed the same antimicrobial properties against *Staphylococcus aureus* 209 bacterial strain and the same NO[•] radicals scavenging activity. On the other hand, the CA solution was more effective in the reaction with OH[•] radicals and inhibited DPPH[•] radicals faster than the CA+A300 composite. The distinctions in activity of the CA solution and the CA+A300 composite are consistent with the data on the CA release. Although only 55÷60% of CA was desorbed from the composite into water and 70% ethanol until equilibrium was reached (within 10–30 min), a more complete and gradual release of the compound was observed when the media for desorption were reaction mixtures used for the Folin-Ciocalteu or DPPH[•] tests. So, the results of this study demonstrated the prolonged CA release and its action as antioxidant and antimicrobial agent in real systems where CA consumption occurs due to the interaction with oxidants and free radicals.

References

- Pilloni, M.; Ennas, G.; Casu, M.; Fadda, A.M.; Frongia, F.; Marongiu, F.; Sanna, R.; Scano, A.; Valenti, D.; Sinico, C. Drug silica nanocomposite: preparation, characterization and skin permeation studies. *Pharmaceutical Development and Technology*, 2013, 18(3), pp. 626–633. DOI: <https://doi.org/10.3109/10837450.2011.653821>
- Chuiko, A.A. Medical chemistry and clinical application of silica. Naukova Dumka: Kyiv, 2003, 417 p. (in Russian).
- Stavinskaya, O.; Laguta, I.; Kazakova, O.; Kuzema, P.; Lupascu, T. Hygroscopic properties of enoxil-silica composites. *Chemistry Journal of Moldova*, 2018, 13(2), pp. 89–92. DOI: <http://dx.doi.org/10.19261/cjm.2018.487>
- Laguta, I.V.; Stavinskaya, O.N.; Kuzema, P.A.; Kazakova, O.A. Coadsorption of ascorbic acid and α -tocopherol antioxidants on partially trimethylsilylated silica surface. *Protection of Metals and Physical Chemistry of Surfaces*, 2013, 49(4), pp. 398–401. DOI: <https://doi.org/10.1134/S2070205113040096>
- Scano, A.; Ebau, F.; Manca, M.L.; Cabras, V.; Cesare Marincola, F.; Manconi, M.; Pilloni, M.; Fadda, A.M.; Ennas, G. Novel drug delivery systems for natural extracts: The case study of *Vitis Vinifera* extract-SiO₂ nanocomposites. *International Journal of Pharmaceutics*, 2018, 551(1-2), pp. 84–96. DOI: <https://doi.org/10.1016/j.ijpharm.2018.08.057>
- Nosach, L.V.; Voronin, E.F. Adsorption modification of high-disperse silica with non-volatile organic compounds in the gaseous dispersion medium. *Physics and Chemistry of Solid State*, 2006, 7(3), pp. 540–543. (in Ukrainian). <http://page.if.ua/uploads/pcss/vol7/0703-25.pdf>
- Lipkovska, N.O.; Barvinchenko, V.M. Supramolecular interactions of natural flavonoids with cationic surfactant ethonium in solutions and on silica surface. *Chemistry, Physics and Technology of Surface*, 2018, 9(1), pp. 92–103. (in Ukrainian). DOI: <https://doi.org/10.15407/hftp09.01.092>
- Shvets, O.; Belyakova, L. Synthesis, characterization and sorption properties of silica modified with some derivatives of β -cyclodextrin. *Journal of Hazardous Materials*, 2015, 283, pp. 643–656. DOI: <https://doi.org/10.1016/j.jhazmat.2014.10.012>
- Ivannikov, R.; Laguta, I.; Stavinskaya, O.; Kuzema, P.; Skorochoch, I.; Roy, A.; Kurdish, I. Biologically active composite based on fumed silica and *Anoectochilus formosanus* Hayata extract. *Chemical Papers*, 2021, 75(6), pp. 2575–2583. DOI: <https://doi.org/10.1007/s11696-021-01513-1>
- Kuzema, P.O.; Laguta, I.V.; Stavinskaya, O.N.; Tsyba, N.N.; Tertykh, V.A. Fumed silica with

- grafted silicon-hydride groups as a redox-active component in the composite with caffeic acid. Reports of the National Academy of Sciences of Ukraine, 2020, 5, pp. 78–85. (in Ukrainian). DOI: <https://doi.org/10.15407/dopovidi2020.05.078>
11. Kazakova, O.; Ivannikov, R.; Laguta, I.; Stavinskaya, O.; Anishchenko, V.; Severinovska, O.; Buyun, L. Chromatographic analysis of orchid extracts and quantum chemical calculations of individual components interaction with silica. Chemistry Journal of Moldova, 2020, 15(1), pp. 95–102. DOI: <http://dx.doi.org/10.19261/cjm.2020.694>
12. Brand-Williams, W.; Cuvelier, M.E.; Berset, C. Use of a free radical method to evaluate antioxidant activity. LWT-Food Science and Technology, 1995, 28(1), pp. 25–30. DOI: [https://doi.org/10.1016/S0023-6438\(95\)80008-5](https://doi.org/10.1016/S0023-6438(95)80008-5)
13. Alonso, A.M.; Dominguez, C.; Guillen, D.A.; Barroso, C.G. Determination of antioxidant power of red and white wines by a new electrochemical method and its correlation with polyphenolic content. Journal of Agricultural and Food Chemistry, 2002, 50(11), pp. 3112–3115. DOI: <https://doi.org/10.1021/jf0116101>
14. Garratt, D.C. The quantitative analysis of drugs. Springer: Boston, MA, 1964, pp. 1-669. DOI: https://doi.org/10.1007/978-1-4613-3380-7_1
15. Yan, J.-K.; Wang, W.-Q.; Ma, H.-L.; Wu, J.-Y. Sulfation and enhanced antioxidant capacity of an exopolysaccharide produced by the medicinal fungus *Cordyceps sinensis*. Molecules, 2013, 18(1), pp. 167–177. DOI: <https://doi.org/10.3390/molecules18010167>
16. Volkogon, V.V.; Nadkernychna, O.V.; Tokmakova, L.M.; Mel'nychuk, T.M.; Chaikovs'ka, L.O.; Nadkernychnyi, S.P.; Sherstoboiev, M.K.; Kozar, S.F.; Kopylov, Je.P.; Krutylo, D.V.; Parhomenko, T.Ju.; Kamienieva, I.O.; Adamchuk-Chala, N.I.; Kovalevs'ka, T.M.; Didovych, S.V.; Volkogon, K.I.; Pyshhur, I.M.; Volkogon, M.V.; Dimova, S.B.; Komok, M.S. Experimental soil microbiology. Agrarna nauka: Kyiv, 2010, 464 p. (in Ukrainian).
17. Dovbii, O.A.; Kazakova, O.A.; Lipkovskaya, N.A. The effect of the structure of cinnamic acid derivatives on their interaction with highly dispersed silica in aqueous medium. Colloid Journal, 2006, 68(6), pp. 707–712. DOI: <https://doi.org/10.1134/S1061933X06060068>
18. Mota, F.L.; Queimada, A.J.; Pinho, S.P.; Macedo, E.A. Aqueous solubility of some natural phenolic compounds. Industrial & Engineering Chemistry Research, 2008, 47(15), pp. 5182–5189. DOI: <https://doi.org/10.1021/ie071452o>
19. Ji, W.; Meng, Q.; Ding, L.; Wang, F.; Dong, J.; Zhou, G.; Wang, B. Measurement and correlation of the solubility of caffeic acid in eight mono and water+ethanol mixed solvents at temperatures from (293.15 to 333.15) K. Journal of Molecular Liquids, 2016, 224 (Part B), pp. 1275–1281. DOI: <https://doi.org/10.1016/j.molliq.2016.10.110>
20. Shalmashi, A.; Eliassi, A. Solubility of L-(+)-ascorbic acid in water, ethanol, methanol, propan-2-ol, acetone, acetonitrile, ethyl acetate, and tetrahydrofuran from (293 to 323) K. Journal of Chemical & Engineering Data, 2008, 53(6), pp. 1332–1334. DOI: <https://doi.org/10.1021/je800056h>

PROPERTIES OF WINEMAKING BY-PRODUCTS OF *FETEASCA NEAGRA* GRAPE SEEDS

Angela Gurev^{ID a*}, Veronica Dragancea^{ID a}, Alexei Baerle^{ID a}, Natalia Netreba^{ID a},
Olga Boestean^{ID a}, Svetlana Haritonov^{ID a}, Boris Gaina^{ID b}

^a Technical University of Moldova, 7, Studentilor str., Chisinau MD-2012, Republic of Moldova

^b Academy of Sciences of Moldova, 1, Stefan cel Mare si Sfant blvd., Chisinau MD-2001, Republic of Moldova
*e-mail: angela.gurev@chim.utm.md; phone: (+373 69) 60 70 90

Abstract. The aim of this study was to perform a quantitative and qualitative assessment of the biologically active compounds in winemaking by-products. The properties of the lipophilic and hydrophilic extracts from the seeds recovered from fermented pomace of the local grapes - *Feteasca Neagra*, grown in three vineyards, in the 2020 season, were studied. The physicochemical indicators of the seeds and the oil quality indicators were determined. The content of carotenoids and polyphenols in the lipophilic extracts was evaluated by spectrophotometric methods. The difference between the total content of polyphenols and flavonoids in the hydrophilic extracts from ground grape seeds (I) and degreased ground grape seeds (II) was registered. Some phenolic and flavanol constituents were identified and quantified using reversed-phase (C₁₈) gradient-elution HPLC/PDA. The Trolox equivalent antioxidant capacity assay proved the increased antioxidant activity of the hydrophilic extracts, with the highest DPPH• scavenging effect of almost 91.70 and 93.81%, an equivalent of 281.66 and 288.27 µM/L Trolox. It was concluded that the seeds recovered from *Feteasca Neagra* by-products are a rich source of functional compounds, with significant antioxidant properties.

Keywords: antioxidant, flavonoid, grape seed, polyphenol, waste.

Received: 20 June 2022/ Revised final: 13 October 2022/ Accepted: 18 October 2022

Introduction

The winemaking industry in the Republic Moldova has one of the most important roles in the national economy. The National Office of Vine and Wine reported that in 2019 the wine industry provided 16% of the agro-industrial complex, generating 3% of the country's Gross Domestic Product. Officially, in 2019, the total area of vineyards in the Republic Moldova was of 124.000 hectares, with 199 registered wineries, of which 69 with their own vineyards [1]. Agro-industrial grape residues - stems, pomace with seeds and liquid filtrate, may exceed 14.5% of the total grape volume [2,3]. Recent research has shown a growing interest in winemaking by-products, which are not being managed anymore as waste, but as a source of functional compounds [4]. The literature shows that grape seeds contain proteins, lipids, carbohydrates, minerals, fibre, and a wide variety of biologically active substances, such as vitamins, carotenoids, sterols, tocopherols, and polyphenols [2-5]. Moreover, grape seeds resulting from the winemaking process, are an accessible source of unsaturated

fats and unsaturated fatty acids, the content of which varies between 8% and 20%, depending on the grape variety, cultivation conditions, and the type of extraction procedure [6,7]. Seeds contain about 62% of the total content of grape polyphenols, some of the most important bioactive substances [8,9]. The most common identified polyphenols are flavonoids, including the gallic acid, flavan-3-ol, catechin, epicatechin, gallic acid, epigallocatechin, epicatechin-3-ol gallate, dimers and trimers of procyanidin, polymers of procyanidin, stilbenes (resveratrol), etc. [7,8].

Several studies have shown that the content of biologically active substances in grapes, depends on several factors, such as cultivation conditions (soil, water, light, temperature, etc.), ripeness, and genotype, which is also the most important factor [10,11]. From the same grape variety can be produced wines with different tastes, depending on the conditions and place of cultivation as well as the processing method [12]. The quantitative and qualitative content of the biologically active substances, recovered from

winemaking by-products, from the same grape variety, is considerably affected by the method used to obtain them (cold or hot pressing, type of extraction method, type of used solvents, temperature regimes, degree of sample grinding, seed moisture, *etc.*) [6,13-15]. Thus, the cultivation conditions, the grape processing method, and the secondary metabolite extraction method used, influences the total content of biologically active substances in the lipophilic and hydrophilic extracts that were obtained after fermentation, from the same grape variety.

Bioactive compounds, recovered from winemaking by-products, have antioxidant, antibacterial [16,17], anti-inflammatory, anticancer [18,19], cardiovascular [20], and hepatic protective properties [21], which can be used in various fields, such as food industries, pharmaceuticals, cosmetics, animal farming, agriculture, *etc.* Winemaking by-products have also caught the interest of food industry researchers. The by-products are considered to be a valuable source of phytonutrients that can be incorporated into various products, thus increasing the nutritional value and turning them into functional foods, with health benefits [2-4,22].

The main aim of this study is to identify the quantitative and qualitative composition of the lipophilic and hydrophilic extracts from the winemaking by-products of the local grapes - *Feteasca Neagra*, grown in three vineyards, as well as to study the antioxidant activity of the extracts. Further, to evaluate the difference between the composition of the extracts and to suggest possible field of applicability of the recovered functional compounds.

Experimental

Materials

The 1,1-diphenyl-2-picrylhydrazyl-hydrate (DPPH) ($\geq 95\%$) 6-hydroxy-2,5,7,8-tetramethylchromane-2-carboxylic acid (Trolox) (purity $\geq 97\%$), were provided by Alpha Aesar (USA). Aluminium chloride hexahydrate ($\geq 98\%$) and the standard compounds: β -carotene ($\geq 95\%$), gallic acid (GA) ($\geq 97\%$), catechin, epicatechin ($\geq 98\%$), rutin ($\geq 94\%$) and quercetin ($\geq 95\%$), were purchased from Sigma-Aldrich (St. Louis, MO, USA). Folin-Ciocalteu phenol reagent (2.1N) was purchased from Chem-Lab NV (Belgium). Ethanol, *n*-hexane, methanol, sodium carbonate, diethyl ether, acetonitrile, chloroform, acetic acid, potassium iodide, sodium thiosulphate, sodium hydroxide, and potassium hydroxide were purchased from Chemapol

(Czech Republic). All reagents used in this study were of analytical or chromatographic grade.

Methods

Sample preparation

The grape seeds were separated from *Feteasca Neagra* grape pomace, grown in the season of 2020, in the vineyards of Hincesti (FNH), Nisporeni (FNN), and Speia (FNS). The grapes were manually collected, at a distance of 1 day, and were further processed and fermented for 7 days in stainless steel containers, at a temperature of 25-26°C, under identical conditions, in the Laboratory of Micro-Vinification of the Department of Oenology and Chemistry of the Technical University of Moldova. The pomace was obtained by pressing and stored at a temperature of -20°C.

Obtaining lipophilic and hydrophilic extracts

The grape seeds, previously washed with distilled water, dried at 60°C for an hour, and ground (100 g), were extracted with *n*-hexane (1:3, v/v) for 48 hours, at room temperature. The mixture was filtered; the extraction procedure was repeated twice. The degreased seed meal was used as written below. The filtrates were combined and the solvent was removed by simple distillation, at a temperature of 60°C. The oil obtained in three repetitions was dried in the oven for 2 hours at 60°C, then treated with anhydrous sodium sulphate. The refractive indices were measured at a temperature of 20°C, using an ABBE Refractometer (ISOLAB Laborgeräte, Germany); the relative density (kg/L) was determined by the pycnometer method, at 20°C [23]; the mass fractions of moisture and volatile substances (%) were calculated by air oven method [23]. To determine the saponification values (mg KOH/1 g oil), a sample of oil was refluxed with potassium hydroxide alcoholic solution and the excess was further titrated with standard hydrochloric acid [23]. The acidity index (mg KOH/1 g oil) was determined by directly titrating the oil in a diethyl ether - alcoholic medium, against standard potassium hydroxide solution [24].

The hydrophilic extracts were obtained from grape seeds (I) separated from pomace and dried for 60 min, at a temperature of 60°C and, from degreased seeds (II), (left after extracting the oil with *n*-hexane). Each variant (I, II) was obtained in three replicates. The ground I and II seed samples, weighted with a three-decimal precision (0.500 g), were placed in test tubes with lids, together with 25 mL of solvent ethanol: water (60:40, v/v). They were used for extraction by *ultrasound-assisted method*

(ISOLAB Laborgeräte GmbH, Germany), for 30 min, at a temperature of 40°C (30 kHz and 300 W).

Extraction of the polyphenols from oil

The extraction of polyphenols from oil was conducted according to the methods described in the literature [25]. A sample of oil weighed on an analytical balance (1.25 g), was dissolved in 2.5 mL of *n*-hexane, while the hydrophilic compounds were extracted with 1.5 mL of a 60% aqueous methyl alcohol solution by vortex stirring. The lipophilic and hydrophilic phases were separated by centrifugation (3500 rpm for 10 min). The procedure was repeated twice. Both methanolic extracts were combined and then analysed.

Evaluation of physicochemical indicators of the seeds

Grape seeds were separated from pomace, washed with distilled water, and dried. The samples were brought to a constant mass, at 105°C. The content of dry matter was determined in the drying oven SPJ SLN 53 SMART (POL-EKO APARATURA, Poland) according to the known methods [26]. To determine the ash content, the samples were calcinated at a temperature of 550°C in a furnace (Omron E5CC, Lithuania) [27]. To calculate the mass fractions of the lipids, weighed samples of ground seeds were placed in three repetitions in a Soxhlet extractor SER 148 (VELP Scientifica, Italy) and extracted for 3 hours by continuous reflux with *n*-hexane in a ratio of 1:10 (sample: solvent m/v).

UV-Vis spectroscopic analysis of grape seed oil

Spectroscopic analysis of the grapeseed oil samples was performed on a DR5000 spectrophotometer (HACH- Lange GmbH, USA-Germany). The concentration of the samples was of 2% of oil in hexane. Carotenoid content was determined as per the calibration graph of standard β -carotene solutions in *n*-hexane and expressed as mg β -carotene equivalent per 100 g of sample (mg β CE/100 g). For the construction of the calibration curve, β -carotene solutions were prepared with a concentration range of 40 to 0.32 mg/L; the absorbances were recorded at a wavelength of 450 nm.

Quantification of total polyphenols

The total content of polyphenols (TPC) was determined using the DR5000 spectrophotometer (HACH- Lange GmbH, USA-Germany), by the method described in the literature [28], using the Folin-Ciocalteu Phenol reagent [29]. The polyphenol content was determined according to the calibration curve of the gallic acid

standard, expressed as mg of GAE/g of seeds. The calibration curve equation (0-500 mg/L, $R^2 = 0.9977$) was used to determine the TPC.

Determination of total flavonoid content

The total flavonoid content (TFC) was determined by the spectrophotometric method, using the same spectrophotometer, according to the method from the literature [28] with aluminium chloride. The absorbance reading for the samples was performed at a 430 nm wavelength. The TFC was determined according to the quercetin (0-160 mg/L, $R^2 = 0.9972$) and rutin (0-160 mg/L, $R^2 = 0.9991$) calibration curve. The results were expressed in milligrams equivalent of quercetin per gram of seeds (mg QE/g) or milligrams equivalent of rutin (mg RE/g).

Reversed-phase HPLC by gradient elution

The Provenience-i LC-2030C 3D Plus Chromatograph (Shimadzu, Japan), with integrated Photodiode Array Detector (PDA) was used. Extracts were filtered through 0.22 μ m PES-filters and chromatographed through C₁₈ type column "Phenomenex" (150 mm x 4.6 mm x 4 μ m x 80 Å) length at an oven temperature of 25°C and flow rate of 0.5 mL/min. Phases: Water (Phase A) and Acetonitrile (Phase B), both containing Acetic Acid 0.1% (v). Gradient program for Phase B: 2 min – 5%, 18 min – 40%, 20-24 min – 90%, 25 min – 5%.

Determination of DPPH• free radical scavenging activity

The antioxidant activities were determined using the reaction of DPPH• with the antioxidants contained in the samples, by the method described in the literature [30], using the DR5000 spectrophotometer (HACH- Lange GmbH, U.S.A.-Germany). Absorbances were read at a 515 nm wavelength. Results are interpreted using the Trolox (Thermo Fisher Scientific, USA) calibration curve (500-3.95 μ mol Trolox/L). To calculate the DPPH• scavenging effect, Eq.(1) was used.

$$DPPH (\% inhibition) = \frac{(A_0 - A_1)}{A_0} \cdot 100\% \quad (1)$$

where, A_0 - the absorbance of control, nm;

A_1 - the absorbance of standard, nm.

Statistical processing of experimental data

Three parallel measurements were conducted to exclude the results with accidental errors and those with high levels of uncertainty [31]. The statistical analysis was performed with

the IBM SPSS Statistics 23 and Microsoft Excel 2010 programs, with a significance level of 95% ($q < 0.05$). Errors ΔX were calculated as 2σ after 3 replications.

Results and discussion

Physicochemical indicators of the seeds from *Feteasca Neagra*

For the sample of the grape seeds of *Feteasca Neagra*, were determined the physicochemical properties and indicators. The mechanical composition of the seeds separated from the fermented pomace of *Feteasca Neagra* grapes, grown in three vineyards in the centre of Moldova, has insignificant differences. A quantity of 100 g of grape seeds collected in Hincesti comprise 58 more seeds than those collected in Speia and 196 more than in Nisporeni (Table 1).

Table 1

The mechanical composition of the seeds separated from *Feteasca Neagra* grape pomace.

Composition	FNN*	FNH*	FNS*
Seeds (g)	100	100	100
Seeds (pcs.)	3822±11	4018±15	3960±8

**Feteasca Neagra* grown on the vineyards from Hincesti (FNH), from Nisporeni (FNN), from Speia (FNS). Results are expressed as average $\pm 2\sigma$ ($n = 3$).

Analysis of the physicochemical indicators revealed that the seeds from Hincesti have a higher content of oil and dry matter. The ratio of the mass fraction of the oil to the mass of the dried seeds is by 11.87% lower in the seeds from Speia grapes, compared to Hincesti, and by 8.03% lower, compared to Nisporeni (Table 2).

Properties of *Feteasca Neagra* seed lipophilic extracts

The ground seeds of FNN, FNH, FNS (previously washed and dried at 60°C for an hour) were extracted with an organic solvent (*n*-hexane), at room temperature. The oil obtained using a cold organic solvent, has an almost 20% lower yield compared with the Soxhlet method. The oil samples have the following organoleptic characteristics: relatively transparent; a pleasant taste of oil; lack of foreign smell and taste. The use of an organic solvent is not a suitable method for obtaining edible oils. Contrariwise, cold pressing is considered to be a harmless method of obtaining vegetable oils as it preserves their functional components [32,33]. The conducted research has shown that hexane, at low temperatures, solubilizes well the fat-soluble components of plant matter: chlorophylls, chlorophyll derivatives, carotenes, tocopherols, sterols, etc. This method could be used in analysing the composition of grapeseed oil.

The physicochemical properties and quality indices of the oil samples (Table 3), extracted with *n*-hexane, at room temperature, from *Feteasca Neagra* grape seeds were determined. The acidity indices of the oil samples are low, with values between 0.51 ± 0.05 and 0.56 ± 0.08 mg KOH/1 g oil. The peroxide values are low, and could not be determined by the classical titrimetric method. The analysed oil samples have the content of water and of volatile substances within the range of 0.073–0.081%. The low values of peroxide, acidity, and other indices are due to the extraction method used.

Table 2

Physicochemical indicators of the seeds from *Feteasca Neagra* grape pomace.

Seed samples	Moisture, %DW	Content of dry matter, %DW	Ash content, %DW	Mass fraction of oil in 100 g of dried seeds, %
FNN	9.67±0.12	90.34±0.16	2.41±0.11	10.10±1.53
FNH	6.53±0.01	93.46±0.01	2.37±0.05	10.53±1.12
FNS	10.13±0.04	89.87±0.04	2.44±0.05	9.30±0.05

DW: dry weight; results are expressed as average $\pm 2\sigma$ ($n = 3$).

Table 3

Quality indices of the *Feteasca Neagra* grapeseed oil, extracted with *n*-hexane at room temperature.

Oil sample	Refractive index	Relative density	Acidity index	Saponification index	Moisture and volatile substances, %
FNN	1.4763±0.0002	0.921±0.011	0.56±0.08	189.7±0.2	0.078±0.002
FNH	1.4764±0.0002	0.921±0.011	0.53±0.02	188.3±0.4	0.073±0.002
FNS	1.4760±0.0001	0.922±0.010	0.51±0.05	189.5±0.6	0.081±0.002

Results are expressed as average $\pm 2\sigma$ ($n = 3$).

The UV-Vis absorption spectra for the FNN, FNH, FNS oil samples were recorded, with an essential difference in the 300–700 nm range. The absorbance values of the oil obtained from *Feteasca Neagra* grape seeds, cultivated in Hincesti, show a higher content of pheophytins (derived from chlorophylls, after the loss of magnesium ions), as per the absorbance values recorded in the 600–620, 650–700 nm intervals (Figure 1) [34].

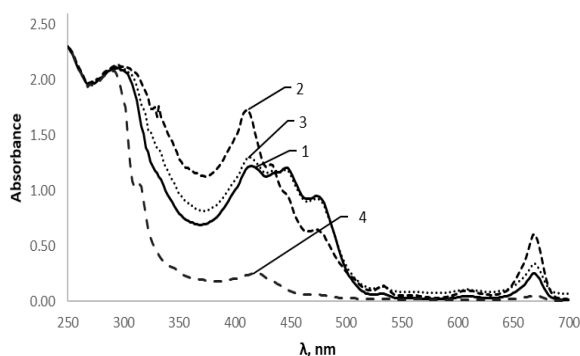


Figure 1. UV-Vis spectra for grapeseed oil samples: from FNN - 1; from FNH - 2; from FNS - 3; unrefined from the supermarket - 4.

According to characteristic absorption bands at 400–540 nm, FNN and FNS grapeseed oils have an increased content of carotenoids. The concentration of carotenoids was calculated using the calibration curve constructed on standard β -carotene solutions. The FNH seed oil has a carotenoid content of 38.71 ± 0.44 mg β CE/100 g oil. FNN and FNS oils have a high content of carotenoids, 49.71 ± 0.43 and 48.53 ± 0.47 mg β CE/100 g oil, respectively. These values fall within the total carotenoid content range of 33.85–59.85 mg β CE/100 g oil, determined for the cold-pressed grape oil by Brazilian researchers [35]. A similar result was recorded for palm oil: 32.7–45.8 mg β CE/100 g of crude palm oil [36]. However, other researchers reported a much lower content of carotenoids in grape seed oil [13].

In the UV-Vis spectra of the unrefined grapeseed oil, local produce, the absorbances for carotenoids and chlorophyll derivatives are missing. Due to the high content of chlorophyll derivatives, the FNH oil is of olive-green colour. The oils from grapes from Nisporeni and Speia are yellow, due to the increased content of carotenoids. Therefore, the colour difference of the 3 oil samples is due to the content of antioxidants. The grapeseed oil P has the lightest colour, probably as a result of thermal treatment and subsequent purification.

The total polyphenol content

Polyphenols are mono- or polycyclic compounds with several hydroxyl functional groups (which may also contain carboxyl and carbonyl groups) attached to aromatic rings. Due to their structure, polyphenols have reducing properties. They form complex compounds with the Folin-Ciocalteu reagent, which absorb in the visible range of the spectrum at 750 nm [25,28]. The components of the oil (phenolic compounds, catechins, epicatechins, oligomeric procyanidins, etc.) were extracted in the hydrophilic phase of the aqueous methyl alcohol solution; it was further spectrophotometrically analysed. The grape seed oils have a reduced content of phenolic compounds (Figure 2), with values between approx. 0.005 and 0.004%; the highest content being in the lipophilic extract from FNN, of 4.89 ± 0.05 mg GAE/100 g of sample. These values are comparable to those from literature, where the total amount of polyphenols in cold-pressed grape seed oil varies from 48 to 153 mg GAE/kg of oil [6]. Other studies have established that the mass part of the phenolic compounds in cold-pressed grape oil constitutes 0.013–0.019% of the total mass of polyphenols embedded in grape seeds; with a reduced TPC of 2.9 mg GAE/kg oil, and a content of catechins and epicatechins of 1.3 mg/kg of oil [7].

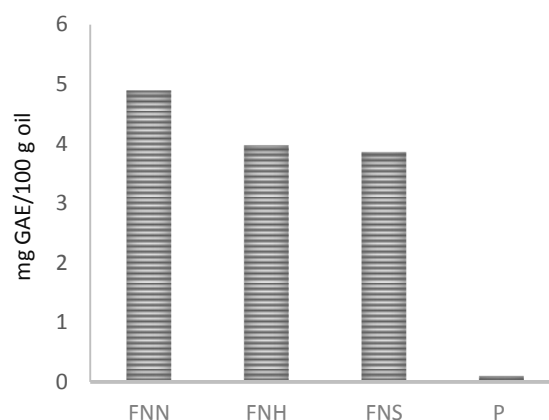


Figure 2. TPC in grapeseed oil. P -unrefined oil from the supermarket. (Results are expressed as average $\pm 2\sigma$ ($n=3$)).

It can be concluded that the lipophilic extracts from the *Feteasca Neagra* grape seeds, obtained at low temperatures and using an organic solvent, contain a higher quality and quantity of functional compounds, if compared with grapeseed oil P from the market. However, TPC in grapeseed oils is much lower than the TPC in crude olive oils from the market, which has an average value of 25 mg GAE/100 g of sample,

or 0.025%. The olive oil, extracted with organic solvents (chloroform-methanol), has a content of polyphenols of up to 57.4 mg GAE/100 g of oil, according to the bibliography [25].

Properties of hydrophilic extracts from *Feteasca Neagra* seeds

The TPC was determined for the hydrophilic extracts I (obtained from ground grape seeds) and II (obtained from ground and degreased seeds, after extracting the oil). According to the results that can be seen in Figure 3, the content of total soluble polyphenols is by 19.26–28.30% higher in all of the extracts II than in the seed extracts I. Hence, after removing the lipids from the seed, the hydrophilic compounds are better solubilized by the polar solvent. The highest TPC, of approximately 4.02%, was registered in extracts FNN II. It can be seen in Figure 3 that in extracts FNN I and II, the TPC of 32.28 ± 2.03 and 40.15 ± 0.16 mg GAE/g seeds respectively, is twice higher than in extracts FNH and FNS.

Several studies state that this difference is due to the influence that various factors can have on the content of polyphenols in grapes and grape seeds, such as humidity, soil fertility, and nitrogen content in the soil, methods of cultivation, climatic conditions and the ripeness of the grapes.

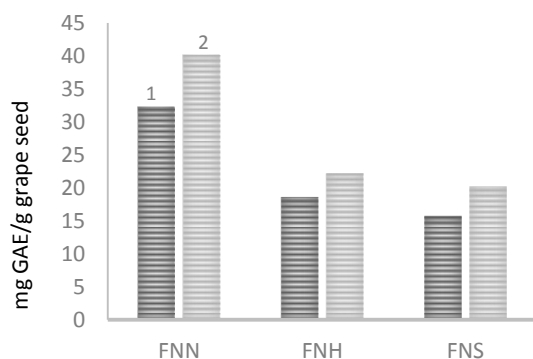


Figure 3. TPC in grape seed extracts I (1) and in grape seed extracts II (2). (Results are expressed as average $\pm 2\sigma$ ($n=3$)).

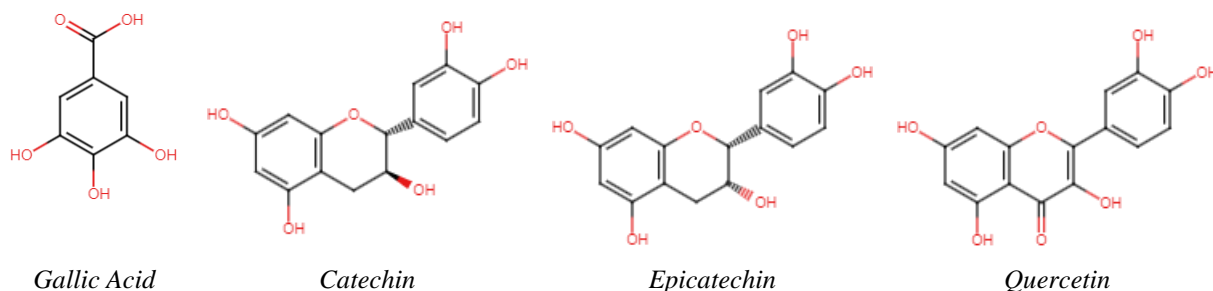


Figure 4. Common polyphenols found in grape seeds.

Another index of grape ripeness, besides the sugar content, is the phenolic ripeness, or changes in the tannin content of the grapes. Grapes harvested from vineyards planted on moderately fertile soil, with a longer sunlight exposure, will have a higher content of polyphenols. Sun rays activate the cluster formation and the synthesis of the secondary metabolites, such as quercetin, which is a good indicator of the amount of sunlight to which the grapes have been exposed [37,38]. It should be mentioned that the TPC values for FNN, FNH, and FNS seeds fall within the data gathered from literature (regarding the content of extractable polyphenols in the seeds of different grape varieties), which is between 22.47 and 72.01 mg GAE/g of dry sample [17], and between 34.63 and 71.24 mg GAE/g of fresh seeds [39].

Gallic acid derivatives and flavonoids, among which flavan-3-ols ((+)-catechin and (-)-epicatechin) and flavonol (quercetin), account for a big part from the total phenolic compounds contained in grape seeds [40], Figure 4.

The TFC in the extracts I and II of *Feteasca Neagra* seeds was determined by the spectrophotometric method, according to the calibration curves recorded for different concentrations of quercetin and rutin. The method is based on the formation of yellow aluminium compounds (III), which absorb in the range of 404–430 nm. Chelate formation is due to the C-3', C-4' hydroxyl groups from ring B and C-3 from ring C of flavan-3-ols and flavon-3-ols (Figure 4), hence quercetin, catechin or rutin solutions can be used as reference substances.

Extract I, from dried at 60°C for an hour, and ground grape seeds, has a higher content of soluble flavonoids (Table 4). In all of the I and II extracts, a higher portion of flavonoids is in form of glycosides; the concentration was calculated in relation to rutin, which is a disaccharide (α -L-rhamnopyranosyl-(1 \rightarrow 6)- β -D-glucopyranoside of quercetin).

A reason for this could be that the functional compounds of the seeds are mostly stored as glycosides, which are also a resource for the growth of the plant. The values calculated in quercetin equivalents for all samples match the data obtained by a group of researchers, who determined by the colorimetric method, with AlCl_3 , that the TFC in 30 grape varieties varies between 1.130 and 3.957 mg QE/g of fresh seeds, depending on the variety [39].

According to the results shown in Table 4, all type I extracts have a higher TFC. TPC, on the contrary, is higher in extracts type II of degreased seeds (Figure 3). This difference is a consequence of the obtaining method that is used: type II extracts were obtained from grape seeds that were washed with distilled water, dried and extracted with *n*-hexane. As a result, the protective layer of tannins (soluble proanthocyanidins) was removed from the surface of the seeds. According to the results (Table 4), *Feteasca Neagra* seeds I, cultivated on the vineyards of Nisporeni, have a higher content of flavonoids, with the following total concentration: 2.74 ± 0.09 mg QE/g of seeds (dried at 60°C , 60 min) however, the concentration expressed in mg RE/g is lower compared to FNH and FNS samples.

The difference between the content of biologically active substances in the FNN, FNH, FNS seeds separated from fermented pomace is admissible within the same grape variety. The phenomenon can be explained by the cultivation conditions [10,11,41] such as altitude, fertility, the physicochemical properties of the soil in the micro zone of the Western Suburbs of Codri, where the Nisporeni wine area is located [42], as well as the viticultural practices [43]. The rest of the technological techniques used (harvesting, processing, grape fermentation, separation of the seeds from the pomace frozen at -20°C , obtaining of the hydrophilic and lipophilic extracts) were done in the same conditions.

Reversed-phase HPLC assay results

To identify the phenolic components in the hydrophilic extracts I and II, their retention time and spectral characteristics were compared to those of the standards: gallic acid (GA), (+)-catechin, and (-)-epicatechin. In addition to the peaks of the available standards, chromatograms showed the presence of several compounds with UV-Vis (PDA) spectra, characteristic for GA-derivates and flavanols A, B, and C, which are yet unidentified compounds, presumably glucosides of Catechin and/or of Epicatechin (Figure 5).

Table 4

TFC concentration in seed extracts of *Feteasca Neagra* grapes.

Sample	TFC			
	Extracts I		Extracts II	
	mg QE/g	mg RE/g	mg QE/g	RE/g
FNN	2.74 ± 0.09	5.44 ± 0.21	1.93 ± 0.08	4.03 ± 0.05
FNH	2.62 ± 0.15	6.99 ± 0.16	1.76 ± 0.05	4.77 ± 0.12
FNS	2.44 ± 0.11	6.65 ± 0.30	1.75 ± 0.03	4.70 ± 0.08

Results are expressed as average $\pm 2\sigma$ ($n = 3$).

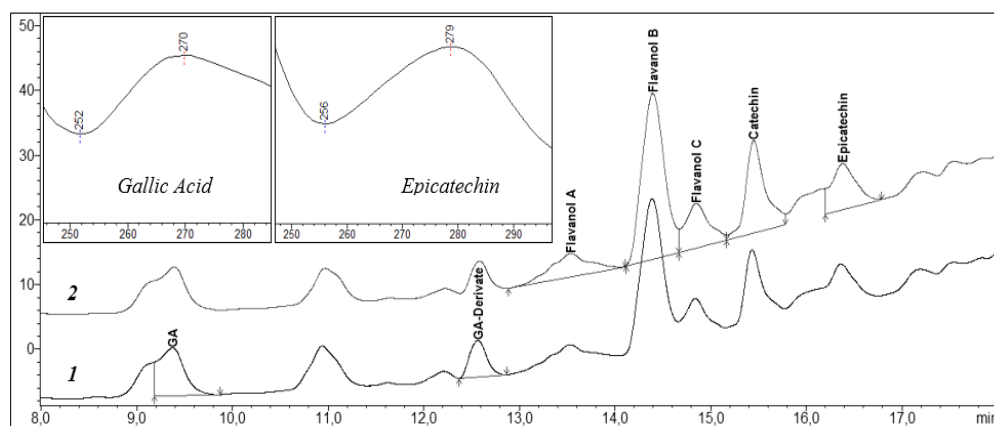


Figure 5. *Feteasca Neagra* grape seeds polyphenols-rich extract chromatograms: (at 271 nm - 1; at 279 nm - 2) and UV-Vis spectra of confirmed compounds - gallic acid (GA) and epicatechin.

The HPLC measurement results are consistent with the results recorded by spectrophotometric methods. The highest content of bioactive substances was detected in FNN extracts I and II. Extracts I from all of the seed samples have a higher content of catechin monomers, hence, a total content of flavanols is higher than in extracts II, from degreased seeds (Table 5).

The values of the total flavanols content in extracts I is within the 490.2 and 699.2 mg/100 g of seed range, on average, by 11% more than in extracts II. The content of gallic acid and gallates is higher in extracts II. Also confirmed by the spectrophotometric analysis (Figure 3), degreasing the seeds favours the release of these polar compounds from the grape seeds. The total content of soluble phenols determined by HPLC is lower than the one determined by the spectrophotometric method. Some non-phenolic substances, organic acids, and saccharides, may interact with the Folin-Ciocalteu reagent, thus TPC may be overestimated. At the same time, the total content of flavanols determined by the HPLC method (Table 5) is close to the TFC values recorded by the spectrophotometric method, with AlCl_3 (Table 4). The difference between the TPC values obtained by the Folin-Ciocalteu method and by HPLC chromatography was also recorded by Greek researchers [44], thus TPC dosed colorimetrically

in 9 grape varieties ranged from 143 to 2228 mg GAE/100 g seeds, while by the HPLC method, values between 55 and 964 mg/100 g seeds were obtained. This source mentions a GA content (measured by the HPLC method) between 1.15 and 17.9 mg/100 g; a content of catechins between 36.4 and 454 mg/100 g, and a content of epicatechins between 17.5 and 249 mg/100 g of seeds. Another study, performed on 7 grape varieties, showed a content of gallic acid between 44.01 and 221.41 mg/100 g, and a content of catechins between 56.42 and 480.50 mg/100 g of fresh grape seeds [45].

Determination of DPPH• Free Radical Scavenging Activity of the grape seeds

The DPPH method implies the spectrophotometric measurement of the changes in the concentration of the DPPH• radical, arising from its reaction with an antioxidant. A freshly prepared methanolic DPPH• solution is purple. The colour fades in the presence of antioxidants. The antioxidant molecules can neutralize the free DPPH• radical, turning it into a colourless reaction product (DPPH-H), reducing so the absorbance of the solution. Consequently, a higher content of antioxidants leads to a more colourless solution. The Trolox equivalent antioxidant capacity assay (TEAC) of the oil samples and the hydrophilic FNN, FNH, FNS extracts was assessed (Table 6).

Table 5

The phenolic compounds identified and quantified using HPLC analysis in *Feteasca Neagra* grape seed extracts (mg/100 g seeds).

Samples	Extracts I					
	Catechin	Epicatechin	Σ Flavanols	Gallic acid	Gallic acid derivatives	Σ Gallates
FNN	80.51 \pm 0.91	49.43 \pm 0.56	699.2 \pm 7.9	18.26 \pm 0.21	14.31 \pm 0.17	32.58 \pm 0.37
FNH	44.49 \pm 0.50	46.45 \pm 0.52	525.9 \pm 5.9	17.68 \pm 0.20	13.78 \pm 0.16	31.46 \pm 0.36
FNS	45.56 \pm 0.51	32.14 \pm 0.36	490.2 \pm 5.5	16.92 \pm 0.19	13.30 \pm 0.15	30.22 \pm 0.34
	Extracts II					
	Catechin	Epicatechin	Σ Flavanols	Gallic acid	Gallic acid derivatives	Σ Gallates
FNN	67.33 \pm 0.76	60.26 \pm 0.68	585.6 \pm 6.6	21.09 \pm 0.24	15.30 \pm 0.18	36.39 \pm 0.41
FNH	49.77 \pm 0.56	51.95 \pm 0.59	479.9 \pm 5.6	20.09 \pm 0.23	14.58 \pm 0.17	34.66 \pm 0.39
FNS	40.15 \pm 0.45	33.71 \pm 0.38	457.5 \pm 5.2	21.26 \pm 0.25	14.60 \pm 0.17	36.13 \pm 0.41

Results are expressed as average $\pm 2\sigma$ ($n = 3$).

Table 6

Antioxidant activity of extracts of *Feteasca Neagra* seeds.

Sample	The Trolox equivalent antioxidant capacity assay					
	Oil		Extracts I		Extracts II	
	% of inhibition DPPH•	Concentration, $\mu\text{mol Trolox/L}$	% of inhibition DPPH•	Concentration, $\mu\text{mol Trolox/L}$	% of inhibition DPPH•	Concentration, $\mu\text{mol Trolox/L}$
FNN	26.11	0.08 \pm 0.02	93.81	288.27 \pm 0.22	91.70	281.66 \pm 0.36
FNH	25.04	0.07 \pm 0.02	93.28	286.62 \pm 0.18	91.44	280.84 \pm 0.34
FNS	25.33	0.07 \pm 0.01	93.54	287.45 \pm 0.27	92.16	283.11 \pm 0.27

All results are reported as the mean of three replicates $\pm 2\sigma$.

To determine the antioxidant activity of the oil samples, extracts were obtained from 1.25 g oil with a 3 mL aqueous methanol solution of 60%. The antioxidant activity was determined for the hydrophilic extracts with the 1:50 (m/v) seed/solvent ratio.

Both our research and the bibliographic data [46,47] prove that fermentation, the only significant process that occurs before the pomace is obtained, does not induce considerable chemical changes and does not affect the antioxidant properties of the grape seeds. It has been established that the hydrophilic and lipophilic extracts of *Feteasca Neagra* grape seeds have an increased antioxidant activity, with the strongest free radical scavenging activity being detected in the hydrophilic extracts I and II, with a DPPH• scavenging effect of almost 91.70 and 93.81%, an equivalent of 281.66 and 288.27 µmol Trolox/L (1408 and 1441 µmol Trolox/100 g of seeds). The antioxidant activity of the extracts depends on the concentration of polyphenols as well as on the concentration of other substances with antioxidant properties (carotenoids, tocopherols, etc.). The data recorded by us fall within the range of the results obtained by a group of researchers who studied the difference between the quantitative and qualitative content of grape seeds from nine clones 'Karaerik' (Turkish table grape cultivar), harvested from different vineyards. The researchers determined that the antioxidant potential of the above-mentioned grape seeds ranged from 1510 to 1918 µmol Trolox/100 g of fresh seeds [48].

The research results have confirmed that grape seeds have a higher TPC and antioxidant potential than most fruits [49]. The seeds recovered from winemaking by-products are rich sources of antioxidants; further research should be conducted in order to identify new areas of applicability and the value the winemaking by-products could bring to the pharmaceutical and food industry.

Conclusions

The conducted research showed that grape seeds from wine by-products are a cheap and accessible source of phytonutrients and biologically active substances. Thus, the properties of the lipophilic and hydrophilic extracts of seeds separated from fermented pomace of *Feteasca Neagra* grapes, cultivated in vineyards from Nisporeni (FNN), Hincesti (FNH), and Speia (Anenii-Noi region) (FNS), in the season of 2020, were elucidated.

According to the UV-Vis absorbance values, *Feteasca Neagra* grape seed oil has an

increased content of chlorophyll derivatives, and the concentration of carotenoids varies from 38.71 to 49.71 mg βCE/100 g oil. The content of total soluble polyphenols (TPC), in all of the oil samples, is a reduced one, FNN having the highest TPC of 0.005%.

It was determined that TPC for the FNN hydrophilic extracts (32.28 and 40.15 mg GAE/g seeds) is almost twice higher than the TPC of FNH and FNS. Studies have shown that degreasing the seeds leads to better solubilization of the polar compounds, which leads to a 28.30% increase in TPC. Nevertheless, washing and extracting the seeds with *n*-hexane has as a consequence the removal of the protective layer of soluble proanthocyanidins from the surface of the seeds, leading to a reduced content of total soluble flavonoids (TFC) in the extracts.

The HPLC measurement results are consistent with the results recorded by spectrophotometric methods; hydrophilic extracts from ground seeds have a higher TFC, with values between 490.20 and 699.20 mg/100 g of seeds, which is on average by 11% higher than that of extracts from degreased ground grape seeds.

It has been established that the hydrophilic and lipophilic extracts of *Feteasca Neagra* grape seeds have an increased antioxidant activity. The strongest free radical scavenging activity was detected in the hydrophilic extracts, with a DPPH• scavenging effect of almost 91.70 and 93.81%, an equivalent of 1408 and 1441 µmol Trolox /100 g of seeds.

The seeds recovered from winemaking by-products retain their antioxidant potential and are an accessible source of phytonutrients and biologically active compounds, which can be recovered and used by the pharmaceutical industry for the production of supplements or as natural additives for functional foods.

Acknowledgments

The research was carried out with the support of the Moldova State project 20.80009.5107.09 – “Improvement of food quality and safety by biotechnology and food engineering”.

References

1. The National Office of Vine and Wine (ONVV), ONVV's Annual report. 2019, 80 p. (in Romanian). <https://wineofmoldova.com/wp-content/uploads/2021/02/RAPORT-ANUAL-2019.pdf>
2. Patel, S. Grape seeds: Grape Seeds: Agro-Industrial Waste with Vast Functional Food

- Potential. In: Emerging Bioresources with Nutraceutical and Pharmaceutical Prospects. Applied Environmental Science and Engineering for a Sustainable Future. Springer:Cham, 2015, pp. 53–69. DOI: https://doi.org/10.1007/978-3-319-12847-4_6
3. Gaina, B.; Cobirman, G.; Golubi, R. Viticultural and wine secondary products and their use (information study). Akademos Journal of Science, Innovation, Culture and Art, 2018, 1(48), pp. 70–74. (in Romanian). <http://akademos.asm.md/taxonomy/term/101>
4. Duca, Gh. Wine and by-products. Chishinau: Stiinta, 2011, 352 p. (in Romanian).
5. Thorngate, J.H.; Singleton, V.L. Localization of procyanidins in grape seeds. American Journal of Enology and Viticulture, 1994, 45(2), pp. 259–262. <https://www.ajevonline.org/content/45/2/259>
6. Rombaut, N.; Savoie, R.; Thomasset, B.; Castello, J.; Van Hecke, E.; Lanoisellè, J.L. Optimization of oil yield and oil total phenolic content during grape seed cold screw pressing. Industrial Crops and Products, 2015, 63, pp. 26–33. DOI: <http://dx.doi.org/10.1016/j.indcrop.2014.10.001>
7. Maier, T.; Schieber, A.; Kammerer, D.R.; Carle, R. Residues of grape (*Vitis vinifera* L.) seed oil production as a valuable source of phenolic antioxidants. Food Chemistry, 2009, 112(3), pp. 551–559. DOI: <https://doi.org/10.1016/j.foodchem.2008.06.005>
8. Xia, E.Q.; Deng, G.F.; Guo, Y.J.; Li, H.B. Biological activities of polyphenols from grapes. International Journal Molecular Sciences, 2010, 11(2), pp. 622–646. DOI: <http://dx.doi.org/10.3390/ijms11020622>
9. Scalbert, A.; Manach, C.; Morand, C.; Rémésy, C.; Jiménez, L. Dietary polyphenols and the prevention of diseases. Critical Reviews in Food Sciences and Nutrition, 2005, 45(4), pp. 287–306. DOI: <http://dx.doi.org/10.1080/10408690509096>
10. Garrido, I.; Uriarte, D.; Hernandez, M.; Llerena, J.L.; Valdes, M.E.; Espinosa, F. The evolution of total phenolic compounds and antioxidant activities during ripening of grapes (*Vitis vinifera* L., cv. *Tempranillo*) grown in semiarid region: Effects of cluster thinning and water deficit. International Journal of Molecular Sciences, 2016, 17(11), pp. 1923. DOI: <https://doi.org/10.3390/ijms17111923>
11. Reynolds, A.G. Ed. Managing wine quality: Viticulture and wine quality. Woodhead Publishing: Cambridge, 2010, pp. 365–444. DOI: <https://doi.org/10.1533/9781845699284.3.365>
12. Gaweł, R.; Day, M.; Van Sluyter, S.C.; Holt, H.; Waters, E.J.; Smith, P.A. White wine taste and mouthfeel as affected by juice extraction and processing. Journal of Agricultural and Food Chemistry, 2014, 62(41), pp. 10008–10014. DOI: <https://doi.org/10.1021/jf503082v>
13. Mohamed, H.B.; Duba, K.S.; Fiori, L.; Abdelgawed, H.; Tlili, I.; Tounekti, T.; Zrig, A. Bioactive compounds and antioxidant activities of different grape (*Vitis vinifera* L.) seed oils extracted by supercritical CO₂ and organic solvent. LWT-Food Sciences and Technology, 2016, 74, pp. 557–562. DOI: <https://doi.org/10.1016/j.lwt.2016.08.023>
14. Ghouila, Z.; Laurent, S.; Henoumont, C.; Vanderelst, L.; Muller, N.R.; Baaliouamer, A. Rich extract on total polyphenols and antioxidant activity obtained by conventional and non-conventional methods from *Ahmeur bouamer* grape seed. Journal of Fundamental and Applied Sciences, 2016, 8(3), pp. 692–711. DOI: <https://doi.org/10.4314/jfas.v8i3.3>
15. Mandić, A.I.; Dilas, S.M.; Četković, G.S.; Čanadanović-Brunet, J.M.; Tumbas, V.T. Polyphenolic composition and antioxidant activities of grape seed extract. International Journal of Food Properties, 2008, 11(4), pp. 713–726. DOI: <https://doi.org/10.1080/10942910701584260>
16. Kalli, E.; Lappa, I.; Bouchagier, P.; Tarantilis, P.A.; Skotti, E. Novel application and industrial exploitation of winery by-products. Bioresources and Bioprocessing, 2018, 5, 46, pp. 1–21. DOI: <https://doi.org/10.1186/s40643-018-0232-6>
17. Xu, C.; Yagiz, Y.; Zhao, L.; Simonne, A.; Lu, J.; Marshall, M.R. Fruit quality, nutraceutical and antimicrobial properties of 58 muscadine grape varieties (*Vitis rotundifolia* Michx.) grown in United States. Food Chemistry, 2017, 215, pp. 149–156. DOI: <https://doi.org/10.1016/j.foodchem.2016.07.163>
18. Iannone, M.; Mare, R.; Paolino, D.; Gagliardi, A.; Froio, F.; Cosco, D.; Fresta, M. Characterization and *in vitro* anticancer properties of chitosan-microencapsulated flavan-3-ols-rich grape seed extracts. International Journal of Biological Macromolecules, 2017, 104(A), pp. 1039–1045. DOI: <https://doi.org/10.1016/j.ijbiomac.2017.07.022>
19. Ferri, M.; Rondini, G.; Calabretta, M.M.; Michelini, E.; Vallini, V.; Fava, F.; Roda, A.; Minnucci, G.; Tassoni, A. White grape pomace extracts, obtained by a sequential enzymatic plus ethanol-based extraction, exert antioxidant, anti-tyrosinase and anti-inflammatory activities. New Biotechnology, 2017, 39(A), pp. 51–58. DOI: <https://doi.org/10.1016/j.nbt.2017.07.002>
20. Vaisman, N.; Niv, E. Daily consumption of red grape cell powder in a dietary dose improves cardiovascular parameters: a double blind, placebo-controlled, randomized study. International Journal of Food Sciences and Nutrition, 2015, 66(3), pp. 342–349. DOI: <http://dx.doi.org/10.3109/09637486.2014.1000840>
21. Ismail, A.F.M.; Salem, A.A.M.; Eassawy, M.M.T. Hepatoprotective effect of grape seed oil against carbon tetrachloride induced oxidative stress in liver of gamma-irradiated rat. Journal of

- Photochemistry and Photobiology B: Biology, 2016, 160, pp. 1–10. DOI: <http://dx.doi.org/10.1016/j.jphotobiol.2016.03.027>
22. Weseler, A.R.; Bast, A. Masquelier's grape seed extract: from basic flavonoid research to a well-characterized food supplement with health benefits. *Nutrition Journal*, 2017, 16(5), pp. 1–19. DOI: <https://doi.org/10.1186/s12937-016-0218-1>
 23. Food Safety and Standards Authority of India (FSSAI), Manual of Methods of Analysis of Foods. Oils and Fats. 2015, 96 p. https://www.fssai.gov.in/upload/uploadfiles/files/OILS_AND_FAT.pdf
 24. ISO 1740:2004 Milkfat products and butter - Determination of fat acidity (Reference method). <https://standards.iteh.ai/catalog/standards/iso/5e98f5b6-2fe4-4b54-8846-ac22f53a45da/iso-1740-2004>
 25. Gutfinger, T. Polyphenols in olive oils. *Journal of the American Oil Chemists Society*, 1981, 58(11), pp. 966–968. DOI: <https://doi.org/10.1007/BF02659771>
 26. ISO 665:2020 Oil seeds - Determination of moisture and volatile matter content. <https://standards.iteh.ai/catalog/standards/iso/ca9695f-bca8-4bb8-afee-ba613cddf714/iso-665-2020>
 27. ISO 749:1977 - Oilseed residues - Determination of total ash. <https://standards.iteh.ai/catalog/standards/iso/9da2aeab-73ec-45d1-9bdc-b7222990aad0/iso-749-1977>
 28. Bouyahya, A.; Dakka, N.; Talbaoui, A.; Moussaoui, N.El.; Abrini, J.; Bakri, Y. Phenolic contents and antiradical capacity of vegetable oil from *Pistacia lentiscus* (L). *Journal of Materials and Environmental Science*, 2018, 9(5), pp. 1518–1524. DOI: <https://doi.org/10.26872/jmes.2018.9.5.167>
 29. Singleton, V.L.; Rossi, J.A. Colorimetry of total phenolics with phosphomolybdic-phosphotungstic acid reagents. *American Journal of Enology and Viticulture*, 1965, 16(3), pp. 144–158. <https://www.ajevonline.org/content/16/3/144>
 30. Paulpriya, K.; Packia Lincy, M.; Tresina Soris, P.; Veerabahu Ramasamy, M. *In vitro* antioxidant activity, total phenolic and total flavonoid contents of aerial part extracts of *Daphniophyllum neilgherrense* (wt.) Rosenth. *Journal of Bio Innovation*, 2015, 4(6), pp. 257–268. www.jbino.com
 31. ISO 5725-1:1994 Accuracy (trueness and precision) of measurement methods and results. <https://www.iso.org/standard/11833.html>
 32. Codex Alimentarius, Standard for Named Vegetable Oils (CXS 210 - 1999). Essential Composition and Quality Factors. <https://www.fao.org/3/y2774e/y2774e04.htm>
 33. Rubalya, V.S.; Neelamegam, P. Selective ABTS and DPPH- radical scavenging activity of peroxide from vegetable oils. *International Food Research Journal*, 2015, 22(1), pp. 289–294. [http://www.ifrj.upm.edu.my/22%20\(01\)%202015/\(42\).pdf](http://www.ifrj.upm.edu.my/22%20(01)%202015/(42).pdf)
 34. Absorption spectra of chlorophyll and carotenoids. www.cfb.unh.edu
 35. Shinagawa, F.B.; de Santana, F.C.; Araujo, E.; Purgatto, E.; Mancini-Filho, J. Chemical composition of cold pressed Brazilian grape seed oil. *Food Science and Technology*, 2018, 38(1), pp.164–171. DOI: <https://doi.org/10.1590/1678-457X.08317>
 36. Szydłowska-Czerniak, A.; Trokowski, K.; Karlovits, G.; Szlyk, E. Effect of refining processes on antioxidant capacity, total contents of phenolics and carotenoids in palm oils. *Food Chemistry*, 2011, 129(3), pp.1187–1192. DOI: <https://doi.org/10.1016/j.foodchem.2011.05.101>
 37. Reshef, N.; Walbaum, N.; Agam, N.; Fait, A. Sunlight modulates fruit metabolic profile and shapes the spatial pattern of compound accumulation within the grape cluster. *Frontiers in Plant Science*, 2017, 8, 70, pp. 1–20. DOI: <https://doi.org/10.3389/fpls.2017.00070>
 38. Haselgrove, L.; Botting, D.; van Heeswijck, R.; Høj, P.B.; Dry, P.R.; Ford, C.; Land, P.G.I. Canopy microclimate and berry composition: The effect of bunch exposure on the phenolic composition of *Vitis vinifera* L. cv. *Shiraz* grape berries. *Australian Journal of Grape and Wine Research*, 2000, 6(2), pp.141–149. DOI: <https://doi.org/10.1111/j.1755-0238.2000.tb00173.x>
 39. Tang, G.Y.; Zhao, C.N.; Liu, Q.; Feng, X.L.; Xu, X.Y.; Cao, S.Y.; Meng, X.; Li, S.; Gan, R.Y.; Li, H.B. Potential of grape wastes as a natural source of bioactive compounds. *Molecules*, 2018, 23(10), 2598, pp. 1–20. DOI: <https://doi.org/10.3390/molecules23102598>
 40. Georgiev, V.; Ananga, A.; Tsołova, V. Recent advances and uses of grape flavonoids as nutraceuticals. *Nutrients*, 2014, 6(1), pp. 391–415. DOI: <https://doi.org/10.3390/nu6010391>
 41. Teixeira, N.; Mateus, N.; de Freitas, V.; Oliveira, J. Wine industry by-product: Full polyphenolic characterization of grape stalks. *Food Chemistry*, 2018, 268, pp. 110–117. DOI: <https://doi.org/10.1016/j.foodchem.2018.06.070>
 42. Ursu, A. Moldova's Soils. Chishinau: Stiinta, 2012, 324 p. (in Romanian).
 43. Maante-Kuljus, M.; Rätsep, R.; Moor, U.; Mainla, L.; Põldma, P.; Koort, A.; Karp, K. Effect of vintage and viticultural practices on the phenolic content of hybrid winegrapes in very cool climate. *Agriculture*, 2020, 10(5), 169, pp. 1–13. DOI: <https://doi.org/10.3390/agriculture10050169>
 44. Guendez, R.; Kallithraka, S.; Makris, D.P.; Kefalas, P. Determination of low molecular weight polyphenolic constituents in grape (*Vitis vinifera* sp.) seed extracts: Correlation with antiradical activity. *Food*

- Chemistry, 2005, 89(1), pp. 1–9. DOI: <https://doi.org/10.1016/j.foodchem.2004.02.010>
45. Özcan, M.M.; Al Juhaimi, F.; Gülcü, M.; Uslu, N.; Geçgel, Ü. Determination of bioactive compounds and mineral contents of seedless parts and seeds of grapes. *South African Journal of Enology and Viticulture*, 2017, 38(2), pp. 212–220. DOI: <http://dx.doi.org/10.21548/38-2-1605>
 46. Dwyer, K.; Hosseinian, F.; Rod, M. The market potential of grape waste alternatives. *Journal of Food Research*, 2014, 3(2), pp. 91–106. DOI: <https://doi.org/10.5539/jfr.v3n2p91>
 47. Ratnasooriya, C.C.; Rupasinghe, H.P.V.; Jameison, A.R. Juice quality and polyphenol concentration of fresh fruits and pomace of selected Nov Scotia-grown grape cultivars. *Canadian Journal of Plant Science*, 2010, 90(2), pp. 193–205. DOI: <https://doi.org/10.4141/CJPS09137>
 48. Kupe, M.; Karatas, N.; Unal, M.S.; Ercisli, S.; Baron, M.; Sochor, J. Phenolic composition and antioxidant activity of peel, pulp and seed extracts of different clones of the turkish grape cultivar ‘Karaerik’. *Plants*, 2021, 10(10), 2154, pp. 1–15. DOI: <https://doi.org/10.3390/plants10102154>
 49. Fu, L.; Xu, B.T.; Xu, X.R.; Gan, R.Y.; Zhang, Y.; Xia, E.Q.; Li, H.B. Antioxidant capacities and total phenolic contents of 62 fruits. *Food Chemistry*, 2011, 129(2), pp. 345–356. DOI: <https://doi.org/10.1016/j.foodchem.2011.04.079>

NOVEL Zn(II) BINUCLEAR AND Ni(II) 1D POLYMERIC COORDINATION COMPOUNDS BASED ON DIANILINEGLYOXIME AND DICARBOXYLIC ACIDS: SYNTHESIS AND STRUCTURE

Dumitru Ureche^{a*}, Ion Bulhac^a, Sergiu Shova^a, Paulina Bourosh^b

^aInstitute of Chemistry, 3, Academiei str., Chisinau MD 2028, Republic of Moldova

^bInstitute of Applied Physics, 5, Academiei str., Chisinau MD 2028, Republic of Moldova

*e-mail: dumitru.ureche@ichem.md; d.ureche@yahoo.com; phone: (+373 22) 739 611

Abstract. Two coordination compounds $[\text{Zn}_2(\text{DAnH}_2)_2(1,3\text{-bdc})_2(\text{DMSO})_4]$ (**1**) and $[\text{Ni}(\text{DAnH}_2)(1,4\text{-bdc})(\text{DMF})_2]_n$ (**2**) were synthesized starting from dianilineglyoxime (DAnH_2), 1,3-benzenedicarboxylic acid ($1,3\text{-bdcH}_2$) and 1,4-benzenedicarboxylic acid ($1,4\text{-bdcH}_2$), where DMSO is dimethyl sulphoxide and DMF is dimethylformamide. The molecular and crystal structures of the compounds were studied by infrared spectroscopy and single crystal X-ray diffraction; and for the Zn(II) compound, additionally, the ^1H and ^{13}C NMR spectroscopy was used. The results show that **1** is a binuclear molecular complex while **2** is a unidimensional coordination polymer. In both compounds, the neutral DAnH_2 ligand coordinates in a bidentate-chelate mode, while dianions 1,3-bdc and 1,4-bdc coordinate as bidentate bridges. The ligands are interconnected by intramolecular $\text{O-H}\cdots\text{O}$ hydrogen bonds, involving the oximic groups as proton donors and the carboxylate anions as acceptors. The metal atoms in both compounds have an octahedral geometry.

Keywords: dianilineglyoxime, zinc complex, nickel unidimensional coordination polymer, benzenedicarboxylic acid, X-ray crystallography.

Received: 04 April 2022/ Revised final: 12 August 2022/ Accepted: 16 August 2022

Introduction

The synthesis of dioxime-based complex compounds began in 1905 when L. Chugaev showed that α -dioximes easily coordinated to some transition metals [1]. Nowadays, a large number of coordination compounds based on dioxime ligands are known, and the evolution from mononuclear to bi- and polynuclear complexes is taking place. Those compounds are characterized by high stability, characteristic colours, and specific behaviour towards solvents at high temperatures.

It is well known that in complexes with advanced nuclearity, the function of bridging ligands is realized by additional organic molecules, such as bipyridine [2-5], polycarboxylic [6-9] or inorganic [10,11] anions. A large number of binuclear compounds, including the bridging ligands containing oximic groups [12-16] or a combination of these functions [17], are known. Moreover, compounds that contain modified bridging ligands have already been successfully created [18,19]. A significant number of publications deal with a series of square planar nickel(II), palladium(II) and platinum(II) dioximates with the coordination

number (CN) of the central atom equal to four [20-23], copper(II) binuclear dioximates with tetragonal-pyramidal structure with CN 5 [24-26], and iron(II) [27-29], iron(III) [30], cobalt(II) [31-33], and cobalt(III) [33-37] compounds with metals octahedral geometry with CN 6. In *bis*-dioxime complexes, those ligands usually coordinate as monoanions and participate in the formation of strong intramolecular hydrogen bonds. In addition, iron(II) [38], nickel(II), cobalt(II), copper(II) [39-41], and copper(I) [42] complexes are known where oximes coordinate as neutral ligands, a part of them being *tris*-dioximic compounds. In some complexes, dianilineglyoxime can coordinate with metal atoms in its neutral [43,44], monodeprotonated [43], or bideprotonated [44] forms. Moreover, it has been established that the zinc(II) complex with dianilineglyoxime (DAnH_2) and 1,3-benzenedicarboxylic acid ($1,3\text{-H}_2\text{bdc}$) [7] in dimethyl sulphoxide (DMSO) undergoes modifications over time into a known 3D coordination polymer [45], where DMSO replaces both dimethylformamide (DMF) and DAnH_2 ligands. Recently, new coordination compounds of zinc with fluorine-containing ligands, which

exhibit luminescent properties, have been reported. Based on them, the aggregation-induced emission effect (AIE) was investigated [46,47].

The purpose of the present study was to synthesize new coordination compounds via the interaction of Zn(II) and Ni(II) salts with DAnH₂, 1,3-bdcH₂, and 1,4-benzenedicarboxylic acid (1,4-bdcH₂), and the resulted Zn(II) binuclear complex [Zn₂(DAnH₂)₂(1,3-bdc)₂(DMSO)₄] (1) and Ni(II) one-dimensional coordination polymer [Ni(DAnH₂)(1,4-bdc)(DMF)₂]_n (2).

Experimental

Materials

All reagents were used as purchased from commercial sources. The starting materials were: nickel(II) acetate tetrahydrate, zinc(II) acetate dihydrate, methanol, DMF, ethanol, DMSO, 1,3- and 1,4-bdcH₂, all being purchased from Sigma Aldrich. DAnH₂ was synthesized by condensation of dichloroglyoxime with aniline, according to the method in [48].

General procedure of syntheses

Compounds 1 and 2 have been synthesized according to Scheme 1.

Synthesis of [Zn₂(DAnH₂)₂(1,3-bdc)₂(DMSO)₄] (1)

The dianilineglyoxime (0.054 g, 0.2 mmol) and zinc acetate dihydrate (0.022 g, 0.1 mmol) were dissolved in a DMSO–EtOH mixture (6 mL) in a ratio of 1:1 (v/v). A solution of 1,3-benzenedicarboxylic acid (0.034 g, 0.2 mmol) in EtOH (3 mL) was further added to the obtained mixture, with permanent stirring. The resulted light-yellow reaction mixture was additionally stirred for 10–15 min and then filtered, and the filtrate was left at room temperature for crystallization. After 16 days, block colorless crystals were formed. The compound is soluble in DMSO and insoluble in DMF, methanol, water, and diethyl ether. Yield: 0.09 g, 35 %. Calcd., %: C, 49.41; H, 4.78; N, 8.86; Zn, 10.35; S, 10.15 for C₅₂H₆₀N₈O₁₃S₄Zn₂. Found, %: C, 50.04; H, 4.98; N, 8.99; Zn, 10.37; S, 10.11. The IR spectra (ν, cm⁻¹): 3663 w, 3304 w, 2989 w, 2972 w, 2909 w, 2554 w, 1841 w, 1670 w, 1624 m, 1600 s, 1540 m, 1497 s, 1472 w, 1452 w, 1437m,

1410 vw, 1375 vs, 1314 w, 1293 w, 1282 vw, 1265 vw, 1178 w, 1158 w, 1104 vw, 1090 vw, 1078 m, 1065 w, 1009 vs, 949 m, 934 vw, 913 w, 895 w, 836 w, 807 w, 745 s, 708 s, 694 s, 658 w, 633 w, 607 w, 589 w, 545 w, 516 w, 487 m, 451 w, 428 w.

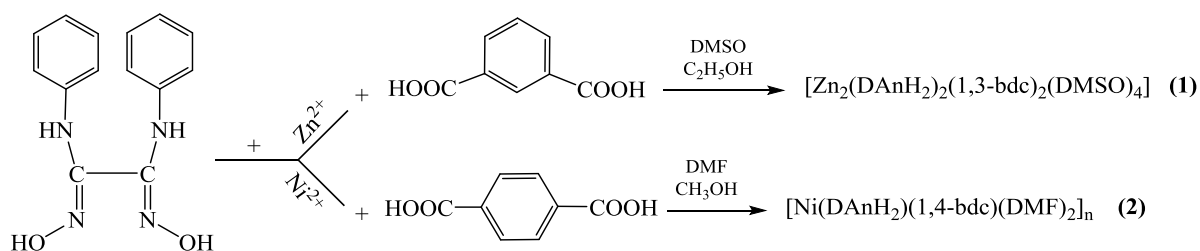
Synthesis of [Ni(DAnH₂)(1,4-bdc)(DMF)₂]_n (2)

Both dianilineglyoxime (0.054 g, 0.2 mmol) and nickel acetate tetrahydrate (0.025 g, 0.1 mmol) were dissolved in a mixture of DMF–MeOH (6 mL) in a ratio of 1:1 (v/v), then a solution of 1,4-H₂bdc (0.034 g, 0.2 mmol) in MeOH (3 mL) was added to the obtained red-black mixture. Gradually, the color of the reaction mixture turned into red-green, after which the mixture was stirred for another 10–15 minutes, filtered, and the filtrate was left to crystallize at room temperature. After three weeks, the green hexagonal prism-shaped crystals soluble in DMSO, less soluble in methanol, and insoluble in water, ethanol, and diethyl ether were formed. Yield: 0.027 g, 42%. Calc., %: C, 52.61; H, 5.05; N, 13.15; Ni, 9.18 for C₂₈H₃₂N₆NiO₈. Found, %: C, 52.48; H, 5.12; N, 13.20; Ni, 9.17. IR spectrum (ν, cm⁻¹): 3316 m, 3045 vw, 2939 vw, 2331 w, 1831 w, 1646 s, 1598 m, 1546 m, 1499 m, 1470 w, 1436 w, 1419 w, 1376 vs, 1315 vw, 1295 m, 1253 w, 1164 vw, 1153 w, 1137 vw, 1105 m, 1077 w, 1063 vw, 1034 vw, 1028 w, 1013 w, 1001 w, 982 vw, 975 vw, 930 vw, 916 m, 886 m, 870 vw, 850 vw, 838 vw, 831 vw, 813 m, 806 m, 753 s, 716 m, 691 s, 678 vw, 660 vw, 628 m, 606 w, 541 s, 508 vw, 481 w.

Physical measurements

Elemental analysis of the synthesized complexes for C, H, and N was performed on a Vario EL (III) Elemental Analyzer, and for metals - on an AAS-1N atomic absorption spectrometer (Carl Zeiss).

Infrared spectra (IR) were recorded on a FT-IR Spectrum-100 Perkin Elmer spectrometer in Nujol (4000–400 cm⁻¹) using the attenuated total reflection (ATR) technique (4000–650 cm⁻¹). Intensities are given as: vs-very strong, s-strong, m-medium, w-weak, and vw-very weak.



Scheme 1. Synthetic pathways to complexes 1 and 2.

^1H , and ^{13}C NMR spectra were recorded in DMSO- d_6 (99.95 %) on a Bruker Advance DRX 400 (400.13, 100.61 and 40.54 MHz). Chemical shifts (δ) are reported in ppm and are referenced to the residual nondeuterated solvent peak (2.50 ppm for ^1H and 39.50 ppm for ^{13}C).

Crystallographic studies

Diffraction data for **1** and **2** were collected on an Xcalibur E diffractometer with a charge-coupled device (CCD) using the graphite-monochromatized MoK α radiation at 160 and 293 K, respectively. The determination of the unit cell parameters and processing of the experimental data were performed using a CrysAlis Oxford Diffraction Ltd. as in [49]. The structures were solved by direct methods and refined by the full-matrix least-squares on weighted F^2 values for all reflections using a SHELXL 2014 software [50]. All non-H atoms in the compounds were refined with anisotropic displacement parameters. The positions of hydrogen atoms in the structures were located on difference Fourier maps or calculated geometrically and refined isotropically in the “rigid body” model with $U = 1.2 \text{ Ueq}$ or 1.5 Ueq of the corresponding O, N, and C atoms. The disordering problems for DMSO ligands were resolved for compound **1**: of the eight DMSO ligands belonging to two crystallographically independent complexes, six were located in two positions. The details of the structure solution and refinement for compounds **1** and **2** are given in Table 1. Selected bond distances and bond angles are given in Table 2. Geometric parameters of hydrogen bonds are listed in Table 3. Both CCDC 2144144 and 2144143 contain the supplementary crystallographic data for this paper. Those data can be obtained free of charge via www.ccdc.cam.ac.uk/data_request/cif, or by emailing data_request@ccdc.cam.ac.uk, or by contacting The Cambridge Crystallographic Data Centre, 12 Union Road, Cambridge CB2 1EZ, UK; fax: +44 1223 336033.

Results and discussion

The IR spectrum of compound **1** shows the absorption maxima at 3662 and 3304 cm^{-1} , which may be attributed to the $\nu(\text{OH})$ and $\nu(\text{NH})$ groups [51]. The very large absorption bands of a low intensity at 2600–1800 cm^{-1} are characteristic to the $\nu(\text{OH})$ vibration of the oximic groups participating in the intramolecular hydrogen bond formation with carboxylic anions. The absorption maxima from 1667 and 1623 cm^{-1} may be attributed to the $\nu(\text{C=O})$ vibration of dicarboxylic ligands and to the $\nu(\text{C=N})$ oximic fragment,

respectively [52,53]. The peaks at 1600 and 1497 cm^{-1} of $\nu(\text{C=C})$ belong to aromatic rings, as well as the peaks of the non-planar deformation of $\delta(\text{CH})$ in a range of 807–694 cm^{-1} . In the IR spectra, also, a band of a high intensity at 1009 cm^{-1} is vivid, which belongs to the $\nu(\text{S=O})$ vibrations of DMSO molecules [52,54].

The IR spectrum of compound **2** has many similarities with that of compound **1**. The absorption bands of $\nu(\text{OH})$ and $\nu(\text{NH})$ groups are localized at 3316 and 3045 cm^{-1} , respectively [51]. Also, there is a large signal with a low intensity at 1831 cm^{-1} , which probably belongs to $\nu(\text{OH})$ vibration of the oximic groups, and, similarly to the case of compound **1**; it participates in the formation of intramolecular hydrogen bonds with carboxylic anions. The maximum of absorption of a high intensity at 1646 cm^{-1} belongs to the $\nu(\text{C=N})$ and $\nu(\text{C=O})$ vibrations of coordinated DMF molecules [51–53]. For benzene rings, the $\nu(\text{C=C})$ vibrations at 1546 and 1499 cm^{-1} , respectively, have been identified as well as those of non-planar deformation $\delta(\text{CH})$ in a range of 753–691 cm^{-1} .

The ^1H NMR spectrum of compound **1** confirms its structure by signals in a weak field at 6.76–7.09 ppm, which reveals the presence of the aromatic protons from the molecule of dianilineglyoxime. The presence of carboxylic dianions is proved by the signal in a range of 7.45–8.24 ppm and the protons from the iminic and the oximic groups are visible at 8.62 ppm and 10.32 ppm, respectively. In the ^{13}C NMR spectrum, there are signals of both aromatic rings. Those of unsubstituted carbon atoms from dianilineglyoxime are well seen in a range of 118.18–121.99 ppm, that of tetrasubstituted - at 139.99 ppm, and of carboxylates - from 128.11 ppm to 135.07 ppm. The signal at 171.78 ppm is attributed to carbon atoms from carboxylic groups and that at 143.43 ppm - to the tetrasubstituted carbon from the oxime group.

The binuclear complex (**1**) crystallizes in the triclinic $P-1$ space group (Table 1). The asymmetric part of the unit cell contains four crystallographically independent Zn(II) ions, four neutral DAnH $_2$ ligands, four bideprotonated carboxylate anions (1,3-bdc) $^{2-}$, and eight DMSO ligands. The crystal contains two crystallographically independent binuclear molecular complexes (denoted A and B); in each of them, two metal atoms are linked together by two bidentate carboxylate bridging ligands (Figure 1(a)). At each of the metal atoms, a bidentate-chelate DAnH $_2$ ligand coordinates, implying two nitrogen atoms, and the

coordination polyhedron of a zinc atom is completed by two monodentate DMSO ligands that are coordinated by oxygen atoms. Thus, the Zn(II) ions have octahedral coordination geometries provided by N_2O_4 sets of donor atoms. The interatomic Zn–N_(oxime) distances in the equatorial plane of the coordination polyhedron of the metal are in a range of 2.130(4)–2.366(4) Å, Zn–O_(bdc) - 2.025(3)–2.093(4) Å, and axial Zn–O_(DMSO) distances - 2.065(4)–2.187(4) Å (Table 2). These are in agreement with the values for Zn(II) complex with dioximes [7]. Each binuclear complex in compound **1** is stabilized by four intramolecular hydrogen bonds between two DAnH₂ ligands and (1,3-bdc)²⁻ residues, the distances donor-acceptor O···O vary in a range of 2.475(5)–2.568(5) Å

(Table 3). The survey of the Cambridge Structural Database [55] identified a binuclear Zn(II)-dioxime complex with the 4,4'-bipyridine as a bridging ligand [56], and the mixed-ligand Zn(II) compounds with dioximes and carboxylates ligands, with mononuclear [57] and polymeric [58] structures.

The binuclear complexes in the crystal of compound **1** are linked in the layers parallel to the *ac* crystallographic plane by intermolecular N–H···O hydrogen bonds, where =NH functional groups act as proton donors and oxygen atoms of oximic ligands as acceptors. The layers are additionally stabilized by weaker hydrogen bonds of C–H···O type, with donor-acceptor distances being in the range of 3.14(2)–3.60(5) Å (Figure 1(b)).

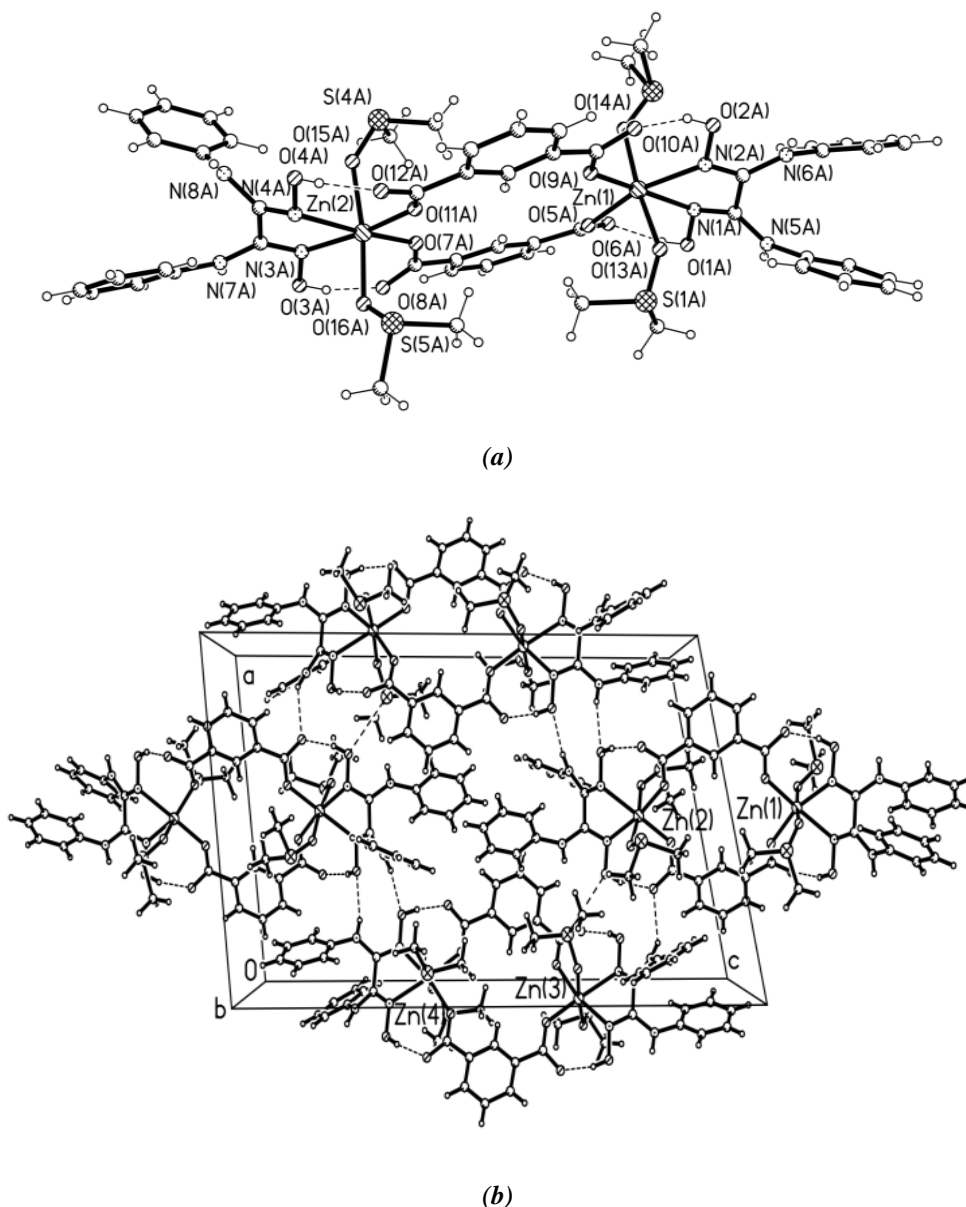


Figure 1. Molecular structure of: binuclear Zn(II) complex **1** (a) and fragment of the H-bonded layer (b).

The coordination compound **2** crystallizes in the monoclinic $P2_1/n$ space group (Table 1), and it is a unidimensional (1D) coordination polymer. The asymmetric part of the unit cell contains Ni(II) metal ion, a DAnH₂ neutral ligand, a (1,4-bdc)²⁻ bideprotonated ligand, and two DMF neutral ligands (Figure 2(a)). Each Ni(II) ion in this polymeric compound (Figure 2(b)) is hexacoordinated and has a distorted octahedral geometry with the N₂O₄ set of donor atoms, two nitrogen atoms belonging to the bidentate-chelate coordinated DAnH₂ neutral ligand, two oxygen atoms from two (1,4-bdc)²⁻ bideprotonated ligands, and two oxygen atoms from two DMF ligands that occupy axial coordinates. The carboxylate ligand is a bridging ligand which coordinates *exo*-bidentate *via* two oxygen atoms from terminal carboxyl groups to two metal atoms. Because of this, one of the positions from the

coordination polyhedron of the metal is occupied by the oxygen atom from the carboxyl group of the neighboring fragment [Ni(DAnH₂)(1,4-bdc)(DMF)₂]. The interatomic Ni–N_(oxime) distances are equal to 2.102(2) and 2.082(2) Å, Ni–O_(bdc) – 2.013(2) and 2.040(2) Å, Ni–O_(DMF) – 2.081(2) and 2.083(2) Å (Table 2).

The 1D coordination polymer **2** in the crystal is stabilized in a zig-zag form with Ni–Ni separation across the (1,4-bdc)²⁻ bridging ligand equal to 11.086 Å, the polymeric step being of 14.011 Å.

In the crystal of compound **2**, a system of intra- and intermolecular hydrogen bonds was registered. The intramolecular hydrogen bonds O_(oxime)–H···O_(carb.) with donor-acceptor distances 2.538(3) and 2.536(3) Å (Table 3) form two seven-membered pseudo-chelate rings which stabilize an extended Ni(II) equatorial platform in the polymeric complex.

Table 1

Crystal data and details of data collection for (1) and (2).

Parameter	Value	
	1	2
Empirical formula	C ₅₂ H ₆₀ N ₈ O ₁₃ S ₄ Zn ₂	C ₂₈ H ₃₂ NiN ₆ O ₈
<i>M</i>	1312.06	639.30
Temperature, K	160(2)	293(2)
Crystal system	Triclinic	Monoclinic
Space group	<i>P</i> -1	<i>P</i> 2 ₁ / <i>n</i>
<i>a</i> , Å	16.7185(3)	14.6306(5)
<i>b</i> , Å	16.7218(4)	14.0111(5)
<i>c</i> , Å	24.8930(4)	15.9393(6)
α , °	94.7468(15)	90
β , °	96.1010(14)	109.175(4)
γ , °	119.152(2)	90
<i>V</i> , Å ³	5970.3(2)	3086.1(2)
<i>Z</i>	4	4
ρ_{calcd} , g/cm ³	1.450	1.376
μ , mm ⁻¹	1.016	0.686
<i>F</i> (000)	2720	1336
Crystal size, mm	0.28×0.18×0.08	0.42×0.32×0.07
2 θ range, °	1.52–25.50	2.95–25.05
Index ranges	–20 ≤ <i>h</i> ≤ 18, –19 ≤ <i>k</i> ≤ 20, –30 ≤ <i>l</i> ≤ 30	–17 ≤ <i>h</i> ≤ 17, –10 ≤ <i>k</i> ≤ 16, –18 ≤ <i>l</i> ≤ 18
Reflections collected/independent reflections (<i>R</i> _{int})	55923/21896(0.0513)	11361/5439(0.0397)
Reflections with <i>I</i> > 2 σ (<i>I</i>)	13893	3927
Completeness, %	98.6 (θ = 25.24°)	99.5 (θ = 25.05°)
Parameters	1675	394
GOOF	1.006	1.003
Final <i>R</i> indices (<i>I</i> > 2 σ (<i>I</i>))	<i>R</i> ₁ = 0.0632 <i>wR</i> ₂ = 0.1350	<i>R</i> ₁ = 0.0489 <i>wR</i> ₂ = 0.1050
<i>R</i> indices (all data)	<i>R</i> ₁ = 0.1120 <i>wR</i> ₂ = 0.1536	<i>R</i> ₁ = 0.0757 <i>wR</i> ₂ = 0.1202
$\Delta\rho_{\text{max}}$, $\Delta\rho_{\text{min}}$, e Å ⁻³	1.821–1.298	0.354–0.290

Table 2

Selected bond lengths (Å) and bond angles (°) in 1 and 2.

Structure of 1			
Bond	Bond length, Å	Bond	Bond length, Å
Zn(1)–N(1A)	2.309(4)	Zn(3)–N(1B)	2.366(4)
Zn(1)–N(2A)	2.128(4)	Zn(3)–N(2B)	2.139(4)
Zn(1)–O(5A)	2.023(3)	Zn(3)–O(5B)	2.050(3)
Zn(1)–O(9A)	2.053(3)	Zn(3)–O(9B)	2.030(3)
Zn(1)–O(13A)	2.188(4)	Zn(3)–O(13B)	2.145(3)
Zn(1)–O(14A)	2.074(4)	Zn(3)–O(14B)	2.039(4)
Zn(2)–N(3A)	2.167(4)	Zn(4)–N(3B)	2.166(4)
Zn(2)–N(4A)	2.290(4)	Zn(4)–N(4B)	2.299(4)
Zn(2)–O(7A)	2.047(3)	Zn(4)–O(7B)	2.041(3)
Zn(2)–O(11A)	2.035(3)	Zn(4)–O(11B)	2.091(3)
Zn(2)–O(15A)	2.131(4)	Zn(4)–O(15B)	2.132(8)
Zn(2)–O(16A)	2.068(4)	Zn(4)–O(16B)	2.061(3)
Bond angle	Bond angle value, °	Bond angle	Bond angle value, °
N(1A)–Zn(1)–N(2A)	71.4(1)	N(1B)–Zn(3)–N(2B)	71.4(1)
N(1A)–Zn(1)–O(5A)	93.3(3)	N(1B)–Zn(3)–O(5B)	96.3(1)
N(1A)–Zn(1)–O(9A)	174.2(1)	N(1B)–Zn(3)–O(9B)	170.8(1)
N(1A)–Zn(1)–O(13A)	90.4(1)	N(1B)–Zn(3)–O(13B)	82.7(2)
N(1A)–Zn(1)–O(14A)	91.4(2)	N(1B)–Zn(3)–O(14B)	94.4(2)
N(2A)–Zn(1)–O(5A)	163.6(1)	N(2B)–Zn(3)–O(5B)	167.4(1)
N(2A)–Zn(1)–O(9A)	104.3(1)	N(2B)–Zn(3)–O(9B)	102.0(1)
N(2A)–Zn(1)–O(13A)	79.1(1)	N(2B)–Zn(3)–O(13B)	87.0(1)
N(2A)–Zn(1)–O(14A)	95.0(2)	N(2B)–Zn(3)–O(14B)	88.9(2)
O(5A)–Zn(1)–O(9A)	90.6(1)	O(5B)–Zn(3)–O(9B)	90.0(1)
O(5A)–Zn(1)–O(13A)	95.7(1)	O(5B)–Zn(3)–O(13B)	88.8(1)
O(5A)–Zn(1)–O(14A)	91.1(2)	O(5B)–Zn(3)–O(14B)	94.9(2)
O(9A)–Zn(1)–O(13A)	84.9(1)	O(9B)–Zn(3)–O(13B)	90.7(1)
O(9A)–Zn(1)–O(14A)	92.9(2)	O(9B)–Zn(3)–O(14B)	91.8(2)
O(13A)–Zn(1)–O(14A)	172.9(2)	O(13B)–Zn(3)–O(14B)	175.6(2)
N(3A)–Zn(2)–N(4A)	72.7(1)	N(3B)–Zn(4)–N(4B)	71.6(1)
N(3A)–Zn(2)–O(7A)	101.6(1)	N(3B)–Zn(4)–O(7B)	102.5(1)
N(3A)–Zn(2)–O(11A)	170.7(1)	N(3B)–Zn(4)–O(11B)	169.2(1)
N(3A)–Zn(2)–O(15A)	83.3(2)	N(3B)–Zn(4)–O(15B)	80.1(2)
N(3A)–Zn(2)–O(16A)	87.5(1)	N(3B)–Zn(4)–O(16B)	90.1(1)
N(4A)–Zn(2)–O(7A)	171.6(2)	N(4B)–Zn(4)–O(7B)	173.7(1)
N(4A)–Zn(2)–O(11A)	98.2(1)	N(4B)–Zn(4)–O(11B)	97.6(1)
N(4A)–Zn(2)–O(15A)	82.0(2)	N(4B)–Zn(4)–O(15B)	93.6(3)
N(4A)–Zn(2)–O(16A)	91.9(1)	N(4B)–Zn(4)–O(16B)	90.4(2)
O(7A)–Zn(2)–O(11A)	87.3(1)	O(7B)–Zn(4)–O(11B)	88.3(1)
O(7A)–Zn(2)–O(15A)	91.6(2)	O(7B)–Zn(4)–O(15B)	83.1(3)
O(7A)–Zn(2)–O(16A)	94.3(2)	O(7B)–Zn(4)–O(16B)	91.8(2)
O(11A)–Zn(2)–O(15A)	90.8(2)	O(11B)–Zn(4)–O(15B)	100.9(2)
O(11A)–Zn(2)–O(16A)	94.6(1)	O(11B)–Zn(4)–O(16B)	90.1(1)
O(15A)–Zn(2)–O(16A)	172.3(2)	O(15B)–Zn(4)–O(16B)	167.7(2)
Structure of 2			
Bond	Bond length, Å	Bond	Bond length, Å
Ni–N(1)	2.102(2)	Ni–O(6) ^{#1}	2.040(2)
Ni–N(2)	2.082(2)	Ni–O(8)	2.081(2)
Ni–O(3)	2.013(2)	Ni–O(7)	2.083(2)
Bond angle	Bond angle value, °	Bond angle	Bond angle value, °
N(1)–Ni–N(2)	76.58(10)	N(2)–Ni–O(8)	91.75(10)
N(1)–Ni–O(3)	176.26(10)	O(3)–Ni–O(6) ^{#1}	84.49(9)
N(1)–Ni–O(6) ^{#1}	98.68(10)	O(3)–Ni–O(7)	89.27(10)
N(1)–Ni–O(7)	88.75(10)	O(3)–Ni–O(8)	90.82(10)
N(1)–Ni–O(8)	91.34(10)	O(6) ^{#1} –Ni–O(7)	89.75(9)
N(2)–Ni–O(3)	100.29(10)	O(6) ^{#1} –Ni–O(8)	87.14(10)
N(2)–Ni–O(6) ^{#1}	175.11(9)	O(7)–Ni–O(8)	176.86(10)
N(2)–Ni–O(7)	91.32(10)		

^{#1} $-x+1/2, y+1/2, -z+1/2$ (2).

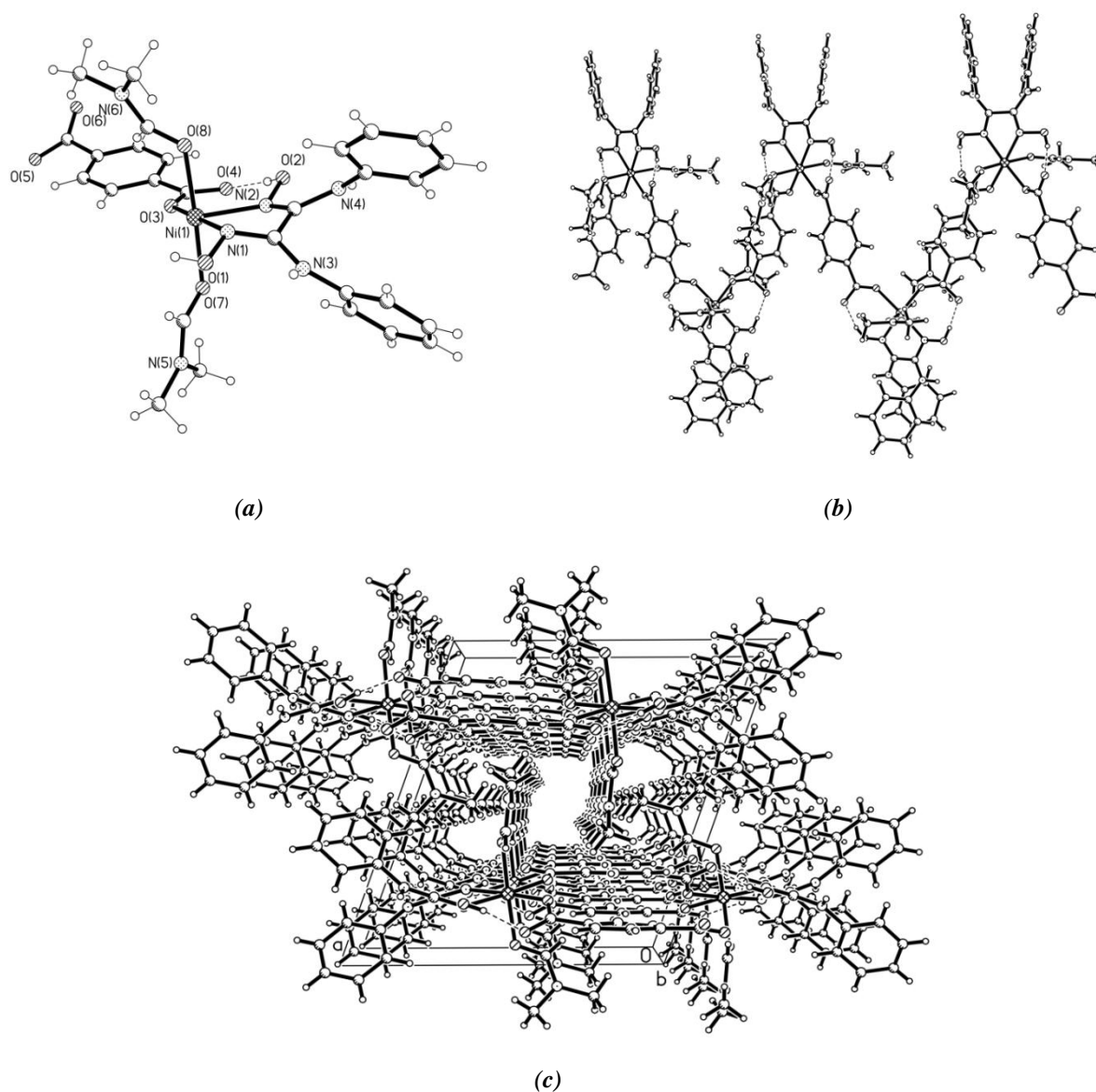


Figure 2. The asymmetric part of coordination polymer 2 with partial numbering of atoms (a); fragment of 1D coordination polymer (b); a perspective view of crystal packing (c).

Table 3

Geometric parameters of intra- and intermolecular hydrogen bonds in the structures of 1 and 2.

$D-H\cdots A$	$D-H, \text{\AA}$	$H\cdots A, \text{\AA}$	$D\cdots A, \text{\AA}$	$DHA, ^\circ$
<i>Structure of 1</i>				
$N(5A)-H(5A)\cdots O(2B)^{\#1}$	0.88	2.10	2.965(5)	167
$N(8A)-H(8A)\cdots O(3B)^{\#3}$	0.88	2.01	2.846(5)	158
$N(5B)-H(5B)\cdots O(8A)^{\#4}$	0.88	2.23	2.901(5)	132
$N(6B)-H(6B)\cdots O(1A)^{\#1}$	0.88	2.32	3.057(5)	142
$N(7B)-H(7B)\cdots O(4A)^{\#3}$	0.88	2.18	3.007(5)	158
$N(8B)-H(8B)\cdots O(10A)^{\#5}$	0.88	2.30	3.021(5)	139
$O(1A)-H(1A)\cdots O(6A)$	0.84	1.72	2.525(4)	161
$O(2A)-H(2A)\cdots O(10A)$	0.84	1.77	2.564(4)	157
$O(3A)-H(3A)\cdots O(8A)$	0.84	1.71	2.531(4)	165
$O(4A)-H(4A)\cdots O(12A)$	0.84	1.73	2.536(4)	160
$O(1B)-H(1B)\cdots O(6B)$	0.84	1.76	2.550(5)	156
$O(2B)-H(2B)\cdots O(10B)$	0.84	1.69	2.500(4)	162
$O(3B)-H(3B)\cdots O(8B)$	0.84	1.64	2.470(5)	171
$O(4B)-H(4B)\cdots O(12B)$	0.84	1.74	2.538(5)	158

Continuation of Table 3

$D-H\cdots A$	$D-H, \text{\AA}$	$H\cdots A, \text{\AA}$	$D\cdots A, \text{\AA}$	$DHA, ^\circ$
Structure of 2				
$O(1)-H(1O)\cdots O(5)^{\#1}$	0.82	1.74	2.538(3)	164
$O(2)-H(2O)\cdots O(4)$	0.82	1.73	2.536(3)	166
$N(3)-H(1N)\cdots O(2)^{\#3}$	0.86	2.20	3.048(4)	167
$N(4)-H(2N)\cdots O(1)^{\#4}$	0.86	2.19	3.011(4)	160
$^{\#1} -x+1, -y+1, -z+1; ^{\#2} x, y+1, z; ^{\#3} -x+2, -y+1, -z; ^{\#4} x+1, y, z+1; ^{\#5} x, y-1, z$ (1); $^{\#1} -x+1/2, y+1/2, -z+1/2; ^{\#2} -x+1/2, y-1/2, -z+1/2; ^{\#3} -x+3/2, y+1/2, -z+1/2; ^{\#4} -x+3/2, y-1/2, -z+1/2$ (2).				

Those coordination chains are joined together by intermolecular hydrogen bonds of the $N-H\cdots O$ type, the donor-acceptor distances being equal to 3.048(4) and 3.011(4) Å (Figure 2(c), Table 3), where amino =NH groups are proton donors and oxygen atoms from the oximic groups are acceptors. A detailed analysis of the fine hydrogen bonding system of the $C-H\cdots O$ type shows that DMF ligands do not participate in the formation of intermolecular hydrogen bonds. They generate only intramolecular bonds, stabilizing the polymeric chain; instead, such types of bonds were detected between chains where =CH groups from the aromatic rings of DANH₂ ligand play the role of proton donors.

Conclusions

The synthesis of the studied here coordination compounds in the simultaneous presence of dianilineglyoxime, 1,3- and 1,4-benzendicarboxylic acids, and DMSO/DMF has led to zinc(II) binuclear and nickel(II) polynuclear coordination compounds.

It was proved that, in the reported compounds, dianilineglyoxime coordinates as a neutral ligand in a bidentate-chelate mode, generating a five-membered metallocycle, and 1,3- and 1,4-benzendicarboxylates act as *exo*-bidentate bridging ligands that bind both metal atoms in di- and polynuclear structures, while molecules of DMSO/DMF act as monodentate terminal ligands.

The structure of the nickel(II) coordination compound is a zig-zag chain, which indicates a 1D coordination polymer.

Acknowledgments

This work was supported by State Programs of National Agency for Research and Development of the Republic of Moldova: project no. 20.80009.5007.28 under the title „Development of new multifunctional materials and efficient technologies for agriculture, medicine, technology and the education system based on the metal complexes "s" and "d" with polydentate ligands" and project no. 20.80009.5007.15, under the title

“Implementation of crystal engineering approach and X-ray crystallography for design and creation of hybrid organic/inorganic materials with advanced physical and biologically active functions”.

References

- Chugaev, L.A. Selected Works. Publishing House of the Academy of Sciences of the USSR: Moscow, 1954, 1, 636 p. (in Russian).
- Coropceanu, E.; Rija, A.; Lozan, V.; Bulhac, I.; Duca, G.; Kravtsov, V.Ch.; Bourosh, P. Discrete binuclear cobalt(III) *bis*-dioximates with wheel-and-axle topology as building blocks to afford porous supramolecular metal–organic frameworks. *Crystal Growth & Design*, 2016, 16(2), pp. 814–820.
DOI: <https://doi.org/10.1021/acs.cgd.5b01402>
- Coropceanu, E.; Croitor, L.; Gdaniec, M.; Wicher, B.; Fonari, M. Preparation, spectroscopic and X-ray study of $[Cu_2(Hdmg)_4(\gamma, \gamma'-dpy)]_2 \cdot 4H_2dmg$ and $[Cu_2(Hdmg)_4(\gamma, \gamma'-dpy)] \cdot [Cu(Hdmg)_2(\gamma, \gamma'-dpy)](\gamma, \gamma'-dpy)2H_2dmg$. *Inorganica Chimica Acta*, 2009, 362(7), pp. 2151–2158.
DOI: <https://doi.org/10.1016/j.ica.2008.09.047>
- Croitor, L.; Coropceanu, E.B.; Siminel, A.V.; Kulikova, O.; Zelentsov, V.I.; Datsko, T.; Fonari, M.S. 1,2-Cyclohexanedionedioxime as a useful co-ligand for fabrication of one-dimensional Zn(II) and Cd(II) coordination polymers with wheel-and-axle topology and luminescent properties. *CrystEngComm*, 2012, 14(10), pp. 3750–3758.
DOI: <https://doi.org/10.1039/c2ce00020b>
- Coropceanu, E.B.; Croitor, L.; Siminel, A.V.; Chumakov, Y.; Fonari, M.S. The luminescence attenuation in the solid state by fluoride anion entrapped in the one-dimensional Zn(II) dioximate and mononuclear Cd(II) dioxime compounds. *Polyhedron*, 2016, 109, pp. 107–114.
DOI: <https://doi.org/10.1016/j.poly.2016.01.043>
- Croitor, L.; Coropceanu, E.B.; Duca, G.; Siminel, A.V.; Fonari, M.S. Nine Mn(II), Zn(II) and Cd(II) mixed-ligand coordination networks with rigid dicarboxylate and pyridine-naloxime ligands: Impact of the second ligand in the structures' dimensionality and solvent capacity. *Polyhedron*, 2017, 129, pp. 9–21.
DOI: <https://doi.org/10.1016/j.poly.2017.03.026>

7. Ureche, D.; Bulhac, I.; Rijja, A.; Coropceanu, E.; Bourosh, P. Dianilineglyoxime salt and its binuclear Zn(II) and Mn(II) complexes with 1,3-benzenedicarboxylic acid: synthesis and structures. *Russian Journal of Coordination Chemistry*, 2019, 45(12), pp. 843–855. DOI: <https://doi.org/10.1134/s107032841912008x>
8. Bélombé, M.M.; Nenwa, J.; Wankap Kouamo, J.S.T.; Ponou, S.; Fischer, A. Catena-Poly[[[(oxamide dioxime- κ^2 N,N')copper(II)]- μ -L-tartrato- κ^4 O¹,O²:O³,O⁴] tetrahydrate]: a chiral nanochannel framework hosting solvent water molecules. *Acta Crystallographica Section C*, 2012, 68(5), pp. m131–m134. DOI: <https://doi.org/10.1107/s0108270112016435>
9. Kawata, S.; Kitagawa, S.; Machida, H.; Nakamoto, T.; Kondo, M.; Katada, M.; Kikuchi, K.; Ikemoto, I. Oxamide oxime-based copper(II) coordination polymers. Two- and three-dimensional structures controlled by dicarboxylates. *Inorganica Chimica Acta*, 1995, 229(1-2), pp. 211–219. DOI: [https://doi.org/10.1016/0020-1693\(94\)04247-s](https://doi.org/10.1016/0020-1693(94)04247-s)
10. Croitor, L.; Coropceanu, E.B.; Siminel, A.V.; Kravtsov, V.Ch.; Fonari, M.S. Polymeric Zn(II) and Cd(II) sulfates with bipyridine and dioxime ligands: supramolecular isomerism, chirality, and luminescence. *Crystal Growth & Design*, 2011, 11(8), pp. 3536–3544. DOI: <https://doi.org/10.1021/cg200465f>
11. Endres, H.; Noethe, D.; Rossato, E.; Hatfield, W.E. Monomeric and anion-bridged dimeric and polymeric oxamide oxime complexes of copper(II): preparation, crystal and molecular structures, and magnetic properties. *Inorganic Chemistry*, 1984, 23(22), pp. 3467–3473. DOI: <https://doi.org/10.1021/ic00190a008>
12. Simonov, Yu.A.; Malinovskii, S.T.; Bologa, O.A.; Zavodnik, V.E.; Andrianov, V.I.; Shibanova, T.A. Crystal and molecular structure of μ -oxo-di(bis-dimethylglyoxymatocobalt(III)). *Crystallography Reports*, 1983, 28(4), pp. 682–684. (in Russian).
13. Simonov, Yu.A.; Zavodnik, V.E.; Shkurpelo, A.I.; Bologa, O.A. Crystal and molecular structure of hydroxo-*tris*-(dimethylglyoximate) dimethylglyoxymdicobalt(III) dihydrate perchlorate. *Russian Journal of Structural Chemistry*, 1985, 26(2), pp. 99–106. (in Russian).
14. Chaudhuri, P.; Winter, M.; Della Vedova, B.P.C.; Fleischhauer, P.; Haase, W.; Floerke, U.; Haupt, H.J. Synthesis, electrochemistry, magnetic and spectroscopic properties of an exchange-coupled iron(III)-nickel(II)-iron(III) complex. Crystal structure of $[L_2Fe_2(dm_g)_3Ni](PF_6)_2 \cdot 0.5CH_3OH$ ($L = 1,4,7$ -trimethyl-1,4,7-triazacyclononane; $dm_g =$ dimethylglyoximate(2-)). *Inorganic Chemistry*, 1991, 30(25), pp. 4777–4783. DOI: <https://doi.org/10.1021/ic00025a019>
15. Gradinaru, J.; Malinovskii, S.; Gdaniec, M.; Zecchin, S. Trinuclear *tris*-Co(II) and trans-cobaloxime type Co(III) complexes prepared from Co(II) triflate precursor: Synthesis, structure and properties. *Polyhedron*, 2006, 25(17), pp. 3417–3426. DOI: <https://doi.org/10.1016/j.poly.2006.06.023>
16. Frasson, E.; Bardi, R.; Bezzi, S. Structure of copper-dimethylglyoxime at low temperature. *Acta Crystallographica*, 1959, 12(3), pp. 201–205. DOI: <https://doi.org/10.1107/s0365110x59000573>
17. Liu, X.-W.; You, J.-H.; Wang, Y.-Y.; Yu, Y.-Q.; Su, N.; Guo, A.R. Synthesis, structure, and DFT studies of a novel 1D alternating copper(II) chain polymer with 4,4'-bipyridine and dimethylglyoxime mixed ligand. Synthesis and Reactivity in Inorganic, Metal-Organic, and Nano-Metal Chemistry, 2016, 46(11), pp. 1680–1684. DOI: <https://doi.org/10.1080/15533174.2015.1137045>
18. Xie, L.S.; Park, S.S.; Chmielewski, M.J.; Liu, H.; Kharod, R.A.; Yang, L.; Campbell, M.G.; Dinca, M. Isorecticular linker substitution in conductive metal-organic frameworks with through-space transport pathways. *Angewandte Chemie International Edition*, 2020, 59(44), pp. 19623–19626. DOI: <https://doi.org/10.1002/anie.202004697>
19. Ureche, D.; Rijja, A.; Bulhac, I.; Coropceanu, E.; Bourosh, P. Synthesis and structural study of 2D coordination polymers of Zn(II), Cd(II) and Mn(II) based on diaminobenzoylglyoxime. *Russian Journal of Inorganic Chemistry*, 2020, 65(12), pp. 1838–1847. DOI: <https://doi.org/10.1134/S0036023620120189>
20. Godycki, L.E.; Rundle, R.E. The structure of nickel dimethylglyoxime. *Acta Crystallographica*, 1953, 6(6), pp. 487–495. DOI: <https://doi.org/10.1107/s0365110x5300137x>
21. Mégnamisi-Béloméé, M. Crystal and molecular structure of the linear metal-chain semiconductor *bis*-(1,2-benzoquinonedioximato)platinum(II), $Pt(bqd)_2$. *Journal of Solid State Chemistry*, 1979, 27(3), pp. 389–396. DOI: [https://doi.org/10.1016/0022-4596\(79\)90181-6](https://doi.org/10.1016/0022-4596(79)90181-6)
22. Endres, H.; Keller, H.J.; Moroni, W.; Weiss, J. Oxidation product of *bis*-(1,2-benzoquinonedioximato)nickel(II), $[Ni(BCD)_2]$, with iodine: crystal and molecular structure. *Acta Crystallographica Section B*, 1975, 31(9), pp. 2357–2358. (in German) DOI: <https://doi.org/10.1107/s0567740875007595>
23. Hussain, M.S. Short hydrogen-bonded, column-stacked structure of *bis*-(α -furyl dioximato) palladium(II). *Acta Crystallographica, Section A*, 1984, 40, p. C290. DOI: <https://doi.org/10.1107/S0108767384091376>
24. Boualam, M.; Gleizes, A. Synthesis and crystalline and molecular structure of aqua-bis(diphenylglyoximate)copper(II). *Journal of Crystallography-Crystalline Materials*, 1983,

- 164(1-2), pp. 141-152. (in French). DOI: <https://doi.org/10.1524/zkri.1983.164.1-2.141>
25. Bishop, M.M.; Lee, A.H.W.; Lindoy, L.F.; Turner, P.; Skelton, B.W.; White, A.H. Self-assembly of hydrogen-bonded supramolecular structures based on the neutral pseudo-macrocyclic complex *bis*(dimethylglyoximate)copper(II). *Supramolecular Chemistry*, 2005, 17(1-2), pp. 37-45. DOI: <https://doi.org/10.1080/10610270412331328844>
 26. Koman, M.; Máriássy, M.; Ondrejovič, G. Structure of *bis*(dimethylglyoximate-*N,N'*)(thiourea-*S*)copper(II). *Acta Crystallographica Section C*, 1990, 46(4), pp. 561-562. DOI: <https://doi.org/10.1107/s0108270189008218>
 27. Bourosh, P.; Bulhac, I.; Covaci, O.; Zubareva, V.; Mitina, T. Iron(II) *bis*- α -benzyldioximate complexes with 3- and 4-pyridine hemiacetals as axial ligands: synthesis, structure, and physicochemical properties. *Russian Journal of Coordination Chemistry*, 2018, 44(8), pp. 507-517. DOI: <https://doi.org/10.1134/s1070328418080018>
 28. Bulhac, I.; Bouroş, P.N.; Bologa, O.A.; Lozan, V.; Ciobanică, O.; Lipkowski, J.; Mitina, T.F.; Simonov, Yu.A. Specific features of the structures of iron(II) α -benzyl dioximate solvates with pyridine. *Russian Journal of Inorganic Chemistry*, 2010, 55(7), pp. 1042-1051. DOI: <https://doi.org/10.1134/s0036023610070090>
 29. Prout, C.K.; Wiseman, T.J. The crystal and molecular structure of di[cyclohexane-1,2-dioximate(1-)]di-imidazoleiron(II)(ferrous bisnioximebisimidazole). *Journal of the Chemical Society (Resumed)*, 1964, 0, pp. 497-504. DOI: <https://doi.org/10.1039/jr9640000497>
 30. Dvorkin, A.A.; Simonov, Yu.A.; Malinovskii, T.I.; Bulgak, I.I.; Batyr, D.G. Molecular and crystalline-structure of *bis*-(α -benzyldioximate)-di-(β -picoline)-iron(III) penta-iodide. Report of the Academy of Sciences of USSR, 1977, 234(6), p. 1372. (in Russian).
 31. Chakravorty, A. Structural chemistry of transition metal complexes of oximes. *Coordination Chemistry Reviews*, 1974, 13(1), pp. 1-46. DOI: [https://doi.org/10.1016/s0010-8545\(00\)80250-7](https://doi.org/10.1016/s0010-8545(00)80250-7)
 32. Mandal, D.; Bhuyan, M.; Laskar, M.; Gupta, B.D. Co-C bond homolysis: reactivity difference between alkyl- and benzylcobaloximes. *Organometallics*, 2007, 26(11), pp. 2795-2798. DOI: <https://doi.org/10.1021/om070053q>
 33. Bourosh, P.; Bulhac, I.; Simonov, Yu.A.; Gdaniec, M.; Turta, K.; Siretsanu, L. Structure of the products formed in the reaction of cobalt chloride with 1,2-cyclohexanedione dioxime. *Russian Journal of Inorganic Chemistry*, 2006, 51(8), pp. 1202-1210. DOI: <https://doi.org/10.1134/s0036023606080092>
 34. Bourosh, P.N.; Coropceanu, E.B.; Ciloci, A.A.; Clapco, S.F.; Bologa, O.A.; Bivol, C.M.; Tiurina, J.P.; Bulhac, I. New Co(III) dioximates with hexafluorophosphate ion as stimulators of the proteolytic activity of the micromycete *Fusarium gibbosum* CNMN FD 12. *Russian Journal of Coordination Chemistry*, 2013, 39(11), pp. 777-786. DOI: <https://doi.org/10.1134/s107032841311002x>
 35. Bourosh, P.N.; Coropceanu, E.B.; Rija, A.P.; Bologa, O.A.; Gdaniec, M.; Bulhac, I.I. Structural evidence of $[\text{Rh}(\text{Thio})_6]^{3+}$ and $[\text{Rh}(\text{Thio})_5\text{Cl}]^{2+}$ cations in three novel ionic systems based on Co(III) dioximates. *Journal of Molecular Structure*, 2011, 998(1-3), pp. 198-205. DOI: <https://doi.org/10.1016/j.molstruc.2011.05.033>
 36. Rubin-Preminger, J.M.; Englert, U. Halogen bonding in substituted cobaloximes. *Inorganica Chimica Acta*, 2009, 362(4), pp. 1135-1142. DOI: <https://doi.org/10.1016/j.ica.2008.05.026>
 37. Liebing, P.; Oehler, F.; Wagner, M.; Tripet, P.F.; Togni, A. Perfluoroalkyl cobaloximes: preparation using hypervalent iodine reagents, molecular structures, thermal and photochemical reactivity. *Organometallics*, 2018, 37(4), pp. 570-583. DOI: <https://doi.org/10.1021/acs.organomet.7b00892>
 38. Simonov, Yu.A.; Dvorkin, A.A.; Malinovskii, T.I.; Bel'skii, V.K.; Bulgak, I.I.; Batyr, D.G.; Ozols, L. Crystal structure of *tris*(1,2-cyclohexanedione dioxime)iron(II) oxalate monohydrate. *Russian Journal of Coordination Chemistry*, 1985, 11(11), pp. 1554-1558. (in Russian).
 39. Simonov, Yu.M.; Botoshanskii, M.M.; Malinovskii, T.I.; Batyr, D.G.; Ozol, L.D.; Bulgak, I.I. Structure of *cis*-dichloro-*bis*(1,2-cyclohexanedione dioxime) nickel(II). Report of the Academy of Sciences of USSR, 1979, 246(3), pp. 609-613. (in Russian). <http://mi.mathnet.ru/rus/dan/v246/i3/p609>
 40. Simonov, Yu.A.; Botoshanskii, M.M.; Bulgak, I.I.; Batyr, D.G.; Malinovskii, T.I. Crystal structure of *tris*-(1,2-cyclohexanedione dioxime)nickel(II) sulfate dihydrate. *Russian Journal of Coordination Chemistry*, 1981, 7(4), pp. 612-618. (in Russian).
 41. Ozol, L.D.; Botoshanskii, M.M.; Bulgak, I.I.; Batyr, D.G.; Simonov, Yu.A. X-ray diffraction analysis of isostructural octahedral complexes of cobalt(II), nickel(II), and copper(II) with α -dioximes. *Russian Journal of Inorganic Chemistry*, 1980, 25(4), pp. 1137-1139. (in Russian).
 42. Simonov, Yu.A.; Dvorkin, A.A.; Malinovskii, T.I.; Batyr, D.G.; Bulgak, I.I.; Ozol, L.D. Crystal and molecular structure of

- catena- μ -iodo-(1,2-cyclohexane dionedioxime) copper(I). Report of the Academy of Sciences of USSR, 1982, 263(5), pp. 1135-1138. (in Russian).
<http://mi.mathnet.ru/rus/dan/v263/i5/p1135>
43. Coropceanu, E.B.; Ureche, D.; Rija, A.P.; Ciloci, A.A.; Clapco, S.F.; Dvornina, E.G.; Bulhac, I.I.; Cocu, M.; Bourosh, P.N. Synthesis and structures of nickel(II) complexes based on dianilineglyoxime. Stimulation of the proteolytic properties by $[\text{Ni}(\text{DAnH})_2] \cdot 0.25\text{H}_2\text{O}$. Russian Journal of Coordination Chemistry, 2021, 47(1), pp. 17–25.
 DOI: <https://doi.org/10.1134/S1070328421010024>
 44. Ureche, D.; Bulhac, I.; Shova, S.; Bourosh, P. Pseudomacrocyclic bis(dianilineglyoximate) cobalt(III) complex cations: synthesis and structures. Russian Journal of Coordination Chemistry, 2022, 48(6), pp. 333–343. DOI: <https://doi.org/10.1134/S1070328422060070>
 45. Zevaco, T.A.; Männle, D.; Walter, O.; Dinjus, E. An easy way to achieve three-dimensional metal–organic coordination polymers: synthesis and crystal structure of dizinc diisophthalate *bis*-dimethylsulfoxide monohydrate: $[\text{Zn}_2(\text{ip})_4(\text{DMSO})_2(\text{H}_2\text{O}) \cdot 3\text{DMSO}]_n$. Applied Organometallic Chemistry, 2007, 21(11), pp. 970–977. DOI: <https://doi.org/10.1002/aoc.1325>
 46. Diana, R.; Panunzi, B.; Tuzi, A.; Caruso, U. Two tridentate pyridinyl-hydrazone zinc(II) complexes as fluorophores for blue emitting layers. Journal of Molecular Structure, 2019, 1197, pp. 672–680. DOI: <https://doi.org/10.1016/j.molstruc.2019.07.098>
 47. Diana, R.; Panunzi, B. Zinc(II) and AlEgens: the „Clip Approach” for a novel fluorophore family. A review. Molecules, 2021, 26(14), 4176, pp. 1–31. DOI: <https://doi.org/10.3390/molecules26144176>
 48. Rija, A.; Bulhac, I.; Coropceanu, E.; Gorincioi, E.; Calmîc, E.; Barbă, A.; Bologa, O. Synthesis and spectroscopic study of some coordinative compounds of Co(III), Ni(II) and Cu(II) with dianiline- and disulfanilamideglyoxime. Chemistry Journal of Moldova, 2011, 6(2), pp. 73–78.
 DOI: [https://doi.org/10.19261/cjm.2011.06\(2\).16](https://doi.org/10.19261/cjm.2011.06(2).16)
 49. CrysAlis RED, O.D.L. Version 1.171.34.76. 2003.
<https://www.rigaku.com/products/crystallography/crysalis>
 50. Sheldrick, G.M.; Crystal structure refinement with SHELXL. Acta Crystallographica Section C, 2015, 71(1), pp. 3–8.
 DOI: <https://doi.org/10.1107/s2053229614024218>
 51. Bellamy, L.J. The Infrared Spectra of Complex Molecules. Wiley: New York, 1954, 590 p.
 DOI: <https://doi.org/10.1007/978-94-011-6017-9>
 52. Tarasevich, B.N. IR spectra of the main classes of organic compounds. Reference Materials. MGU: Moscow, 2012, 55 p. (in Russian).
http://www.chem.msu.su/rus/teaching/tarasevich/Tarasevich_IR_tables_29-02-2012.pdf
 53. Gordon, A.J.; Ford, R.A. The Chemist's Companion. A Handbook of Practical Data, Techniques and References. Wiley: New York, 1972, 560 p. <https://www.wiley.com/en-us/The+Chemist's+Companion:+A+Handbook+of+Practical+Data,+Techniques,+and+References-p-9780471315902>
 54. Nakanishi, K. Infrared Absorption Spectroscopy. Holden-Day: Tokyo, 1962, 233 p.
 55. Allen, F.H. The Cambridge Structural Database: a quarter of a million crystal structures and rising. Acta Crystallographica Section B, 2002, 58(3), pp. 380–388.
 DOI: <https://doi.org/10.1107/s0108768102003890>
 56. Croitor, L.; Coropceanu, E.B.; Jeanneau, E.; Dementiev, I.V.; Goglidze, T.I.; Chumakov, Y.M.; Fonari, M.S. Anion-induced generation of binuclear and polymeric Cd(II) and Zn(II) coordination compounds with 4,4'-bipyridine and dioxime ligands. Crystal Growth & Design, 2009, 9(12), pp. 5233–5243.
 DOI: <https://doi.org/10.1021/cg900746w>
 57. Coropceanu, E.; Croitor, L.; Ciloci, A.; Clapco, S.; Labliuc, S.; Codreanu, S.; Fonari, M. Synthesis and structure of some zinc and cadmium 1,2-cyclohexanedione dioximines. Russian Journal of Coordination Chemistry, 2017, 43(7), pp. 433–440.
 DOI: <https://doi.org/10.1134/S1070328417070053>
 58. Croitor, L.; Coropceanu, E.B.; Masunov, A.E.; Rivera-Jacquez, H.J.; Siminel, A.V.; Fonari, M.S. Mechanism of nonlinear optical enhancement and supramolecular isomerism in 1D polymeric Zn(II) and Cd(II) sulfates with pyridine-4-aldoxime ligands. The Journal of Physical Chemistry C, 2014, 118(17), pp. 9217–9227.
 DOI: <https://doi.org/10.1021/jp5007395>

SYNTHESIS, CHARACTERIZATION AND ANTIBACTERIAL ACTIVITY OF FERROCENE LIGANDS AND THEIR BINUCLEAR COMPLEXES

Ozan Süleyman Ürgüt^{a*}, Aydın Tavman^b, Muazzez Gürkan Eser^c

^aDepartment of Chemistry, Faculty of Arts and Sciences, Tekirdag Namik Kemal University, Namik Kemal District, Degirmenalti Campus, 1, Campus str., Suleymanpasa-Tekirdag 59030, Turkey

^b Department of Chemistry, Engineering Faculty, Istanbul University-Cerrahpasa, University District, 7, Baglarici str., Avclar-Istanbul 34320, Turkey

^cDepartment of Biology, Faculty of Arts and Sciences, Tekirdag Namik Kemal University, Namik Kemal District, Degirmenalti Campus, 1, Campus str., Suleymanpasa-Tekirdag 59030, Turkey

*e-mail: ourgut@nku.edu.tr, phone: (+90 282) 25 026 52

Abstract. 6-Chloro-2-ferrocenyl-1H-benzimidazole and (E)-((4-chloro-2-hydroxyphenylimino) methyl)ferrocene ligands and their Fe(III), Co(II), Cu(II), Zn(II) and Pd(II) complexes were synthesized. The structures of compounds were confirmed on the basis of elemental analysis, FT-IR, ¹H and ¹³C NMR, UV-Vis spectroscopy and mass spectrometry. In addition, magnetic moment and molar conductivity measurements were performed for the complexes. The Fe(III), Cu(II), Zn(II) and Co(II) complexes do not manifest electrolytic properties while Pd(II) complexes have electrolytic properties. All the complexes coordinate in a 1:1 M:L ratio. Benzimidazoles have a potential to be used as antibacterial agents alternative to current antibiotics to which bacteria gain resistance day by day. The antibacterial activity of the ligands and the complexes was investigated against *Staphylococcus aureus* and *Escherichia coli*. The obtained complexes generally show considerable high activity compared to the ligands, and it was revealed that the complexes of benzimidazole presented a more pronounced activity in comparison to other investigated compounds. The high activities of the Co complex of the benzimidazole ligand and the Zn complex of the Schiff base ligand against *Staphylococcus aureus* (2 and 4 mg/mL, respectively), are noteworthy.

Keywords: azomethine, binuclear complex, organometallic, transition metal complex, antibacterial property.

Received: 23 May 2022/ Revised final: 08 August 2022/ Accepted: 11 August 2022

Introduction

Many organometallic cyclic molecules have been synthesized in recent years, especially metallocenes, which are of particular interest as they have different coordination abilities and can withstand multiple electron transfer processes. Ferrocene is one of the most popular metallocene complex. Ferrocene derivatives have received great interest due to their potential applications as sensitive electrochemical sensors, nonlinear optical materials, antibacterial and anticancer drugs, nanotube materials, catalysts, ionic recognition and redox fluorescent switch [1,2]. There has been great interest in the functionalization of metallocene molecules; addition of ferrocene to some coordination compounds increases their cytotoxic activity. The affinity of the two cyclopentadiene rings in ferrocene to bond and the redox ability of the central iron explain this success, allowing ferrocene to be tuned to different challenges [3]. Benzimidazole is a bicyclic organic compound

formed by the fusion of benzene and imidazole rings [4]. Ferrocene-based benzimidazole derivatives are attracting much attention for the synthesis of new heterocyclic complexes with many applications including ionic recognition, metal complexes, fluorescent probes, enantioselective and heterogeneous catalysts [5]. The properties that ferrocene gives to heterocyclic moiety are now of great interest to researchers [6].

Schiff bases obtained from amino and aldehyde compounds contain an azomethine group (-HC=N-), which is an important class of ligands that coordinate with metal ions through the nitrogen atom. The presence of azomethine group is important in elucidating the mechanism of biological transformation and racemization reaction [7]. Ferrocenyl bonded to Schiff base compounds creates a link between organometallic chemistry and molecular biotechnology.

Schiff base molecules have great potential sites for biochemically active compounds related to intermolecular hydrogen bonding and proton

transfer equilibrium. The transition metal complexes of some Schiff bases are of interest because of their antifungal, antibacterial and antitumor activities, as well as their spectroscopic properties and applications [8].

The aim of this study was to synthesize ferrocene derivatives of benzimidazole and Schiff base ligands structurally similar and to obtain their metal complexes, to examine and compare the structural properties and antibacterial effects of all the compounds. Thus, the 6-Chloro-2-ferrocenyl-1*H*-benzimidazole, **L1**, and (*E*)-((4-chloro-2-hydroxyphenylimino)methyl)ferrocene, **HL2**, ligands, and their Fe(III), Co(II), Cu(II), Zn(II) and Pd(II) complexes were synthesized and characterized. The antibacterial activity of the ligands and the complexes was tested against *Escherichia coli* and *Staphylococcus aureus* strains.

Experimental

Generalities

Dichloromethane (anhydrous, $\geq 99.8\%$), acetic acid ($\geq 99.8\%$), ethyl alcohol, methyl alcohol ($\geq 99.8\%$), acetonitrile, acetone ($\geq 99.5\%$), ethyl acetate, *n*-hexane, dimethyl sulfoxide (DMSO), potassium chloride (99.0-99.5%), boric acid, ferrocenecarboxaldehyde, 2-amino-4-chlorophenol, 4-chloro-*o*-phenylenediamine, iron(III) chloride, copper(II) chloride dihydrate, cobalt(II) chloride hexahydrate, zinc(II) chloride, and palladium(II) chloride hexahydrate were purchased from Sigma-Aldrich and Supelco and used without further purification.

Elemental analysis data were obtained by using a Thermo Finnigan Flash EA 1112 analyzer.

Molar conductivity of the complexes was measured on a VWR Phenomenal conductometer CO 3000 L in dimethylformamide (DMF) at $25 \pm 1^\circ\text{C}$.

Magnetic moment measurements for the paramagnetic complexes were carried out on a Sherwood Scientific apparatus (MK1) at room temperature by Gouy's method.

FT-IR spectra were recorded on a Bruker Optics Vertex 70 spectrometer using ATR (Attenuated Total Reflection) techniques.

^1H NMR (500 MHz, DMSO- d_6) and ^{13}C NMR (125 MHz, DMSO- d_6) spectra were registered on a Varian Unity Inova 500 NMR spectrometer.

The electron spray ionization-mass spectroscopic (ESI-MS) analyses were carried out in positive ion modes using a Thermo Finnigan LCQ Advantage MAX LC/MS/MS.

UV-Vis spectra were performed on a Shimadzu UV-2600UV-Vis Spectrometer at molar concentration of 10^{-2} in DMSO.

Synthesis

6-Chloro-2-ferrocenyl-1*H*-benzimidazole (**L1**)

The novel **L1** was synthesized according to the literature method with a minor modification [9]. To the well stirred solution of ferrocenecarboxaldehyde (0.214 g, 0.001 mol) in ethanol (10 mL) was added 0.001 mol H_3BO_3 and stirred with gentle heating for 30 minutes followed by addition of an ethanolic solution of 4-chloro-*o*-phenylenediamine (0.142 g, 0.001 mol). The reaction mixture was further refluxed with continuous stirring for 2 hours; the progress of the reaction was monitored with thin layer chromatography (TLC) upon completion of the reaction. The reaction was terminated with water and allowed to cool to room temperature, and then filtered with vacuum. The filtered claret red product was washed with ethanol. The obtained solid phase was filtered, washed with ethanol several times and dried in a vacuum drying oven, giving a clear yellow solid compound. A quantity of 0.239 g (71%) of the reaction product **L1** was obtained with m.p. $267\text{--}269^\circ\text{C}$. Anal. calcd. for $\text{C}_{17}\text{H}_{13}\text{ClFeN}_2$ (formula weight: 336.0): C, 60.66; H, 3.89; N, 8.32%; found: C, 59.87; H, 4.12; N, 8.11%. ESI-MS (m/z , %): 337.2 ($[\text{M}+\text{H}]^+$, 100), 199.2 (10.4). Molar conductivity Λ_{M} (DMF, 25°C , $\text{S}\cdot\text{m}^2/\text{mol}$): 4.80. FT-IR (ATR, cm^{-1}): 3093 br $\nu(\text{N-H})$, 1624 w $\nu(\text{C=N})$, 1562 m, 1427 m $\nu(\text{C=C, Fc})$, 1408 m $\nu(\text{C=C})$, 1057 m $\nu(\text{Ar-Cl})$, 800 s $\nu(\text{C-H, Fc})$, 486 s $\nu(\text{Cp-Fe, Fc})$, 428 m $\nu(\text{Cp-Fe, Fc})$. UV-Vis (λ_{max} / nm): 446 br, 312 s, 265 m. ^1H NMR, δ_{H} ppm: 12.51 (1H, br, H3), 7.68 (1H, m, H4), 7.12 (1H, m, H6), 6.46 (1H, m, H7), 4.48 (2H, s, H11), 4.22 (2H, s, H12), 4.15 (5H, s, H13). ^{13}C NMR, δ_{C} ppm: 154.61 (C-2), 139.82 (C-9), 133.49 (C-8), 125.71 (C-5), 121.47 (C-6), 114.98 (C-7), 108.67 (C-4), 73.28 (C-10), 69.98 (C-11), 69.40 (C-12), 67.41 (C-13). [$\text{Fe}(\text{L1})\text{Cl}_3(\text{H}_2\text{O})$] (**1a**)

A quantity of 0.337 g **L1** (0.001 mol) was dissolved in methanol (20 mL) in a 50 mL round-bottomed flask and FeCl_3 (0.162 g, 0.001 mol) in methanol : water (20 mL : 2 mL) was added to **L1** solution and the mixture was heated gently until 20 mL remained, and then refluxed for 2 hours; the progress of the reaction was monitored with TLC upon completion of the reaction. The product was filtered and kept at room temperature for slow evaporation. The resulting dark green solid was collected by filtration and purified with acetone. A quantity of

0.435 g (78%) of the reaction product **1a** was obtained with m.p. 280–282°C (decomp.). Anal. calcd. for $C_{17}H_{15}Cl_4Fe_2N_2O$ (formula weight: 514.9): C, 39.51; H, 2.93; N, 5.42%; found: C, 40.39; H, 2.78; N, 6.55%. ESI-MS (m/z , %): 512.9 ($[(M-2H)]^+$, 18). Magnetic moment, μ_{eff} : 6.20 μ_B . Molar conductivity Λ_M (25°C, $S \cdot m^2/mol$): 30.6. FT-IR (ATR, cm^{-1}): 3304 m, br $\delta(N-H)$, 1620 s $\delta(C=N)$, 1442 s $\delta(C=C, Fc)$, 1409 s $\delta(C=C)$, 1062 m $\delta(Ar-Cl)$, 810 m $\delta(C-H, Fc)$, 478 m $\delta(Fe-N)$, 422 m $\delta(Cp-Fe, Fc)$. UV-Vis ($\lambda_{\text{max}} / nm$): 309 s, 293 br, 261 sh, 229 sh.

[Zn(L1)Cl₂(H₂O)] (1b)

A quantity of 0.337 g **L1** (0.001 mol) was dissolved in methanol (20 mL) in a 50 mL round-bottomed flask; $ZnCl_2 \cdot 6H_2O$ (0.244 g, 0.001 mol) in methanol : water (40 mL : 4 mL) was added to **L1** solution and the mixture was heated gently until 20 mL remained and then refluxed for 3 hours; the progress of the reaction was monitored with TLC upon completion of the reaction. The mixture was filtered and kept at vacuum for evaporation. The resulting brown solid was collected by filtration and purified with methanol. A quantity of 0.398 g (81%) of the reaction product **1b** was obtained with m.p. 170–172°C (decomp.). Anal. calcd. for $C_{17}H_{15}Cl_3FeN_2OZn$ (formula weight: 490.9): C, 41.59; H, 3.08; N, 5.71%; found: C, 40.82; H, 3.64; N, 5.18%. ESI-MS (m/z , %): 535.3 ($[M+C_2H_5OH]$, 100). Magnetic moment, μ_{eff} : 1.10 μ_B . Molar conductivity Λ_M (25°C, $S \cdot m^2/mol$): 20.7. FT-IR (ATR, cm^{-1}): 3203 m, br $\nu(N-H)$, 1620s $\nu(C=N)$, 1427 m $\nu(C=C, Fc)$, 1408 m $\nu(C=C)$, 1060 w $\nu(Ar-Cl)$, 802 w $\nu(C-H, Fc)$, 547 w $\nu(Zn-N)$, 482 m $\nu(Cp-Fe, Fc)$, 426 m $\nu(Cp-Fe, Fc)$. UV-Vis ($\lambda_{\text{max}} / nm$): 450 br, 344 br, 304 sh, 228 sh.

[Cu(L1)Cl₂(H₂O)] (1c)

A quantity of 0.337 g of **L1** (0.001 mol) was dissolved in methanol (20 mL) in a 50 mL round-bottomed flask; $CuCl_2 \cdot 2H_2O$ (0.170 g, 0.001 mol) in methanol : water (20 mL : 2 mL) was added to **L1** solution and the mixture was heated gently until 20 mL remained and then refluxed for 3 hours; the progress of the reaction was monitored with TLC upon completion of the reaction. The mixture was filtered and kept in vacuum for evaporation. The resulting brown solid was collected by filtration and purified with methanol/*n*-hexane (30/70) mixture. A quantity of 0.414 g (85%) of the reaction product **1c** was obtained with m.p. > 300°C. Anal. calcd. for $C_{17}H_{15}Cl_3CuFeN_2O$ (formula weight: 486.89): C, 41.75; H, 3.09; N, 5.73%; found: C, 40.98;

H, 3.45; N, 5.09%. ESI-MS (m/z , %): 487.5 ($[M]^+$, 50.01). Magnetic moment, μ_{eff} : 1.80 μ_B . Molar conductivity Λ_M (25°C, $S \cdot m^2/mol$): 31.0. FT-IR (ATR, cm^{-1}): 3321 m, br $\nu(N-H)$, 1581 s $\nu(C=N)$, 1444 s $\nu(C=C, Fc)$, 1413 s $\nu(C=C)$, 1062 m $\nu(Ar-Cl)$, 810 m $\nu(C-H, Fc)$, 596 m $\nu(Cu-N)$, 474 m $\nu(Cp-Fe, Fc)$, 430 m $\nu(Cp-Fe, Fc)$. UV-Vis ($\lambda_{\text{max}} / nm$): 290 s, 285 sh, 229 sh.

[Co(L1)Cl₂(H₂O)₃] (1d)

A quantity of 0.337 g **L1** (0.001 mol) was dissolved in methanol (20 mL) in a 50 mL round-bottomed flask; $CoCl_2 \cdot 6H_2O$ (0.238 g, 0.001 mol) in methanol : water (20 mL : 2 mL) was added to **L1** solution and the mixture was heated gently until 20 mL remained and then refluxed for 2.5 hours; the progress of the reaction was monitored with TLC upon completion of the reaction. The mixture was filtered and kept in vacuum for evaporation. The resulting dark green solid was collected by filtration and purified with ethyl acetate/*n*-hexane (10/90) mixture. A quantity of 0.457 g (88%) of the reaction product **1d** was obtained with m.p. > 300°C. Anal. calcd. for $C_{17}H_{19}Cl_3CoFeN_2O_3$ (formula weight: 518.90): C, 39.23; H, 3.68; N, 5.38%; found: C, 39.47; H, 3.73; N, 4.74%. ESI-MS (m/z , %): 520.48 ($[M+1]^+$, 100). Magnetic moment, μ_{eff} : 5.11 μ_B . Molar conductivity Λ_M (25°C, $S \cdot m^2/mol$): 31.8. FT-IR (ATR, cm^{-1}): 3388 m $\nu(N-H)$, 1562 m $\nu(C=N)$, 1427 m $\nu(C=C, Fc)$, 1406 m $\nu(C=C)$, 1057 w $\nu(Ar-Cl)$, 798 m $\nu(C-H, Fc)$, 551 w $\nu(Co-N)$, 486 s $\nu(Cp-Fe, Fc)$, 426 m $\nu(Cp-Fe, Fc)$. UV-Vis ($\lambda_{\text{max}} / nm$): 436 br, 312 s, 267 sh, 227 sh.

[Pd(L1)Cl(H₂O)]Cl (1e)

A quantity of 0.337 g **L1** (0.001 mol) was dissolved in methanol (20 mL) in a 50 mL round-bottomed flask; $PdCl_2$ (0.177 g, 0.001 mol) and KCl (0.149 g, 0.002 mol) stirred in methanol : water (50 mL : 5 mL) and added to **L1** solution. Reaction mixture was heated gently until 20 mL remained and then refluxed for 4 hours; the progress of the reaction was monitored with TLC upon completion of the reaction. The mixture was filtered and kept in vacuum for evaporation. The resulting brown solid was collected by filtration and purified with *n*-hexane. A quantity of 0.378 g (71%) of the reaction product **1e** was obtained with m.p. > 300°C. Anal. calcd. for $C_{17}H_{15}Cl_3FeN_2OPd$ (formula weight: 531.90): C, 38.38; H, 2.84; N, 5.27%; found: C, 38.97; H, 2.66; N, 5.55%. ESI-MS (m/z , %): 551.2 ($[M+]$, 17). Magnetic moment, μ_{eff} : 2.20 μ_B . Molar conductivity Λ_M (25°C, $S \cdot m^2/mol$): 104.1. FT-IR (ATR, cm^{-1}): 3385 m, br $\nu(N-H)$, 1620 m $\nu(C=N)$, 1438 m $\nu(C=C, Fc)$, 1408 m $\nu(C=C)$,

1060 w $\nu(\text{Ar-Cl})$, 802 w $\nu(\text{C-H, Fc})$, 503 w $\nu(\text{Cp-Fe, Fc})$, 482 m $\nu(\text{Pd-N})$, 426 m $\nu(\text{Cp-Fe, Fc})$. UV-Vis ($\lambda_{\text{max}} / \text{nm}$): 308 s, 265 m, 229 sh. (E)-((4-Chloro-2-hydroxyphenylimino)methyl)ferrocene (**HL2**)

Ferrocenecarboxaldehyde (0.214 g, 0.001 mol) was dissolved in toluene (25 mL) in a 100 mL round-bottomed flask. 2-Amino-4-chlorophenol (0.143 g, 0.001 mol) and CH_3COOH (0.060 g, 0.001 mol, 1.05 g/mL) was stirred in toluene (40 mL); 2-amino-4-chlorophenol mixture was added to ferrocenecarboxaldehyde solution drop-wise during a period of 10 min. The dean stark apparatus was used to increase the reaction yield by removing the water formed from the reaction environment. The reaction mixture was refluxed with dean stark apparatus for 3 hours [10]; the progress of the reaction was monitored with TLC upon completion of the reaction. The reaction was filtered with vacuum. The filtered claret red product was collected by filtration and purified with acetone and then acetonitrile. A quantity of 0.239 g (72%) of the reaction product **HL2** was obtained with m.p. 114–116°C. Anal. calcd. for $\text{C}_{17}\text{H}_{14}\text{ClFeNO}$ (formula weight: 339.6): C, 60.12; H, 4.16; N, 4.12%; found: C, 60.01; H, 4.76; N, 4.98%. ESI-MS ($m/z, \%$): 340.0 ($[\text{M}]^+$, 100). Molar conductivity Λ_{M} (25°C, $\text{S}\cdot\text{m}^2/\text{mol}$): 22.9. FT-IR (ATR, cm^{-1}): 3317 br, m $\nu(\text{O-H})$, 1581 m $\nu(\text{C=N})$, 1495 m $\nu(\text{C=C, Fc})$, 1425 m $\nu(\text{C=C})$, 1090 w $\nu(\text{Ar-Cl})$, 820 w $\nu(\text{C-H, Fc})$, 490 w $\nu(\text{Cp-Fe, Fc})$, 411 m $\nu(\text{Cp-Fe, Fc})$. UV-Vis ($\lambda_{\text{max}} / \text{nm}$): 442 m, 421 m, 302 sh. ^1H NMR, δ_{H} ppm: 9.88 (1H, s, H1), 8.58 (1H, s, H2), 7.72 (1H, s, H4), 7.16 (1H, s, H6), 6.61 (1H, m, H7), 4.80 (2H, m, H11), 4.66 (2H, m, H12), 4.29 (5H, s, H13). ^{13}C NMR, δ_{H} ppm: 163.17 (C-2), 148.88 (C-8), 142.81 (C-9), 126.42 (C-4), 122.59 (C-5), 115.73 (C-6), 113.65 (C-7), 79.22 (C-10), 72.82 (C-11), 71.25 (C-12), 69.34 (C-13).

$[\text{Fe}(\text{HL2})\text{Cl}_3(\text{H}_2\text{O})]\cdot\text{H}_2\text{O}$ (**2a**)

A quantity of 0.339 g (0.001 mol) **HL2** was dissolved in methanol (20 mL) in a 50 mL round-bottomed flask; FeCl_3 (0.162 g, 0.001 mol) in methanol : water (20 mL : 2 mL) was added to **HL2** solution and the mixture was heated gently until 20 mL remained and then refluxed for 4 hours; the progress of the reaction was monitored with TLC upon completion of the reaction. The brown precipitate was filtered and kept at room temperature for slow evaporation. The obtained brown precipitate was washed a few times with methanol, and dried under vacuum. A quantity of 0.403 g (75%) of the reaction product **2a** was obtained with m.p. > 300°C. Anal.

calcd. for $\text{C}_{17}\text{H}_{18}\text{Cl}_4\text{Fe}_2\text{NO}_3$ (formula weight: 537.8): C, 37.96; H, 3.37; N, 2.60%; found: C, 37.23; H, 3.98; N, 2.54%. ESI-MS ($m/z, \%$): 538.8 ($[\text{M}+\text{H}]^+$, 46), ($[\text{M}-\text{H}_2\text{O}]$, 15). Magnetic moment, μ_{eff} : 5.70 μ_{B} . Molar conductivity Λ_{M} (25°C, $\text{S}\cdot\text{m}^2/\text{mol}$): 37.9. FT-IR (ATR, cm^{-1}): 3211 s, br $\nu(\text{O-H})$, 1614 m $\nu(\text{C=N})$, 1492 m $\nu(\text{C=C, Fc})$, 1417 m $\nu(\text{C=C})$, 1118 w $\nu(\text{Ar-Cl})$, 801 m $\nu(\text{C-H, Fc})$, 747 m $\nu(\text{Fe-O})$, 476 w $\nu(\text{Cp-Fe, Fc})$, 467 w $\nu(\text{Fe-N})$, 428 w $\nu(\text{Cp-Fe, Fc})$. UV-Vis ($\lambda_{\text{max}} / \text{nm}$): 340 br, 260 s, 234 sh. $[\text{Zn}(\text{HL2})\text{Cl}_2]\cdot\text{H}_2\text{O}$ (**2b**)

A quantity of 339 g (0.001 mol) **HL2** was dissolved in methanol (20 mL) in a 50 mL round-bottomed flask; $\text{ZnCl}_2\cdot 6\text{H}_2\text{O}$ (0.244 g, 0.001 mol) in methanol : water (40 mL : 4 mL) was added to **HL2** solution and the mixture was heated gently until 20 mL remained and then refluxed for 2 hours; the progress of the reaction was monitored with TLC upon completion of the reaction. The reaction mixture was filtered and allowed to cool. The resulting claret red precipitate was washed with a few times with *n*-hexane and dried under vacuum. A quantity of 0.445 g (90%) of the reaction product **2b** was obtained with m.p. 120–122°C. Anal. calcd. for $\text{C}_{17}\text{H}_{16}\text{Cl}_3\text{FeNO}_2\text{Zn}$ (formula weight: 490.9): C, 41.34; H, 3.27; N, 2.84%; found: C, 41.78; H, 3.07; N, 2.76%. ESI-MS ($m/z, \%$): 490.4 ($[\text{M}]^+$, 48). Magnetic moment, μ_{eff} : 1.90 μ_{B} . Molar conductivity Λ_{M} (25°C, $\text{S}\cdot\text{m}^2/\text{mol}$): 14.1. FT-IR (ATR, cm^{-1}): 3369 s, br $\nu(\text{O-H})$, 1597 s $\nu(\text{C=N})$, 1479 m $\nu(\text{C=C, Fc})$, 1456 m $\nu(\text{C=C})$, 1107 w $\nu(\text{Ar-Cl})$, 812 m $\nu(\text{C-H, Fc})$, 570 w $\nu(\text{Zn-N})$, 471 s $\nu(\text{Zn-O})$, 403 w $\nu(\text{Cp-Fe, Fc})$. UV-Vis ($\lambda_{\text{max}} / \text{nm}$): 437 br, 418 br, 301 sh, 234 s. $[\text{Cu}(\text{HL2})\text{Cl}_2]\cdot\text{H}_2\text{O}$ (**2c**)

A quantity of 0.339 g (0.001 mol) **HL2** was dissolved in methanol (20 mL) in a 50 mL round-bottomed flask; $\text{CuCl}_2\cdot 2\text{H}_2\text{O}$ (0.170 g, 0.001 mol) in methanol : water (30 mL : 3 mL) was added to **HL2** solution and the mixture was heated gently until 20 mL remained and then refluxed for 2 hours; the progress of the reaction was monitored with TLC upon completion of the reaction. The reaction mixture was filtered and allowed to cool. The resulting brown precipitate was collected by filtration and purified with dichloromethane/*n*-hexane (20/80) mixture. A quantity of 0.340 g (69%) of the reaction product **2c** was obtained with m.p. 240–242°C. Anal. calcd. for $\text{C}_{17}\text{H}_{16}\text{Cl}_3\text{CuFeNO}_2$ (formula weight: 492.1): C, 41.49; H, 3.28; N, 2.85%; found: C, 40.93; H, 3.78; N, 2.14%. ESI-MS ($m/z, \%$): 491.0 ($[\text{M}-1]^+$, 54.5). Magnetic moment, μ_{eff} : 1.72 μ_{B} . Molar conductivity Λ_{M} (25°C,

S·m²/mol): 26.3. FT-IR (ATR, cm⁻¹): 3319 m, br ν (O–H), 1568 m ν (C=N), 1492 m ν (C=C, Fc), 1423 m ν (C=C), 1091 w ν (Ar–Cl), 819 w ν (C–H, Fc), 667 w ν (Cu–N), 442 w ν (Cu–O), 422 w ν (Cp–Fe, Fc), 408 w ν (Cp–Fe, Fc). UV-Vis (λ_{max} / nm): 420 br, 290 br, 229 sh. [Co(HL2)Cl₂(H₂O)₂]·H₂O (**2d**)

A quantity of 0.339 g (0.001 mol) **HL2** was dissolved in methanol (20 mL) in a 50 mL round-bottomed flask; CoCl₂·6H₂O (0.238 g, 0.001 mol) in methanol : water (60 mL : 6 mL) was added to **HL2** solution and the mixture was heated gently until 20 mL remained and then refluxed for 4 hours; the progress of the reaction was monitored with TLC upon completion of the reaction. The reaction mixture was filtered and kept in vacuum for evaporation. The resulting brown solid was collected by filtration and purified with methanol/*n*-hexane (40/60) mixture. A quantity of 0.438 g (84%) of the reaction product **2d** was obtained with m.p. 148–150°C (decomp.). Anal. calcd. for C₁₇H₂₀Cl₃CoFeNO₄ (formula weight: 521.90): C, 39.00; H, 3.85; N, 2.68%; Found: C, 38.42; H, 4.03; N, 1.98%. ESI-MS (*m/z*, %): 520.2 ([M–1]⁺, 100). Magnetic moment, μ_{eff} : 4.41 BM. Molar conductivity Λ_{M} (25°C, S·m²/mol): 44.6. FT-IR (ATR, cm⁻¹): 3097 m ν (O–H), 1570 m ν (C=N), 1485 m ν (C=C, Fc), 1410 m ν (C=C), 1105 w ν (Ar–Cl), 818 m ν (C–H, Fc), 586 w ν (Co–N), 515 w ν (Co–O), 478 m ν (Cp–Fe, Fc), 457 m ν (Cp–Fe, Fc). UV-Vis (λ_{max} / nm): 442 br, 421 br, 259 s. [Pd(HL2)Cl(H₂O)]Cl (**2e**)

A quantity of 0.339 g (0.001 mol) **HL2** was dissolved in methanol (20 mL) in a 50 mL round-bottomed flask. PdCl₂ (0.177 g, 0.001 mol) and KCl (0.149 g, 0.002 mol) stirred in methanol : water (50 mL : 5 mL) and added to **HL2** solution. The reaction mixture was heated gently until 20 mL remained and then refluxed for 5 hours; the progress of the reaction was monitored with TLC upon completion of the reaction. The reaction mixture was filtered and allowed to cool. The resulting brown precipitate was collected by filtration and purified with dichloromethane/*n*-hexane (30/70) mixture. A quantity of 0.378 g (70%) of the reaction product **2e** was obtained with m.p. > 300°C. Anal. calcd. for C₁₇H₁₆Cl₃FeNO₂Pd (formula weight: 532.90): C, 38.17; H, 3.01; N, 2.62%; found: C, 38.87; H, 3.57; N, 2.32%. ESI-MS (*m/z*, %): 532.0 ([M–H]⁺, 100). Magnetic moment, μ_{eff} : 0.00 μ_{B} . Molar conductivity Λ_{M} (25°C, S·m²/mol): 73.1. FT-IR (ATR, cm⁻¹): 3389 m, br ν (O–H), 1601 m ν (C=N), 1479 w ν (C=C, Fc), 1410 w ν (C=C), 1107 w ν (Ar–Cl), 814 m ν (C–H, Fc), 471

m ν (Pd–N), 430 w ν (Cp–Fe, Fc), 409 w ν (Pd–O). UV-Vis (λ_{max} /nm): 425 m, br, 229 s.

Antibacterial activity evaluation

The synthesized ligands and their complexes were tested against one Gram-positive and one Gram-negative bacteria. The reference strains *Staphylococcus aureus* ATCC 25923 and *Escherichia coli* ATCC 25922 were obtained from the Turkish Republic General Directorate of Public Health, Ankara, Turkey. The bacteria were first grown on blood agar containing 5% sheep blood at 37°C. Later, the bacterial cell concentrations were adjusted to 0.5 McFarland and the bacteria were inoculated on Mueller Hinton agar plates under aseptic conditions using sterile cotton swabs. According to Balouiri, M. *et al.* the agar well diffusion method was then applied by forming 6 mm wells with the help of sterile pipette tips [11]. Different concentrations of the ligand and complexes were prepared by two-fold serial dilutions in DMSO starting from 256 mg/mL to 1 mg/mL. DMSO was also used as the negative control while 10 μ g Gentamicin sulphate (Sigma-Aldrich, Darmstadt, Germany) was used as positive control. A volume of 50 μ L of each concentration was added to the wells. The plates were kept at 37±0.1°C for 24 hours. After a careful visual inspection, the zones of antibacterial activity were determined and the diameter of clear zone around each well was measured in mm as an indicator of antibacterial activity of each compound and were compared with that of the standard antibiotic Gentamicin.

Results and discussion

Synthesis and characterisation

Synthesis of the **L1** and **HL2** ligands were given in Schemes 1 and 2, ferrocenecarboxaldehyde and 4-chloro-*o*-phenylenediamine (for **L1**) or 2-amino-4-chlorophenol (for **HL2**) were reacted in a 1:1 mole ratio. Also, the ligands and metal chlorides (FeCl₃, CoCl₂·6H₂O, CuCl₂·2H₂O, ZnCl₂·6H₂O and PdCl₂) reacted at a mole ratio of 1:1 to produce dinuclear metal complexes. **L1** is a monodentate ligand, and coordinates with metal ions through the imine nitrogen atom (C=N) [2]. Schiff base ligand (**HL2**) has a bidentate coordination. It can binary “grab” a metal atom over oxygen and nitrogen atoms [7]. The structure of ligands and complexes were characterized by the melting point, elemental analysis, FT-IR, ¹H and ¹³C NMR, UV-Vis

spectroscopy and mass spectrometry (ESI-MS) techniques. Molar conductivity and magnetic moment measurements were applied for further characterization of the complexes. A generalisation of analytical data and physical properties of ligands and complexes is given in Table S1 (see the Supplementary material).

Infrared spectroscopy characterization

Investigation of FT-IR peaks is important for comparison of ligand and metal complexes. Especially, C=N bands are characteristic for benzimidazoles, and the C=N and O–H bands for Schiff bases. The interaction between ligand and metal occur with these functional groups.

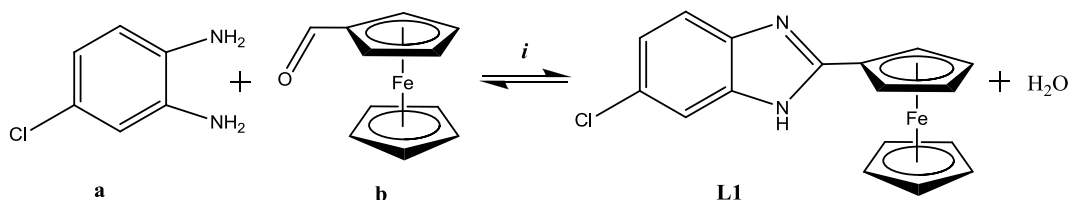
In the FT-IR spectra of the ligands, the medium bands at 1624 cm^{-1} (**L1**) and 1584 cm^{-1} (**HL2**) must belong to the C=N groups. The corresponding wavenumbers in the complexes are detected at the $1620\text{--}1562\text{ cm}^{-1}$ (**1a-e**) and $1614\text{--}1568\text{ cm}^{-1}$ ranges (**2a-e**). The C=N stretching frequencies of the complexes has been changed as it binds with metals *via* the C=N nitrogen atom [12,13].

For the functional ferrocene group, the characteristic C–H (out-of-plane) peaks were observed at $700\text{--}830\text{ cm}^{-1}$ range, C=C stretching at $1420\text{--}1470\text{ cm}^{-1}$ range, Cp–Fe stretching at around 400 and 500 cm^{-1} [14]. The NH band,

which can be observed at 3093 cm^{-1} in the benzimidazole ligand, shifts to 3300 cm^{-1} upon complex formation [15]. The O–H peak for **HL2** is observed at 3317 cm^{-1} [16]. The broad band between $3000\text{--}2500\text{ cm}^{-1}$ in the complexes could be attributed to the hydrogen bonding because of the coordinated and uncoordinated (lattice) water molecules. However, in the literature, it is seen that the O–H peak in the complexes of some Schiff bases with metals originates from the water in the environment [16,17]. Therefore, the O–H peaks in the compounds (**2a-e**) between 3389 and 3098 cm^{-1} could belong to H_2O . The appearance of the characteristic metal-nitrogen and metal-oxygen vibrations indicates the bidentate bonding of the Schiff base ligand to the metal ion [3,16-21].

NMR spectroscopy characterization

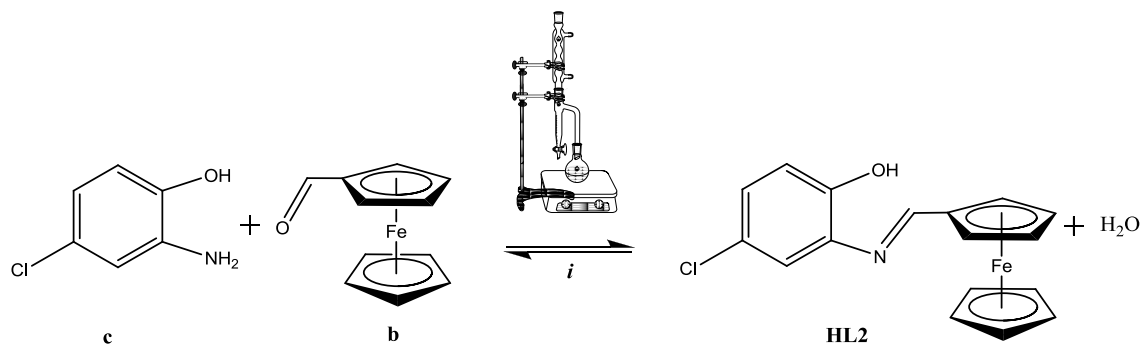
NMR spectra of the Pd(II) and Zn(II) complexes could not be recorded because of the paramagnetic effect of the ferrocene group. The characteristic single N–H signal of **L1** was observed at 12.51 ppm [22]. Phenolic OH and azomethine CH=N protons of Schiff base ligand (**HL2**) give singlet at 9.88 and 8.58 ppm , respectively [12,21]. The protons of the benzene ring of benzimidazole and Schiff base ligands were found in the range 6.46 to 7.72 ppm [23].



Reagent and conditions: i) EtOH solvent, H_3BO_3 catalyst, reflux 2 hours, 71%.

(a) 4-chloro-*o*-phenylenediamine; (b) ferrocenecarboxaldehyde

Scheme 1. Synthesis of 6-chloro-2-ferrocenyl-1H-benzimidazole (L1) ligand.



Reagent and conditions: i) toluene / acetic acid solvent mixture, reflux with Dean Stark apparatus 3 hours, 72%.

(c) 2-amino-4-chlorophenol; (b) ferrocenecarboxaldehyde

Scheme 2. Synthesis of (E)-((4-chloro-2-hydroxyphenylimino)methyl)ferrocene (HL2) ligand.

The chemical structure of the ligands, **L1** and **HL2**, are shown in Figure 1. There are 3 different types of protons in the ferrocene moiety H11 (two protons), H12 (two protons) and H13 (five protons). Chemical shift values of these protons are compatible with the literature [24].

The chemical shift values of the benzene rings of **L1** and **HL2** are at the range of 108.67-126.42 ppm for C4, C6 and C7 carbon atoms, and 125.71-122.59 ppm for substituted C5 carbons. Chemical shift values for the quaternary carbon atoms, C8 and C9, on the benzene ring, were observed at 133.49 ppm and 139.82 ppm (**L1**), and at 142.81 and 148.88 ppm (**HL2**), respectively. The chemical shift value for the benzimidazole ligand (**L1**) of the C2 (C=N) carbon was found to be 154.61 ppm and 163.17 ppm for the Schiff base (**HL2**) [22,25-27]. There are four different types of carbons in the ferrocene moiety of **L1** and **HL2**: C10 (one carbon), C11 (two carbons), C12 (two carbons) and C13 (five carbons). The ipso-carbon (C10) on the substituted Cp ring is observed at 73.29 ppm and 79.22 ppm for **L1** and **HL2**, respectively. C11 relates to two carbons adjacent to the carbon (C10) on the cyclopentadienyl (C₅H₄) ring with ferrocene bonds. C12, other protons in the cyclopentadienyl ring where ferrocene is attached to benzimidazole. The third type are the C13 carbons in the unsubstituted cyclopentadienyl (C₅H₅) ring. Chemical shift values of these carbons are compatible with the literature (Figures S1-S4) [25-27].

UV-Vis spectra analysis

The peaks observed in the low range (200–300 nm) represent the transition $\pi \rightarrow \pi^*$ in the aromatic rings of the ligands and complexes [25-27]. The 300–350 nm bands involve $\pi \rightarrow \pi^*$ transitions of the C=N group in Schiff base compounds containing ferrocene. In addition to this band, a weaker absorption is observed in the 430–460 nm range. This band indicates $d-d$ transitions in ferrocene-containing complexes but it is not always observed. The weak $d-d$ transitions found in Schiff bases cannot be clearly determined in UV-Vis spectroscopy (Figures 2 and 3) [13,28].

Metal ligand interaction in Fe(III) complexes can be observed as a shoulder band at 300 nm (**1a**) and 340 nm (**2a**) in the UV-vis spectrum [29]. Since Zn(II) complexes (**1b**, **2b**) have d^{10} electronic configuration, the $d-d$ transition was not observed. The band observed around 300–350 nm is due to the charge transfer transition between the ligand and the Zn(II) ion (L \rightarrow M; O \rightarrow M) [30].

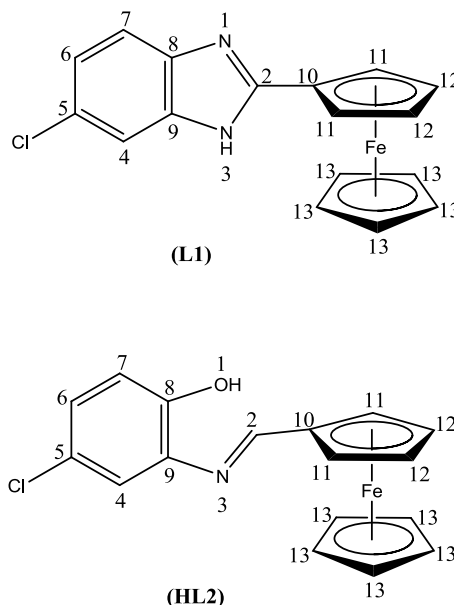


Figure 1. The chemical structure of the **L1** and **HL2** ligands.

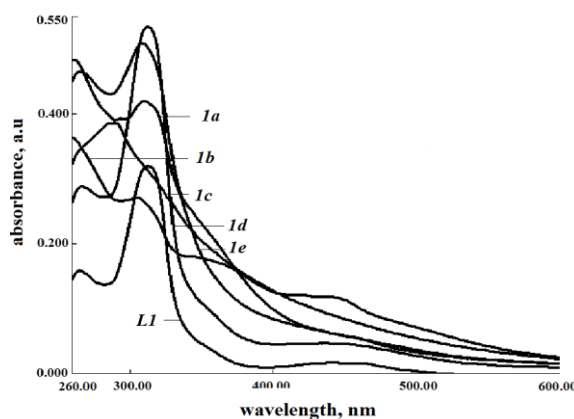


Figure 2. UV-Vis spectra of **L1**, **1a**, **1b**, **1c**, **1d** and **1e** at a concentration of 10^{-2} M in DMSO.

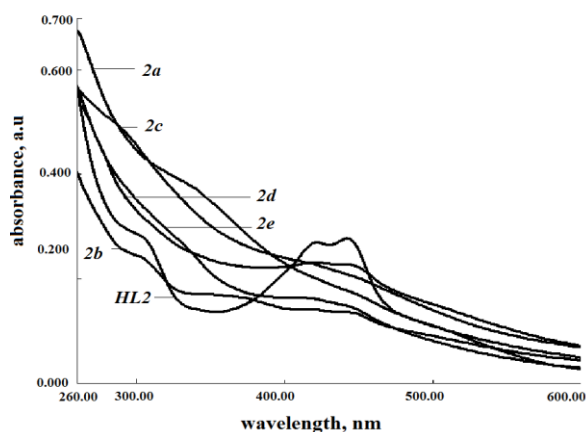


Figure 3. UV-Vis spectra of **HL2**, **2a**, **2b**, **2c**, **2d** and **2e** at a concentration of 10^{-2} M in DMSO.

The observed band at 290 nm (**1c**) and shoulder at 300 nm (**2c**) in the spectra of Cu(II) complexes is attributed to the charge transfer between metal and ligands assuming a square-planar configuration [31]. Co(II) (**1d**, **2d**) complexes have six coordinates and have octahedral structures, if **1d** and **2d** complexes have a $2a \rightarrow 1g$ transition, they will present a weak band at 530 nm. Absorptions between 250 and 330 nm are due to the ligand to metal charge transfer transition [32]. Pd(II) complexes (**1e**, **2e**) bonding with the ligand give a band at 280–340 nm in the UV-Vis spectrum. Non-bonding Pd(II) halides give bands at 450 nm [33].

Molar conductivity and magnetic moment measurements

Molar conductivity data of the complexes give useful information about the structure of the complexes. According to the molar conductivity data, Pd(II) complexes having molar conductivity values of 104.1 and 73.1 S·m²/mol, respectively for **1e** and **2e**, are 1:1 electrolytes. Only these two complexes react with AgNO₃ to form the AgCl salt. There was no precipitation of AgCl in the other complexes, indicating that the chloride anions are inside the coordination sphere of the complexes. Fe(III), Cu(II), Zn(II) and Co(II) complexes are not electrolytes since their molar conductivity value is in the range of 20.7–44.6 S·m²/mol. The molar conductivity values for the 1:1 electrolyte in DMF should generally be higher than 50 S·m²/mol [33,34].

Room temperature magnetic moment values of complex compounds match the predicted geometry and structural properties. Magnetic moment values (μ_{eff}) of the complexes are shown in the Experimental section. Many paramagnetic compounds containing ferrocene functional groups exhibit higher magnetic moment values than expected [35]. Also, diamagnetic Pd²⁺ complexes may show paramagnetic character since they have ferrocene. This unexpected situation indicates that the diamagnetic character of Fe²⁺ in the ferrocene group disappears with the unpaired electron pair found in ferrocene [34–36].

The magnetic moment values of Fe³⁺ complexes are 5.6–6.1 μ_B for high spin and 1.8–2.1 μ_B for low spin octahedral geometry [34–36]. The magnetic moment values of **1a** and **2a** are 6.2 and 5.7 μ_B respectively so their structures are estimated to be octahedral with high spin. Due to the diamagnetism of Zn²⁺ and Pd²⁺ ions, the μ_B values of the complexes **1b**, **2b**, **1e** and **2e** must be zero. However, the μ_B values both

of the complexes are positive due to paramagnetic effect of the ferrocene group [34–36]. Magnetic moment values of Cu²⁺ complexes, **1c** and **2c**, are 1.8 μ_B and 1.72 μ_B respectively, corresponding to one unpaired electron expected for d⁹ square-planar Cu²⁺ complexes [7,18–20]. Magnetic moment values of the Co²⁺ complexes are found as 5.11 μ_B for **1d** and 4.41 μ_B for **2d**. Co²⁺ complexes in the range of 4.3–5.2 μ_B in octahedral compounds are obtained [34–36]. The d⁸ electron configuration complexes are generally square planar, and in a small number of samples are tetrahedral. Although the coordination number is 3 in the empirical formulas of **1e** and **2e** in the results of the elemental analysis, these complexes may be in dimeric structure. In this case, the coordinated Cl anion can act as a bridging ligand and become a 4-coordinated structure. Therefore, it is highly probable that the Pd²⁺ complexes, **1e** and **2e**, are square planar.

Antibacterial activity evaluation of the complexes

The antibacterial activity of the ligands and the complexes was evaluated against a Gram-positive (*Staphylococcus aureus*) and a Gram-negative (*Escherichia coli*) bacterial strains. These bacteria are members of the normal flora of humans. Some strains of these bacteria have become resistant to many antibiotics. This situation is especially important for the normal flora bacteria which have developed to be antibiotic resistant and result in nosocomial infections [37,39]. Benzimidazoles have a potential to be used as antibacterial agents as alternative to current antibiotics to which bacteria gain resistance day by day [40]. Results of the antibacterial evaluation of the obtained compounds are summarized in Table 2.

Table 2
Concentration (mg/mL) of the compound showing significant inhibition compared to Gentamicin.

Compounds	<i>E. coli</i>	<i>S. aureus</i>
L1	>256	>256
1a	>256	>256
1b	128	16
1c	64	64
1d	64	2
1e	32	8
HL2	64	16
2a	128	64
2b	128	4
2c	32	64
2d	32	32
2e	64	128

The minimum inhibitory concentration of Gentamicin antibiotic for the bacteria used in this study was given to be less than 2 mg/mL by The European Committee on Antibacterial Susceptibility Testing (EUCAST) [41]. If the zone diameter of the compound was 30-50% of the Gentamicin inhibition zone, which was 16 mm for *E. coli* and 20 mm for *S. aureus*, the inhibition was accepted as significant. The concentration which exerts a significant inhibition compared to the reference antibiotic is given in Table 2.

The negative control DMSO was ineffective in inhibiting all the bacterial strains, as expected [42,43]. **L1** was ineffective against both bacteria even at the highest concentration tested in this study (>256 mg/mL). The complexes of **L1** showed considerably high antibacterial activity, except for **1a**. This result can be explained by Tweedy's Chelation Theory, which states that the activities of chemical compounds increase when they form complexes [42,43].

Chelation decreases the polarity of the metal as a partial positive charge of the metal atom is shared with the donor groups and possible electron delocalization occurs over the entire ring. This increases the lipophilic character of the chelates, which promotes their passage through the lipid layers of the bacterial membrane. The complexes of both ligands have a higher inhibition effect on *Staphylococcus aureus*. Moreover, the bacteriostatic effects of the complexes **1d**, **1e**, **2b**, **2d** and **2e** on *Staphylococcus aureus* are noticeable. The full potentials of the complexes could not be totally observable due to the precipitation of the complexes dissolved in DMSO when came across with the water molecules present in agar. The precipitations of the complexes are especially obvious starting from the concentration of 16 mg/mL. Nevertheless, the order of activities can be shown as **1d** > **1e** > **1b** > **1c** > **1a** = **L1** for *Staphylococcus aureus* and **1e** > **1d** > **1c** > **1b** > **1a** = **L1** for *Escherichia coli*. The order for **HL2** and its complexes is as follows: **2b** > **HL2** > **2d** > **2a** = **2c** > **2e** for *Staphylococcus aureus* and **2c** = **2d** > **2e** > **HL2** > **2a** = **2b** for *Escherichia coli*. The effect of a structural change between **L1** and **HL2** was very obvious, the **L1** was ineffective against bacteria, however, **HL2** was effective on both bacteria, especially on *Staphylococcus aureus*. This can be explained by the cell wall differences between Gram-positive and Gram-negative bacteria (Figures S5-S8, Supplementary material). The cell wall of Gram-positive bacteria is more permeable and therefore some antibacterial agents can act more

effectively on Gram-positive bacteria [42]. The high activity of **1d** (Co²⁺ complex) and **2b** (Zn²⁺ complex) against *Staphylococcus aureus* (2 and 4 mg/mL, respectively), is quite remarkable.

Conclusions

In this study, a ferrocenyl benzimidazole derivative, 6-chloro-2-ferrocenyl-1*H*-benzimidazole (**L1**) and a ferrocenyl Schiff base, (*E*)-((4-chloro-2-hydroxyphenylimino)methyl)ferrocene (**HL2**) ligands and their complexes with Fe(III), Co(II), Cu(II), Zn(II) and Pd(II) chloride were synthesized and characterized. All complexes reacted in a 1:1 metal:ligand ratio.

Molar conductivity data showed that Fe(III), Cu(II), Zn(II) and Co(II) complexes are not electrolytes whereas the Pd(II) complexes are 1:1 electrolyte. According to the obtained data, it is estimated that Fe(III) and Co(II) complexes have octahedral geometry, Zn(II) and Cu(II) complexes manifest tetrahedral geometry and Pd(II) complexes present square plane geometry. Due to the characteristics of the ligands, **HL2** complexes have a chelate structure whereas the complexes of **L1** are not. Antibacterial activity of the ligands and the complexes were tested towards *Escherichia coli* and *Staphylococcus aureus*. It was observed that especially benzimidazole derivative complexes (**1b** – **1e**) show higher activity compared to the ligand and this situation is considered to be related to the non-chelate structures of benzimidazole compound complexes. The activities of **1d** (Co²⁺ complex) and **2b** (Zn²⁺ complex) against *Staphylococcus aureus* (2 and 4 µg/mL, respectively), are notable for being considerably higher than the others.

Acknowledgments

This work was supported by Scientific Research Projects Coordination Unit of Istanbul University – Cerrahpasa, project no.: FDK-2017-23684.

Supplementary information

Supplementary data are available free of charge at <http://cjm.asm.md> as PDF file.

References

1. Patra, M.; Gasser, G. The medicinal chemistry of ferrocene and its derivatives. *Nature Reviews Chemistry*, 2017, 1, 0066, pp. 1–12. DOI: <https://doi.org/10.1038/s41570-017-0066>
2. Cunningham, L.; Benson, A.; Guiry, P.J. Recent developments in the synthesis and applications of chiral ferrocene ligands and organocatalysts in

- asymmetric catalysis. *Organic & Biomolecular Chemistry*, 2020, 18(46), pp. 9329–9370.
DOI: <https://doi.org/10.1039/D0OB01933J>
3. Astruc, D. Why is ferrocene so exceptional? *European Journal of Inorganic Chemistry*, 2017, 1, pp. 6–29.
DOI: <https://doi.org/10.1002/ejic.201600983>
 4. Wagner, E.C.; Millet, W.H. Benzimidazole. *Organic Syntheses*, 1939, 19, pp. 12–15.
DOI: <https://doi.org/10.15227/orgsyn.019.0012>
 5. Zapata, F.; Caballero, A.; Espinosa, A.; Tarraga, A.; Molina, P. Triple channel sensing of Pb(II) ions by a simple multiresponsive ferrocene receptor having a 1-deazapurine backbone. *Organic Letters*, 2008, 10(1), pp. 41–44.
DOI: <https://doi.org/10.1021/ol702541y>
 6. Vigato, P.A.; Tamburini, S. The challenge of cyclic and acyclic Schiff bases and related derivatives. *Coordination Chemistry Reviews*, 2004, 248(17–20), pp. 1717–2128.
DOI: <https://doi.org/10.1016/j.cct.2003.09.003>
 7. Kumar, S.; Dhar, D.N.; Saxena, P.N. Applications of metal complexes of Schiff bases - a review. *Journal of Scientific & Industrial Research*, 2009, 68, pp. 181–187.
<http://nopr.niscpr.res.in/bitstream/123456789/3170/1/JSIR%2068%283%29%20181-187.pdf>
 8. Karimi-Jaberi, Z.; Amiri, M. An efficient and inexpensive synthesis of 2-substituted benzimidazoles in water using boric acid at room temperature. *E-Journal of Chemistry*, 2012, 9(1), pp. 167–171.
DOI: <https://doi.org/10.1155/2012/793978>
 9. Vazzana, I.; Terranova, E.; Mattioli, F.; Sparatore, F. Aromatic Schiff bases and 2,3-disubstituted-1,3-thiazolidin-4-one derivatives as antiinflammatory agents. *Arkivoc*, 2004, 5, pp. 364–374.
DOI: <https://doi.org/10.3998/ark.5550190.0005.531>
 10. Balouiri, M.; Sadiki, M.; Ibsouda, S.K. Methods for *in vitro* evaluating antimicrobial activity: a review. *Journal of Pharmaceutical Analysis*, 2016, 6(2), pp. 71–79.
DOI: <https://doi.org/10.1016/j.jpha.2015.11.005>
 11. Tavman, A. Synthesis, spectral characterization of 2-(5-methyl-1*H*-benzimidazol-2-yl)-4-bromo/nitro-phenols and their complexes with zinc(II) ion, and solvent effect on complexation. *Spectrochimica Acta Part A*, 2006, 63(2), pp. 343–348.
DOI: <https://doi.org/10.1016/j.saa.2005.05.020>
 12. Tavman, A.; Agh-Atabay, N.M.; Neshat, A.; Guçin, F.; Dulger, B.; Hacı, D. Structural characterization and antimicrobial activity of 2-(5-*H*-methyl-1*H*-benzimidazol-2-yl)-4-bromo/nitro-phenol ligands and their Fe(NO₃)₃ complexes. *Transition Metal Chemistry*, 2006, 31, pp. 194–200.
DOI: <https://doi.org/10.1007/s11243-005-6368-1>
 13. Garnovskii, A.D.; Sennikova, E.V.; Kharisov, B.I. Coordination aspects in modern inorganic chemistry. *The Open Inorganic Chemistry Journal*, 2009, 3(1), pp. 1–20. DOI: <https://doi.org/10.2174/1874098700903010001>
 14. Hariprasath, K.; Deepthi, B.; Sudheer Babu, I.; Venkatesh, P.; Sharfudeen, S.; Soumya, V. Metal complexes in drug research - a review. *Journal of Chemical and Pharmaceutical Research*, 2010, 2(4), pp. 496–499. <https://www.jocpr.com/articles/metal-complexes-in-drug-research--a-review.pdf>
 15. Elseman, A.M.; Shalan, A.E.; Rashad, M.M.; Hassan, A.M.; Ibrahim, N.M.; Nassar, A.M. Easily attainable new approach to mass yield ferrocenyl Schiff base and different metal complexes of ferrocenyl Schiff base through convenient ultrasonication-solvothermal method. *Journal of Physical Organic Chemistry*, 2017, 30(6), pp. e3639–e3648.
DOI: <https://doi.org/10.1002/poc.3639>
 16. Socrates, G. *Infrared and Raman Characteristic Group Frequencies*. John Wiley & Sons Ltd.: New York, USA, 2001, 366 p. ISBN: 0-471-85298-8
 17. Saxena, A.K.; Saxena, S.; Rai, A.K. Some titanium(IV) complexes of 1,3-dihydro-1,3-dioxo- α -(Substituted)-2*H*-isoindole-2-acetates. *Synthesis and Reactivity in Inorganic Metal-Organic Chemistry*, 1990, 20(1), pp. 21–37.
DOI: <https://doi.org/10.1080/00945719008049867>
 18. Amjad, M.; Sumrra, S.H.; Akram, M.S.; Chohan, Z.H. Metal-based ethanolamine-derived compounds: a note on their synthesis, characterization and bioactivity. *Journal of Enzyme Inhibition and Medicinal Chemistry*, 2016, 31(S4), pp. 88–97. DOI: <https://doi.org/10.1080/14756366.2016.1220375>
 19. Tendero, M.J.L.; Benito, A.; Lloris, J.M.; Martínez-Mañez, R.; Soto, J.; Paya, J.; Edwards, A.J.; Raithby, P.R. Synthesis and characterisation of the new diaza ferrocene macrocycle 1,1'-(2,6-diazahepta-1,6-diene) ferrocene and its parent amine 1,1'-(2,6-diazaheptane) ferrocene. *Inorganica Chimica Acta*, 1996, 247(1), pp. 139–142. DOI: [https://doi.org/10.1016/0020-1693\(95\)04952-5](https://doi.org/10.1016/0020-1693(95)04952-5)
 20. Cinarli, A.; Gürbüz, D.; Tavman, A.; Birteksöz, A.S. Synthesis, spectral characterizations and antimicrobial activity of some Schiff bases of 4-chloro-2-aminophenol. *Bulletin of the Chemical Society of Ethiopia*, 2011, 25(3), pp. 407–417.
DOI: <https://doi.org/10.4314/bcse.v25i3.68593>
 21. Yamamoto, T.; Sugiyama, K.; Kanbara, T.; Hayashi, H.; Etori, H. Preparation and properties of π -conjugated poly(benzimidazole-4,7-diyl)s. *Macromolecular Chemistry and Physics*, 1998, 199(9), pp. 1807–1813.
DOI: [https://doi.org/10.1002/\(SICI\)1521-3935\(19980901\)199:9<1807::AID-MACPI1807>3.0.CO;2-2](https://doi.org/10.1002/(SICI)1521-3935(19980901)199:9<1807::AID-MACPI1807>3.0.CO;2-2)
 22. D'Antona, N.; Morrone, R.; Gambera, G.; Pedotti, S. Enantio-recognition of planar “metallocenic” chirality by a nitrile hydratase/amidase bienzymatic system. *Organic & Biomolecular Chemistry*, 2016, 14, pp. 4393–4399.
DOI: <https://doi.org/10.1039/C6OB00689B>

23. Toro, P.; Klahn, A.H.; Pradines, B.; Lahoz, F.; Pascual, A.; Biot, C.; Arancibia, R. Organometallic benzimidazoles: Synthesis, characterization and antimalarial activity. *Inorganic Chemistry Communications*, 2013, 35, pp. 126–129.
DOI: <https://doi.org/10.1016/j.inoche.2013.06.019>
24. Liu, Y.-T.; Lian, G.-D.; Yin, D.-W.; Su, B.-J. Synthesis, characterization and biological activity of ferrocene-based Schiff base ligands and their metal (II) complexes. *Spectrochimica Acta Part A*, 2013, 100, pp. 131–137.
DOI: <https://doi.org/10.1016/j.saa.2012.03.049>
25. Shabbir, M.; Akhter, Z.; Ahmad, I.; Ahmed, S.; Bolte, M.; Ismail, H.; Mirza, B. Ferrocene-based Schiff bases copper(II) complexes: synthesis, characterization, biological and electrochemical analysis. *Inorganica Chimica Acta*, 2017, 463, pp. 102–111.
DOI: <https://doi.org/10.1016/j.ica.2017.04.034>
26. Tavman, A.; Cinarli, A.; Gürbüz, D.; Birteksöz, A.S. Synthesis, characterization and antimicrobial activity of 2-(5-H/Me/F/Cl/NO₂-1*H*-benzimidazol-2-yl)-benzene-1,4-diols and some transition metal complexes. *Journal of the Iranian Chemical Society*, 2012, 9(5), pp. 815–825.
DOI: <https://doi.org/10.1007/s13738-012-0098-z>
27. Shi, Y.-C.; Yang, H.-M.; Shen, W.-B.; Yan, C.-G.; Hu, X.-Y. Syntheses and crystal structures of ferrocene-containing enamines and their copper complexes. *Polyhedron*, 2004, 23(1), pp. 15–21.
DOI: <https://doi.org/10.1016/j.poly.2003.08.017>
28. Berreau, L.M. Coordination and bioinorganic chemistry of aryl-appended *tris*(2-pyridylmethyl) amine ligands. *Comments on Inorganic Chemistry*, 2007, 28(3-4), pp. 123–171.
DOI: <https://doi.org/10.1080/02603590701572940>
29. Abd-Elzaher, M.M. Synthesis, characterization, and antimicrobial activity of cobalt(II), nickel(II), copper(II) and zinc(II) complexes with ferrocenyl Schiff bases containing a phenol moiety. *Applied Organometallic Chemistry*, 2004, 18(4), pp. 149–155. DOI: <https://doi.org/10.1002/aoc.608>
30. El-Tabl, A.S.; Issa, R.M. Preparation and characterization of new nickel(II), cobalt(II) and copper(II) complexes of 3,11-diacetyl-2,12-dioxo-5,9-diazatrideca-3,11-diene; reactivity towards ammonia, 1,2-diaminopropane, hydroxylamine and copper(II) acetylacetonate compounds. *Journal of Coordination Chemistry*, 2004, 57(6), pp. 509–524.
DOI: <https://doi.org/10.1080/00958970410001696816>
31. Kohtoku, M.; Honma, H.; Takai, O. Electroless plating catalyst performance of a cationic moiety bearing palladium complex. *Journal of the Electrochemical Society*, 2014, 161(14), pp. D806–D812.
DOI: <https://doi.org/10.1149/2.0861414jes>
32. Geary, W.J. The use of conductivity measurements in organic solvents for the characterisation of coordination compounds. *Coordination Chemistry Reviews*, 1971, 7(1), pp. 81–122. DOI: [https://doi.org/10.1016/S0010-8545\(00\)80009-0](https://doi.org/10.1016/S0010-8545(00)80009-0)
33. Zhang, X.; Wang, J.; Gao, Y.; Zeng, X.C. Ab initio study of structural and magnetic properties of TM_n(ferrocene)_{n+1} (TM = Sc, Ti, V, Mn) sandwich clusters and nanowires (n = ∞). *ACS Nano*, 2009, 3(3), pp. 537–545.
DOI: <https://doi.org/10.1021/nn800794c>
34. Montazeri-zohori, M.; Musavi, S.A.; Naghiha, A.; Veyseh, S. Some new IIB group complexes of an imidazolidine ligand: Synthesis, spectral characterization, electrochemical, thermal and antimicrobial properties. *Journal of Chemical Sciences*, 2014, 126, pp. 227–238.
DOI: <https://doi.org/10.1007/s12039-013-0555-y>
35. Munyaneza, A.; Kumar, G.; Morobe, I.C. Synthesis, characterization and *in vitro* biological activities of pyrazolylpalladium(II) complexes towards selected strains. *Synthesis and Catalysis: Open Access*, 2018, 3(1:2), pp. 1–8.
DOI: <https://doi.org/10.4172/2574-0431.100020>
36. Poorabbas, B.; Mardaneh, J.; Rezaei, Z.; Kalani, M.; Pouladfar, G.; Alami, M.H.; Soltani, J.; Shamsi-Zadeh, A.; Abdoli-Oskooi, S.; Saffar, M.J.; Alborzi, A. Nosocomial infections: multicenter surveillance of antimicrobial resistance profile of *Staphylococcus aureus* and Gram negative rods isolated from blood and other sterile body fluids in Iran. *Iranian Journal of Microbiology*, 2015, 7(3), pp. 127–135.
<https://www.ncbi.nlm.nih.gov/pmc/articles/PMC4676981/>
37. Toval, F.; Köhler, C.D.; Vogel, U.; Wagenlehner, F.; Mellmann, A.; Fruth, A.; Schmidt, M.A.; Karch, H.; Bielewska, M.; Dobrindt, U. Characterization of *Escherichia coli* isolates from hospital inpatients or outpatients with urinary tract infection. *Journal of Clinical Microbiology*, 2014, 52(2), pp. 407–419.
DOI: <https://doi.org/10.1128/JCM.02069-13>
38. Zhang, Q.; Yue, C.; Zhang, Y.; Lü, Y.; Hao, Y.; Miao, Y.; Li, J.; Liu, Z. Six metal-organic frameworks assembled from asymmetric triazole carboxylate ligands: synthesis, crystal structures, photoluminescence properties and antibacterial activities. *Inorganica Chimica Acta*, 2018, 473, pp. 112–120.
DOI: <https://doi.org/10.1016/j.ica.2017.12.036>
39. EUCAST, European Committee on Antibacterial Susceptibility Testing. Breakpoint tables for interpretation of MICs and zone diameters, version 10.0, 2020.
https://eucast.org/clinical_breakpoints/
40. Lambert, P.A. Cellular impermeability and uptake of biocides and antibiotics in Gram-positive bacteria and mycobacteria. *Journal of Applied Microbiology*, 2002, 92(s1), pp. 46S–54S. DOI: <https://doi.org/10.1046/j.1365-2672.92.5s1.7.x>
41. Tweedy, B.G. Plant extracts with metal ions as potential antimicrobial agents. *Phytopathology*, 1964, 55, pp. 910–918.
<https://apsjournals.apsnet.org/journal/phyto>

ISOMERIZATION OF LIMONENE ON ZEOLITE-CONTAINING CATALYSTS BASED ON KAOLIN

Lyubov Patrylak^{id a,b*}, Stepan Zubenko^{id a}, Serhy Konovalov^{id a}, Anzhela Yakovenko^{id a},
Volodymyr Povazhnyi^{id a}, Oleksandra Pertko^{id a}, Yulia Voloshyna^{id a},
Oleksandr Melnychuk^{id a}, Mykhailo Filonenko^{id a,c}

^aV.P. Kukhar Institute of Bioorganic Chemistry and Petrochemistry of National Academy of Sciences of Ukraine,
1, Murmanska str., Kyiv 02094, Ukraine

^bNational Technical University of Ukraine "Igor Sikorskyi Kyiv Polytechnic Institute",
37, Peremohy ave., Kyiv 03056, Ukraine

^cNational Pedagogical Dragomanov University, 9, Pyrogoва str., Kyiv 01601, Ukraine
*e-mail: lkpg@ukr.net

Abstract. The aim of the work was to study the isomerization of limonene on zeolite-containing biporous acid catalysts based on kaolin. Zeolite catalysts were synthesized from Ukrainian kaolin and characterized by using XRD, XRF, DTA/TG, IR-spectroscopy, low-temperature nitrogen adsorption, and pyridine sorption. Micro-mesoporous materials isomerize limonene at 160°C. The main reaction product on acid catalysts was terpinolene, while the original metakaolin microsphere catalyzes mainly the limonene condensation. The maximum yield of isomers is of 60–65% at 80–90% conversion. The obtained results show that the studied samples do not have a significant accumulation of carbonaceous deposits because limonene has high solubility, which helps to remove intermediate products of transformation from the surface of the samples.

Keywords: kaolin, zeolite, limonene isomerization, terpinolene yield.

Received: 20 June 2022/ Revised final: 08 September 2022/ Accepted: 14 September 2022

Introduction

Terpenes and terpenoids are well-known substances of biological origin, which until now have been used mainly as additives to perfumes with antiseptic properties. However, in recent years, a new trend has emerged regarding their possible use in bioprocessing to produce valuable chemicals [1,2]. Thus, the well-known "green" solvent limonene, obtained as a by-product of citrus processing and the paper industry, can be converted into *p*-cymene, a valuable intermediate for fine organic synthesis.

The conversion of limonene to *p*-cymene is still poorly understood. The modern idea about the mechanism of the transformation reaction of limonene into *p*-cymene consists of the sequential unfolding of isomerization of limonene into terpenoids (terpinolene, α - and γ -terpinene) and subsequent dehydroaromatization of the latter [3,4]. The process of isomerization of unsaturated compounds, in contrast to linear alkanes, requires catalysts with acid centers of not very high strength [5,6] or the use of lower process temperatures. Terpenoids are also valuable substances used in medicine and perfumery, as

well as in fine organic synthesis [7-12]. Terpinolene is an intermediate for the production of terpenoid acid [10-13]. It can be used to start and finish radical polymerization reactions involving unsaturated monomers [13].

Limonene transformation has been investigated using natural clay minerals [14-16] and titanium-containing mesoporous molecular sieves [17,18]. Approaches to the activation of the limonene molecule on Brønsted acid centers associated with titanium were proposed [17]. Quantitative conversions were achieved at the transitions from 150–160°C and 170°C, but only for 23–24 hours of the process. In all cases, considerable polymerization is observed on the source clays, and the yields of isomerization products are low (up to 20%), while additional modification with iron, manganese, and nickel ions significantly improves the selectivity for *p*-cymene. The synthesis of zeolites on the basis of kaolin allows for the combination of the zeolite phase and the matrix (residual kaolin) within the same sample, as well as the presence of micro- and meso-porosity [19].

The purpose of this study was to look into the isomerization of limonene using kaolin-based biporous acid catalysts containing zeolite, with improved diffusion properties.

Experimental

Materials

Kaolin (Prosyana deposit, Dnipropetrovsk region, Ukraine) was utilized for zeolite synthesis. The mineralogical composition of kaolin was as follows: 97 wt% of kaolinite, 3 wt% of mica, and quartz in trace amounts. The content of oxides in wt% was: 46% of SiO₂, 38% of Al₂O₃, 1.12% of Fe₂O₃, 1.16% of TiO₂, 0.12% of CaO, 0.28% of MgO, 0.6% of K₂O, 0.11% of Na₂O, 12.4% of H₂O.

The analytical grade reagents used in this study (NaOH, Ca(NO₃)₂·4H₂O, La(NO₃)₃·6H₂O, NH₄NO₃, Na₂SiO₃) were obtained from Ukrainian commercial sources and were used as received without further purification. Nitrogen and helium of high purity (99.99%) were applied in the measurements. In the experiments, pyridine and *n*-hexane (Sigma Aldrich, 99.0% for GC), as well as limonene (Merck, 98%), were used.

Methods and instruments

Synthesis of catalysts

In order to synthesize micro-mesoporous zeolites with improved diffusion properties, the latter were synthesized in situ in preformed kaolin microspheres (20–100 μm). To start with, the original kaolin was dispersed in water by adding sodium pyrophosphate. Ultrasound was used to improve homogenization. The formation of the microspheres (MS-1) from kaolin powder was performed using a disk spray dryer, in which the aqueous kaolin suspension was fed to the centrifugal disk and sprayed into the ascending stream of hot air (350–400°C).

By calcining microspherical kaolin at 730 and 1000°C for 2 hours metakaolin and a mixture of aluminosilicate spinel with reactive silicon oxide were obtained. The synthesis of zeolite of the faujasite type was carried out in the presence of an aqueous solution of alkali in accordance with the method described in [20]. Synthetic granules were prepared by mixing microspherical metakaolin with spinel and sodium silicate. The weight ratio of metakaolin to spinel was 1:1 or 1:2 for samples K1 and K2 respectively. Solutions of sodium hydroxide, seed (10% wt.), and additional water were added to granules. Amorphous seed (Na₂O/SiO₂= 1.0; SiO₂/Al₂O₃= 17.6; H₂O/Na₂O= 17.7) was pre-aged for 20 hours at 35–40°C. The syntheses were performed in glass flasks at 100°C for

20 hours. Then the granules were washed with hot water to pH= 9, dried at 100°C for 2 hours, and used as a basis for the preparation of the catalyst.

The catalysts were prepared by successive ion exchanges of the native zeolite sodium for calcium, lanthanum, and ammonium from aqueous solutions of nitrates of these salts (1, 1.5, and 3 mol/L) at 80–150°C for 3 hours. After each ion exchange, the samples were calcined in a muffle furnace at 550°C for 2 hours. Finally, the samples were further exchanged for ammonium without calcination.

The SiO₂/Al₂O₃ ratios according to X-ray fluorescence analysis were 2.1 and 1.6 for samples K1 and K2, which correspond to zeolite type X [21]. In terms of exchange capacity, the chemical composition of the synthesized samples was as follows (%): NH₄⁺(50), Ca²⁺(12), La³⁺(35), Na⁺(3) for K1 sample and NH₄⁺(40), Ca²⁺(17), La³⁺(40), Na⁺(3) for K2 sample.

Catalyst characterization

The porous properties of kaolin-based materials were assessed using low temperature (-196°C) nitrogen adsorption/desorption isotherms obtained with a Nova 1200e (Quantochrome) surface area and a pore size analyzer. Using nitrogen adsorption data at *p/p_s* values between 0.06 and 0.2, the specific surface areas (*S^{BET}*) were estimated using the conventional Brunauer–Emmett–Teller (BET) method [22]. The *t*-plot approach was used to determine the micropore volumes (*V_{micro}*) and micropore surface areas (*S_{micro}*). The Eq.(1) was used to get the average pore size *R*.

$$R = 2V^{\Sigma}/S^{BET} \quad (1)$$

where, *V^Σ* – the total pore volume, cm³/g;
S^{BET} – the specific surface area, m²/g.

The *R^{BJH}* is based on the Barrett–Joiner–Halenda (BJH) theory [23], while the *R^{DFT}* is based on the density-functional theory (DFT) [24].

The Lewis and Brønsted acidity of the samples was investigated using pyridine sorption with IR-spectroscopic control in the 1400–1700 cm⁻¹ range (Shimadzu IR Affinity-1S FTIR spectrometer). The samples were loaded into a special holder after being pressed into 5–10 mg tablets without a binder. The latter was then placed in a spectral cell, and the samples were activated for 1 hour in a vacuum at 380°C. The spectral probe was absorbed for 30 min at 150°C. To remove physically adsorbed pyridine, the latter was desorbed at 250°C for 30 min before recording IR spectra at 50°C.

The samples were subjected to *simultaneous thermogravimetric (TG) and differential thermal analysis (DTA)* in the temperature range of 20–1000°C using a Linseis STA 1400 system type derivatograph at a heating rate of 10°C/min. Calcined alumina at 1200°C was used as a reference material. Samples of 25 mg of zeolite were used in this study.

X-ray fluorescence analysis was used to determine the elemental composition of synthesized catalysts (Oxford Instruments X-Supreme 8000 analyzer, Great Britain).

The *diffraction pattern* of the original zeolite was recorded on a Rigaku MiniFlex600 diffractometer in CuK α radiation in the region of 2θ angles 2–80° with a step of 0.02° and a rotation speed of 5°/12 min. The acceleration voltage was 40 kV, and the anode current was 15 mA.

Catalytic testing

The limonene conversion was realized at atmospheric pressure in argon on a pre-activated catalyst in a closed system. The glass reactor tube was charged with 1.5 g of catalyst, and the unit was sealed. The catalyst was activated for 1.5 hour at 380°C in a vacuum. The reactor was heated using a sand bath with an electric stove. After cooling to 40°C, the argon supply was switched on until atmospheric pressure was reached and the magnetic stirrer was lowered into the catalyst bed (at the activation stage, the magnetic stirrer armature was held above the catalyst bed by a magnet). The glass stopper was opened and 10 g of limonene was loaded through the funnel, after which the hole was closed with a silicone stopper.

An oil bath filled with silicone oil was preheated on a heated magnetic stirrer to 160–170°C. After reaching the set temperature, the reactor was immersed in an oil bath and started stirring (speed 250 rpm). The reaction continued for 2–3 hours. Liquid samples were taken every hour.

Analysis of reaction products

Limonene conversion products were determined by using an Agilent 7890A gas chromatograph with a flame ionization detector, a split separator, and a J&W HP-5 capillary column (30 m, 0.32 mm, 0.25 μ m, (5% phenyl)–methylsiloxane). Liquid samples for analysis (about 0.05 g) were placed in a 4 mL vial and dissolved in 3 mL of *n*-hexane. Chromatographic analysis was performed under the following conditions: evaporator temperature – 250°C; flow separation – 30:1; carrier gas flow (helium) – 2.5 cm³/min (steady

flow mode); temperature program of the thermostat of the chromatographic column – 70°C/12 min – heating to 180°C at a speed of 120°C/min – heating to 320°C at a speed of 35°/min; detector temperature – 250°C; sample volume – 1 μ L. The concentration of the components in the catalyst composition was calculated as the ratio of the corresponding peak area to the sum of the areas of all the peaks represented in the chromatogram.

Results and discussion

Catalysts characterization

After all ion exchanges, zeolite-containing catalysts K1 and K2 have the same origin with only a slight difference in their chemical composition, which has been indicated above. According to silica to alumina ratio studies by X-ray fluorescence analysis, a zeolite phase is presented by low silica X-type zeolite. X-ray diffraction investigations have been conducted in order to confirm this. The XRD data for kaolin-based samples show the formation of crystalline phases (Figure 1). The main characteristic lines of the faujasite-type zeolites can be seen in the diffractograms of the samples synthesized from kaolin (2θ = 6.1, 9.9, 11.7, 15.4, 18.4, 20.0, 21.0, 22.5, 23.3, 23.5, 26.7, 29.1, 30.1, 31.0, 32.0, 33.5, 37.2°) [21]. Some X-ray amorphous halo is observed at the level of 2θ = 25.0–30.0° in kaolin samples, and may reflect the presence of unconverted metakaolin, which is X-ray amorphous. The peaks observed at 2θ = 45.0° and 2θ = 67.0° indicate the presence of aluminosilicate spinel in the samples. Thus, the XRD and XRF data show that the catalysts were synthesized from kaolin, with the zeolite phase represented by X-type zeolite with minor admixtures of aluminosilicate spinel. The SiO₂ to Al₂O₃ ratio is close to 2.

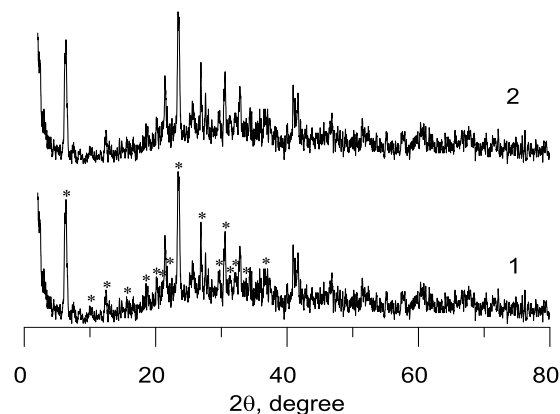


Figure 1. XRD patterns for K2 (1) and K1 (2) samples. (* - the main characteristic lines of faujasite phase).

Figure 2 depicts the low-temperature nitrogen adsorption/desorption isotherms for zeolite-containing catalysts and the original kaolin microsphere (MS-1).

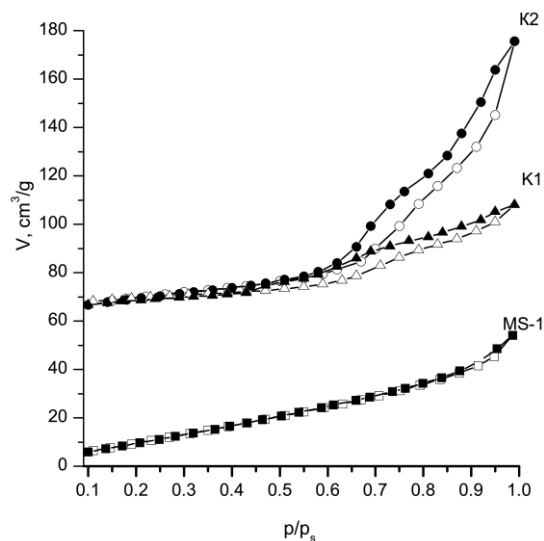


Figure 2. Isotherms of low-temperature nitrogen adsorption for a number of samples from kaolin.

According to the IUPAC classification, isotherms correspond to type IV and reflect the combination of microporosity and mesoporosity in the samples [22]. The latter is reflected by the presence of hysteresis loops of varying sizes caused by capillary condensation in mesopores ranging in size from 2 to 50 nm. Such a loop is

relatively weak in the case of the original kaolin microspheres (MS-1), larger in the case of K1, and the largest in the case of K2. The isotherm of the MS-1 sample clearly shows that there is no microporosity in the kaolin sample, as there is virtually no nitrogen adsorption at low saturation pressures. As a result, the synthesized catalysts are micro-mesoporous objects, also known as hierarchical zeolites.

From low-temperature nitrogen adsorption/desorption isotherms for kaolin-based zeolite-containing samples using BET, BJH, and DFT approaches, a range of the porous properties of the samples were calculated (Table 1). The specific surface area of kaolin microspheres MS-1 was initially 55 m²/g. Zeolite-containing samples based on it (K1, K2) have significantly higher specific surfaces of 250–260 m²/g.

The highest specific content of mesopores (74%) is in the sample K2 with the largest hysteresis loop. Distributions of pores by size, shown in Figures 3 and 4, demonstrate that the same sample has the largest dominant pores of about 3 nm according to BJH and 4 nm according to DFT.

Interestingly, for all samples synthesized in situ, the peaks of the predominant pores do not have sharp peaks and are quite wide, having many peaks of varying intensities, while in the case of synthetic zeolites, peaks are usually sharp, single, and much narrower.

Table 1

Adsorption characteristics of catalysts.									
	S^{BET} , m²/g	S^t , m²/g	$S^{t_{micro}}$, m²/g	$V^{t_{micro}}$, cm³/g	V^t , cm³/g	$V^{t_{micro}}/V^t$, %	R^{DFT} , nm	$R^{BJH(des)}$, nm	R , nm
K1	252	34	217	0.10	0.17	62	1.1	1.8	1.3
K2	260	98	162	0.07	0.27	26	4.1	3.3	2.1
MS-1	55	33	22	0.02	0.08	22	2.4	1.5	3.1

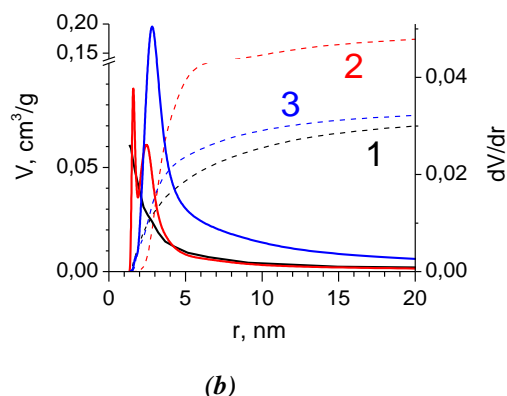
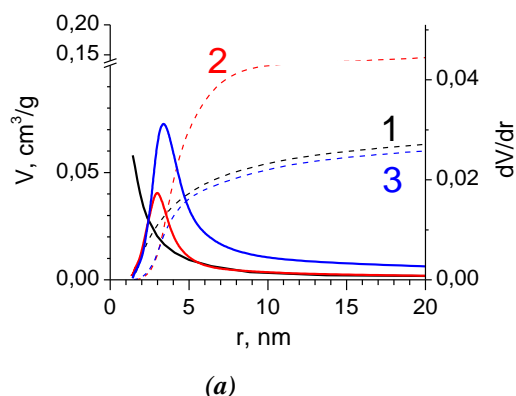


Figure 3. Integral and differential pore size distributions calculated from BJH theory using the adsorption (a) and desorption (b) branches of isotherms for MS-1 (1), K1 (2), and K2 (3).

Thus, the pore variance is larger for samples with an available binder or matrix component. Sample K2 has the largest volume of mesopores of 0.2 cm³/g, for other kaolin-containing samples, the range is from 0.06 to 0.08 cm³/g (Figures 3,4).

The total acidity of the samples was evaluated by following the sorption of pyridine under static conditions. The number of acid centers in mmol/g was 0.20, 0.90, and 1.04 for MS-1, K1, and K2, respectively. Figure 5 shows the acidity of the samples by sorption of pyridine monitored by IR spectroscopy. The bands at 1543 cm⁻¹ and 1454 cm⁻¹ indicate the presence of Brønsted and Lewis acid centers on the surface of the samples, respectively [25,26]. While the band at 1489 cm⁻¹ indicates both types of sites, Brønsted acidity dominates the catalysts. Based on the assumption that the Brønsted and Lewis acid centers represented by the band at 1489 cm⁻¹ are equally distributed, the number of Brønsted and Lewis acid sites was calculated to be 0.6 and 0.3 mmol/g for the K1 sample, as well as 0.68 and 0.36 mmol/g for the K2 sample. The total number of acid sites for samples K1 and K2 is comparable with the number of acid sites for powder faujasite-type zeolite (1.11 mmol/g) [5] or 1.2 mmol/g [27].

Isomerization of limonene

Limonene transformation can occur according to reaction Scheme 1 in a few ways. The original metakaolin microspheres MS-1 and the samples obtained on its basis showed different catalytic activities in the conversion of limonene (Figure 6).

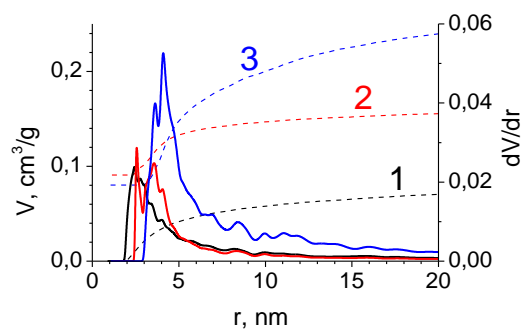


Figure 4. DFT-calculated integral and differential pore size distributions for samples MS-1 (1), K1 (2), and K2 (3).

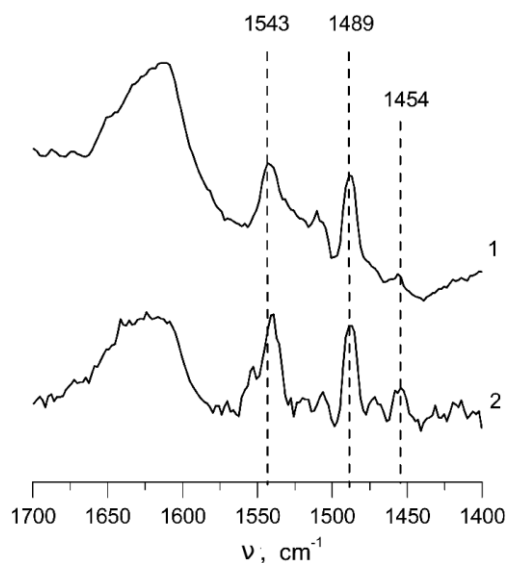
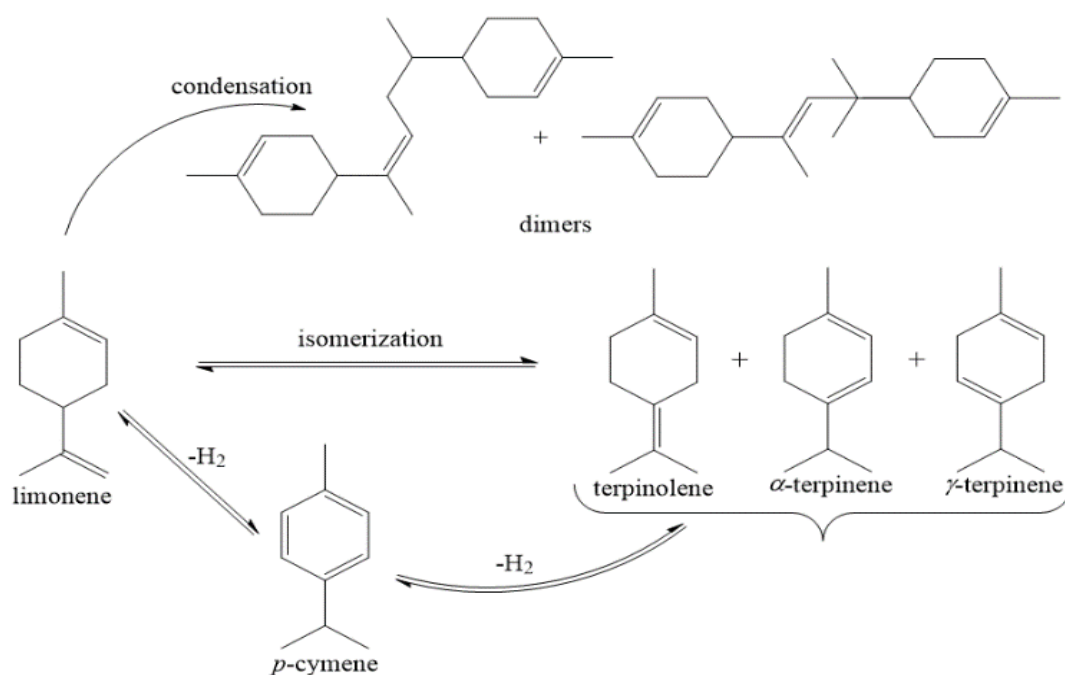


Figure 5. IR spectra of adsorbed pyridine on catalysts K1 (1) and K2 (2).



Scheme 1. Possible ways of limonene transformation.

If the products on MS-1 for 50% conversion consisted primarily of terpinolene, with a selectivity of 50%, the process selectivity for this isomer dropped sharply to 10% for high conversions. In fact, the formation of dimeric compounds changes in antibat, increasing by up to 40%. Selectivity for α - and γ -terpinenes was 20% and 10%, respectively. There is an increase in selectivity for *p*-cymene up to 10% for the high limonene conversions. The latter from 90 min is more than 90%. As for the yields of the respective products, there is an opposite drop and an increase in the yields of terpinolene and dimers. The maximum yield of α - and γ -terpinene was observed for 90 min and was 18% and 15%. The yield of *p*-cymene increases linearly over time to 10% for 3 hours (Figure 6).

On the polycationic catalyst K2, the selectivity for terpinolene also decreases (Figure 7). However, the dimers are practically unchanged, and the selectivity for α -terpinene increases. The yields on this sample are higher and are up to 60% and 66% of isomers at 90 and 120 min.

Yields of dimers and *p*-cymene are low, up to 5% and 2%, respectively. Catalyst K1 shows lower conversions (up to 60% in 3 hours), increasing linearly over time (Figure 7(c)). The selectivity for all products changes only slightly with rising conversion. As a result, the yields of all products increase linearly (Figure 7(c)), the highest yields are being characteristic of terpinolene (up to 30%) and γ -terpinene (up to 15%). The total yield of isomers for 3 hours was 50%. This is higher than on the titanium-containing mesoporous molecular sieves (20%) at 150–160°C [17,18]. Values of selectivity for terpinolene on samples K1 and K2 are higher (up to 50%) than on the mesoporous zeolites (20–30% or 35–40%) [17,18]. Whereas α -terpinene selectivity is similar (20–30%).

Due to the fact that the K2 sample has greater mesoporosity, it achieves roughly the same performance at 90 min as the K1 catalyst does at 180 min. The peculiarities of the product distribution in favor of terpinolene observed on the samples indicate, first, that the isomerization of limonene to terpinolene is the simplest because the migration of the double bond occurs only within the alkyl radical in this case. This stage of the reaction is the first one according to the mechanism proposed in a previously published study [17]. The second reaction step is the transformation of terpinolene to α -terpinene and after that, the latter transforms to γ -terpinene. The obtained product ratios (terpinolene: α -terpinene: γ -terpinene: *p*-cymene) with a terpinolene predominance on the second hour (25:10:5:1) are similar to those reported in the literature (10:7:4:1) [17,18].

Further transfer of the double bond to the ring is much more difficult. Interestingly, also on MS-1, the yield of *p*-cymene increases in parallel with the increase in the yield of dimers. The latter may be due to the fact that similar to the alkylation reaction of isobutane with butenes, when the formation of a certain number of oligomeric compounds promotes hydride transfer, the saturation of hydrogen-unsaturated oligomers occurs due to the dehydrogenation of terpenes to form *p*-cymene. This process is less intense in the absence of a metal component, but it still manifests to some extent.

In the case of MS-1, terpinolene is first formed for up to 60 min, and then the process abruptly turns into dimerization. Apparently, the number of relatively strong Brønsted acid centers in metakaolin is so small that they are rapidly deactivated. After that, only centers, which can oligomerize the unsaturated compounds, remain on the surface of the sample.

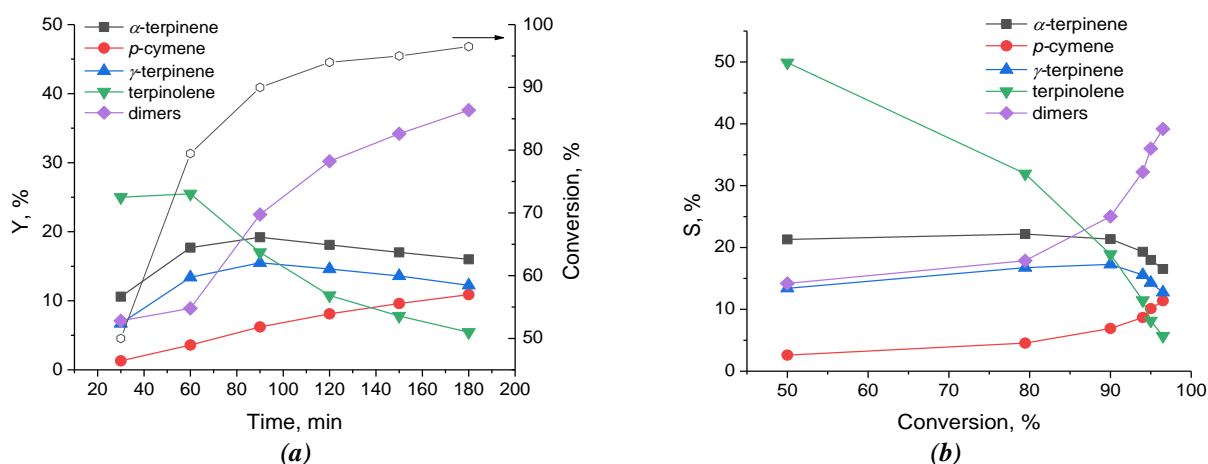
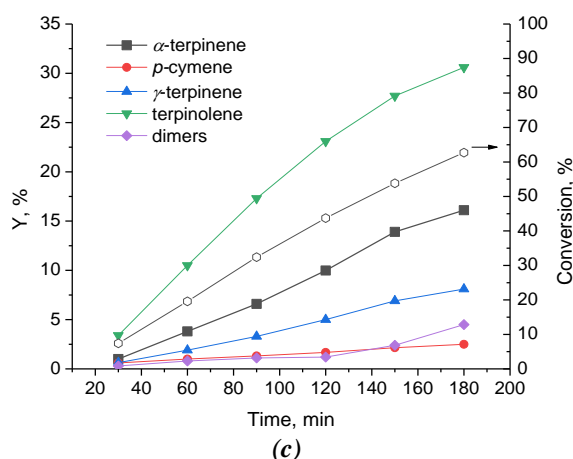
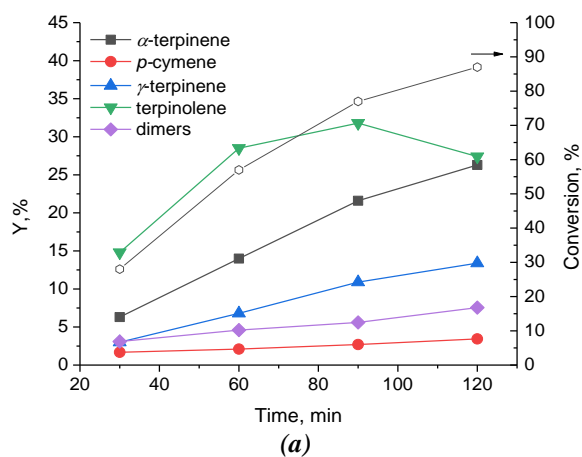


Figure 6. Conversion, product yields vs. reaction time (a), and selectivity vs. conversion (b) on the sample MS-1.

On acid zeolite catalysts, the acid centers are clearly stronger, and therefore the process is not aimed at dimerization, but isomerization of limonene. Furthermore, with a higher proportion of meso-porosity, the yields of isomers are higher in the case of the K2 catalyst (Figure 7).

As a result, limonene isomerization occurs properly not only on mesoporous molecular sieves [17,18], but also on catalysts that combine micro- and mesoporosity.



Investigation of deactivated catalysts

Figure 8 shows the DTA/TG curves for the samples studied in the conversion of limonene. After the reaction, the analyzed samples were washed with hexane. As can be seen from the DTA curves of samples K1 and K2 when heated to 400°C, endothermic minima are observed, indicating the process of desorption from catalysts at temperatures of approximately 100, 200, and 300°C.

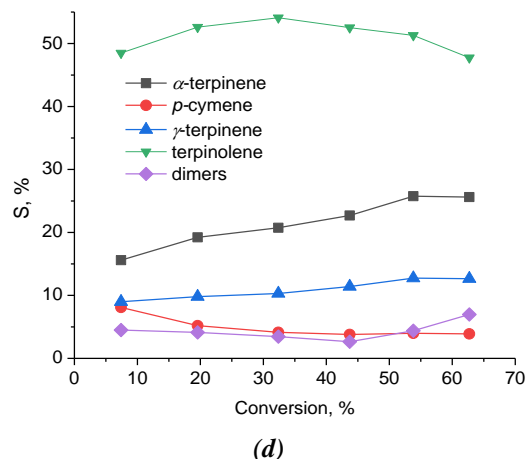
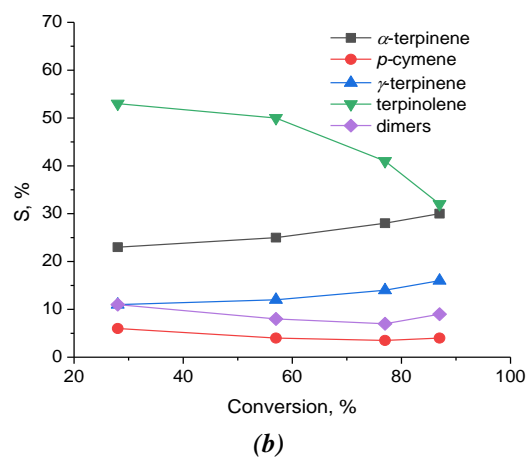


Figure 7. Conversion, product yields (a, c) vs. reaction time, and selectivity vs. conversion (b, d) on the samples K2 (a, b) and K1 (c, d).

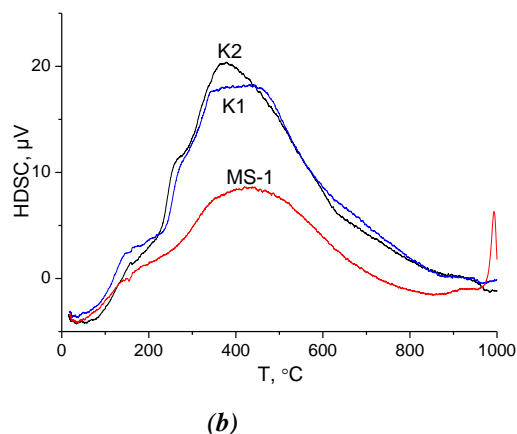
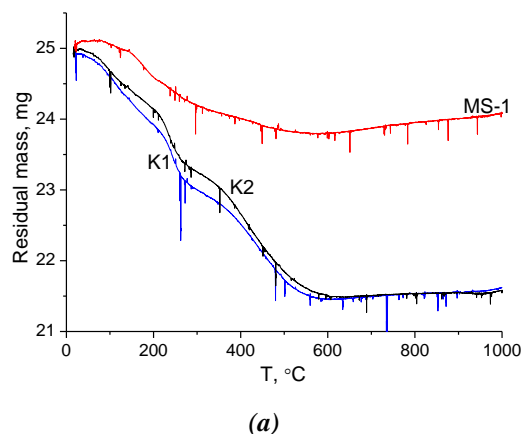


Figure 8. TG (a) and DTA (b) curves of MS-1, K1, and K2 deactivated samples.

There are three sections with different rates of weight loss: in the first and third, they are close, while in the second section, the speed increases. This appears to be due to the loss of various substances in the sample, at first glance. Hexane can be desorbed first, then limonene. However, the observed pattern is most likely caused by desorption from various structural elements, specifically the external surface of zeolite crystals, mesopores, and micropores. This assumption is confirmed by the existence of basically one desorption site in the case of the MS-1 microsphere sample, which has only mesopores. It is interesting that if for the first two samples, 3.5 mg were lost, which is 14%, in the case of MS-1, the weight loss was only 1 mg, or 4% of the mass. Whereas in the conversion of limonene, the largest number of dimer compounds were formed on it, which, however, were not retained on the catalyst, but were desorbed into the liquid medium. It is possible that this is due, firstly, to the low strength of the acid centers of MS-1, and secondly, to the high solubility of limonene as such. For both samples of the microsphere on the DTA curve, there is a

pronounced exothermic peak of about 950–980°C, which characterizes the phase transition [28].

In order to compare the changes that the samples underwent after the reaction was carried out, the catalysts were subjected to IR spectroscopy investigations. Figure 9 shows the IR spectra of fresh and deactivated samples in limonene isomerization. For all samples, the most intense absorption band is associated with antisymmetric valence vibrations of alumina-oxygen tetrahedra in zeolites and metakaolin [21]. Moreover, for zeolites, it is shifted to the lower frequency range (950 cm^{-1}) and for metakaolin, it is shifted to the higher frequency range (1050 cm^{-1}). Bands at 550 and 700 cm^{-1} are also observed, which reflect the deformation and symmetric valence oscillations of alumina-oxygen tetrahedra. They are again shifted to a higher frequency range for metakaolin. The fundamental difference between the spectra of fresh samples and catalysts after the reaction is the bifurcation of the band at 1000 cm^{-1} . The latter can be caused by non-planar oscillations of the terminal vinyl group $\delta\text{-CH}$ in the limonene molecule, which are reflected by the absorption band at 995–985 cm^{-1} .

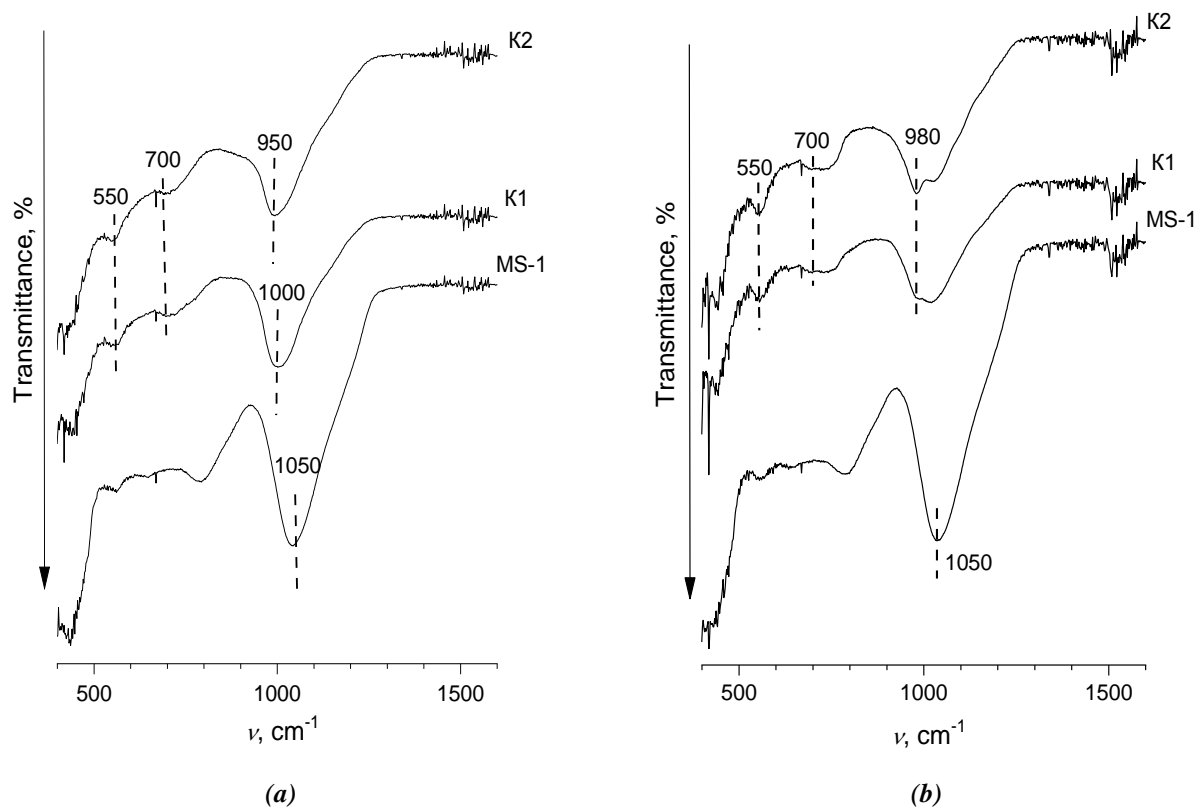


Figure 9. IR spectra of fresh (a) and deactivated (b) in limonene transformation catalysts.

Conclusions

Two faujasite-type zeolite-containing catalysts from Ukrainian kaolin were synthesized. The acid catalysts were prepared by successive ion exchanges of the native zeolite sodium for calcium, lanthanum, and ammonium. The Brønsted and Lewis acidity of the samples was confirmed by pyridine adsorption with IR control.

The XRD and XRF data show that the zeolite phase is represented by X-type zeolite with minor admixtures of aluminosilicate spinel. The SiO₂ to Al₂O₃ ratio for two samples is close to 2. The biporous structure of the samples with varying amounts of micro- and mesopores is confirmed by low-temperature nitrogen adsorption/desorption.

Limonene isomerization on biporous zeolite-containing catalysts synthesized from Ukrainian kaolin was conducted for the first time. The possibility of limonene isomerization on micro-mesoporous zeolite-containing materials is demonstrated, with the increased mesoporosity aiding in the reduction of reaction time.

It was found that the original metakaolin microsphere primarily catalyzes terpene dimerization, whereas terpinolene is the main product of isomerization on polycationic zeolite-containing catalysts. For an 80–90% conversion rate, the maximum yield of isomers is 60–65%. Because limonene has high solubility, it helps to remove intermediate products from the surface of the samples. It was discovered that neither the original microsphere nor the catalysts had a significant accumulation of coke precursors.

Acknowledgments

The publication contains the results of studies conducted with a grant from the National Research Foundation of Ukraine project 2020.01/0042.

References

1. Esteban, J.; Yustos, P.; Ladero, M. Catalytic processes from biomass-derived hexoses and pentoses: a recent literature overview. *Catalysts*, 2018, 8(12), pp. 637–678. DOI: <https://doi.org/10.3390/catal8120637>
2. Teong, S.P.; Yi, G.; Zhang, Yu. Hydroxymethylfurfural production from bioresources: past, present and future. *Green Chemistry*, 2014, 16(4), pp. 2015–2026. DOI: <https://doi.org/10.1039/C3GC42018C>
3. Satira, A.; Espro, C.; Paone, E.; Calabrò, P.S.; Pagliaro, M.; Ciriminna, R.; Mauriello, F. The limonene biorefinery: from extractive technologies to its catalytic upgrading into *p*-cymene. *Catalysts*, 2021, 11(3), pp. 387–403. DOI: <https://doi.org/10.3390/catal11030387>
4. Makarouni, D.; Lycourghiotis, S.; Kordouli, E.; Bourikas, K.; Kordulis, C.; Dourtoglou, V.




Transformation of limonene into *p*-cymene over acid activated natural mordenite utilizing atmospheric oxygen as a green oxidant: a novel mechanism. *Applied Catalysis B: Environmental*, 2018, 224, pp. 740–750.

DOI: <https://doi.org/10.1016/j.apcatb.2017.11.006>

5. Patrylak, L.K.; Pertko, O.P.; Yakovenko, A.V.; Voloshyna, Yu.G.; Povazhnyi, V.A.; Kurmach, M.M. Isomerization of linear hexane over acid-modified nanosized nickel-containing natural Ukrainian zeolites. *Applied Nanoscience*, 2022, 12, pp. 411–425. DOI: <https://doi.org/10.1007/s13204-021-01682-1>
6. Brei, V.V.; Melezhyk, O.V.; Prudius, S.V.; Levchuk, M.M.; Patrylak, K.I. Superacid WO_x/ZrO₂ catalysts for isomerization of *n*-hexane and for nitration of benzene. *Studies in Surface Science and Catalysis*, 2002, 143, pp. 387–395. DOI: [https://doi.org/10.1016/S0167-2991\(00\)80679-5](https://doi.org/10.1016/S0167-2991(00)80679-5)
7. Johnson, Jr.W.E. Process for the isomerization of limonene to terpinolene. USA Patent, 1985, No. US4551570A. <https://patents.google.com/patent/US4551570A/en>
8. Aricu, A. The natural product chemistry of terpenoids – a tribute to the remarkable legacy of academician Pavel Vlad. *Chemistry Journal of Moldova*, 2021, 16(1), pp. 8–29. DOI: <http://dx.doi.org/10.19261/cjm.2021.856>
9. Ito, K.; Ito, M. The sedative effect of inhaled terpinolene in mice and its structure–activity relationships. *Journal of Natural Medicines*, 2013, 67, pp. 833–837. DOI: <https://doi.org/10.1007/s11418-012-0732-1>
10. Deck, P.; Birkert, O. Addition of H₂S to terpenes for producing novel molar mass regulators for radical polymerisations. USA Patent, 2010, No. US20100010267A1. <https://patents.google.com/patent/US20100010267A1/en>
11. Okumura, N.; Yoshida, H.; Nishimura, Yu.; Kitagishi, Ya.; Matsuda, S. Terpinolene, a component of herbal sage, downregulates AKT1 expression in K562 cells. *Oncology Letters*, 2012, 3(2), pp. 321–324. DOI: <https://doi.org/10.3892/ol.2011.491>
12. Ma, Y.; Marston, G. Formation of organic acids from the gas-phase ozonolysis of terpinolene. *Physical Chemistry Chemical Physics*, 2009, 11(21), pp. 4198–4209. DOI: <https://doi.org/10.1039/b818789d>
13. Ikeda, Yo.; Takamatsu, C.; Matsuyama, K. Raw-material for pregellation, method for preparation of pregel, pregel, method for production of molded material, and molded material. European Patent, 1990, No. EP0376662A2. <https://patents.google.com/patent/EP0376662A2/en>
14. Retajczyk, M.; Wróblewska, A.; Szymańska, A.; Michalkiewicz, B. Isomerization of limonene over natural zeolite-clinoptilolite. *Clay Minerals*, 2019, 54(2), pp. 121–129. DOI: <https://doi.org/10.1180/clm.2019.18>

15. Martin-Luengo, M.A.; Yates, M.; Rojo, E.S.; Arribas, D.H.; Aguilar, D.; Hitzky, E.R. Sustainable *p*-cymene and hydrogen from limonene. *Applied Catalysis A: General*, 2010, 387(1-2), pp. 141–146. DOI: <https://doi.org/10.1016/j.apcata.2010.08.016>
16. Catrinescu, C.; Fernandes, C.; Castilho, P.; Breen, C. Influence of exchange cations on the catalytic conversion of limonene over Serra de Dentro (SD) and SAz-1 clays: correlations between acidity and catalytic activity/selectivity. *Applied Catalysis A: General*, 2006, 311, pp. 172–184. DOI: <http://dx.doi.org/10.1016/j.apcata.2006.06.023>
17. Retajczyk, M.; Wróblewska, A. Isomerization and dehydroaromatization of *R*(+)-limonene over the Ti-MCM-41 catalyst: effect of temperature, reaction time and catalyst content on product yield. *Catalysts*, 2019, 9(6), pp. 508–519. DOI: <https://doi.org/10.3390/catal9060508>
18. Retajczyk, M.; Wróblewska, A. The isomerization of limonene over the Ti-SBA-15 catalyst – the influence of reaction time, temperature, and catalyst content. *Catalysts*, 2017, 7(9), pp. 273–287. DOI: <https://doi.org/10.3390/catal7090273>
19. Patrylak, L.; Likhnyovskyi, R.; Vypyraylenko, V.; Leboda, R.; Skubiszewska-Zieba, J.; Patrylak K. Adsorption properties of zeolite-containing microspheres and FCC catalysts based on Ukrainian kaolin. *Adsorption Science and Technology*, 2001, 19(7), pp. 525–540. DOI: <https://doi.org/10.1260/0263617011494376>
20. Patrylak, L.K.; Yakovenko, A.V. Alkylation of isobutane with butenes under microcatalytic conditions in pulse mode. *Issues of Chemistry and Chemical Technology*, 2021, 1, pp. 55–61. (in Ukrainian). DOI: <http://dx.doi.org/10.32434/0321-4095-2021-134-1-55-61>
21. Breck, D.W. *Zeolite Molecular Sieves: Structure, Chemistry, and Use*. John Wiley: New York, 1973, 771 p.
22. Rouquerol, F.; Rouquerol, J.; Sing, K. *Adsorption by Powders and Porous Solids: Principles, Methodology and Applications*. Academic Press: San Diego, 1999, 467 p.
23. Barrett, E.P.; Joyner, L.G.; Halenda, P.P. The determination of pore volume and area distributions in porous substances. I. Computations from nitrogen isotherms. *Journal of the American Chemical Society*, 1951, 73(1), pp. 373–380. DOI: <https://doi.org/10.1021/ja01145a126>
24. Ravikovitch, P.I.; Haller, G.L.; Neimark, A.V. Density functional theory model for calculating pore size distributions: pore structure of nanoporous catalysts. *Advances in Colloid and Interface Science*, 1998, 76-77, pp. 203-226. DOI: [https://doi.org/10.1016/S0001-8686\(98\)00047-5](https://doi.org/10.1016/S0001-8686(98)00047-5)
25. Cejka, J.; Van Bakkum, H.; Corma, A.; Schueth, F. Eds. *Introduction to zeolite molecular sieves*. Elsevier: New York, 2007, pp. 787–836. DOI: [https://doi.org/10.1016/S0167-2991\(07\)80810-X](https://doi.org/10.1016/S0167-2991(07)80810-X)
26. Rabo, J.A. *Zeolite chemistry and catalysis*. American Chemical Society: Washington, 1976, 796 p.
27. Lakiss, L.; Vicente, A.; Gilson, J.-P.; Valtchev, V.; Mintova, S.; Vimont, A.; Bedard, R.; Abdo, S.; Bricker, J. Probing the Brønsted acidity of the external surface of faujasite-type zeolites. *ChemPhysChem*, 2020, 21(16), pp. 1873–1881. DOI: <https://doi.org/10.1002/cphc.202000062>
28. Alver, B.E.; Sakizci, M.; Yörükoğulları, E. Investigation of clinoptilolite rich natural zeolites from Turkey: a combined XRF, TG/DTG, DTA and DSC study. *Journal of Thermal Analysis and Calorimetry*, 2010, 100(1), pp. 19–26. DOI: <https://doi.org/10.1007/s10973-009-0118-0>

ONE-POT SYNTHESIS OF SUBSTITUTED BENZIMIDAZOLE DERIVATIVES UNDER ULTRASONIC IRRADIATION USING ZnFe_2O_4 REUSABLE CATALYST

Dhanraj Kamble ^a, Anil Shankarwar ^a, Yuvraj Sarnikar ^b, Radhakrushna Tigote ^c,
Mubarak Shaikh ^d, Pravin Chavan ^{e*}

^a Department of Chemistry, Sarswati Bhuvan Education Society's, College of Science,
Paithan gate Road, Gulmandi-03, Aurangabad 431001, Maharashtra, India

^b Department of Chemistry, Dayanand Science College, Barshi Road, Prakash nagar, Latur 413531,
Maharashtra, India

^c Department of Chemistry, Dr. B. A. M. University (Aurangabad) Sub-campus, Near to MIDC-Sector-2,
Osmanabad 413501, Maharashtra, India

^d Department of Chemistry, Radhabai kale Mahila Mahavidyalaya, near to Tarakpur road Bus stand,
Ahemadnagar- 414001, Maharashtra, India

^e Department of Chemistry, Doshi Vakil Arts College and G.C.U.B. Science & Commerce College,
Goregaon, Lonere-Goregaon Road, Goregaon, Raigad 402103, Maharashtra, India

*e-mail: chemistrypr141286@gmail.com; phone: (+91 90) 28 137 355

Abstract. An efficient one-pot synthesis of benzimidazole derivatives by the condensation between various *o*-phenylenediamine and substituted aromatic aldehyde using ZnFe_2O_4 as a nano-catalyst under ultrasonic irradiation conditions was described. Remarkable advantages of the present synthetic strategy over the previously reported methods are shorter reaction times, higher isolated yields and simple work-up procedure. The presence of electron withdrawing and electron donating groups on the aromatic rings did not affect the yield of the product. The ZnFe_2O_4 catalyst was recycled after completion of reaction and was reused.

Keywords: one pot reaction, substituted benzimidazole, ultrasound irradiation, ZnFe_2O_4 catalyst, biological activity.

Received: 01 August 2022/ Revised final: 10 October 2022/ Accepted: 13 October 2022

Introduction

Nitrogen containing heterocycles are of great importance due to the synthetic utility and extensive attention in organic chemistry and benzimidazole is one amongst them [1-3]. The NH group in benzimidazole is very weakly basic and relatively strongly acidic and benzimidazoles are able to form salts [4]. Outstanding uses of benzimidazoles in medicinal as well pharmaceutical fields include treating fungus pathogens, to treat nematode and trematode infection in animals and humans, stopping hyphal growth. Other benzimidazoles play an important role as preservative agents in fruits, paints, textiles, leather industry, papermaking process. Various pharmaceutical drugs have been manufactured from benzimidazole ring such as astemizole, esomeprazole, nitazene, etonitazene, clonitazene, anti-tuberculosis *etc.* [5-7]. Several authors have reviewed the spectrum of benzimidazole's

pharmacological activity [8-11]. Numerous of its derivatives exhibit pharmacological effects and thus have been promoted in commercialization of medications as shown in Figure 1, therefore there is a continuous interest in developing new methods of synthesis and improving the existing ones.

In recent years, various methods have described syntheses of substituted benzimidazoles using several catalysts, such as rose Bengal [12], *p*-toluenesulfonic acid/graphene and *N,N*-dimethyl aniline/graphene [13], NH_4Cl [14], $[\text{Yb}(\text{OPf})_3]$ [15], $\text{In}(\text{OTf})_3$ [16], FeCl_3 [17], $\text{VO}(\text{acac})_2$ [18], I_2 [19], NH_4OAc [20], nano-catalyst such as CoFe_2O_4 [21], Co/SBA-15 [22], ZnO [23], MNPs@Cu-PMT [24], MNP-IL [25], ZnS [26], $\text{Co}(\text{OH})_2/\text{CoO(II)}$ [27], CuMVs [28] and MIL-53(Fe) [29]. Many of these processes endure limitations, such as extreme reaction conditions, low yields, dreary work-up procedures and co-occurrence of several side reactions.

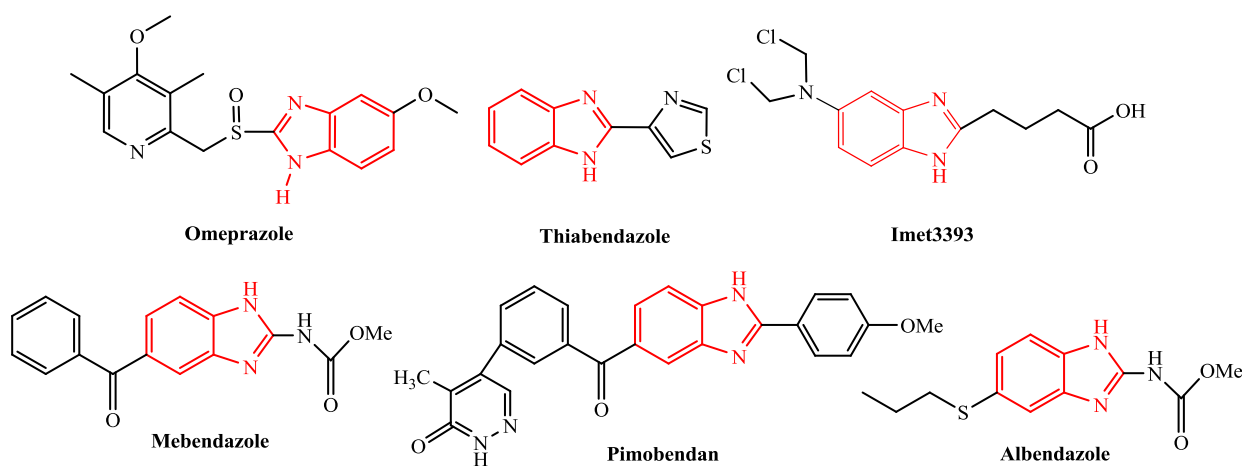


Figure 1. Benzimidazole incorporated drug molecules.

The introduction of green methods to overcome these limitations is still an important experimental challenge. Recently, ZnFe_2O_4 mixed metaloxide nanoparticles have been broadly used in modern heterocyclic organic synthesis. ZnFe_2O_4 is one of the economically efficient, insoluble in organic solvents, easily recoverable, having low surface area, heterogeneous, and inexpensive nanocatalyst [30-33]. Use of ZnFe_2O_4 nanocatalyst in organic synthesis resulted in several advantages such as commercially efficient, yield improvement, time reduction, suitable experimental procedure to work up and easily recovery of catalyst etc. Some examples of synthesized heterocyclic compounds by using ZnFe_2O_4 nanocatalyst are 2,3-dihydroquinazolin 4(1*H*)ones [34] and pyrano[2,3-*d*]pyrimidines [35] derivatives. Also, nanocatalyzed reactions in ultrasonic technique have given excellent yield of product within time [36] in comparison to other.

Thus, above mentioned heterocycles having tremendous significance in various areas, organic chemists have challenge to overwhelm them by searching a surrogate for the conventional bases, which can work in water, and to develop efficient methods for this nucleus using milder, non-hazardous and inexpensive reagents. In continuation to the earlier work, herein it is explored the straightforward synthesis of benzimidazoles by condensation of *o*-phenylenediamine and benzaldehyde under ultrasonication, in hydrated ethanol as a solvent, using ZnFe_2O_4 nanoparticles as catalyst. According to the literature survey, there are no available reports in the literature for the above mentioned procedure.

Herein the aim of this study is the synthesis of benzimidazole derivatives using ZnFe_2O_4 nanoparticles as a catalyst under ultrasonic irradiation.

Experimental

Generalities

All chemicals were purchased from Aura Chemical Laboratory and purified before starting the reactions. The ZnFe_2O_4 nano-catalyst was also purchased from Aura Chemical Laboratory. Ultrasonic bath sonicator conditions were established at: 230 V AC, 50 Hz, liquid holding capacity 5.5 L and temperature 70°C. Melting point values were registered on a SRS Opti-melt instrument and all synthesized compounds were analyzed by means of ^1H and ^{13}C NMR spectroscopy (Bruker), using $\text{DMSO-}d_6$ solvent and TMS as internal standard, at 400 and 100 MHz respectively. Electrospray ionization coupled to mass spectrometry method was carried out on ESI QTOF instrument. IR spectra were recorded on a Perkin Elmer FTIR spectrometer using KBr pallets. Elemental analysis was performed on an Elementer-Vario MICRO cube Analyzer Instrument.

General procedure for synthesis of substituted benzimidazole derivatives (3a-j)

The reaction mixture (*o*-phenylenediamine **1a-c** (0.1 mol), aromatic aldehydes **2a-j** (0.1 mol) and a nano-catalyst in 3 mL of solvent) was ultrasonically irradiated for 30 minutes. The progress of the reaction was monitored by TLC plate using (7:3) ethyl acetate and *n*-hexane. After completion of reaction, 10 mL of ethanol was added to reaction mass and the resulting mixture was stirred for 5 minutes. The obtained solution was filtered to remove the catalyst. The solvent was distilled out under reduced pressure. The product was purified by column chromatography using (1:1) *n*-hexane and ethyl acetate. NMR data of synthesized compounds are presented in supplementary material.

Anti-tuberculosis activity testing

The investigation of *in vitro* anti-tuberculosis activity of synthesized substituted benzimidazole derivatives **3a-j** was carried out by the CLAIRO COMBI method [37]. The synthesized compounds **3a-j** were tested against *M. Tuberculosis* bacterial stain with reference to standard Streptomycin by using Liquefied sterile Lowenstein-Jensen agar media [37].

Results and discussion

An efficient and green protocol for the synthesis of benzimidazoles **3a-j** using ZnFe_2O_4 catalyst is established. To synthesize the target molecule, ultrasound assisted (70°C) condensation of substituted *o*-phenylenediamine **1a-c** with aromatic aldehydes **2a-j** one-pot synthesis was carried out, according to Scheme 1. To establish the efficiency and advantages of the catalytic activity of ZnFe_2O_4 , the synthesis was

also carried out in the same reaction conditions (ethanol as solvent, and temperature of 70°C), by using other catalysts (see Table 1). Results demonstrate that the ZnFe_2O_4 nano-catalyst is more efficient than the other catalyst (Table 1, Entry 6).

To determine the optimum quantity of ZnFe_2O_4 nano-catalyst, the condensation of *o*-phenylenediamine (**1a**) and benzaldehyde (**2a**) was carried out in hydrated ethanol as solvent under ultrasonic irradiation at 70°C (water as a liquid used in the ultrasonic bath) using variable quantities of ZnFe_2O_4 nano-catalyst as presented in Table 2. In Table 2, Entry 3, the results show that 10 mol% nano-catalyst produced an excellent product of yield. Further increase in the concentration of catalyst did not improve the yields. It was therefore concluded that the optimum concentration of catalyst was 10 mol%.

Table 1

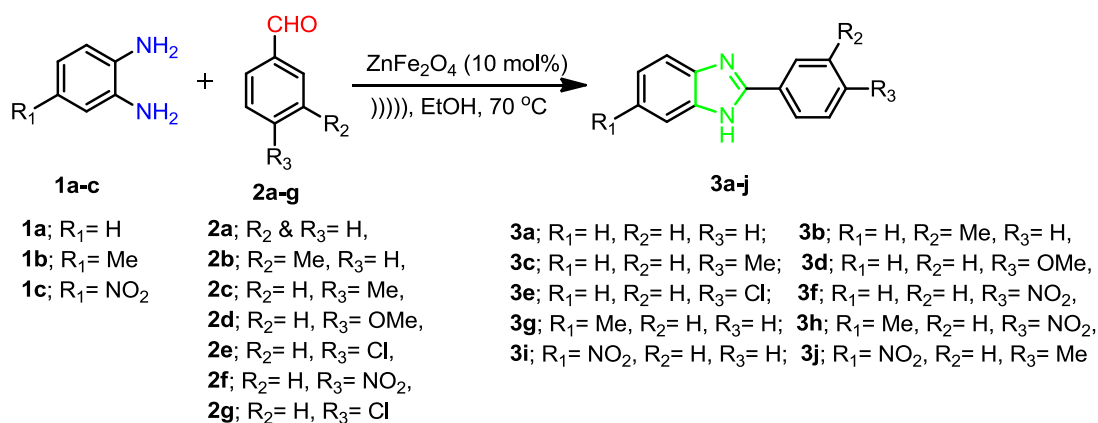
Evaluation of the different catalysts under ultrasonic irradiation conditions for synthesis of 2-phenyl-1H-benzimidazole **3a**.

Entry	Catalyst (10 mol%)	Time (min)	Yield (%)
1.	-	30	25
2.	NH_4Cl	30	47
3.	$\text{Yb}(\text{OTf})_3$	30	60
4.	FeCl_3	30	40
5.	CdCl_2	30	20
6.	ZnFe_2O_4	30	92

Table 2

Screening of amount of ZnFe_2O_4 nano-catalyst under ultrasonic irradiation for the synthesis of 2-phenyl-1H-benzimidazole **3a**.

Entry	Catalyst (mol%)	Time (min)	Yield (%)
1.	-	30	0
2.	5	30	76
3.	10	30	92
4.	15	30	93
5.	20	30	93



Scheme 1. Synthesis of substituted benzimidazole derivatives **3a-j** using ZnFe_2O_4 nano-particles.

Screening of various solvents for model reaction with reflux condenser such as acetonitrile (ACN), ethanol (EtOH), dichloromethane (DCM), dichloroethane (DCE) and water (H₂O), different amounts of product yield observed due to chemical properties of solvent under ultrasonic conditions. In EtOH solvent, the percentage of product yield was excellent (Table 3, Entry 2); maximum yield of product was observed after 28 minutes (**3a**) [38].

In the next step, the reaction with regard to the temperature parameter was examined. Initially, the reaction was carried out at room temperature and then elevated to 50, 65 and 70°C, respectively. It is observed that the yield of the product was considerably enhanced by increasing the temperature (Table 4, Entries 1-4).

Hence, the cyclo-condensation accomplishes smoothly at 70°C and is more efficient with respect to reaction time and excellent yield of the desired product **3a**. After screening the reaction conditions, the synthesis of substituted benzimidazole derivatives (**3a-j**) was carried out by the reaction of different diamines (**1a-j**) with various aromatic aldehydes (**2a-j**).

Thus, substituted benzimidazole derivatives **3a-j** were synthesized using the ultrasonic irradiation method and the yield of reactions were found between 88-92% due to the ultrasonic effect. From that, electron withdrawing substituent of reactants showed slightly higher percentage of product yield. All prepared benzimidazole derivatives **3a-j** showed significant amount of product yield (Table 5).

Table 3

Screening of various solvents under ultrasonic irradiation at 70°C for synthesis of 2-phenyl-1H-benzimidazole **3a**.

Entry	Solvent	Time (min)	Yield (%)
1.	ACN	30	79
2.	EtOH	30	92
3.	DCM	30	64
4.	DCE	30	71
5.	H ₂ O	30	0

Table 4

Screening of ultrasonic temperature for synthesis of 2-phenyl-1H-benzimidazole **3a**.

Entry	Temperature (°C)	Time (min)	Yield (%)
1.	r.t.	30	20
2.	50	30	65
3.	65	30	85
4.	70	30	92

Table 5

Synthesis of substituted benzimidazole derivatives **3a-j** using recyclable ZnFe₂O₄ nano-catalyst.

Sr. No.	Compound	Time (min)	Yield ^a (%)		Melting point values (°C)	
			Found	Reported [Ref.]	Found	Reported [Ref.]
1.	3a	25	92	90 [38]	285-287	288-290 [38]
2.	3b	27	90	-	287-289	-
3.	3c	28	88	-	276-278	-
4.	3d	24	89	87 [38]	234-236	230-232 [38]
5.	3e	25	91	-	294-296	-
6.	3f	22	92	95 [38]	306-308	303-304 [38]
7.	3g	26	89	90 [38]	245-247	232-233 [38]
8.	3h	23	90	95 [38]	240-242	235-238 [38]
9.	3i	24	91	87 [38]	203-205	198-200 [38]
10.	3j	25	89	-	286-288	-

Reaction conditions- *o*-phenylenediamine (0.1 mole), Aromatic aldehydes (0.1 mole), ZnFe₂O₄ nanoparticles catalyst (10 mol%), 3 mL ethanol solvent and ultrasonic irradiation for 70°C, ultrasonic bath liquid - water.

^a yield refers to the isolated product, characterized by NMR, IR, MS spectral analysis.

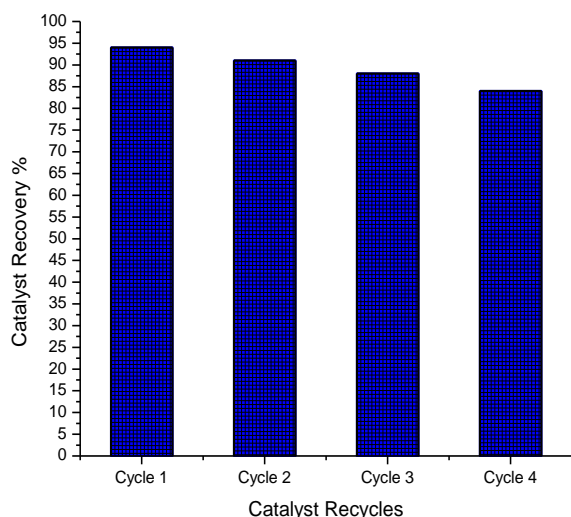


Figure 2. Recyclability of ZnFe_2O_4 nanoparticles catalyst.

Further, the catalyst was recovered by a simple filtration method as shown in Figure 2. The recovered catalyst was implemented again in the optimized reactions 4 times by using 94, 91, 88 and 84% of recovered catalyst. The recycled catalyst gave very good yield of product.

Antituberculosis analysis

Benzimidazoles were showed to detain efficient antituberculosis activity [39]. Hence, the newly synthesized substituted benzimidazole derivatives **3a-j** were evaluated for the antitubercular activity by the zone of inhibition method. Streptomycin was used as a reference standard drug. The obtained results show that the newly synthesized substituted benzimidazole derivatives **3a-j** possessed moderate antitubercular activity (Table 6) and thus have scope in treating tuberculosis (moderate to good). Among all the synthesized compounds **3a-j**, compound **3i** exhibited excellent antitubercular activity compared to the standard drug.

Table 6

Anti-tuberculous activity for prepared substituted benzimidazoles derivatives 3a-j.

Entry	Product	<i>M. Tuberculosis</i> (inhibition zone in diameter mm)
1.	3a	8
2.	3b	10
3.	3c	7
4.	3d	9
5.	3e	8
6.	3f	12
7.	3g	8
8.	3h	12
9.	3i	13
10.	3j	11
11.	Standard	14

Antituberculosis results (Table 6) clearly indicated that the electron withdrawing groups containing benzimidazoles products displayed anti-tuberculous activity as **3i** (13 mm), **3f**, **3h** (12 mm), but not greater than standard (14 mm).

Conclusions

In conclusion, herein is reported the synthesis of substituted benzimidazole derivatives from various *o*-phenylenediamine, different aromatic aldehydes using ZnFe_2O_4 as a recyclable nano-catalyst in ethanol solvent under ultrasonic irradiation conditions. This methodology provides an easier, facile, safe and environmentally benign green protocol synthesis.

The optimized methodology offers reduced reaction time 22 to 28 minutes, recyclability of catalyst up to four cycles with better yields up to 88 to 92%. The main aim of the investigation claims application of ultrasonic irradiation and recyclability of catalyst to synthesize various substituted benzimidazole derivatives by reducing the cost of products, waste and pollution.

All synthesized substituted benzimidazole derivatives exhibited moderate **3c** (7 mm) to good **3h** (12 mm), **3i** (13 mm) anti-tuberculosis activity. Compound 6-nitro-2-phenyl-1*H*-benzo[d]imidazole exhibited excellent anti-tubercular activity comparable to that of the standard drug (14 mm).

Acknowledgments

The authors are grateful to Dr. Arun Kharat, School of Life Sciences, New Delhi, India- 110067, for helping proof-reading the manuscript.

Supplementary information

Supplementary data are available free of charge at <http://cjm.asm.md> as PDF file.





References

- Teague, S.J.; Barber, S.; King, S.; Stein, L. Synthesis of benzimidazole based JNK inhibitors. *Tetrahedron Letters*, 2005, 46(27), pp. 4613–4616. DOI: <https://doi.org/10.1016/j.tetlet.2005.04.145>
- Tatsuta, M.; Kataoka, M.; Yasoshima, K.; Sakakibara, S.; Shogase, Y.; Shimazaki, M.; Yura, T.; Li, Y.; Yamamoto, N.; Gupta, J.; Urbahns, K. Benzimidazoles as non-peptide luteinizing hormone-releasing hormone (LHRH) antagonists. Part 3: Discovery of 1-(1*H*-benzimidazol-5-yl)-3-*tert*-butylurea derivatives. *Bioorganic and Medicinal Chemistry Letters*, 2005, 15(9), pp. 2265–2269. DOI: <https://doi.org/10.1016/j.bmcl.2005.03.030>
- Townsend, L.B.; Wise, D.S. The synthesis and chemistry of certain anthelmintic benzimidazoles. *Parasitology Today* 1990, 6(4), pp. 107–112. DOI: [https://doi.org/10.1016/0169-4758\(90\)90226-t](https://doi.org/10.1016/0169-4758(90)90226-t)

4. Baliharova, V.; Skalova, L.; Maas, R.F.M.; De Vrieze, G.; Bull, S.; Fink-Gremmels, J. The effects of benzimidazole anthelmintics on P4501A in rat hepatocytes and HepG2 cells. *Research in Veterinary Science*, 2003, 75(1), pp. 61–69. DOI: [https://doi.org/10.1016/s0034-5288\(03\)00033-x](https://doi.org/10.1016/s0034-5288(03)00033-x)
5. Lutz, P. Benzimidazole and its derivatives - from fungicides to designer drugs. A new occupational and environmental hazards. *Medycyna Pracy*, 2012, 63(4), pp. 505–513. <https://pubmed.ncbi.nlm.nih.gov/22994080/>
6. Antoci, V.; Cucu, D.; Zbancioc, G.; Moldoveanu, C.; Mangalagiu, V.; Amariuca-Mantu, D.; Aricu, A.; Mangalagiu, I.I. Bis-(imidazole/benzimidazole)-pyridine derivatives: synthesis, structure and antimycobacterial activity. *Future Medical Chemistry*, 2020, 12(3), pp. 207–222. DOI: <https://doi.org/10.4155/fmc-2019-0063>
7. Mantu, D.; Antoci, V.; Moldoveanu, C.; Zbancioc, G.; Mangalagiu, I.I. Hybrid imidazole (benzimidazole)/pyridine (quinoline) derivatives and evaluation of their anticancer and antimycobacterial activity. *Journal of Enzyme Inhibition and Medicinal Chemistry*, 2016, 31(sup2), pp. 96–103. DOI: <https://doi.org/10.1080/14756366.2016.1190711>
8. Habib, N.S.; Soliman, R.; Ashour, F.A.; El-Taiebi, M. Synthesis and antimicrobial testing of novel oxadiazolylbenzimidazole derivatives. *Pharmazie*, 1997, 52(10), pp. 746–749. <https://pubmed.ncbi.nlm.nih.gov/9362087/>
9. Spasov, A.A.; Yozhitsa, I.N.; Bugaeva, L.I.; Anisimova, V.A. Benzimidazole derivatives: Spectrum of pharmacological activity and toxicological properties (a review). *Pharmaceutical Chemistry Journal*, 1999, 33, pp. 232–243. DOI: <https://doi.org/10.1007/bf02510042>
10. Navarrete-Vazquez, G.; Cedillo, R.; Hernandez-Campos, A.; Yepez, L.; Hernandez-Luis, F.; Valdez, J.; Morales, R.; Cortes, R.; Hernandez, M.; Castillo, R. Synthesis and antiparasitic activity of 2-(Trifluoromethyl) benzimidazole derivatives. *Bioorganic and Medicinal Chemistry Letters*, 2001, 11(2), pp. 187–190. DOI: [https://doi.org/10.1016/s0960-894x\(00\)00619-3](https://doi.org/10.1016/s0960-894x(00)00619-3)
11. Salahuddin; Shaharyar, M.; Mazumder, A. Benzimidazoles: A biologically active compounds. *Arabian Journal of Chemistry*, 2017, 10, pp. S157–S17. DOI: <https://doi.org/10.1016/j.arabjc.2012.07.017>
12. Kovvuri, J.; Nagaraju, B.; Kamal, A.; Srivastava, A.K. An efficient synthesis of 2-substituted benzimidazoles via photocatalytic condensation of *o*-phenylenediamines and aldehydes. *ACS Combinatorial Science*, 2016, 18(10), pp. 644–650. DOI: <https://doi.org/10.1021/acscmbosci.6b00107>
13. Sharghi, H.; Asemani, O.; Tabaei, S.H.M. Simple and mild procedures for synthesis of benzimidazole derivatives using heterogeneous catalyst systems. *Journal of Heterocyclic Chemistry*, 2008, 45(5), pp. 1293–1298. DOI: <https://doi.org/10.1002/jhet.5570450506>
14. Kathirvelan, D.; Yuvaraj, P.; Babu, K.; Nagarajan, A.S.; Reddy, B.S.R. A green synthesis of benzimidazoles. *Indian Journal of Chemistry*, 2013, 52B, pp. 1152–1156. <http://nopr.niscair.res.in/handle/123456789/20511>
15. Kedar, M.S.; Dighe, N.S.; Pattan, S.R.; Musmade, D.S.; Thakur, D.; Bhosale, M.; Gaware, V.M. Benzimidazole in medicinal chemistry: an overview. *Der Pharma Chemica*, 2010, 2(2), pp. 249–256. <https://www.derpharmachemica.com/pharmachemica/benzimidazole-in-medicinal-chemistry-an-overview.pdf>
16. Trivedi, R.; De, S.K.; Gibbs, R.A. A convenient one-pot synthesis of 2-substituted benzimidazoles. *Journal of Molecular Catalysis A: Chemical*, 2006, 245(1–2), pp. 8–11. DOI: <https://doi.org/10.1016/j.molcata.2005.09.025>
17. Singh, M.P.; Sasmal, S.; Lu, W.; Chatterjee, M.N. Synthetic utility of catalytic Fe(III)/Fe(II) redox cycling towards fused heterocycles: A facile access to substituted benzimidazole, bisbenzimidazole and imidazopyridine derivatives. *Synthesis*, 2000, 10, pp. 1380–1390. DOI: <https://doi.org/10.1055/s-2000-7111>
18. Dey, M.; Deb, K.; Dhar, S.S. VO(acac)₂ catalyzed condensation of *o*-phenylenediamine with aromatic carboxylic acids/aldehydes under microwave radiation affording benzimidazoles. *Chinese Chemical Letters*, 2011, 22(3), pp. 296–299. DOI: <https://doi.org/10.1016/j.ccllet.2010.10.031>
19. Gogoi, P.; Konwar, D. An efficient and one-pot synthesis of imidazolines and benzimidazoles via anaerobic oxidation of carbon–nitrogen bonds in water. *Tetrahedron Letters*, 2006, 47(1), pp. 79–82. DOI: <https://doi.org/10.1016/j.tetlet.2005.10.134>
20. Sharghi, H.; Asemani, O.; Khalifeh, R. New one-pot procedure for the synthesis of 2-substituted benzimidazoles. *Synthetic Communications*, 2008, 38(7), pp. 1128–1136. DOI: <https://doi.org/10.1080/00397910701863657>
21. Jithendra Kumara, S.K.; Krishnamurthy, G.; Sunil Kumar, N.; Naik, N.; Praveen, T.M. Sustainable synthesis of magnetically separable SiO₂/Co@Fe₂O₄ nanocomposite and its catalytic applications for the benzimidazole synthesis. *Journal of Magnetism and Magnetic Materials*, 2018, 451, pp. 808–821. DOI: <https://doi.org/10.1016/j.jmmm.2017.10.125>
22. Rajabi, F.; De, S.; Luque, R. An efficient and green synthesis of benzimidazole derivatives using SBA-15 supported cobalt nanocatalysts. *Catalysis Letters*, 2015, 145, pp. 1566–1570. DOI: <https://doi.org/10.1007/s10562-015-1546-z>
23. Paul, B.; Vadivel, S.; Dhar, S.S.; Debbarma, S.; Kumaravel, M. One-pot green synthesis of zinc oxide nano rice and its application as sonocatalyst for degradation of organic dye and synthesis of

- 2-benzimidazole derivatives. *Journal of Physics and Chemistry of Solids*, 2017, 104, pp. 152–159.
DOI: <https://doi.org/10.1016/j.jpcs.2017.01.007>
24. Mobinikhaledi, A.; Moghanian, H.; Ghazvini, S.M.B.H.; Dalvand, A. Copper containing poly(melamine-terephthaldehyde)-magnetite mesoporous nanoparticles: a highly active and recyclable catalyst for the synthesis of benzimidazole derivatives. *Journal of Porous Materials*, 2017, 25, pp. 1123–1134.
DOI: <https://doi.org/10.1007/s10934-017-0524-9>
 25. Nezhad, E.R.; Tahmasebi, R. Ionic liquid supported on magnetic nanoparticles as an efficient and reusable green catalyst for synthesis of benzimidazole derivatives under solvent and solvent-free conditions. *Asian Journal of Green Chemistry*, 2019, 3(1), pp 34–42.
DOI: <http://doi.org/10.22034/AJGC.2018.65743>
 26. Hakimi, F.; Niri, M.D.; Taba, S.H.B.; Golrasan, E. A facile synthesis of benzimidazole derivatives over zinc sulfide nanoparticles as heterogeneous catalyst. *Asian Journal of Green Chemistry*, 2020, 4(3), pp. 239–248.
DOI: <http://doi.org/10.22034/AJGC/2020.3.1>
 27. Adharvana Chari, M.; Shobha, D.; Sasaki, T. Room temperature synthesis of benzimidazole derivatives using reusable cobalt hydroxide (II) and cobalt oxide (II) as efficient solid catalysts. *Tetrahedron Letters*, 2011, 52(43), pp. 5575–5580.
DOI: <https://doi.org/10.1016/j.tetlet.2011.08.047>
 28. Kaur, N.; Kaur, S.; Kaur, G.; Bhalla, A.; Srinivasan, S.; Chaudhary, G.R. Metallovesicles as smart nanoreactors for green catalytic synthesis of benzimidazole derivatives in water. *Journal of Materials Chemistry A*, 2019, 7(29), pp. 17306–17314.
DOI: <https://doi.org/10.1039/c9ta05441c>
 29. Azadeh, N. Metal-organic framework MIL-53(Fe) as a highly efficient reusable catalyst for the synthesis of 2-aryl-1*H*-benzimidazole. *Chemical Methodologies*, 2019, 3(6), pp. 704–712. DOI: <https://doi.org/10.33945/SAMI/CHEMM.2019.6.8>
 30. Zhang, M.; Liu, Y.-H.; Shang, Z.-R.; Hu, H.-C.; Zhang, Z.-H. Supported molybdenum on graphene oxide/Fe₃O₄: An efficient, magnetically separable catalyst for one-pot construction of spiro-oxindole dihydropyridines in deep eutectic solvent under microwave irradiation. *Catalysis Communications*, 2017, 88, pp. 39–44.
DOI: <https://doi.org/10.1016/j.catcom.2016.09.028>
 31. Bangale, S.; Jondhale, V.; Pansare, D.; Chavan, P. Reusable ZnCr₂O₄ nano catalyzed one pot three-component cycloaddition reaction for synthesis of azetidine derivatives under ultrasound irradiation. *Polycyclic Aromatic Compounds*, 2021, 41, pp. 1–13. DOI: <https://doi.org/10.1080/10406638.2021.1983617>
 32. Jadhav, S.; Farooqui, M.; Chavan, P.; Hussain, S.; Rai, M. ZnFe₂O₄ nano-catalyzed one-pot multi-component synthesis of substituted tetrahydropyranoquinoline under neat ultrasonic irradiation. *Polycyclic Aromatic Compounds*, 2022, 42(5), pp. 2067–2075. DOI: <https://doi.org/10.1080/10406638.2020.1825005>
 33. Chavan, P.; Salve, A.; Shelke, R.; Pansare, D. A facile synthesis and biological screening of pyrimidine derivatives under ultrasonic irradiations by ZnCr₂O₄ nano-particles catalyst. *Letters in Applied NanoBioScience*, 2022, 11(1), pp. 2996–3005. DOI: <https://doi.org/10.33263/LIANBS111.29963005>
 34. Rupnar, B.D.; Kachave, T.R.; Jawale, P.D.; Shisodia, S.U.; Pawar, R.P. Green and efficient synthesis of 2,3-dihydroquinazolin-4(1*H*)-ones in aqueous medium using ZnFe₂O₄ catalyst under microwave irradiation. *Journal of the Iranian Chemical Society*, 2017, 14, pp. 1853–1858.
DOI: <https://doi.org/10.1007/s13738-017-1124-y>
 35. Khazaei, A.; Ranjbaran, A.; Abbasi, F.; Khazaei, M.; Moosavi-Zare, A.R. Synthesis, characterization and application of ZnFe₂O₄ nanoparticles as a heterogeneous ditopic catalyst for the synthesis of pyrano[2,3-*d*] pyrimidines. *RSC Advances*, 2015, 5(18), pp. 13643–13647.
DOI: <https://doi.org/10.1039/c4ra16664g>
 36. Chavan, P.; Bangale, S.; Pansare, D.; Shelke, R.; Jadhav, S.; Tupare, S.; Kamble, D.; Rai, M. Synthesis of substituted pyrimidine using ZnFe₂O₄ nanocatalyst via one pot multi-component reaction ultrasonic irradiation. *Journal of Heterocyclic Chemistry*, 2020, 57(9), pp. 3326–3333.
DOI: <https://doi.org/10.1002/jhet.4048>
 37. Government of India, The Ayurvedic Pharmacopoeia of India. New Delhi: Department of Indian Systems of Medicine & Homeopathy, 2001, Part-1, Vol. II, 155 p. <https://cdn.ayush.gov.in/wp-content/uploads/2021/03/Ayurvedic-Pharmacopoeia-of-India-part-1-volume-IX.pdf>
 38. Ghafari, H.; Joorabchi, N.; Emami, A.; Zand, H.R.E. Covalent modification of graphene oxide with vitamin b1: preparation, characterization and catalytic reactivity for synthesis of benzimidazole derivatives. *Industrial & Engineering Chemistry Research*, 2017, 56(22), pp. 6462–6467.
DOI: <https://doi.org/10.1021/acs.iecr.7b00182>
 39. Yadav, S.; Narasimhan, B.; Lim, S.M.; Ramasamy, K.; Vasudevan, M.; Shah, S.A.A.; Mathur, A. Synthesis and evaluation of antimicrobial, antitubercular and anticancer activities of benzimidazole derivatives. *Egyptian Journal of Basic and Applied Sciences*, 2018, 5(1), pp. 100–109.
DOI: <https://doi.org/10.1016/j.ejbas.2017.11.001>

MILD ACIDIC CHARCOAL CATALYZED SYNTHESIS OF 3,4-DIHYDROPYRIMIDIN-2(1H)-ONE/-THIONE DERIVATIVES

Rajendra Patil ^a, Jagdish Chavan ^a, Shivnath Patel ^a, Vaishali Shinde ^b, Anil Beldar ^{a*}

^aDepartment of Chemistry, Poojya Sane Guruji Vidya Prasarak Mandal's Sajan Isan Patil Arts, Girdhar Barku Patel Science and Shahada Taluka Kharedi Vikri Sangh Commerce College, Khetia Road Shahada, Nandurbar 425409, India

^bDepartment of Chemistry, Savitribai Phule Pune University, Ganeshkhind Road, Pune 411007, India
*e-mail: dragbeldar@gmail.com; phone: (+91) 94 20 134 233

Abstract. A mild catalyst system with comparative reduction in amount of catalyst was demonstrated. The multicomponent synthesis of 3,4-dihydropyrimidin-2(1H)-ones and -thiones using acetic acid supported on activated charcoal as a mild acid catalyst in ethanol under both conventional as well as microwave irradiation conditions has been achieved. The obtained catalyst system is more efficient under microwave irradiation than under conventional conditions with shorter reaction times (3-9 min) and excellent yields (78-94 %).

Keywords: Biginelli reaction, acetic acid, acidic charcoal, microwave irradiation.

Received: 20 September 2022/ Revised final: 18 November 2022/ Accepted: 20 November 2022

Introduction

Polymer supported reagents have been utilized successfully for the synthesis of substituted 3,4-dihydropyrimidin-2(1H)-ones (or thiones) (DHPMs) [1]. Several polymers-based efficient catalysts were reported for the Biginelli advancements, such as biocatalysts [2], clays and minerals, alumina [3], silica [4], cyclodextrins, hetero-polyacids[5], hetero-polyanions, and organo-catalysts [6]. Organic polymers such as resins, calixarenes, cyclodextrins and polymeric carbon were found to be effective catalysts and catalyst support [6]. A polymeric form of carbon was employed as catalyst in the form of expandable graphite [7] and graphite [8] for synthesizing DHPMs. The use of polymeric carbon as a support for the LaCl_3 catalyst supported on graphite [9] under microwave conditions; sulphonated carbon materials prepared using concentrated sulphuric acid, at elevated temperature [10]; sulphuric acid immobilized on activated charcoal in *n*-hexane-acetonitrile under reflux conditions [11], were reported as catalytic conditions for the one-pot multicomponent Biginelli reaction, thereby providing heterogeneous protocol. However, the limitations such as the use of sulphuric acid as a catalyst and longer reaction times require the development of simpler and safer method.

Thus, the purpose of the study was to synthesize 3,4-dihydropyrimidin-2(1H)-one

and -thione derivatives by using charcoal supported acetic acid as the catalyst system. The optimized method employed in this study allows to overcome the use of hazardous strong acids, expensive catalysts and to employ a cheap and readily available catalyst system.

Experimental

Generalities

All starting reagents, including aromatic aldehydes, ethyl acetoacetate, urea, thiourea, acetic acid, charcoal, ethanol, ethyl acetate, petroleum ether *etc.*, were purchased from commercial sources Loba Chemie Pvt. Ltd., Merck Specialities Pvt. Ltd. and used without further purification. *Melting point values* were determined using the conventional method and are uncorrected. Reactions were monitored by *thin layer chromatography* on silica gel 60 F254 plates. A conventional household microwave oven operating at 800 W was used for irradiation. All the synthesized products are known compounds and were identified by comparing their melting points and spectra data with those reported in the literature.

Preparation of mild acidic charcoal

To a 50 mL round bottom flask fitted on a magnetic stirrer containing 10 mL ethanol was added 1 mL of glacial acetic acid and stirred to get a homogeneous solution. Further, to a homogenized solution of ethanolic acetic acid, 1 g

of activated charcoal was added in portions and stirred for 10 min to ensure uniform adsorption. Ethanol was then removed by rotary evaporator to get dry acetic acid adsorbed charcoal powder. The loading of acetic acid on charcoal was found 14–16 mmol/g (80–91%), determined titrimetrically using 0.01 N NaOH for a 0.1 g sample of mild acidic charcoal with phenolphthalein indicator.

The conventional method for the synthesis of 3,4-dihydropyrimidin-2(1H)-ones and -thiones

A 50 mL round bottom flask containing the mixture of aldehyde (**1**) (10 mmol), ethyl acetoacetate (**2**) (10 mmol), urea/thiourea (**3**) (12 mmol) and 0.1 g mild acidic charcoal catalyst was refluxed with 10 mL ethanol for the appropriate time. The progress of the reaction was monitored by TLC using the ethyl acetate and *n*-hexane solvent system. After reaction completion, the warm reaction mixture was filtered on a filtration funnel to separate the charcoal residue. The charcoal residue was washed with ethanol (3×3 mL). The products were obtained from the filtrate after removal of ethanol by rotary evaporator. The recrystallization of crude products from ethanol afforded good to excellent yields of DHPMs and thiones [12].

Microwave irradiation method for the synthesis of 3,4-dihydropyrimidin-2(1H)-ones and -thiones

To an Erlenmeyer flask containing a mixture of aldehyde (10 mmol), ethyl acetoacetate (10 mmol), urea/thiourea (12 mmol) in 10 mL ethanol was added 0.1 g mild acidic charcoal catalyst subjected to microwave irradiation for the indicated period of time. The reaction mixture was irradiated with a time interval of 1 min and the reaction progress was monitored using TLC. After reaction completion, the work-up procedure was employed as described in the conventional method.

5-(Ethoxycarbonyl)-6-methyl-4-phenyl-3,4-dihydropyrimidin-2(1H)-one (4a)

IR (KBr, cm^{-1}): 3480, 3247, 2980, 1728, 1705, 1646, 1466, 1222, 1090. ^1H NMR (400 MHz, δ , ppm) ($\text{DMSO}-d_6$): δ 9.17 (s, 1H), 7.75–7.69 (m, 1H), 7.37–7.27 (m, 2H), 7.24 (ddt, J = 6.9, 3.3, 1.5 Hz, 3H), 5.15 (d, J = 3.4 Hz, 1H), 3.99 (q, J = 7.0 Hz, 2H), 2.25 (s, 3H), 2.09 (s, 2H), 1.10 (t, J = 7.1 Hz, 3H). MS (m/z): 261 ($M+1$) [13].

5-Ethoxycarbonyl-6-methyl-4-(4-hydroxyphenyl)-3,4-dihydropyrimidin-2(1H)-one (4b)

IR (KBr, cm^{-1}): 3520, 3362, 2991, 1737, 1705, 1652, 1566, 1250. ^1H NMR (400 MHz, δ , ppm) ($\text{DMSO}-d_6$): δ 9.33 (s, 1H), 9.08 (d,

J = 2.2 Hz, 2H), 7.62–7.56 (m, 2H), 7.07–6.99 (m, 3H), 6.83 (s, 1H), 6.73–6.65 (m, 3H), 5.05 (d, J = 3.3 Hz, 2H), 3.98 (q, J = 7.1 Hz, 3H), 2.23 (s, 5H), 2.09 (s, 1H), 1.10 (t, J = 7.1 Hz, 5H), 1.06 (s, 1H). [13].

5-(Ethoxycarbonyl)-6-methyl-4-(4-nitrophenyl)-3,4-dihydropyrimidin-2(1H)-one (4c)

IR (KBr, cm^{-1}): 3343, 3107, 2981, 1704, 1651, 1520, 1347, 1213. ^1H NMR (400 MHz, δ , ppm) ($\text{DMSO}-d_6$): δ 9.37 (s, 1H), 8.25–8.17 (m, 2H), 7.91 (dd, J = 3.5, 2.0 Hz, 1H), 7.54–7.47 (m, 2H), 5.27 (d, J = 3.3 Hz, 1H), 3.98 (q, J = 7.1 Hz, 2H), 2.26 (s, 3H), 1.09 (t, J = 7.1 Hz, 3H). [14].

5-(Ethoxycarbonyl)-4-(4-methoxyphenyl)-6-methyl-3,4-dihydropyrimidin-2(1H)-one (4d)

IR (KBr, cm^{-1}): 3479, 3413, 3246, 2928, 1724, 1705, 1651, 1513, 1224, 1220. ^1H NMR (400 MHz, δ , ppm) ($\text{DMSO}-d_6$): δ 9.13 (s, 1H), 8.25–8.17 (m, 2H), 7.91 (dd, J = 3.5, 2.0 Hz, 1H), 7.54–7.47 (m, 2H), 5.27 (d, J = 3.3 Hz, 1H), 3.98 (q, J = 7.1 Hz, 2H), 2.26 (s, 3H), 1.09 (t, J = 7.1 Hz, 3H). [14].

5-(Ethoxycarbonyl)-4-(*n*-propyl)-6-methyl-3,4-dihydropyrimidine-2(1H)-one (4e)

IR (KBr, cm^{-1}): 3237, 3015, 1735, 1712, 1666, 1599, 1287. ^1H NMR (400 MHz, δ , ppm) (CDCl_3): δ 8.04 (s, 1H), 5.85 (s, 1H), 4.33 (dt, J = 7.6, 3.5 Hz, 1H), 4.28–4.12 (m, 2H), 2.30 (s, 3H), 2.19 (s, 2H), 1.67–1.39 (m, 2H), 1.30 (t, J = 7.1 Hz, 4H), 0.93 (t, J = 7.1 Hz, 3H). [15].

5-Ethoxycarbonyl-4-(phenyl)-6-methyl-3,4-dihydropyrimidin-2(1H)-thione (4f)

IR (KBr, cm^{-1}): 3380, 3186, 2986, 1720, 1703, 1660, 1586, 1270. ^1H NMR (400 MHz, δ , ppm) ($\text{DMSO}-d_6$): δ 9.81 (s, 1H), 9.65 (s, 1H), 7.37–7.21 (m, 5H), 5.17 (d, J = 3.4 Hz, 1H), 4.00 (q, J = 7.1 Hz, 2H), 2.29 (s, 3H), 1.10 (s, 3H). MS (m/z): 277 ($M+1$). [12].

5-Ethoxycarbonyl-6-methyl-4-(2-hydroxyphenyl)-3,4-dihydropyrimidin-2(1H)-thione (4g)

IR (KBr, cm^{-1}): 3487, 3290, 2857, 1750, 1698, 1634, 1534, 1232. ^1H NMR (400 MHz, δ , ppm) ($\text{DMSO}-d_6$): δ 1.07 (t, J = 7.6 Hz, 3H), 2.4 (s, 3H), 4.1 (q, J = 7.6 Hz, 2H), 5.68 (s, 1H), 6.91–7.15 (m, 4H), 7.72 (s, 1H), 9.65 (s, 1H), 9.95 (s, 1H). MS (m/z): 293 ($M+1$). [16].

5-(Ethoxycarbonyl)-6-methyl-4-(4-chlorophenyl)-3,4-dihydropyrimidin-2(1H)-thione (4h)

IR (KBr, cm^{-1}): 3410, 3269, 2897, 1755, 1631, 1575, 1365, 1268. ^1H NMR (400 MHz, δ , ppm) (CDCl_3): δ 7.52 (d, J = 8.7 Hz, 1H), 6.92–6.81 (m, 2H), 6.16 (q, J = 1.3 Hz, 1H), 4.14 (t, J = 5.9 Hz, 2H), 3.56 (t, J = 6.5 Hz, 2H), 2.42 (d, J = 1.2 Hz, 3H), 2.17–2.06 (m, 2H). [12].

5-Ethoxycarbonyl-4-(4-methoxyphenyl)-6-methyl-3,4-dihydropyrimidin-2(1H)-thione (4i)

IR (KBr, cm^{-1}): 3463, 3192, 2889, 1737, 1708, 1653, 1573, 1243. ^1H NMR (400 MHz, δ , ppm) ($\text{DMSO}-d_6$): δ 9.9 (s, 1H), 9.60 (s, 1H), 7.13 (d, J = 8.7 Hz, 2H), 6.89 (d, J = 8.7 Hz, 2H), 5.11 (d, J = 3.4 Hz, 1H), 4.01 (q, J = 7.1 Hz, 2H), 3.72 (s, 3H), 2.28 (s, 3H), 1.11 (t, J = 7.0 Hz, 3H). [12].

5-Ethoxycarbonyl-4-(*n*-propyl)-6-methyl-3,4-dihydropyrimidin-2(1H)-thione (4j)

IR (KBr, cm^{-1}): 3337, 3019, 1745, 1705, 1651, 1520, 1320. ^1H NMR (400 MHz, δ , ppm) (CDCl_3): δ 8.41 (s, 1H), 7.94 (s, 1H), 4.37 (dt, J = 7.7, 3.7 Hz, 1H), 4.28–4.09 (m, 2H), 2.32 (s, 3H), 2.18 (s, 1H), 1.69–1.55 (m, 1H), 1.55–1.43 (m, 1H), 1.46 (s, 1H), 1.47–1.30 (m, 1H), 1.30 (s, 1H), 1.28 (d, J = 7.1 Hz, 2H), 0.92 (t, J = 7.0 Hz, 3H). [17].

Results and discussion

Firstly, the heterogeneous mild acid catalyst system was developed by using glacial acetic acid and activated charcoal as solid support (1:1 v/w ratio) to achieve the synthesis of DHPMs and -thiones. Titrimetrically, the loading of acetic acid was determined to 80–91% per 0.1 g support. The model Biginelli reaction was performed using benzaldehyde, ethyl acetoacetate and urea (1:1:1.2) in ethanol with the different amounts of mild acidic charcoal catalyst. Both conventional

as well as microwave irradiation (800 W, 40%) methods were demonstrated to optimize the catalyst amount (Scheme 1).

The optimized catalytic conditions showed satisfactory results with respect to the yield and purity of the compounds under both reaction conditions with 0.1 g, as described in Table 1. No significant change in reaction time and in yield was observed with the catalyst amount higher than 0.1 g; therefore 0.1 g of mild acidic charcoal as a catalyst was employed for the synthesis of Biginelli derivatives. The microwave method was apparently more efficient than the conventional method with notably short reaction time and excellent yields of products (Table 1 and Table 2).

Table 1

Effect of catalyst amount on the conventional and on the microwave assisted model Biginelli reaction.

Entry	Catalyst, g	Conventional method		Microwave irradiation	
		Time, min	Yield, %	Time, min	Yield, %
1	0.025	120	79	12	83
2	0.050	90	83	9	88
3	0.075	60	88	7	91
4	0.100	40	90	3	94
5	0.125	40	88	3	94
6	0.150	40	88	3	93

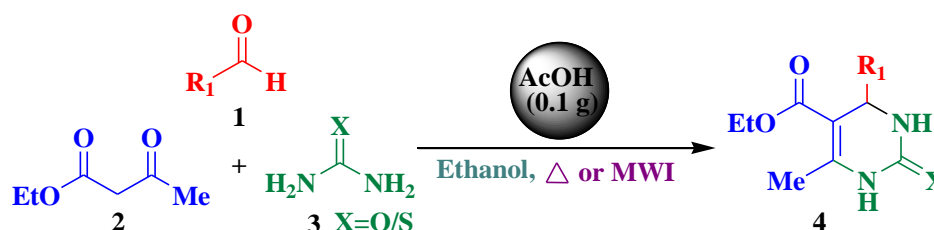
Optimization of acidic charcoal catalyst amount.

Table 2

Mild acidic charcoal catalyzed synthesis of dihydropyrimidin-2(1H)-ones and -thiones under conventional, as well as microwave irradiation conditions.

Entry	Product	R1	X	Conventional heating		Microwave irradiation		Melting point, °C	
				Time, min	Yield, %	Time, min	Yield, %	Observed	Reported
1	4a	C ₆ H ₅ -	O	40	90	3	94	200-202	200-202[12]
2	4b	4-OH-	O	40	76	4	84	228-230	228-230[12]
3	4c	4-NO ₂ -	O	35	88	3	92	208-210	210-212[16]
4	4d	4-OCH ₃ -	O	140	72	8	79	194-196	196-198[12]
5	4e	<i>n</i> -Propyl	O	90	92	4	94	180-182	180-182[15]
6	4f	C ₆ H ₅ -	S	120	88	5	92	204-206	205-207[12]
7	4g	2-OH-	S	120	76	6	84	206-208	206-208[16]
8	4h	4-Cl-	S	40	85	3	87	178-180	180-182[12]
9	4i	4-OCH ₃ -	S	140	74	9	78	154-156	154-156[12]
10	4j	<i>n</i> -Propyl	S	90	90	4	94	148-150	148-152[17]

Mild acidic charcoal employed as a catalyst for the synthesis of different Biginelli derivatives.



Scheme1. Mild acidic charcoal catalyzed Biginelli reaction.

The mild acidic charcoal catalyst was then employed to synthesize DHPM and -thione derivatives using substituted aromatic aldehydes, ethyl acetoacetate and urea or thiourea. To verify the catalytic efficiency of mild acidic charcoal, DHPM and -thione derivatives were prepared under microwave irradiation and conventional refluxing conditions. Under both conditions the mild acid charcoal catalyst was found efficient, but under microwave conditions the efficiency was appreciably good (yielding 78–94%) in comparison to conventional conditions (72–98% yielding) (Table 2).

The aldehydes bearing electron releasing and electron withdrawing groups were reacted successfully under both conventional and microwave conditions. The evaluation of mild acidic charcoal catalyst for Biginelli multicomponent cyclo-condensation proved to be

noteworthy. The use of acetic acid for the Biginelli reaction reported in the literature has been compared with the mild acidic charcoal catalyzed by microwave irradiation displayed in Table 3.

Some of the methods used acetic acid solvent in the presence of acid catalyst such as Lewis acids and protic acids. The mild acidic charcoal catalyst proved a short reaction time (3 min) and excellent yield (94%). Compared to conventional heating conditions, MWI conditions required shorter reaction times (Table 3). The comparison shown in Table 4 could be accounted for a summary of microwave assisted methods for the synthesis of DHPMs and -thiones. The variety of reported methods involved different amounts of catalyst and variations in reaction times, with varied ranges of DHPMs yields.

Table 3

Comparison of methods used acetic acid for the Biginelli reaction.

Entry	AcOH, mL	Solvent, mL	Catalyst	Activation mode	T, °C	Time, min	Yield, %	Ref.
1	0.1	THF (30)	CuCl /BF ₃ .OEt ₂	Heat	66	480	82	[18]
2	3	EtOH (1)	FeCl ₃	MWI	120	10	74	[19]
3	10	AcOH	H ₃ BO ₃	Heat	100	30	94	[20]
4	25	EtOH (10)	-	Heat	78	240	90	[21]
5	1	EtOH (50)	-	Heat	78	240	87	[22]
6	20	AcOH	HCl	Heat	100	480	93	[23]
7	20	AcOH	HCl	Heat	100	480	52*	[24]
8	20	AcOH	Meldrum's acid	Heat	118	600	41	[25]
9	1	EtOH (10)	AcOH-Charcoal	MWI	-	3	94	This work

*With 1,3-diphenyl-1,3-propanedione; AcOH: acetic acid; EtOH: ethanol; THF: tetrahydrofuran.

Some methods which employed acetic acid are compared.

Table 4

Comparison of microwave assisted protocols for Biginelli reaction.

Entry	Catalyst used (amount)	Solvent, mL	Time, min	Yield, %	Ref.
1	FeCl ₃ /Si-MCM-41 (0.03 g/ 20 wt %)	-	3	89	[26]
2	Acidic Al ₂ O ₃ (20 g)	Methanol (30)	6	86	[27]
3	Acidic Al ₂ O ₃ or montmorillonite K ₁₀ clay (20 g)	EtOH (10)	8	75	[28]
4	I ₂ - Al ₂ O ₃ (neutral) (0.5 g)	-	1	90	[29]
5	ZrO ₂ -pillared clay (0.25 g)	-	5	94	[30]
6	PEG-SO ₃ H	-	6	91	[31]
7	Polystyrene sulphonic acid [PSSA] (20% solution)	Water	20	89	[32]
8	LaCl ₃ -graphite (1.5 g)	-	8	85	[9]
9	FeCl ₃ /Nanopore Silica (0.05 g)	-	15	75	[33]
10	Al ₂ O ₃ -SO ₃ H (0.5 g)	-	2	88	[28]
11	N-Bromosuccinamide (0.35g)	-	30	75	[34]
12	nanosized Ni _{0.45} Zn _{0.55} Fe ₂ O ₄ (0.03 g)	-	10	67	[35]
13	[PyPS] ₃ PW ₁₂ O ₄₀ (0.314 g)	-	5	95	[36]
14	3D printed α-Al ₂ O ₃ (0.350 g)	-	10	95	[37]
15	AcOH-Charcoal (0.1 g)	EtOH (10)	3	94	This work

Different catalyst systems under microwave irradiation conditions are compared.

Table 5

Comparison of solid supported organic catalysts for Biginelli reaction.

Entry	Catalyst used (amount)	Reaction conditions	Time, min	Yield, %	Ref.
1	PsMImPF ₆ (0.1 g)	AcOH (40 mL), 100 °C	120	98	[38]
2	PANI-HBF ₄ .DHS (5 wt %)	EtOH, reflux	360	97	[39]
3	PANI-PTSA (5 wt %)	Methanol (10 mL), reflux	120	97	[40]
4	Ps-AlCl ₃ (1.28 g)	EtOH (10 mL), reflux	180	89	[41]
5	PS-AFDPAT (0.65 g)	EtOH (50 mL), reflux	300	90	[42]
6	PVSA (10 mol%)	EtOH or H ₂ O (5 mL),	60	88/94	[43]
7	PPF-SO ₃ H (0.25 g)	EtOH (15 mL), reflux	480	81	[44]
8	NSPVP (4 mol%)	Solvent free, 100 °C	6	90	[45]
9	PSBIL (50 mg)	EtOH (5 mL), 110 °C	1080	91	[46]
10	PANI-FeCl ₃ (0.2 g)	Acetonitrile, reflux	1440	83	[47]
11	H ₂ SO ₄ - Charcoal (133 % w/w)	<i>n</i> -Hexane- Acetonitrile, reflux	35	95	[11]
12	AcOH-Charcoal (0.1 g)	EtOH (10 mL), MWI	3	94	This work

Organic polymer supported catalysts for the Biginelli reaction are compared.

Few of the methods involved relatively more amount of catalyst (10–25 mL) and in some cases yields were good (82–93 %); with relatively more reaction time (240–480 min). The catalysts supported on clays, acidic alumina, nano-silica etc. and also, heteropolyacids and nanopolymers as catalysts were compared. In addition, the present charcoal supported acetic acid catalyst was also compared with the solid supported organic catalysts under different reaction conditions for the synthesis of Biginelli DHPMs and -thiones as per the Table 5.

The described solid supported organic catalysts in the Table 5 provided good yields comparable to the conventional reaction conditions with longer reaction times. The preparation methods for the solid or polymer supported organic catalyst, presented in Table 5, involve multiple steps and needs more expensive characterization methods. The functionalized polymers, resins as a catalyst were compared under both solvent and solvent-free conventional heating conditions. Concentrated sulphuric acid supported on charcoal support employed as a catalyst under conventional refluxing conditions was also compared. The reusability of recovered charcoal support for six cycles after activation and adsorption with acetic acid as per the procedure for preparation of mild acidic charcoal catalyst has also been demonstrated.

Conclusions

In conclusion, acetic acid adsorbed on activated charcoal as a mild catalyst was efficiently screened for the synthesis of Biginelli DHPMs and -thiones. The estimated adsorption of acetic acid on charcoal was observed as 80–91% per 0.1 g sample of charcoal. The amount of acetic acid as catalyst also reduced considerably

due to the large surface area provided by charcoal particles which also capably improved the yields. The increase in yields can also be supported by large surface area provided for reactants by charcoal particles.

The use of cheap, green, and easily available charcoal as solid support for acetic acid makes the method environment friendly. In the present article, a simple and convenient synthesis of known DHPMs and -thiones using mild acidic charcoal as catalyst was reported. In future, using the optimized protocol synthesis of novel DHPMs and -thiones will be planned.

Acknowledgments

The authors thank the Central Instrumentation Facility, Savitribai Phule Pune University, Pune for the characterization facility.

Supplementary information

Supplementary data are available free of charge at <http://cjm.asm.md> as PDF file.

References

- Patil, R.; Chavan, J.; Beldar, A. Review Biginelli reactions: Reagent support based approaches. *World Journal of Pharmacy and Pharmaceutical Sciences*, 2016, 5(11), pp. 419-432. DOI: <https://doi.org/10.20959/wjpps201611-7959>
- Zanin, L.L.; Brito Matos, T.K.; Leitão, A.; Ellena, J.; Porto, A.L.M. Biocatalytic kinetic resolution to access enantiomerically enriched dihydropyrimidinone/thiones through recognition of a remote stereocentre. *European Journal of Organic Chemistry*, 2022, 2022(38), pp. e202200331. DOI: <https://doi.org/10.1002/ejoc.202200331>
- Zanin, L. L.; Porto, A. L. HClO₄-Al₂O₃ as a prominent catalyst in the synthesis of 3, 4-dihydropyrimidin-2 (1*H*)-ones/thiones under environmentally friendly solvent conditions.

- ChemistrySelect, 2020, 5(28), pp. 8604-8608. DOI: <https://doi.org/10.1002/slct.202001830>
4. Chopda, L.V.; Dave, P.N. Recent advances in homogeneous and heterogeneous catalyst in Biginelli reaction from 2015-19: A concise review. ChemistrySelect, 2020, 5(19), pp. 5552-5572. DOI: <https://doi.org/10.1002/slct.202000742>
 5. Chopda, L.V.; Dave, P.N. Heteropoly-12-tungstophosphoric acid $H_3[PW_{12}O_{40}]$ over natural bentonite as a heterogeneous catalyst for the synthesis of 3, 4-dihydropyrimidin-2-(1H)-ones. Arabian Journal of Chemistry, 2020, 13(6), pp. 5911-5921. DOI: <https://doi.org/10.1016/j.arabjc.2020.04.034>
 6. Patil, R.V.; Chavan, J.U.; Dalal, D.S.; Shinde, V.S.; Beldar, A.G. Biginelli reaction: polymer supported catalytic approaches. ACS combinatorial science, 2019, 21(3), pp. 105-148. DOI: <https://doi.org/10.1021/acscmbosci.8b00120>
 7. Zhang, Y.Q.; Wang, C.; Li, G.S.; Li, J.C.; Liu, H.M.; Wu, Q.H. One-pot synthesis of 3,4-dihydropyrimidin-2 (1H)-ones catalyzed by expandable graphite. Chinese Journal of Organic Chemistry, 2005, 25(10), pp. 1265-1267. http://sioc-journal.cn/Jwk_yjhx/EN/Y2005/V25/I10/1265
 8. Dhumaskar, K.L.; Meena, S.N.; Ghadi, S.C.; Tilve, S.G. Graphite catalyzed solvent free synthesis of dihydropyrimidin-2(1H)-ones/thiones and their antidiabetic activity. Biorganic & Medicinal Chemistry Letters, 2014, 24(13), pp. 2897-2899. DOI: <https://doi.org/10.1016/j.bmcl.2014.04.099>
 9. Khabazzadeh, H.; Saidi, K.; Sheibani, H. Microwave-assisted synthesis of dihydropyrimidin-2(1H)-ones using graphite supported lanthanum chloride as a mild and efficient catalyst. Biorganic & Medicinal Chemistry Letters, 2008, 18(1), pp. 278-280. DOI: <https://doi.org/10.1016/j.bmcl.2007.10.087>
 10. Moghaddas, M.; Davoodnia, A.; Heravi, M.M.; Tavakoli-Hoseini, N. Sulfonated carbon catalyzed Biginelli reaction for one-pot synthesis of 3,4-dihydropyrimidin-2(1H)-ones and -thiones. Chinese Journal of Catalysis. 2012, 33(4-6), pp. 706-710. DOI: [https://doi.org/10.1016/s1872-2067\(11\)60377-x](https://doi.org/10.1016/s1872-2067(11)60377-x)
 11. Dilmaghani, K.A.; Zeynizadeh, B.; Parasajam, H. The efficient synthesis of 3,4-dihydropyrimidin-2-(1H)-ones and their sulfur derivatives with H_2SO_4 immobilized on activated charcoal. Phosphorus, Sulfur, and Silicon and the Related Elements, 2012, 187(4), pp. 544-553. DOI: <https://doi.org/10.1080/10426507.2011.631644>
 12. Heirati, S.Z.D.; Shirini, F.; Shojaei, A.F. PEG-SANM nanocomposite: a new catalytic application towards clean and highly efficient Biginelli-like reaction under solvent-free conditions. RSC Advances, 2016, 6(71), pp. 67072-67085. DOI: <https://doi.org/10.1039/C6RA11201C>
 13. Chopda, L.V.; Dave, P.N. 12-Tungstosilicic acid $H_4[W_{12}SiO_{40}]$ over natural bentonite as a heterogeneous catalyst for the synthesis of 3, 4-dihydropyrimidin-2 (1H)-ones. ChemistrySelect, 2020, 5(8), pp. 2395-2400. DOI: <https://doi.org/10.1002/slct.201904962>
 14. Chopda, L.V.; Dave, P.N. 12-Phosphomolybdic acid $H_3[PMo_{12}O_{40}]$ over natural bentonite as a heterogeneous catalyst for the synthesis of 3,4-dihydropyrimidin-2-(1H)-ones. Results in Chemistry, 2021, 3, pp. 100169. DOI: <https://doi.org/10.1016/j.rechem.2021.100169>
 15. Darehkordi, A.; Hosseini, M.S. Montmorillonite modified as an efficient and environment friendly catalyst for one-pot synthesis of 3,4-dihydropyrimidin-2(1H) ones. Iranian Journal of Materials Science and Engineering, 2012, 9(3), pp. 49-57. <http://ijmse.iust.ac.ir/article-1-242-en.html>
 16. Ahmed, B.; Khan, R.A.; Habibullah; Keshari, M. An improved synthesis of Biginelli-type compounds via phase-transfer catalysis. Tetrahedron Letters, 2009, 50(24), pp. 2889-2892. DOI: <https://doi.org/10.1016/j.tetlet.2009.03.177>
 17. Wang, L.; Zhou, M.; Chen, Q.; He, M.-Y. Facile Biginelli-type reactions catalysed by super acidic ionic liquid under solvent-free conditions. Journal of Chemical Research, 2012, 36, pp. 712-714. DOI: <https://doi.org/10.3184/174751912X13518654161237>
 18. Hu, E.H.; Sidler, D.R.; Dolling, U.-H. Unprecedented catalytic three component one-pot condensation reaction: an efficient synthesis of 5-alkoxycarbonyl-4-aryl-3,4-dihydropyrimidin-2(1H)-ones. The Journal of Organic Chemistry, 1998, 63(10), pp. 3454-3457. DOI: <https://doi.org/10.1021/jo970846u>
 19. Stadler, A.; Yousefi, B.H.; Dallinger, D.; Walla, P.; Van der Eycken, E.; Kaval, N.; Kappe, C.O. Scalability of microwave-assisted organic synthesis. from single-mode to multimode parallel batch reactors. Organic Process Research & Development, 2003, 7(5), pp. 707-716. DOI: <https://doi.org/10.1021/op034075+>
 20. Tu, S.; Fang, F.; Miao, C.; Jiang, H.; Feng, Y.; Shi, D.; Wang, X. One-pot synthesis of 3,4-dihydropyrimidin-2(1H)-ones using boric acid as catalyst. Tetrahedron Letters, 2003, 44(32), pp. 6153-6155. DOI: [https://doi.org/10.1016/s0040-4039\(03\)01466-7](https://doi.org/10.1016/s0040-4039(03)01466-7)
 21. Mamedov, V.A.; Mustakimova, L.V.; Gubaidullin, A.T.; Vdovina, S.V.; Litvinov, I.A.; Reznik, V.S. Dichloroacetylaryl methanes as two-carbon synthons in the Biginelli reaction. Chemistry of Heterocyclic Compounds, 2006, 42, pp. 1229-1232. DOI: <https://doi.org/10.1007/s10593-006-0230-z>
 22. El-Hamouly, W.S.; El-Khamry, A.M.A.; Abbas, E.M.H. Synthesis of new 4-aryl-isoxazolo[5,4-d]pyrimidin-6-one(thione) and 4-aryl-

- pyrazolo[3,4-d]pyrimidin-6-one derivatives of potential antihypertensive activity. *Indian Journal of Chemistry*, 2006, 45B, pp. 2091-2098.
23. Aslanoğlu, F.; Akbaş, E.; Sönmez, M.; Anıl, B. Studies on reactions of pyrimidine compounds: synthesis and reactions of 5-benzoyl-4,6-diphenyl-1,2,3,4-tetrahydro-2-thioxopyrimidine. Phosphorus, Sulfur, and Silicon and the Related Elements, 2007, 182(7), pp. 1589-1597. DOI: <https://doi.org/10.1080/10426500701263554>
 24. Akbal, E.; Aslanoğlu, F.; Şener, A.; Anıl, B. A simple one-pot synthesis of 1,2,3,4-tetrahydro-2-thioxopyrimidine derivatives. *Journal of Heterocyclic Chemistry*, 2008, 45(5), pp. 1457-1460. DOI: <https://doi.org/10.1002/jhet.5570450532>
 25. Svetlik, J.; Veizerova, L. A different role of Meldrum's acid in the Biginelli reaction. *Helvetica Chimica Acta*, 2011, 94(2), pp. 199-205. DOI: <https://doi.org/10.1002/hlca.201000193>
 26. Choudhary, V.R.; Tillu, V.H.; Narkhede, V.S.; Borate, H.B.; Wakharkar, R.D. Microwave assisted solvent-free synthesis of dihydropyrimidinones by Biginelli reaction over Si-MCM-41 supported FeCl₃ catalyst. *Catalysis Communication*, 2003, 4(9), pp. 449-453. DOI: [https://doi.org/10.1016/S1566-7367\(03\)00111-0](https://doi.org/10.1016/S1566-7367(03)00111-0)
 27. Kidwai, M.; Mohan, R.; Saxena, S. Solid supported Hantzsch-Biginelli reaction for syntheses of pyrimidine derivatives. *Russian Chemical Bulletin*, 2003 52, pp. 2457-2460. DOI: <https://doi.org/10.1023/B:RUCB.0000012370.16259.4f>
 28. Kidwai, M.H.; Bala, S.; Mishra, A.D. Microwave assisted synthesis of thiadiazolopyrimidin-2-thiones. *Indian Journal of Chemistry*, 2004, 43B, pp. 2485-2487.
 29. Saxena, I.; Borah, D.C.; Sarma, J.C. Three component condensations catalyzed by iodine-alumina for the synthesis of substituted 3,4-dihydropyrimidin-2(1H)-ones under microwave irradiation and solvent-free conditions. *Tetrahedron Letters*, 2005, 46(7), pp. 1159-1160. DOI: <https://doi.org/10.1016/j.tetlet.2004.12.081>
 30. Singh, V.; Sapehiyia, V.; Srivastava, V.; Kaur, S. ZrO₂-pillared clay: An efficient catalyst for solventless synthesis of biologically active multifunctional dihydropyrimidinones. *Catalysis Communication*, 2006, 7(8), pp. 571-578. DOI: <https://doi.org/10.1016/j.catcom.2005.12.021>
 31. Wang, X.; Quan, Z.; Wang, F.; Wang, M.; Zhang, Z.; Li, Z. PEG-SO₃H as Catalyst for 3,4-Dihydropyrimidinones via Biginelli Reaction Under Microwave and Solvent-Free Conditions. *Synthetic Communication*, 2006, 36(4), pp. 451-456. DOI: <https://doi.org/10.1080/00397910500383519>
 32. Polshettiwar, V.; Varma, R.S. Biginelli reaction in aqueous medium: a greener and sustainable approach to substituted 3,4-dihydropyrimidin-2(1H)-ones. *Tetrahedron Letters*, 2007, 48(41), pp. 7343-7346. DOI: <https://doi.org/10.1016/j.tetlet.2007.08.031>
 33. Ahn, B.J.; Gang, M.S.; Chae, K.; Oh, Y.; Shin, J.; Chang, W. A microwave-assisted synthesis of 3,4-dihydro-pyrimidin-2-(1H)-ones catalyzed by FeCl₃-supported Nanopore Silica under solvent-free conditions. *Journal of Industrial and Engineering Chemistry*, 2008, 14(3), pp. 401-405. DOI: <https://doi.org/10.1016/j.jiec.2008.01.008>
 34. Khrustalev, D.P. Biginelli reaction under microwave irradiation conditions without a solvent. *Russian Journal of General Chemistry*, 2009, 79, pp. 164-165. DOI: <https://doi.org/10.1134/S1070363209010356>
 35. Dey, S.; Gomes, R.; Mondal, R.; Dey, S.K.; Dasgupta, P.; Poddar, A.; Reddy, V.R.; Bhaumik, A.; Kumar, S. Stable room temperature magnetic ordering and excellent catalytic activity of mechanically activated high surface area nanosized Ni_{0.45}Zn_{0.55}Fe₂O₄. *RSC Advances*, 2015, 5(96), pp. 78508-78518. DOI: <https://doi.org/10.1039/c5ra14773e>
 36. Fu, R.; Yang, Y.; Lai, W.; Ma, Y.; Chen, Z.; Zhou, J.; Chai, W.; Wang, Q.; Yuan, R. Efficient and green microwave-assisted multicomponent Biginelli reaction for the synthesis of dihydropyrimidinones catalyzed by heteropolyanion-based ionic liquids under solvent-free conditions. *Synthetic Communication*, 2014, 45(4), pp. 467-477. DOI: <https://doi.org/10.1080/00397911.2014.976346>
 37. Azuaje, J.; Tubío, C.R.; Escalante, L.; Gómez, M.; Guitián, F.; Coelho, A.; Caamaño, O.; Gil, A.; Sotelo, E. An efficient and recyclable 3D printed α-Al₂O₃ catalyst for the multicomponent assembly of bioactive heterocycles. *Applied Catalysis A: General*, 2017, 530, pp. 203-210. DOI: <https://doi.org/10.1016/j.apcata.2016.11.031>
 38. Wang, Z.T.; Wang, S.C.; Xu, L.W. Polymer-supported ionic-liquid-catalyzed synthesis of 1,2,3,4-tetrahydro-2-oxypyrimidine-5-carboxylates via Biginelli reaction. *Helvetica Chimica Acta*, 2005, 88(5), pp. 986-989. DOI: <https://doi.org/10.1002/hlca.200590093>
 39. Palaniappan, S.; John, A. A novel polyaniline-fluoroboric acid-dodecylhydrogensulfate salt: versatile reusable polymer based solid acid catalyst for organic transformations. *Journal of Molecular Catalysis A: Chemistry*, 2005, 233(1-2), pp. 9-15. DOI: <https://doi.org/10.1016/j.molcata.2005.02.002>
 40. Gangadasu, B.; Palaniappan, S.; Amarnath, C.A.; Rao, V.J. Polyaniline salts and complexes: Efficient and reusable catalyst for the one-pot synthesis of 5-(methoxycarbonyl)-6-methyl-4-phenyl-3,4-dihydropyrimidin-2(1h)-one. *Journal of Applied Polymer Science*, 2006, 102(2), pp. 1741-1745. DOI: <https://doi.org/10.1002/app.24374>
 41. Wang, L.; Cai, C. Polystyrene-Supported AlCl₃: A highly active and reusable heterogeneous catalyst

- for the one-pot synthesis of dihydropyrimidinones. *ChemInform*, 2009, 40(15).
DOI: <https://doi.org/10.1002/chin.200915160>
42. Lei, M.; Wu, D.-D.; Wei, H.-G.; Wang, Y.-G. Polymer-supported 4-aminoformoyldiphenylammonium triflate (PS-AFDPAT): An effective and recyclable catalyst for the Biginelli reaction. *Synthetic Communication*, 2009, 39(3), pp. 475-483.
DOI: <https://doi.org/10.1080/00397910802393109>
 43. Rahmatpour, A. Polyvinylsulfonic acid: an efficient, water-soluble and reusable Brønsted acid catalyst for the three-component synthesis of 3,4-dihydropyrimidin-2(1H)-ones/thiones in water and ethanol. *Catalysis Letters*, 2012, 142, pp. 1505-1511.
DOI: <https://doi.org/10.1007/s10562-012-0873-6>
 44. Shi, X.-L.; Yang, H.; Tao, M.; Zhang, W. Sulfonic acid-functionalized polypropylene fiber: highly efficient and recyclable heterogeneous Brønsted acid catalyst. *RSC Advances*, 2013, 3(12), pp. 3939-3945.
DOI: <https://doi.org/10.1039/c3ra23187a>
 45. Shirini, F.; Abedini, M.; Pourhasan-Kisomi, R. *N*-Sulfonic acid poly(4-vinylpyridinium) chloride as a highly efficient and reusable catalyst for the Biginelli reaction. *Chinese Chemical Letters*, 2014, 25(1), pp. 111-114.
DOI: <https://doi.org/10.1016/j.cclet.2013.09.005>
 46. Khiratkar, A.G.; Muskawar, P.N.; Bhagat, P.R. Polymer-supported benzimidazolium based ionic liquid: an efficient and reusable Brønsted acid catalyst for Biginelli reaction. *RSC Advances*, 2016, 6(107), pp. 105087-105093.
DOI: <https://doi.org/10.1039/c6ra23781a>
 47. Patel, H.A.; Sawant, A.M.; Rao, V.J.; Patel, A.L.; Bedekar, A.V. Polyaniline Supported FeCl₃: An effective heterogeneous catalyst for Biginelli reaction. *Catalysis Letters*, 2017, 147, pp. 2306-2312.
DOI: <https://doi.org/10.1007/s10562-017-2139-9>

RESIN ACIDS AS RAW MATERIAL FOR THE PREPARATION OF CYCLODEXTRIN COMPLEXES LOADED WITH DEHYDROABIETITIC ACID AND CHROMENOL HYBRID

Marina Zveaghintseva^a, Eugenia Stingaci^a, Serghei Pogrebnoi^{a,b}, Lucian Lupascu^a,
Alic Barba^a, Gheorghe Duca^a, Vladimir Valica^b, Livia Uncu^b, Victor Kravtsov^c,
Dumitru Terteac^{a,d}, Alexandr Brinzan^e, Fliur Macaev^{a,b*}

^aInstitute of Chemistry, 3, Academiei str., Chisinau MD-2028, Republic of Moldova

^b“Nicolae Testemitanu” State University of Medicine and Pharmacy, 165, Stefan cel Mare blvd.,
Chisinau MD-2004, Republic of Moldova

^cInstitute of Applied Physics, 5, Academiei str., Chisinau MD-2028, Republic of Moldova

^dPractical Scientific Institute of Horticulture and Food Technology, 59, Vierul str.,
Chisinau MD-2070, Republic of Moldova

^eInstitute of Biology Bucharest, Romanian Academy of Science,
296, Splaiul Independentei str., Bucuresti 060031, Romania

*e-mail: fliur.macaev@ichem.md

Abstract. In this work new methods to obtain complexes from β -cyclodextrin and dehydroabietic acid with chromenol-triazol hybrid with the sizes limits of approximately 0.1-250 μm are reported. Kneading, co-evaporation and co-precipitation for the resolution of racemic 2-tert-butyl-3-(1*H*-1,2,4-triazol-1-yl)-2*H*-chromen-2-ol for obtaining micro- and nanoparticles have been optimized. *In vitro* dissolution studies of the synthesized compounds in phosphate buffer (pH 6.8) showed an improved dissolution rate of chromenol-triazol hybrid in the inclusion complexes compared to the free form. It has been found that β -complexes of β -cyclodextrin loaded with dehydroabietic acid and chromenol hybrid show good antibacterial activity with MIC and MBC values ranging from 0.72 to 44.45 μM . The evaluation results revealed that all compounds showed good antifungal activity with MIC values ranging from 0.02 to 0.4 mM and MFC from 0.07 to 0.52 mM better than the reference drugs ketoconazole (MIC and MFC values at 0.28-1.88 and 0.38 mM to 2.82 mM, respectively), bifonazole (MIC and MFC values at 0.32-0.64 and 0.64-0.81 mM) and nistatin (MIC and MFC values at 0.55-0.65 mM and 0.65-0.79 mM).

Keywords: β -cyclodextrin, dehydroabietic acid, 2-tert-butyl-3-(1*H*-1,2,4-triazol-1-yl)-2*H*-chromen-2-ol, chromenol-triazol hybrid, antimicrobial activity.

Received: 22 April 2022/ Revised final: 01 August 2022/ Accepted: 05 August 2022

Introduction

In recent years, interest in natural biologically active substances and their synthetic analogues has been growing steadily. However, most biologically active organic compounds are poorly soluble in water and, as a consequence, have low bioavailability. An important and well-designed approach to increase water solubility of certain organic moieties is the formation of host-guest inclusion complexes with specific molecules able to participate in this interaction. For example, β -cyclodextrin (β -CD) is a well-known host molecule able to form inclusion complexes in both solution and solid phase with a wide variety of solid and/or liquid hydrophobic compounds [1-4]. Moreover,

crystalline bioactive ingredients are strongly preferred, since they are relatively easy to isolate, and the rejection of impurities inherent to the crystallization process and their physical-chemical stability, so most marketed pharmaceuticals consist of molecular crystals. In such crystalline assemblies the intermolecular interactions play a crucial role [5-8]. It is interesting to note that co-crystal co-formers are non-volatile molecules at ambient conditions. The existence of a space that can expand or contract to fit the solvents in the crystal structure appears to be important for the formation of pseudo-polymorphism with diverse solvents, regardless of whether the space is intramolecular or between molecular complexes. However, the most significant

problems involved in the application of the small molecules as bioactive compounds are their sometimes-low efficacy or high cytotoxicity. This can be solved by modification of bioactive ingredients involved in the complex formation, as well as through formulation of encapsulated compositions with the use of different natural or semisynthetic agents, like dehydroabietic acid (DHA) **1** (Figure 1) and cycloheptaamylose, as well [9-11]. The discovery that **1** itself possess fungicidal properties against *Aspergillus terreus* has stimulated interest in investigation of the acid **1** chemistry and has given impetus to search for other biological properties [12-14].

The aim of this work was to obtain complexes of β -cyclodextrin with water-insoluble biologically active compounds such as natural dihydroabietic acid and chromenol-triazole hybrid and to study their physicochemical properties and activity.

Experimental

Materials

β -Cyclodextrin (batch CYL-3190) was purchased from CycloLab R&D Ltd. (Hungary), anhydrous Na_2SO_4 .

The solvents including, methanol (MeOH), methylene chloride and acetonitrile (MeCN) were of reagent grade and used without additional purification. Removal of all solvents was carried out under reduced pressure.

Methods

^1H and ^{13}C NMR spectra were recorded in $\text{DMSO}-d_6$ on a Bruker Avance DRX 400 spectrometer. Chemical shifts are given in ppm in the δ scale and referred to $\text{DMSO}-d_6$ (δ_{H} at 2.50 ppm) and to $\text{DMSO}-d_6$ (δ_{C} 39.52 ppm), respectively. The coupling constants (J) are reported in Hertz (Hz). The H, H-COSY, H, C-HSQC and H, C-HMBC experiments were recorded using standard pulse sequences, in the version with z -gradients, as delivered by Bruker Corporation. Carbon substitution degrees were established by the DEPT pulse sequence.

The IR spectra were registered on a Spectrum-100 FT-IR spectrometer (Perkin-Elmer) by the ATR technique.

Elemental analyses for C, H, and N were carried out by using an Elementar Vario EL analyser.

Melting point values (uncorrected) were determined on a Boetius apparatus.

Thin-layer chromatography was carried out on Merck aluminum TLC plates, silica gel 60 coated with fluorescent indicator F254.

The morphology of the system was studied at VEGA TESCAN TS 5130 MM scanning electron microscope (SEM).

X-ray diffraction measurements were carried out on an Xcalibur E diffractometer equipped with a CCD area detector and a graphite monochromator utilizing $\text{MoK}\alpha$ radiation at room temperature. All calculations to solve and refine the structure were carried out with the programs SHELXS97 and SHELXL2014 [15,16]. Crystallographic data were deposited with the Cambridge Crystallographic Data Centre, CCDC 1985718.

For dissolution studies, 200 mg of substance and quantities of the inclusion complexes containing an equivalent amount of 1,2,4-triazole were used. The experiments were conducted under physiological conditions, at $37 \pm 0.5^\circ\text{C}$, using 900 mL of phosphate buffer (pH 6.8), with 24 hours stirring. Further, the suspensions were centrifuged and the absorbance of the supernatant was read at 319 nm after filtration through a $0.45 \mu\text{m}$ filter.

Dehydroabietic acid (**1**) was isolated from commercial disproportionate rosin as described before [17] in 85% yield, $[\alpha]_{\text{D}}^{20} +59.8$ (c 0.01, MeOH), m.p. $168\text{--}170^\circ\text{C}$. IR (ν , cm^{-1}): 2956 (carboxyl), 2928 (carboxyl), 2870, 2645, 1687 (C=O), 1458, 1458, 1388 ($\text{C-(CH}_3)_2$), 1279 (deformation vibrations OH), 1191, 1137, 951, 817, 719, 665. ^1H NMR: δ 12.2 (1H, s, $\text{CO}_2\text{H-19}$); 7.15 (1H, d, $J = 8.2$, H-11); 6.96 (1H, dd, $J = 8.0, 1.7$, H-12); 6.86 (1H, d, $J = 1.7$, H-14); 2.77 (1H, m, overlapping, H-16); 2.7–2.9 (2H, m, overlapping, H-7); 2.28 (1H, $J = 12.0$, H-1 $_{\alpha}$); 2.0 (1H, dd, $J = 12.3, 2.0$, H-5 $_{\alpha}$); 1.69–1.82 (1H, m, overlapping, H-6 $_{\beta}$); 1.67 (1H, t, $J = 12.0$, H-3 $_{\alpha}$); 1.6–1.73 (1H, $J = 7.8, 1.4$, H-2); 1.57 (1H, d, $J = 12.0$, H-3 $_{\beta}$); 1.36–1.45 (1H, m, overlapping, H-6 $_{\alpha}$); 1.26 (1H, tt, $J = 12.0, 3.3$, H-1 $_{\beta}$); 1.15 (3H, s, $\text{CH}_3\text{-18}$); 1.15 (6H, d, $J = 6.8$, $(\text{CH}_3)_2\text{-15,17}$); 1.11 (3H, s, $\text{CH}_3\text{-20}$). ^{13}C NMR: δ 179.9 (C-19); 147.2 (C-9); 145.5 (C-13); 134.6 (C-8); 124.5 (C-11); 124.2 (C-12); 46.8 (C-4); 45.2 (C-5); 38.2 (C-1); 36.9 (C-10); 36.7 (C-3); 33.3 (C-15); 30.0 (C-7); 25.3 (C-20); 24.4 (C-16,17); 21.6 (C-6); 18.6 (C-2); 16.8 (C-18). Calculated (%) for $\text{C}_{20}\text{H}_{28}\text{O}_2$: C 79.96, H 9.39. Found (%): C 79.5, H 9.0.

2-*tert*-butyl-3-(1*H*-1,2,4-triazol-1-yl)-2*H*-chromen-2-ol (BTC) (**2**) and 3,3-dimethyl-1-(1*H*-1,2,4-triazol-1-yl)butan-2-one (**4**) were synthesized according to previously described procedures [18,19].

The co-crystal (**6**) was obtained by co-crystallisation after reflux of an equal amount of dehydroabietic acid (**1**) and chromenol-triazol hybrid (**2**) in MeCN. Yield 70%, white crystals, (MeCN), m.p. 136–138°C, $[\alpha]_D^{20} +33.8$ (*c* 0.0072, MeOH). IR (ν , cm^{-1}): 3318 (hydrogen bonds), 3314 (OH), 2956 (carboxyl), 2924 (carboxyl), 2868, 2573, 1698 (C=O), 1462 (C-CH₃), 1400, 1292, 1255, 1126 (C-O-C), 1055, 973, 893, 752 (=CH-), 673, 655. ¹H NMR: δ 12.2 (1H, CO₂H-19); 8.67 (1H, s); 8.18 (1H, s); 8.0 (1H, s, OH); 7.29 (1H, dd, *J* = 7.4, 0.8); 7.25 (1H, td, *J* = 7.8, 1.4); 7.13 (1H, s); 7.15 (1H, d, *J* = 8.2, H-11); 6.96 (1H, dd, *J* = 8.0, 1.7, H-12); 6.92 (1H, td, *J* = 7.8, 1.4); 6.89 (1H, d, *J* = 8.2); 6.86 (1H, d, *J* = 1.7, H-14); 2.77 (1H, m, overlapping, H-16); 2.7–2.9 (2H, m, overlapping, H-7); 2.28 (1H, *J* = 12.0, H-1_a); 2.0 (1H, dd, *J* = 12.3, 2.0, H-5_a); 1.69–1.82 (1H, m, overlapping, H-6_β); 1.67 (1H, t, *J* = 12.0, H-3_a); 1.6–1.73 (1H, *J* = 7.8, 1.4, H-2); 1.57 (1H, d, *J* = 12.0, H-3_β); 1.36–1.45 (1H, m, overlapping, H-6_a); 1.26 (1H, tt, *J* = 12.0, 3.3, H-1_β); 1.15 (3H, s, CH₃-18); 1.15 (6H, d, *J* = 6.8, (CH₃)₂-15,17); 1.11 (3H, s, CH₃-20); 0.76 (9H, s). ¹³C NMR: δ 179.9 (C-19); 152.9; 151.8; 147.2 (C-9); 145.1; 145.5 (C-13); 134.6 (C-8); 131.1; 129.8; 128.1; 124.5 (C-11); 124.2 (C-12); 123.3; 121.4; 118.7; 114.8; 103.8; 46.8 (C-4); 45.2 (C-5); 42.9; 38.2 (C-1); 36.9 (C-10); 36.7 (C-3); 33.3 (C-15); 30.0 (C-7); 25.3 (C-20); 24.6; 24.4 (C-16,17); 21.6 (C-6); 18.6 (C-2); 16.8 (C-18). Calculated (%) for C₃₅H₄₅N₃O₄; C 73.52, H 7.35. Found (%) C 73.2, H 7.1.

The system (**7**) was obtained using the kneading method, where the molar ratio of the components dehydroabietic acid (**1**) and chromenol-triazol hybrid (**2**) was 1:1, the working temperature being 20±2°C. A sufficient amount of distilled water was added to the mixture in order to form a paste. The paste was kneaded using a pestle for 90 minutes: the first 60 minutes by adding distilled water to compensate its losses by evaporation and maintain the appearance of pasta; next 30 minutes the mixture was milled to a fine powder. The obtained powder was stored in a parafilm sealed sample tube at room temperature (20±2°C). M.p. 131–134°C, IR (ν , cm^{-1}): 3350, 3314 (hydrogen bonds), 3314 (OH), 2956 (carboxyl), 2925 (carboxyl), 2870, 2572, 1695 (C=O), 1460 (C-CH₃), 1400, 1286, 1256, 1127 (C-O-C), 1057, 969, 892, 752 (=CH-), 673, 655. ¹H NMR: δ 12.15 (1H, s, CO₂H-19); 8.67 (1H, s, H-3'); 8.18 (1H, s, H-4'); 8.0 (1H, s, OH); 7.29 (1H, dd, *J* = 7.4, 0.8); 7.25 (1H, td, *J* = 7.8, 1.4); 7.13 (1H, s); 7.15 (1H, d, *J* = 8.2, H-11); 6.96 (1H, dd, *J* = 8.0, 1.7, H-12); 6.92 (1H, td, *J* = 7.8, 1.4);

6.89 (1H, d, *J* = 8.2); 6.86 (1H, d, *J* = 1.7, H-14); 2.77 (1H, m, overlapping, H-16); 2.7–2.9 (2H, m, overlapping, H-7); 2.28 (1H, *J* = 12.0, H-1_a); 2.0 (1H, dd, *J* = 12.3, 2.0, H-5_a); 1.69–1.82 (1H, m, overlapping, H-6_β); 1.67 (1H, t, *J* = 12.0, H-3_a); 1.6–1.73 (1H, *J* = 7.8, 1.4, H-2); 1.57 (1H, d, *J* = 12.0, H-3_β); 1.36–1.45 (1H, m, overlapping, H-6_a); 1.26 (1H, tt, *J* = 12.0, 3.3, H-1_β); 1.15 (3H, s, CH₃-18); 1.15 (6H, d, *J* = 6.8, (CH₃)₂-15,17); 1.11 (3H, s, CH₃-20); 0.76 (9H, s). ¹³C NMR: δ 179.9 (C-19); 152.9; 151.8; 147.2 (C-9); 145.1; 145.5 (C-13); 134.6 (C-8); 131.1; 129.8; 128.1; 124.5 (C-11); 124.2 (C-12); 123.3; 121.4; 118.7; 114.8; 103.8; 46.8 (C-4); 45.2 (C-5); 42.9; 38.2 (C-1); 36.9 (C-10); 36.7 (C-3); 33.3 (C-15); 30.0 (C-7); 25.3 (C-20); 24.6; 24.4 (C-16,17); 21.6 (C-6); 18.6 (C-2); 16.8 (C-18). Calculated (%) for C₃₅H₄₅N₃O₄; C 73.52, H 7.35. Found (%) C 73.2, H 7.1.

The binary system (**8**) based on chromenol-triazol hybrid **2** and β-CD **3** has been prepared by the kneading method, the molar ratio of the components was 1:1, the working temperature being 20±2°C. In an agate mortar were added appropriate amounts of β-cyclodextrin and of chromenol-triazol hybrid, previously weighed on the electronic analytical balance.

A sufficient amount of distilled water was added to the mixture in order to form a paste. The paste was kneaded using a pestle for 90 minutes: the first 60 minutes by adding distilled water to compensate its losses by evaporation and maintain the appearance of pasta; next 30 minutes the mixture was milled to a fine powder. The obtained powder was stored in a parafilm sealed sample tube, at room temperature (20±2°C). M.p. 150–210°C. IR (ν , cm^{-1}): 3290 (νOH), 2927 (δCCH), 1651, 1459, 1414, 1153, 1077, 1023, 998, 947, 855, 758 (δ CCO), 752. ¹H NMR: δ 8.67 (1H, s); 8.18 (1H, s); 8.0 (1H, s, OH); 7.28 (1H, dd, *J* = 7.4, 0.8); 7.25 (1H, td, *J* = 7.8, 1.4); 7.14 (1H, s); 6.90 (1H, td, *J* = 7.8, 1.4); 6.89 (1H, d, *J* = 8.2); 5.73 (2H, dd, OH-2,3_{β-CD}); 4.82 (1H, d, H-1_{β-CD}); 4.48 (1H, t, OH-6_{β-CD}); 3.63 (3H, m, H-3,-5,-6_{β-CD}); 3.29 (2H, m, H-2,-4_{β-CD}); 0.76 (9H, s). ¹³C NMR: δ 152.9; 151.8; 145.1; 131.1; 129.8; 128.1; 123.3; 121.4; 118.7; 114.8; 103.8; 102.4 (C-1_{β-CD}); 82.0 (C-4_{β-CD}); 73.5 (C-3_{β-CD}); 72.8 (C-2_{β-CD}); 72.5 (C-5_{β-CD}); 60.4 (C-6_{β-CD}); 42.9 (C-16'); 24.6 (C-17'-19'). Calculated (%) for C₅₇H₈₇N₃O₄₂; C 48.67, H 6.19. Found (%) C 48.2, H 5.8.

The system (**9**) based on acid **1**, chromenol-triazol hybrid **2** and β-CD **3** was obtained using the following procedure: to a stirred solution of β-CD in 50% aqueous MeOH was added in small

portions the mixture of dehydroabietic acid (**1**) and chromenol-triazol hybrid **2** in MeOH, and the reaction mixture was stirred for additional 24 hours. After evaporation of the solvents under vacuum and drying at heating (up to 60°C) for 3 hours, the remaining solid system (**9**) was stored in sealed with parafilm sample tube, at room temperature (20±2°C). M.p. 170–245°C. IR (ν , cm⁻¹): 3294 (ν OH), 2925 (δ CCH), 1698, 1460, 1415, 1153, 1078, 1024, 999, 939, 820, 752. ¹H NMR: δ 8.68 (1H, s); 8.17 (1H, s); 8.0 (1H, s, OH); 7.30 (1H, dd, J = 7.4, 0.8); 7.25 (1H, td, J = 7.8, 1.4); 7.13 (1H, s); 7.15 (1H, d, J = 8.2, H-11); 6.96 (1H, dd, J = 8.0, 1.7, H-12); 6.92 (1H, td, J = 7.8, 1.4); 6.89 (1H, d, J = 8.2); 6.86 (1H, d, J = 1.7, H-14); 5.71 (2H, dd, OH-2,3 β -CD); 4.83 (1H, d, H-1 β -CD); 4.47 (1H, t, OH-6 β -CD); 3.64 (3H, m, H-3,-5,-6 β -CD); 3.31 (2H, m, H-2,-4 β -CD); 2.77 (1H, m, overlapping, H-16); 2.7–2.9 (2H, m, overlapping, H-7); 2.28 (1H, J = 12.0, H-1 α); 2.0 (1H, dd, J = 12.3, 2.0, H-5 α); 1.69–1.82 (1H, m, overlapping, H-6 β); 1.67 (1H, t, J = 12.0, H-3 α); 1.6–1.73 (1H, J = 7.8, 1.4, H-2); 1.57 (1H, d, J = 12.0, H-3 β); 1.36–1.45 (1H, m, overlapping, H-6 α); 1.26 (1H, tt, J = 12.0, 3.3, H-1 β); 1.15 (3H, s, CH₃-18); 1.15 (6H, d, J = 6.8, (CH₃)₂-15,17); 1.11 (3H, s, CH₃-20); 0.76 (9H, s). The signal of the carboxyl group is not expressed due to the strong influence of intramolecular hydrogen bonds. ¹³C NMR: δ 179.9 (C-19); 152.9; 151.8; 147.2 (C-9); 145.1; 145.5 (C-13); 134.6 (C-8); 131.1; 129.8; 128.1; 124.5 (C-11); 124.2 (C-12); 123.3; 121.4; 118.7; 114.8; 103.8; 102.4 (C-1 β -CD); 82.0 (C-4 β -CD); 73.5 (C-3 β -CD); 72.8 (C-2 β -CD); 72.5 (C-5 β -CD); 60.4 (C-6 β -CD); 46.8 (C-4); 45.2 (C-5); 42.9 (C-16'); 38.2 (C-1); 36.9 (C-10); 36.7 (C-3); 33.3 (C-15); 30.0 (C-7); 25.3 (C-20); 24.6; 24.4 (C-16,17); 21.6 (C-6); 18.6 (C-2); 16.8 (C-18). Calculated (%) for C₇₇H₁₁₅O₃₉; C 54.17, H 6.74. Found (%) C 53.7, H 6.3.

The system (**10**) based on acid **1**, chromenol-triazole hybrid **2**, and β -CD **3**, was prepared by the kneading method, same as the system (**8**). Molar ratio of components 1:1:1, working temperature 20±2°C. M.p. 150–245°C. IR (ν , cm⁻¹): 3676 (H₂O), 3277, 2972, 2902, 1693, 1451, 1154, 1126, 1077, 1050, 1027, 758 (δ CCO), 751. ¹H NMR: δ 8.68 (1H, s); 8.17 (1H, s); 8.0 (1H, s, OH); 7.29 (1H, dd, J = 7.4, 0.8); 7.25 (1H, td, J = 7.8, 1.4); 7.12 (1H, s, overlapping); 7.15 (1H, d, J = 8.2, H-11); 6.96 (1H, dd, J = 8.0, 1.7, H-12); 6.92 (1H, td, J = 7.8, 1.4); 6.89 (1H, d, J = 8.2); 6.86 (1H, d, J = 1.7, H-14); 5.72 (2H, dd, OH-2,3 β -CD); 4.83 (1H, d, H-1 β -CD); 4.48 (1H, t, OH-6 β -CD); 3.61 (3H, m, H-3,-5,-6 β -CD); 3.39 (2H, m, H-2,-4 β -CD); 2.77 (1H,

m, overlapping, H-16); 2.7–2.9 (2H, m, overlapping, H-7); 2.28 (1H, J = 12.0, H-1 α); 2.0 (1H, dd, J = 12.3, 2.0, H-5 α); 1.69–1.82 (1H, m, overlapping, H-6 β); 1.67 (1H, t, J = 12.0, H-3 α); 1.6–1.73 (1H, J = 7.8, 1.4, H-2); 1.57 (1H, d, J = 12.0, H-3 β); 1.36–1.45 (1H, m, overlapping, H-6 α); 1.26 (1H, tt, J = 12.0, 3.3, H-1 β); 1.15 (3H, s, CH₃-18); 1.15 (6H, d, J = 6.8, (CH₃)₂-15,17); 1.11 (3H, s, CH₃-20); 0.76 (9H, s). The signal of the carboxyl group is not expressed due to the strong influence of intramolecular hydrogen bonds. ¹³C NMR: δ 179.9 (C-19); 152.9; 151.8; 147.2 (C-9); 145.1; 145.5 (C-13); 134.6 (C-8); 131.1; 129.8; 128.1; 124.5 (C-11); 124.2 (C-12); 123.3; 121.4; 118.7; 114.8; 103.8; 102.4 (C-1 β -CD); 82.0 (C-4 β -CD); 73.5 (C-3 β -CD); 72.8 (C-2 β -CD); 72.5 (C-5 β -CD); 60.4 (C-6 β -CD); 46.8 (C-4); 45.2 (C-5); 42.9 (C-16'); 38.2 (C-1); 36.9 (C-10); 36.7 (C-3); 33.3 (C-15); 30.0 (C-7); 25.3 (C-20); 24.6; 24.4 (C-16,17); 21.6 (C-6); 18.6 (C-2); 16.8 (C-18). Calculated (%) for C₇₇H₁₁₅O₃₉; C 54.17, H 6.74. Found (%) C 53.8, H 6.4.

Antimicrobial activity

For the evaluation of the antimicrobial activity, the successive double dilution method was used. For this, at the initial stage, 1 mL of Sabouraud broth for test fungi and 1 mL of the Peptone broth for bacteria were introduced into a series of 10 tubes. Subsequently, 1 mL of the analysed compound was dropped into the first test tube, then, the obtained mixture was pipetted, after which 1 mL of it was transferred to the next tube, so the procedure was repeated until the tube no. 10 of the series. At the same time, 24 hour test-microbial cultures were prepared. On the second day, a preliminary analysis of the results was made. The last tube from the series in which no visible growth of microbial strains has been detected is considered to be the minimal inhibitory concentration (MIC) of the compound. For the estimation of the minimal bactericidal and fungicidal concentrations (MBC and MFC), the contents of the test tubes with MIC and with higher concentrations were seeded on Sabouraud and Peptone agar from Petri dishes. The concentration of the tested compound that does not allow the growth of any colony of microbial strains is considered to be the minimal fungicidal and bactericidal concentrations of the compound [19].

The antimicrobial activity of dehydroabietic acid (**1**), BTC **2** and microparticulate systems was evaluated against different bacterial species: *Bacillus subtilis*, *Pseudomonas fluorescens*, *Erwinia amylovora*,

Erwinia carotovora and *Xanthomonas campestris*. As well as fungi species: *Aspergillus fumigatus*, *Aspergillus versicolor*, *Aspergillus ochramensis*, *Aspergillus niger*, *Trichoderma viride*, *Penicillium funiculosum*, *Penicillium ochrochloron*, *Penicillium verrucosum* var. *cyclopium*, *Candida albicans*, *Saccharomyces cerevisiae*, *Plasmodium falciparum* 3D7 and Dd2 cultures.

Results and discussion

Recently it was demonstrated that (Z)-4,4-dimethyl-1-(4-nitrophenyl)-2-(1*H*-1,2,4-triazol-1-yl)pent-1-en-3-one with anti-tuberculosis activity can be easily prepared from 3,3-dimethyl-1-(1*H*-1,2,4-triazol-1-yl)butan-2-one (**4**) [20]. Chromenes are widespread in natural products and attracted much attention by medicinal chemistry researchers [17,21]. From the point of view of bioactivity, the hybrid system of 1,2,4-triazol and chromenol is an interesting subject for study. In order to reduce duration of treatment, frequency and quantity of the administered doses of antibacterial agents, and to reduce the side effects, the recent discovery of a new drugs and different micro- and nanoparticle β -CD based systems have been proposed [10,11,17,22-26]. Recently attention has only been paid to the tandem reactions of salicylic

aldehydes or salicylic imines with α,β -unsaturated compounds [21]. Some years ago an α,β -unsaturated ketone containing a 1,2,4-triazolyl and pivaloyl groups directly attached to the carbon-carbon double bond was synthesized by the interaction of **4** with a 4-nitrobenzaldehyde [20]. It was found that an applicable route to 1*H*-1,2,4-triazol functionalized chromene **2** would go through the coupling of substituted triazolylethanones with salicylic aldehyde [16].

Herein, it was proposed the preparation of β -CD **3** particles containing biological active compounds: DHA **1** and BTC **2** (Figure 1).

Thus, the synthesis of 1*H*-1,2,4-triazole-functionalized chromenol (BTC) **2** was carried out for the first time using tandem reactions of compound **4** with salicylic aldehyde (Scheme 1) [18].

Two different sets of conditions for the achieving of the co-precipitation were tried to obtain the co-crystal particles of the dehydroabietic acid **1** with chromenol-triazol hybrid **2**. This particular system was chosen, since the two epimers of racemic compound **5** have opposite configuration at stereogenic center (quaternary carbon atom on the hydroxyl group) and one of them may produce more stable systems with **1**.

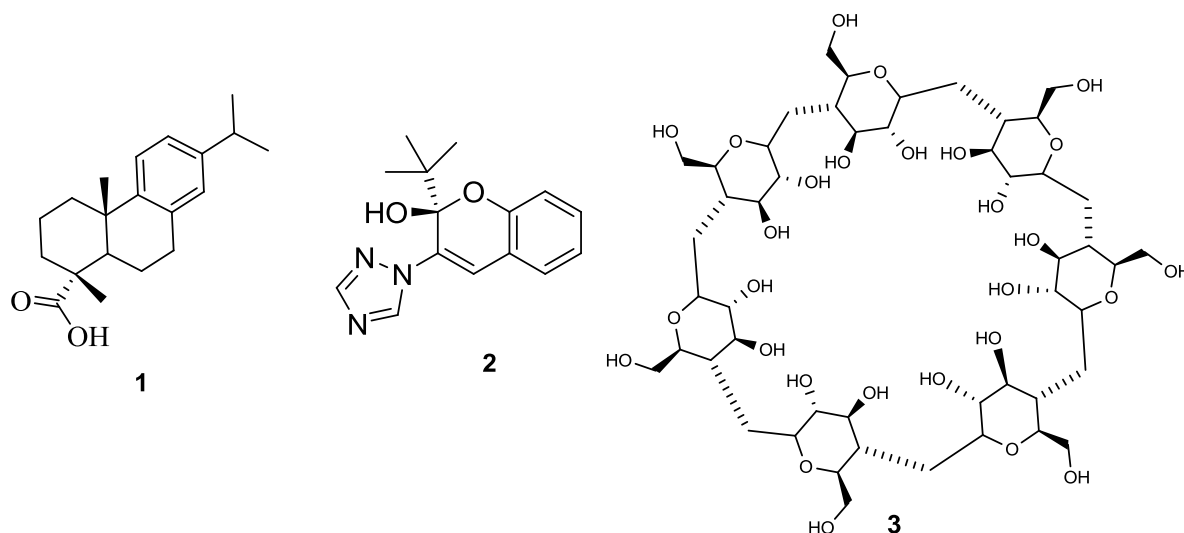
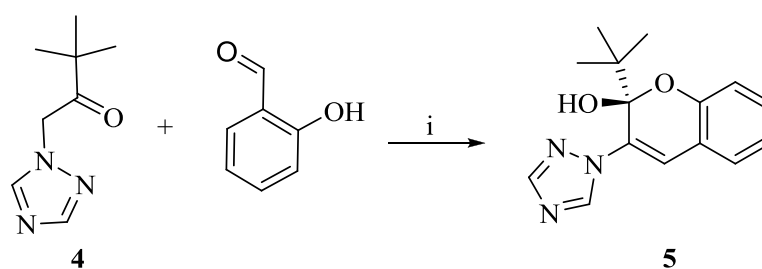


Figure 1. Chemical structures of dehydroabietic acid **1** and target chromene-triazol hybrid **2**.



Reagents and conditions: (i) benzene, piperidine/AcOH (cat, reflux), 5 h, 70%.

Scheme1. Synthesis of 1*H*-1,2,4-triazol functionalized chromenol.

X-ray diffraction results

The molecular structure and intermolecular interactions among ingredients of the co-crystal **6** were characterized by the single crystal X-ray diffraction method. The colourless needle-like crystals of **6** belong to the non-centrosymmetric orthorhombic space group $P2_12_12_1$, have the unit cell parameters $a = 6.5059(6)$, $b = 10.990(2)$, $c = 44.484(7)$ Å, $V = 3180.6(8)$ Å³, and represent the co-crystals with 1:1 stoichiometry formed by natural acid **1** and hybrid **5** components, Figure 2(a).

The structure of the co-crystal **6** was refined using 4893 [$R(\text{int}) = 0.0681$] independent reflections to $R1 = 0.0899$ and $wR2 = 0.0953$ for 1750 reflections with $I > 2\sigma(I)$ and $\text{GOF} = 1.006$. The maximum and minimum residual electron densities in the difference synthesis were 0.150 and $-0.154 \text{ e} \cdot \text{\AA}^{-3}$.

The interaction of dehydroabietic acid with compound **2** yielded a material that was a DHA-BTC co-crystallization product **6**. It has been found that the rate of formation of DHA-BTC systems is very sensitive to the composition of the medium. For example, more than 70% of the expected material is formed (TLC data) within 4 hours when the solvent is MeCN at 80°C. The product is then isolated by filtration.

As the stereo configuration of diterpenoid acid **1** is well established, the crystal structure unambiguously indicates the *S*-configuration of the chiral atom in BTC. In the crystal the acid **1** and chromenol-triazol hybrid **5** molecules form $\text{O1-H} \cdots \text{N4}' = 2.686(10)$ Å strong hydrogen bond between 1,2,4-triazole and carboxylic groups that results in supramolecular synthon was for the first time reported for co-crystals of a triazole drug with 1,4-dicarboxylic acids [27].

It should be noted however, that the above-mentioned separation was not observed with β -CD **3** as described for ibuprofen [12]. The crystal structure also shows that symmetry related by translation BTC molecules are interlinked in infinite chains along crystallographic axis a by $\text{O20}'\text{-H} \cdots \text{N2}' = 2.785(9)$ Å hydrogen bonds.

Dissolution studies

Previously it was found that ciprofloxacin interacts pharmacodynamically with antifungal agents by altering their growth inhibitory activity against *Candida albicans* and *Aspergillus fumigatus* [28]. It has been hypothesized that the synergistic interactions may have beneficial implications for the outcome of antifungal therapy, for example system antifungal dehydroabietic acid **1** loaded with BTC **2** and β -cyclodextrin **3**.

In the present study, in an attempt to improve the solubility characteristics of micro- and nanoparticle diterpenoid acid **1**, BTC **2** and β -CD **3** based systems, were prepared their crystalline and amorphous forms with defined size and crystallinity.

The kneading method is a relatively simple one, which consists in the precise weighing of the acid **1** and hybrid **5**, mixing and shredding them in dry phase for a few minutes followed by addition of some amount of H₂O. The mixture **7** becomes a paste that has been triturated for 1.5 hours and dried to give the final product.

FTIR and NMR spectral results

The IR-spectra of the components **1**, **2** and **6** are similar to spectrum of **7** with the differences consisting in shifts of band characteristic for OH group: **1** at 1279 cm⁻¹; **2** at 1232 cm⁻¹, 3069 cm⁻¹; **6** at 1255 cm⁻¹, 3318 cm⁻¹; **7** at 1285 cm⁻¹ and 3113 cm⁻¹ (Figure S1).

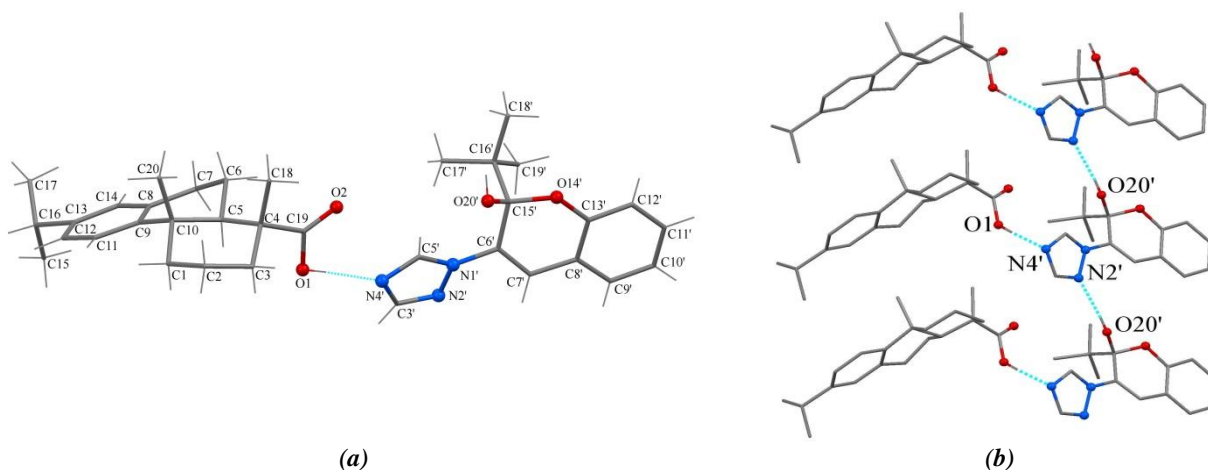


Figure 2. View of the formula unit of **6** with numbering scheme illustrates the stereo configuration of **1** and **2** components and their interaction via O-H...N hydrogen bond (a). Hydrogen bonded chain in the crystal of **6** (b).

The structure of co-crystal **6** and system **7** was studied by NMR spectroscopy, which is a very sensitive method that allows to establish the nature of the intermolecular interaction. The presence of intermolecular interaction in the structure of co-crystal **6** was established by comparing the NMR spectra of the initial compounds **1** and **2**. The main difference was the shift of the signals of the aromatic part of the chromenol molecule, the vinyl proton, and the *tert*-butyl group to a lower field. The similarity of several aspects of the NMR spectrum of system **7** with that of co-crystal **6** led to a preliminary determination of the structure and to a tentative assignment of structure to this material (Figure S2).

The interaction of BTC **2** with β -CD **3**, which has not been studied previously, was found to yield system **8**. Analysis of the FTIR spectra shows that it is mainly the sum of the spectra of its components. It is worth noting that some of the absorption bands of the compounds disappear in the spectrum of the system **8**. These are, for instance, the bands at 755 cm^{-1} and 2926 cm^{-1} in the β -CD spectrum, which correspond to the vibrations ($\delta\text{CCO} + \delta\text{CCH}$) and $\nu_{\text{as}}\text{CH}$, respectively, and the bands at 750 cm^{-1} , 1459 cm^{-1} (C=N, triazole ring) and 1509 cm^{-1} (benzene ring) in the 2*H*-chromenole spectrum. Also, one can observe a shift of characteristic bands at 755 cm^{-1} (β -CD) and 750 cm^{-1} (2*H*-chromenole) to 752 cm^{-1} and 758 cm^{-1} , decrease in the intensity of absorption bands of 2*H*-chromenole at 1459 cm^{-1} (C=N, triazole ring) and 1509 cm^{-1} (benzene ring). All these observations have prompted us to conclude that the 2*H*-chromenole molecules are incorporated into the β -cyclodextrin structure and that there are interaction forces between the compounds, as a result of the formation of the inclusion complex.

A ternary dehydroabietic acid **1**: chromenol-triazol hybrid **6**: β -CD **3** system by using two techniques was obtained. The co-evaporation method (the first one) involved the use of 50% aqueous MeOH solution of β -CD mixed with dehydroabietic acid **1**: chromenol-triazol hybrid **6** in MeOH, stirring for 24 hours followed by evaporation under vacuum and drying at heating (up to 60°C) for 3 hours. Analysis of IR spectra of system **9** showed that the characteristic absorption bands of chromenol at 1459 cm^{-1} and 1509 cm^{-1} and dehydroabietic acid at 1686 cm^{-1} and 1279 cm^{-1} (C-C stretching vibrations) disappeared and the absorption band of the cyclodextrin shifted from 3289 cm^{-1} to 3294 cm^{-1} . The kneading method (the second

one), as already mentioned, consisted in precise weighing the “host” and the “guest” ingredients followed by additional mixing with an amount of water. The resulting system has been dried and then crushed. In the second method, the same pattern is observed, and the absorption band at 3674 cm^{-1} indicates the presence of water molecules in system **10** (Figure S3).

The ^1H NMR spectra of the systems showed interaction between aromatic protons and the internal CD protons, when the isopropyl-1,2,3,4-tetrahydronaphthalene fragment enters into the CD cavities, as well as when the chromene ring is inside the CD cavities. On the other hand, in the case of triazole ring protons, their chemical shifts cannot be confidently attributed to the formation of the inclusion complex (Figure S4).

In vitro dissolution studies of the synthesized compounds compared to the pure in water phosphate buffer (pH= 6.8) showed an improved dissolution rate of chromenol-triazol hybrid in the inclusion complexes compared to the free form in the following order: DHA **1**: BTC **2** : β -CD **3** > DHA **1**: BTC **2**: β -CD **3**: H_2O > BTC **2**: β -CD **3** > co-cristal **6** > DHA **1**: BTC **2**.

SEM results

The scanning electron microscopy (SEM) image Figure 4(a) showed that the diameter of particles from system **7** was approximately 50–100 μm and such data implicated with optimal uniformity of the prepared system.

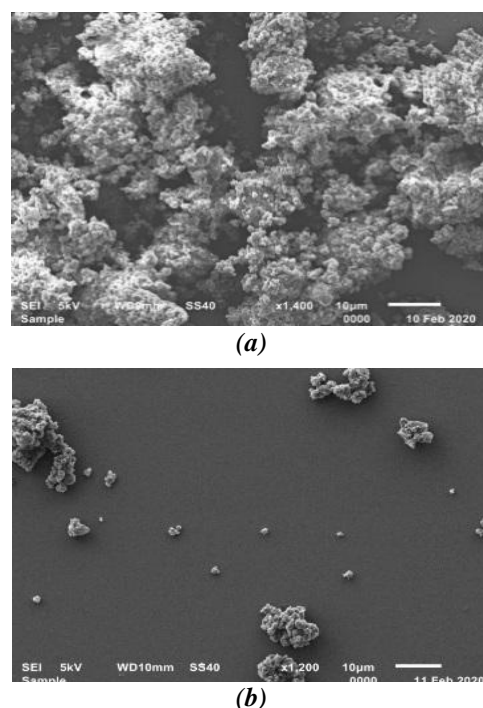


Figure 4. SEM micrographs for dry (a) and wet (b) particles of system **7**.

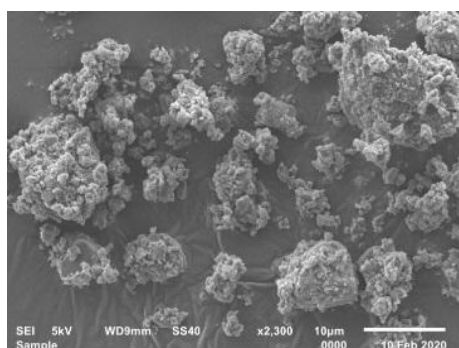
The solubility of system **7** in water increased compared to the initial compounds - DHA (**1**) and BTC **2**. The morphology of the system after dissolution studies is characterized by the formation of a solid clot with main size range of the obtained particles falling in the limits of approximately 0.1–50 μm Figure 4(b).

The system **8** consists of a mixture of irregularly shaped micro- and nanoparticles with predominance of the first. Wet particles of the system **8** are characterized by the formation of a firm gel and solid plates. The main size ranges of the obtained needle-like particles are approximately 0.1–250 μm . β -CD is a solubilizer and increases the solubility of the BTC **2**.

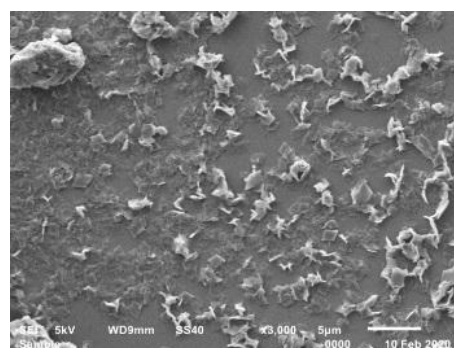
The particles surface of system **9** is smooth, in comparison with those of systems **7-8**, which

have many rough edges. SEM analysis shows that dehydroabietic acid **1**, BTC **2**, and β -CD **3** are in close contact with each other and sufficiently dispersed, indicating that system **9** was successfully obtained, Figure 5. The visualized particle sizes showed that the wet particles of system **9** had homogenous morphology and did not produce aggregated structures, Figure 6(b).

SEM investigation showed that the average sizes of the dehydroabietic acid **1**: BTC **2**: β -CD **3** particles were from 0.4 μm up to 3.9 μm , respectively. In case of the system dehydroabietic acid **1**: BTC **2** coated with β -CD and H_2O the formation of a firm gel has not been observed. Wet particles of system **10** are characterized by the formation of solids in the sizes limits of approximately 0.1–250 μm , Figure 7(b).

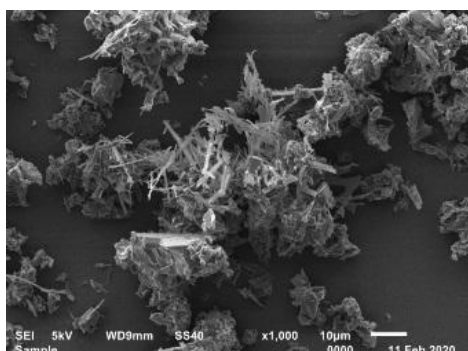


(a)

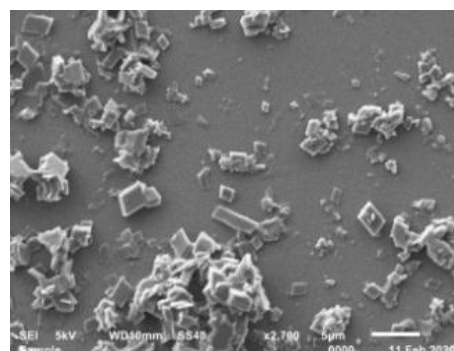


(b)

Figure 5. SEM micrographs for dry (a) and wet (b) particles of system **8**.

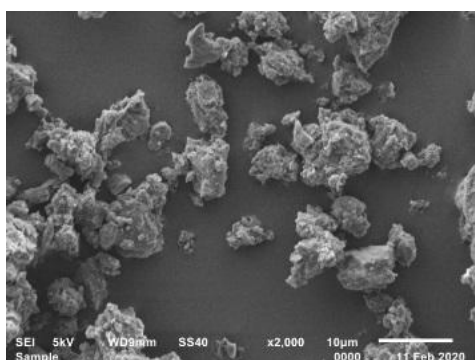


(a)

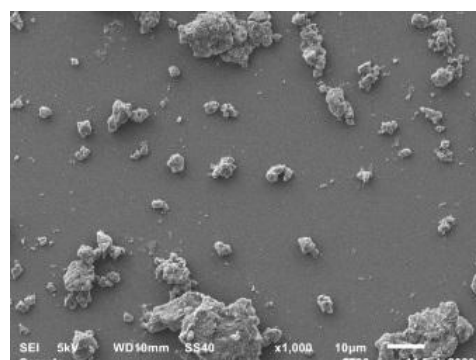


(b)

Figure 6. SEM micrographs for dry (a) and wet (b) particles of system **9**.



(a)



(b)

Figure 7. SEM micrographs for dry (a) and wet (b) particles of system **10**.

The surface of the particles of systems **10** is almost similar to that of the particles of dry systems **8-9**, which have many rough edges, probably due to the presence of β -cyclodextrin, which adheres to the surface of the matrix.

Antimicrobial activity

All tested compounds showed good antibacterial activity with MIC and MBC values ranging from 0.72 to 44.45 mM. Systems **9** and **10** appeared to be the most active among all tested compounds. In contrast, low efficiency of the BTC **2** against the *Plasmodium falciparum* remained essentially unchanged in both 3D7 and Dd2 cultures over the entire duration of the experiment, although fluctuating within 10% variation has been noted. The evaluation results revealed that all compounds showed good antifungal activity against *A. fumigatus*, *T. viride*, *C. albicans*, *S. cerevisiae*, *A. versicolor*, *A. ochraceus*, with MIC values ranging from 0.02 mM to 0.4 mM and MFC from 0.07 mM to 0.52 mM better than reference drugs ketoconazole (MIC and MFC values at 0.28–1.88 mM and 0.38 mM to 2.82 mM respectively), bifonazole (MIC and MFC values at 0.32–0.64 mM and 0.64–0.81 mM) and nistatin (MIC and MFC values at 0.55–0.65 mM and 0.65–0.79 mM) (Table S1).

The order of compounds can be presented as follows: **6>7>10>8>9>2>1**. The best antifungal activity as in case of antibacterial is displayed by systems **9**, **10** with MIC at 0.07 mM and MFC at 0.08–0.09 mM, while compound **1** showed the lowest activity. Thus, the antifungal potency of compounds against *Candida albicans* can be presented as follows: **6>7>9>10>8>2>1**, while against *Aspergillus fum* and the *Trichoderma viride*. : **9>6>10>8>2>1**. The most sensitive fungal appeared to be *Candida albicans*, while *Trichoderma viride* was the most resistant one. The results reveal that all prepared systems display a higher antifungal activity as compared to nystatin, which is used to treat *Candida* infections of the skin including oesophageal candidiasis, thrush, vaginal vast infections and diaper rash (Table S2).

Some differences in antifungal activity according to the method of synthesis could be noticed. Thus, the antifungal activity decreases in the following order of the preparation methods: co-evaporation, co-crystallisation, kneading.

This may be attributed to the differences in the enhanced solubility of the prepared systems, which should lead to different level of disruption

of the fungal and bacteria cell membrane by extraction of the sterols and lipids, interaction of the positively charged cyclodextrins with negatively charged lipids or anionic phospholipids, or reduction of total blood cholesterol content by cyclodextrins. These effects have been well described in different examples [8,22]. The morphology of the obtained particles varies from spherical to irregularly-shaped with size range from 0.001 to 0.25 mM. The FTIR as well as NMR spectra analysis has revealed molecular interactions between active compounds and β -cyclodextrin-polymeric matter of the particles.

Conclusions

Complexes of β -cyclodextrin and dehydroabiatic acid with chromenol-triazol hybrid were synthesized. In summary, kneading, co-evaporation and co-precipitation as example of the resolution technology of racemic 2-*tert*-butyl-3-(1*H*-1,2,4-triazol-1-yl)-2*H*-chromen-2-ol for obtaining micro- and nanoparticles have been optimized.

The morphology of the obtained particles varied from spherical to irregular shape with sizes from 0.001 to 0.25 mM. The particle diameter of system **7** (DHA-BTC) decreased from 50–100 μ m to 0.1–50 μ m. Based on the increase in solubility of systems **8-10**, molecular interactions between active compounds: dehydroabiatic acid, chromenol-triazole hybrid, and β -cyclodextrin according to FTIR and NMR spectra indicate complex formation.

The obtained β -cyclodextrin: dehydroabiatic acid : chromenol-triazole hybrid systems showed good activity against *Aspergillus fumigatus*, *Trichoderma viride*, *Penicillium funiculosum*, *Penicillium ochrochloron*, *Penicillium verrucosum* var. *Cyclopium*, *Candida albicans* and *Saccharomyces cerevisiae*. The antibacterial activity of the obtained systems was higher compared to the initial components: 5.75-fold for dehydroabiatic acid and 2-fold for the chromenol-triazole hybrid. The complexes from β -cyclodextrin and dehydroabiatic acid with chromenol-triazol hybrid were 2 and 1.5 times more active against the genus *Pseudomonas fluorescens* compared to the reference preparations ampicillin and chloramphenicol, respectively. It was shown that the solubility of the obtained complexes increased in comparison with the solubility of the reference compounds.

The use of cyclodextrins to obtain inclusion complexes of biologically active substances

seems to be a promising direction, which leads to physicochemical properties and bioavailability of biologically active compounds.

Acknowledgments

The authors M.Z., E.S., S.P., L.L. and F.M. are grateful for the funding of this research under the Moldovan State Program (2020-2023) project no. 20.80009.5007.17 "Hybrid materials functionalized with carboxyl groups based on plant metabolites with activity against human and agricultural pathogens".

V.V., L.U. and F.M. are grateful to the Moldovan State Program (2020-2023) project no. 20.80009.8007.14 "Complex researches for the development of new local anti-infective pharmaceuticals for optimizing the pharmacotherapy of dental, oropharyngeal and auricular diseases".

The author Gh.D. is grateful to the Moldovan State Program (2020-2023) project no. 20.80009.5007.27 "Physico-chemical mechanisms of redox processes with electron transfer involved in vital, technological and environmental systems".

The author V.K. is grateful to the Moldovan State Program (2020-2023) project no. 20.80009.5007.15 "Implementation of crystal engineering approach and X-ray crystallography for design and creation of hybrid organic/inorganic materials with advanced physical and biologically active functions" and appreciates the contribution of the National Collection of Non-Pathogenic Microorganisms for the offering of the microbial cultures for testing.

Supplementary information

Supplementary data are available free of charge at <http://cjm.asm.md> as PDF file.

References

- García-Villén, F.; Viseras, C. Clay-based pharmaceutical formulations and drug delivery systems. *Pharmaceutics*, 2020, 12(12), 1142, pp. 1–4. DOI: <https://doi.org/10.3390/pharmaceutics12121142>
- Conceição, J.; Adeoye, O.; Cabral-Marques, H.; Concheiro, A.; Alvarez-Lorenzo, C.; Lobo, J.M.S. Orodispersible carbamazepine/hydroxypropyl- β -cyclodextrin tablets obtained by direct compression with five-in-one co-processed excipients. *AAPS PharmSciTech*, 2020, 21(2), 39, pp.1–10. DOI: <https://doi.org/10.1208/s12249-019-1579-5>
- Sepúlveda, B.; Quispe, C.; Simirgiotis, M.; García-Beltrán, O.; Areche, C. Gastroprotective effects of new diterpenoid derivatives from *Azorella cuatrecasii* Mathias & Constance obtained using a β -cyclodextrin complex with microbial and chemical transformations. *Bioorganic & Medicinal Chemistry Letters*, 2016, 26(14), pp. 3220–3222. DOI: <https://doi.org/10.1016/j.bmcl.2016.05.081>
- Fernández-Ferreiro, A.; Bargiela, N.F.; Varela, M.S.; Martínez, M.G.; Pardo, M.; Ces, A.P.; Méndez, J.B.; Barcia, M.G.; Lamas, M.J.; Otero-Espinar, F.J. Cyclodextrin-polysaccharide-based, in situ-gelled system for ocular antifungal delivery. *Beilstein Journal of Organic Chemistry*, 2014, 10, pp. 2903–2911. DOI: <https://doi.org/10.3762/bjoc.10.308>
- Datta, S.; Grant, D.J.W. Crystal structures of drugs: advances in determination, prediction and engineering. *Nature Reviews Drug Discovery*, 2004, 3, pp. 42–57. DOI: <https://doi.org/10.1038/nrd1280>
- Almarsson, O.; Zaworotko, M.J. Crystal engineering of the composition of pharmaceutical phases. Do pharmaceutical co-crystals represent a new path to improved medicines? *Chemical Communications*, 2004, 17, pp. 1889–1896. DOI: <https://doi.org/10.1039/b402150a>
- Huang, L.; He, J.; Lu, R.; Ge, X.; Guo, J. Investigation on a host-guest inclusion system by β -cyclodextrin derivative and its analytical application. *Bioorganic & Medicinal Chemistry Letters*, 2011, 21(4), pp. 1113–1117. DOI: <https://doi.org/10.1016/j.bmcl.2010.12.125>
- Ivancic, A.; Macaev, F.; Aksakal, F.; Boldescu, V.; Pogrebnoi, S.; Duca, Gh. Preparation of alginate-chitosan-cyclodextrin micro- and nanoparticles loaded with anti-tuberculosis compounds. *Beilstein Journal of Nanotechnology*, 2016, 7, pp. 1208–2018. DOI: <https://doi.org/10.3762/bjnano.7.112>
- Tolstikov, G.A.; Tolstikova, T.G.; Shults, E.E.; Tolstikov, S.E.; Khvostov, M.V. Resin acids from russian forest conifers. *Chemistry and pharmacology*. Academic Publishing House "Geo", 2011, 396 p. (in Russian).
- Halbrook, N.J.; Lawrence, R.V. The isolation of dehydroabietic acid from disproportionated rosin. *The Journal of Organic Chemistry*, 1966, 31(12), pp. 4246–4247. DOI: <https://doi.org/10.1021/jo01350a510>
- Varan, G.; Benito, J.M.; Mellet, C.O.; Bilensoy, E. Development of polycationic amphiphilic cyclodextrin nanoparticles for anticancer drug delivery. *Beilstein Journal of Nanotechnology*, 2017, 8, pp. 1457–1468. DOI: <https://doi.org/10.3762/bjnano.8.145>
- Skvara, J.; Nezbeda, I.; Izak, P. Molecular dynamics study of racemic mixtures. II. Temperature dependence of the separation of ibuprofen racemic mixture with β -cyclodextrin in methanol solvent. *Journal of Molecular Liquids*, 2020, 302, 112575, pp. 1–6. DOI: <https://doi.org/10.1016/j.molliq.2020.112575>
- Savluchinske-Feio, S.; Curto, M.J.M.; Gigante, B.; Roseiro, J.C. Antimicrobial activity of resin acid

- derivatives. Applied Microbiology and Biotechnology, 2006, 72(3), pp. 430–436.
DOI: <https://doi.org/10.1007/s00253-006-0517-0>
14. Zhou, Z.; Wang, X.; Zhou, T. Synthesis and antibacterial activity of benzenesulfonylhydrazone derivatives of methyl dehydroabietate. Russian Journal of General Chemistry, 2019, 89(4), pp. 819–823.
DOI: <https://doi.org/10.1134/S1070363219040297>
15. Pavlova, A.; Mikhalechenko, O.; Rogachev, A.; Il'ina, I.; Korchagina, D.; Gatilov, Y.; Tolstikova, T.; Volcho, K.; Salakhutdinov, N. Synthesis and analgesic activity of stereoisomers of 2-(3(4)-hydroxy-4(3)-methoxyphenyl)-4,7-dimethyl-3,4,4a,5,8,8a-hexahydro-2H-chromene-4,8-diols. Medicinal Chemistry Research, 2015, 24, pp. 3821–3830.
DOI: <https://doi.org/10.1007/s00044-015-1426-5>
16. Zveaghintseva, M.; Stingaci, E.; Pogrebnoi, S.; Smetanscaia, A.; Valica, V.; Uncu, L.; Kravtsov, V.Ch.; Melnic, E.; Petrou, A.; Glamočlija, J.; Soković, M.; Carazo, A.; Mladěnka, P.; Poroikov, V.; Geronikaki, A.; Macaev, F.Z. Chromenol derivatives as novel antifungal agents: synthesis, *in silico* and *in vitro* evaluation. Molecules, 2021, 26(14), 4304, pp. 1–21.
DOI: <https://doi.org/10.3390/molecules26144304>
17. Macaev, F.; Zveaghintseva, M.; Stingaci, E.; Pogrebnoi, S.; Duca, Gh. Process for the synthesis of 3,3-dimethyl-1-(1*H*-1,2,4-triazol-1-yl)butane-2-one. Patent MD 4505, BOPI, 2017, nr. 8, p. 28.
<http://www.db.agepi.md/Inventions/details/a%202016%200146>
18. Macaev, F.; Zveaghintseva, M.; Stingaci, E.; Pogrebnoi, S.; Duca, Gh. Use of (Z)-4,4-dimethyl-1-(4-nitrophenyl)-2-(1*H*-1,2,4-triazol-1-yl)pent-1-en-3-one as antituberculous agent. Patent MD 4519, BOPI, 2017, 10, pp. 27–28.
<http://www.db.agepi.md/Inventions/details/a%202017%200068>
19. Shi, Y.-L.; Shi, M. The synthesis of chromenes, chromanes, coumarins and related heterocycles *via* tandem reactions of salicylic aldehydes or salicylic imines with α,β -unsaturated compounds. Organic and Biomolecular Chemistry, 2007, 5, pp. 1499–1504.
DOI: <https://doi.org/10.1039/B618984A>
20. Boldescu, V.; Bratu, I.; Borodi, Gh.; Kacso, I.; Bende, A.; Duca, Gh.; Macaev, F.; Pogrebnoi, S.; Ribkovskaia, Z. Study of binary systems of β -cyclodextrin with a highly potential anti-mycobacterial drug. Journal of Inclusion Phenomena and Macrocyclic Chemistry, 2012, 74, pp. 129–135.
DOI: <https://doi.org/10.1007/s10847-011-0091-7>
21. Mohammed, N.N.; Pandey, P.; Khan, N.S.; Elokely, K.M.; Liu, H.; Doerksen, R.J.; Repka, M.A. Clotrimazole–cyclodextrin based approach for the management and treatment of Candidiasis - a formulation and chemistry-based evaluation. Pharmaceutical Development Technology, 2016, 21(5), pp. 619–629. DOI: <https://doi.org/10.3109/10837450.2015.1041041>
22. Macaev, F.; Boldescu, V.; Geronikaki, A.; Sucman, N. Recent advances in the use of cyclodextrins in antifungal formulations. Current Topics in Medicinal Chemistry, 2013, 13(21), pp. 2677–2683. DOI: <https://doi.org/10.2174/15680266113136660194>
23. Tiwari, G.; Tiwari, R.; Rai, A.K. Cyclodextrins in delivery systems: Applications. Journal of Pharmacy and BioAllied Sciences, 2010, 2(2), pp. 72–79.
DOI: <https://doi.org/10.4103/0975-7406.67003>
24. Minea, B.; Nastasa, V.; Moraru, R.F.; Kolecka, A.; Flonta, M.M.; Marincu, I.; Man, A.; Toma, F.; Lupse, M.; Doroftei, B.; Marangoci, N.; Pinteala, M.; Boekhout, T.; Mares, M. Species distribution and susceptibility profile to fluconazole, voriconazole and MXP-4509 of 551 clinical yeast isolates from a Romanian multi-centre study. European Journal of Clinical Microbiology & Infectious Diseases, 2015, 34, pp. 367–383.
DOI: <https://doi.org/10.1007/s10096-014-2240-6>
25. Sheldrick, G.M. Crystal structure refinement with SHELXL. Acta Crystallographica Section C, 2015, C71, pp. 3–8.
DOI: <http://doi.org/10.1107/S2053229614024218>
26. Sheldrick, G.M. A short history of SHELX. Acta Crystallographica Section A, 2008, A64, pp. 112–122.
<https://doi.org/10.1107/S0108767307043930>
27. Remenar, J.F.; Morissette, S.L.; Peterson, M.L.; Moulton, B.; MacPhee, J.M.; Guzmán, H.R.; Almarsson, Ö. Crystal engineering of novel cocrystals of a triazole drug with 1,4-dicarboxylic acids. Journal of American Chemical Society, 2003, 125(28), pp. 8456–8457.
DOI: <https://doi.org/10.1021/ja035776p>
28. Method of serial dilutions in broth. Saint-Petersburg Pasteur Institute. (in Russian). http://www.dntpasteur.ru/metodic2_4_2_2.php